Universidad de La Laguna
Oficina de Sede Electrónica
Entrada
Nº registro: 2021/12258
Nº reg. oficina: OF002/2021/12092
Fecha: 18/02/2021 08:49:19

Doctorado en Territorio y Sociedad. Evolución Histórica en un Espacio Tricontinental (África, América y Europa)

INVESTIGATING MICROSCOPIC AND MOLECULAR ORGANIC MATTER TO EXPLORE THE ROLE OF CLIMATE IN NEANDERTHAL SOCIAL AND CULTURAL EVOLUTION AT A REGIONAL SCALE

A thesis presented

by

Rory Connolly

to

Departamento de Geografía e Historia

in partial fulfilment of the requirements

for the degree of

Doctor of Philosophy

in the subject of

Archaeology

Universidad de La Laguna

San Cristóbal de La Laguna, Tenerife

February 2021

Universidad
de La Laguna

Thesis advisor: Dr Carolina Mallol

Facultad de Humanidades

Departamento de Geografía e Historia

UDI de Arqueología, Prehistoria e Historia Antigua

Universidad de La Laguna

La Dra. Carolina Mallol Duque, profesora titular de Prehistoria del Departamento de Geografía e Historia (UDI de Arqueología, Prehistoria e Historia Antigua) de la Universidad de La Laguna

CERTIFICA:

Que la Tesis Doctoral titulada “Investigating microscopic and molecular organic matter to explore the role of Neanderthal social and cultural evolution at a regional scale” presentada por Rory Connolly ha sido realizada bajo mi dirección y reúne las condiciones de calidad y rigor científico para que pueda ser presentada y defendida ante la comisión nombrada al efecto.

Y para que así conste y surta los efectos oportunos, firmo el presente certificado en San Cristóbal de La Laguna, Febrero de 2021.

Dra. Carolina Mallol Duque

INVESTIGATING MICROSCOPIC AND MOLECULAR ORGANIC MATTER TO EXPLORE THE ROLE OF CLIMATE IN NEANDERTHAL SOCIAL AND CULTURAL EVOLUTION AT A REGIONAL SCALE

ABSTRACT

The role of climate change is a recurrent theme in debates concerning the replacement of Neanderthals by anatomically modern humans across Europe and western Asia. The Iberian Peninsula is widely regarded as a key geographic location for understanding this process, owing to the apparent late survival of Neanderthal populations along its southern and western fringes. Despite this, relatively few long-term terrestrial palaeoclimate records are available against which hypotheses concerning climatic and ecological factors can be tested. Global climatic datasets from analyses of ice-cores obtained from the polar regions have provided a framework for understanding broad fluctuations in climate over geological timescales. At a higher scale of resolution, analysis of speleothems and palynological studies of marine cores off the Atlantic and Mediterranean coasts provide our most complete records of Pleistocene conditions throughout Iberia. Nevertheless, the extent to which these records accurately reflect regional and local terrestrial conditions in the areas inhabited by Neanderthal groups remains unclear. The persistence of locally favourable conditions in certain parts of the peninsula during periods of wider global climatic downturn cannot be discounted, and relatively few site-specific palaeoecological studies from human occupation contexts have been carried out. This presents a challenge for understanding long-term human-environment dynamics and the processes which drove the Middle to Upper Paleolithic transition.

Compound-specific isotope analyses of sedimentary organic compounds, particularly hydrocarbons derived from fossil leaf waxes (*n*-alkanes), have recently emerged as a powerful palaeoclimate proxy for reconstructing palaeohydrological (hydrogen isotope) and palaeoecological (carbon isotope) conditions at a high spatial and temporal resolution. This technique has been successfully applied in a wide range of terrestrial environments, however, has rarely been utilised in archaeological contexts. Here we combine compound-specific carbon and hydrogen isotope analysis of sedimentary *n*-alkanes with archaeological soil micromorphology, a well-established geoarchaeological method, to better understand the sedimentary context of the target organic compounds and any potential biases which might arise due to anthropogenic activity or post-depositional processes. We investigate palaeoenvironmental conditions at the Middle Palaeolithic sites of Abric del Pastor (MIS 5/4) and El Salt (MIS 3) in Alcoy, Eastern Iberia, in combination with traditional palaeoenvironmental proxies employed in archaeological research, including charcoal, microvertebrates, macro-faunal remains and pollen. In addition, an experimental study has been carried out to assess the degree of thermal alteration on hydrogen isotope signatures of different plant organs of *Celtis australis*, a common anthropogenic fuel source at the study sites. Our results reveal the strengths of integrated microscopic and molecular approaches to address archaeological questions, highlight new avenues for future research, and add new levels of detail to our understanding of the regional environmental variability that framed the disappearance of Neanderthal populations in Eastern Iberia.

INVESTIGAR LA MATERIA ORGÁNICA MICROSCÓPICA Y MOLECULAR PARA EXPLORAR EL PAPEL DEL CLIMA EN LA EVOLUCIÓN SOCIAL Y CULTURAL DE LOS NEANDERTALES A ESCALA REGIONAL

RESUMEN

El rol de la variabilidad climática es un tema recurrente en las discusiones que rodean la sustitución de los neandertales por los humanos modernos en toda Europa y Asia occidental. La Península Ibérica se considera un lugar geográfico clave para entender este proceso, debido a la aparente pervivencia de las poblaciones neandertales en las regiones meridionales y occidentales de su territorio. A pesar de ello, se dispone de relativamente pocos registros paleoclimáticos terrestres lo suficientemente amplios para contrastar las hipótesis existentes sobre el rol de factores climáticos y ecológicos. Los análisis de las sondas de hielo de las regiones polares han aportado datos esenciales para construir modelos climáticos globales que abarcan escalas de tiempo geológicas. Los estudios palinológicos regionales de las sondas marinas de las costas atlánticas y mediterráneas son los registros paleoclimáticos pleistocénicos más completos para el estudio del ámbito ibérico. Sin embargo, aún no está claro hasta qué punto estos registros reflejan con exactitud las condiciones terrestres regionales y locales. No se puede descartar la persistencia de condiciones favorables a nivel local durante los periodos de enfriamiento global, y se han llevado a cabo relativamente pocos estudios paleoecológicos específicos de los contextos de ocupación humana correspondientes. Esto supone un reto para entender la dinámica sociedad-clima a largo plazo y durante la transición del Paleolítico Medio al Superior.

El análisis de isótopos específicos de compuestos orgánicos sedimentarios, concretamente de hidrocarburos derivados de ceras de hojas fósiles (*n*-alcanos), ha surgido recientemente como proxy ambiental alternativo que facilita la reconstrucción de las condiciones paleohidrológicas (isótopos de hidrógeno) y paleoecológicas (isótopos de carbono) con una alta resolución espacial y temporal. Esta técnica ha sido aplicada con éxito en una amplia gama de entornos terrestres, pero rara vez se ha utilizado en contextos arqueológicos. En esta tesis, combinamos el análisis de los isótopos de carbono e hidrógeno específicos de los *n*-alcanos sedimentarios con la micromorfología de suelos arqueológicos, técnica fundamental para caracterizar el contexto sedimentario de los compuestos orgánicos objeto de estudio y así detectar cualquier posible sesgo antrópico o natural, como la biodegradación. Aplicamos estas técnicas para investigar las condiciones ambientales en los yacimientos del Paleolítico Medio de Abric del Pastor (MIS 5/4) y El Salt (MIS 3) en Alcoy, Iberia oriental, en combinación con proxis paleoambientales tradicionalmente empleados en estudios arqueológicos: el carbón vegetal, los restos de macro y microvertebrados y el polen. Además, se realizó un estudio experimental para evaluar la influencia de la alteración térmica en las huellas isotópicas de hidrógeno en diferentes partes anatómicas de *Celtis australis*. Nuestros resultados ponen de manifiesto el gran potencial de la aplicación integrada de técnicas microscópicas y moleculares para la reconstrucción paleoambiental y contribuyen un aumento en el grado de detalle de los datos paleoambientales actuales de cara a nuestra comprensión de la variabilidad ambiental regional existente durante el periodo de desaparición de las poblaciones neandertales de Iberia oriental.

Acknowledgements

I am extremely grateful to many people for all the support I have received throughout the course of this research. I owe a great debt of gratitude to my supervisor, **Dr Carolina Mallol**, for her guidance and encouragement over the last four years. Sincere thanks also go to all of the members of PALEOCHAR and AMBI Lab for their constant help and support throughout, as well as for creating an excellent research atmosphere to conduct this work. I must extend a very special thank you in particular to **Dr Antonio V. Herrera-Herrera** for his continual guidance, help getting to grips working with organic biomolecules, and his constant availability for technical support.

Thank you to all of my colleagues and **co-authors** who have contributed their analyses to the case studies included here and helped to teach me the value of truly interdisciplinary and collaborative research. Access to El Salt and Abric del Pastor and a great deal assistance were provided by **Dr Cristo M. Hernández** and **Prof Bertila Galván**. I am also grateful to all of the students and specialists who have dedicated their time and hard work to the excavation campaigns over the years, without which this research would not have been possible.

Thank you to **Dr Glenn Lambrecht** and **Lucia Leierer** for their friendship and fruitful discussions on topics related to the contents of this thesis. Very special thanks are also reserved for **Dr Marion Dowd**, **Dr James Bonsall**, **Sam Moore**, **Chris Read**, **Dr Fiona Beglane,** and **Dr Shirley Markley** at the Institute of Technology Sligo, all of whom have been a great source of encouragement and inspiration throughout the years.

I am deeply grateful to my girlfriend, **Alessia Ronchi**, for her enduring support, encouragement, reassurance, and infinite patience during the work for this thesis. Thank you also to my parents and friends who are always available and willing to help in any way they can.

Finally, this research was supported by the **European Research Council (ERC)**, **Spanish Ministry of Science, Innovation and Universities** and the **Government of Valencia Cultural Heritage Department**, to whom I am very thankful.

Contents

List of Figures

Chapter 3

Chapter 4

Chapter 5

List of Tables

Chapter 3

Chapter 4

Chapter 5

Chapter 1: Introduction

1.1. Neanderthal demise and the Middle to Upper Palaeolithic Transition

The disappearance of Neanderthals approximately 38 kya (Higham et al., 2014) and their subsequent replacement by anatomically modern humans (AMH) coincides with a significant cultural and technological shift in the archaeological record, commonly referred to as the Middle to Upper Palaeolithic transition (MUPT). Despite constituting one of the richest and most well-studied archaeological and palaeontological records in the world, built through more than a century of focused research throughout Europe and western Asia, much debate still surrounds the nature and timing of the major biological and cultural changes that define the MUPT (Roebroeks, 2008; Blockley et al., 2008; Galván et al., 2014; Higham et al., 2014; Hublin, 2015; Greenbaum et al., 2018; Mihailović, 2019).

Neanderthals and AMH diverged from a common ancestor between 550 - 765 kya (Prüfer et al., 2014). At present, the earliest secure dates for Neanderthal remains suggest that the species emerged approximately 400 kya, with a geographic distribution throughout much of Europe and western Asia. Genetic evidence demonstrates that interactions between Neanderthals and AMH, perhaps occurring as early as 100 kya in the region around the Levant, resulted in multiple episodes of genetic introgression and hybridisation (Sankararaman et al., 2014; Kuhlwilm et al., 2016; McCoy et al., 2017; Villanea and Schraiber, 2019; Price, 2020). This corresponds with archaeological and palaeontological evidence which demonstrates some degree of overlap in the geographic range of both Neanderthals and AMH for as much as 15,000 years in the Levant and perhaps a few thousand years in Western Europe (i.e. contemporaneous habitation or coexistence within a region, though not necessarily overlapping or involving a high degree of contact at the local scale) (Shea, 2003; Gravina et al., 2005; Nigst et al., 2014). Archaeologically, the MUPT is expressed as a diachronic and regionally variable succession of distinct stone tool industries (d'Errico et al., 1998; Bocquet-Appel and Demars, 2000; Conard, 2011; Welker et al., 2016; Marín-Arroyo et al., 2018; Nigst, 2019). In Europe, incoming AMH groups, associated with Early Upper Palaeolithic (EUP) industries, arrived by at least 45-43 kya, eventually replacing the Mousterian industries associated with Neanderthals (Hublin, 2015; Roberts and Bricher, 2018). However, the authorship of certain transitional industries which have characteristics similar to both Mousterian and EUP assemblages remain the subject of ongoing debate (Welker et al., 2016; Villa et al., 2018)). There is disagreement as to the extent of the interaction, acculturation and genetic exchange which occurred between Neanderthals and AMH, however, what is clear is that by approximately 38 kya, Neanderthals had disappeared from the European archaeological record and the regions they formerly occupied came to be inhabited by AMH (Higham et al., 2014).

The complex spatiotemporal patterning involved in this process of cultural and biological replacement has led to numerous, often competing, hypotheses being put forward to explain the demographic collapse of Neanderthal populations. These largely fall into two broad categories, though they are not mutually exclusive. The first of these attributes Neanderthal demise to some form of direct or indirect competition with incoming AMH groups. This includes various models of competitive exclusion (Banks et al., 2008; Klein, 2009; Gilpin et al., 2016), dietary differences (Hockett and Haws, 2005; Richards and Trinkaus, 2009), disadvantageous biological or behavioural capacities (Dibble et al., 2018; Goldfield et al., 2018), differences in life history (Trinkaus, 1995, 2011), cognitive inferiority (Mellars and Stringer, 1989; Klein, 2003), and selectively neutral species drift (Kolodny and Feldman, 2017). The second broad category highlights environmental factors, including viral disease (Underdown, 2008; Wolff and Greenwood, 2010) and significant volcanic eruptions (Golovanova et al., 2010; Morley, 2012; Fedele et al., 2016), but primarily focuses on the role of climate change (d'Errico and Sánchez Goñi, 2003; Jiménez-Espejo et al., 2007; Finlayson and Carrión, 2007). It is the latter with which this thesis is concerned.

1.2. Neanderthals and climate in the Iberian Peninsula

Climatic and environmentally deterministic explanations for Neanderthal replacement by AMH have been prominent since at least the 1980s (Leroyer and Leroi-Gourhan, 1983; Leroyer, 1988) and continue to have much traction (Finlayson, 2004; Sepulchre et al., 2007; Burke et al., 2014; Daura et al., 2017; Staubwasser et al., 2018). Global climatic records from a range of proxy sources suggest that the MUPT occurred during the climatically unstable Marine Isotope Stage 3 (MIS 3) and was preceded by a series of relatively abrupt climatic oscillations (Adams et al., 1999; Maslin et al., 2013; Rasmussen et al., 2014; Sánchez Goñi et al., 2008). The transition itself spanned a number of Dansgaard–Oeschger (DO) millennial-scale cold phases between Greenland Interstadial 12 (GI12) and Greenland Interstadial 8 (GI8) (Rasmussen et al., 2014). In addition, evidence of ice-rafted debris (IRD) from North Atlantic marine sediment cores, among other sources, attests to the significance of Heinrich Events (HE) on northern hemisphere climate conditions (Sánchez Goñi et al., 2008). In particular, HE 5 (*c.* 50 - 47 kya) and HE 4 (*c.* 39 kya) have been argued to have played an important role in the replacement of Neanderthals by AMH (Mellars, 2006; Sepulchre et al., 2007; Müller et al., 2011). It has also been argued that Neanderthals, as a mid-latitude species, only expanded their range into more northern parts of Europe during phases of relative climatic amelioration and, consequently, were detrimentally impacted by the severe cold conditions and global climatic deterioration of MIS 4 (71 - 57 kya), a situation then exacerbated by the subsequent climatic instability during MIS 3 (Finlayson, 2004). From this perspective, the Iberian Peninsula has been proposed as a potentially important 'climatic refugium', which could have provided more hospitable conditions during periods of wider climatic and environmental deterioration, perhaps facilitating the late survival of Neanderthal groups in the southern and western regions

(Zilhão and Pettitt, 2006; Finlayson et al., 2007; Jennings et al., 2011; López-García et al., 2014).

Palaeoclimate data from Greenland ice-cores and deep-sea sediments collected off the Atlantic Iberian margin and in the Western Mediterranean Sea constitute the most complete records for reconstructing environmental conditions in the Iberian Peninsula during MIS 4 and MIS 3 (Sánchez Goñi et al., 2008; Rasmussen et al., 2014). It has been suggested that during Heinrich events, mean annual precipitation (MAP) throughout the Peninsula was approximately 400 mm less than present-day values. This coincided with winter temperatures 6 - 13 °C lower. MAP values during temperate climate phases, on the other hand, were between 600 - 800 mm, with winter temperatures similar to conditions today (Cacho et al., 1999; Sánchez Goñi et al., 2008). It is argued that cold climatic phases marked by low MAP values would have likely seen the development of desert-steppe vegetation over large areas, with a dramatic reduction in vegetation cover to less than 25 % of modern values (d'Errico and Sánchez Goñi, 2003; Sepulchre et al., 2007). It is unclear, however, the extent to which reconstructions based on ice-core and deep-sea sediments, or temporally discontinuous terrestrial palynological sequences, reflect conditions across the whole of the Peninsula. Iberia is characterised by a heterogeneous mountainous topography, which when combined with Atlantic and Mediterranean climatic influences, creates local environmental conditions which can vary significantly even across relatively short distances. While additional sources of information, such palynological, palaeobotanical and palaeontological remains recovered from archaeological contexts (López-García et al., 2013; Daura et al., 2017; Ochando et al., 2019; Fernández-García et al., 2020), continue to provide valuable site-specific data, these proxies rely on physical plant and animal remains which may be subject to taphonomic or preservation biases and often do not survive or are unsuitable for the reconstruction of long-term continuous environmental sequences. This represents a considerable drawback for investigating the role of climate in Neanderthal social and cultural evolution. It is important that archaeologists work to improve the spatio-temporal resolution of climatic reconstructions within and across the Peninsula in order to better test competing hypotheses concerning climatic deterioration during MIS 4 and abrupt climate change events, like HE 4 or HE 5, on Neanderthal populations at the local scale. This is essential if archaeologists are to disentangle the complex causal, probable and correlative relationships between coarse trends in environmental and archaeological records (see Coombes and Barber, 2005; Barnes and Dove, 2015; Contreras, 2016; Arponen et al., 2019). To this end, novel palaeoclimate proxies which focus on the microscopic and molecular record preserved in sediments represent a promising avenue of research and are the focus of the present work.

1.3. Objectives

The aim of this thesis is to present a systematic palaeoenvironmental study of two key Iberian Middle Palaeolithic sites, to yield new sources of information for approaching the relationship between Neanderthals and their environments, as well as to provide a solid base for the application of a novel microscopic and molecular approach in archaeological research. Archaeological soil micromorphology is now a well-established method in geoarchaeological studies across the world but has generally focused on aspects of site formation, post-depositional processes and human behaviour (Goldberg and Berna, 2010; Stoops et al., 2010; Nicosia and Stoops, 2017). Although climatic and environmental signatures are discernable at the microstratigraphic scale (Vliet-Lanoë, 2010), the method has rarely been combined in a systematic fashion with other sedimentary climate proxies, particularly those based on molecular and isotopic analyses of organic compounds (e.g. Bush and McInerney, 2013; Zhang et al., 2014; Jambrina-Enríquez et al., 2016; Jordan et al., 2017; Jansen and Wiesenberg, 2017). It is well known that compound-specific $^{2}H/^{1}H$ and $^{13}C/^{12}C$ ratios ($\delta^{2}H_{wax}$ and $\delta^{13}C_{wax}$) in leaf waxes are determined by climatic and environmental controls (Yang and Huang, 2003; Sachse et al., 2006; Sachse et al., 2012; Collins et al., 2013; Diefendorf and Freimuth, 2017; Wu et al., 2018). The integration of archaeological soil micromorphology and isotopic analyses of sedimentary lipid biomarkers offers a new approach to palaeoclimate reconstruction and the potential to link climate and human behaviour at a high scale of spatial and temporal resolution. There are, however, several challenges involved. For instance, the preservation of these compounds in Pleistocene sediments is not always optimal. In addition, lipid molecular climate proxies have almost exclusively been applied in non-archaeological contexts where the potential for anthropogenic alteration of the climatic signal, for instance through burning, is entirely absent or very limited. Owing to a lack of focused research on the topic, the extent of anthropogenic alteration and the applicability of these methods in archaeological contexts is not well understood. Archaeological soil micromorphology, however, in addition to providing an alternative source of climatic and environmental information, offers one avenue for determining anthropogenic or biogenic impact on sediments and thus the integrity and suitability of sedimentary sequences for lipid molecular analyses. Consequently, in this thesis, these methods are applied together for the first time in Pleistocene archaeosedimentary contexts. The objectives are:

i. To explore the suitability of Pleistocene archaeosediments for lipid molecular and compound-specific isotope analysis of fossil leaf waxes (*n*-alkanes) for palaeoclimate reconstruction.

ii. To characterise the palaeoclimatic framework for the Neanderthal occupations recorded in Abric del Pastor (MIS 5/4) and El Salt (MIS 3).

iii. To investigate the complementarity of archaeological soil micromorphology and molecular sedimentary proxies in tandem with traditional palaeoenvironmental proxies used in archaeological research, specifically charcoal, microvertebrates, macro-faunal remains, pollen and non-pollen palynomorphs.

iv. To determine whether the environmental and climatic data from these sites implicate climate change or abrupt climate events in the disappearance of Neanderthals from Eastern Iberia.

1.4. Hypotheses

The specific hypotheses formulated and tested in this thesis are defined at the outset. In each case, a null hypothesis (H_0) will be examined through the evidence presented in this thesis and tested against a competing alternate hypothesis (H_1).

Hypothesis I:

H_0 – Archaeosediments from Middle Palaeolithic sites in Eastern Iberia *do not* preserve a microscopic and molecular record of Pleistocene climate conditions.

H_1 – Archaeosediments from Middle Palaeolithic sites in Eastern Iberia *do* preserve a microscopic and molecular record of Pleistocene climate conditions.

Hypothesis II:

H_0 – Combined microscopic and molecular analyses of sediments at the study sites *do not* allow accurate and precise reconstruction of past climatic and environmental conditions.

H_1 – Combined microscopic and molecular analyses of sediments at the study sites *do* allow accurate and precise reconstruction of past climatic and environmental conditions.

Hypothesis III:

H_0 – Sedimentary microscopic and molecular climate proxies *cannot* be usefully compared with traditional palaeoenvironmental proxies used in archaeological research.

H_1 – Sedimentary microscopic and molecular climate proxies *can* be usefully compared with traditional palaeoenvironmental proxies used in archaeological research.

Hypothesis IV:

H_0 – Sedimentary microscopic and molecular climate proxies *do not* indicate unstable environmental conditions during MIS 3 in Eastern Iberia.

H_1 – Sedimentary microscopic and molecular climate proxies *do* indicate unstable environmental conditions during MIS 3 in Eastern Iberia.

Hypothesis V:

H_0 – There is *no* consistent relationship between climate change or abrupt climate events and Neanderthal activity at the selected study sites.

H_1 – There *is* a consistent relationship between climate change or abrupt climate events and Neanderthal activity at the selected study sites.

1.5. Thesis structure and rationale

This work is set out in 9 chapters. Chapter 2, which follows, outlines the geoarchaeological and methods employed throughout the work. Chapters 3 to 5 outline three focused case studies which have been published or are being prepared for submission (Chapter 3 was published in *Quaternary Science Reviews* (Connolly et al., 2019)). Chapter 3 describes the application of archaeological soil micromorphology and compound-specific isotope analysis of sedimentary *n*-alkanes at the Middle Palaeolithic site of Abric del Pastor (MIS 5/4). Additional environmental proxies, which include anthracology, micro-vertebrate and macro-faunal analysis, are incorporated into this study to provide a further level of detail in selected stratigraphic units. A similar approach is described in chapter 4, where archaeological soil micromorphology and compound-specific isotope analysis of sedimentary *n*-alkanes are deployed together with a palynological study at the site of El Salt (MIS 3). Chapter 5 describes a laboratory-based experiment which investigates the impact of low-temperature combustion on δ^2H_{wax} values of different plant organs of *Celtis australis*. This study aimed to explore potential weaknesses and new applications of this novel sedimentary climate proxy in archaeological contexts. The common element which runs through all three case studies is methodological; in each, microscopic and molecular methods are applied and show the possibilities and results of integrated research, with the overarching goal of garnering new high-resolution palaeoclimate information to establish the environmental context for the demise of Neanderthals in Eastern Iberia. Several common issues and methodological insights emerged from these case studies, and these are summarised and discussed in Chapter 6 in light of the hypotheses set out previously, followed by references in Chapter 7.

Chapter 2: Methodological background

2.1. Archaeological soil micromorphology

Archaeological deposits, or *archaeosediments*, are typically characterised by a complex interplay between geogenic, biogenic and anthropogenic factors. Information obtained at the microstratigraphic scale of observation has been shown to yield valuable insights into the nature and integrity of these deposits, by elucidating site formation processes, landscape development, environmental conditions, on-site human activities, and bioturbation or other post-depositional disturbances (Nicosia and Stoops, 2017). Soil micromorphology is the study of soils or sediments in their intact state using petrographic thin sections and polarising light microscopy. Early studies of sub-macroscopic soil properties first emerged more than a century ago (Delage and Lagatu, 1904; Agafonoff, 1929; Allen, 1930), although it was through the work of Walter Ludwig Konstantin Ritter von Kubiëna, Professor of Geology at the University of Venice, that the technique of soil micromorphology came to be formalised and more widely known (Kubiëna, 1938, 1958; Kubiëna and Ruhe, 1970). Soil micromorphology found widespread application in pedological studies through the course of the twentieth century, however, Cornwall (1958) was the first to promote its use for addressing strictly archaeological research questions. Few archaeologically oriented studies followed in the subsequent decades (Dalrymple, 1958; Romans and Robertson, 1983), however, from the mid-1980s onward the method began to be more widely applied in archaeological contexts, contributing significantly to the emerging sub-discipline of geoarchaeology, principally through the work of geologists, soil scientists and geoarchaeologists (Courty and Fedoroff, 1985; Fedoroff and Courty, 1987; Macphail, 1987; Courty et al., 1989; Macphail et al., 1990). This flurry of research activity led to the standardisation of terminology used in soil micromorphological descriptions, which facilitated the expansion of the technique and it's more widespread uptake in archaeological studies. The first descriptive guidebook to find widespread use was that of Bullock et al. (1985).

This was later updated and largely replaced by Stoops (2003). An International Working Group in Archaeological Soil Micromorphology was formed in 1990, first meeting at Institute of Archaeology, University College, London, and continues to meet on an annual basis at locations throughout the United Kingdom and Europe. This has provided a platform for researchers at various stages in their careers to interact, exchange knowledge about the application of soil micromorphology in a wide variety of geological and sedimentary contexts. This has no doubt contributed to the significant increase in the number of archaeological soil micromorphological studies that have followed in the subsequent three decades since the working group was first convened (Nicosia and Stoops, 2017; Macphail and Goldberg, 2018).

Archaeological soil micromorphology can also be regarded as having contributed and benefited from concurrent developments in the field of archaeological science and the sub-discipline of microarchaeology (Weiner, 2010). Researchers now commonly complement soil micromorphological descriptions with a range of instrumental analytical techniques designed to add new levels of detail and extract additional information to aid in archaeological interpretation. Many of these techniques which focus on inorganic components can be applied directly to thin sections, such as scanning electron microscopy (SEM) (Ward et al., 2019), energy-dispersive and wave-dispersive X-ray spectroscopy (EDS/EDX/WDX) (Shillito et al. 2009), electron microprobe (EMP) (Schaefer et al., 2004), or Fourier transform infrared spectroscopy (micro-FTIR) (Haaland et al., 2017).

2.1.1. Site formation processes and palaeoenvironments at the microscopic scale

Site-formation processes refer to the combination of factors that ultimately compose the archaeological record. An accurate reconstruction of site formation processes, including the depositional environment and the nature and degree of post-depositional alterations or disturbances, is crucial for understanding the spatial integrity of archaeological materials within site and, hence, for allowing archaeologists to develop robust interpretations (Goldberg and Macphail, 2008). Formation theory in archaeology came to the fore through the seminal work of M.B. Schiffer and the publication of his book *Formation Processes of the Archaeological Record* (Schiffer, 1987). This came on the back of Butzer's *Archaeology as Human Ecology: Method and Theory for a Contextual Approach* (Butzer, 1982), which marked a growing concern with the sedimentary contexts of archaeological sites. It also emerged in an atmosphere of much debate about how archaeologists ought to define and understand archaeological deposits (Schiffer, 1972; Binford, 1983). Schiffer roundly rejected the assumption that past human activities define the spatial patterning of excavated archaeological materials, an idea which had widespread acceptance among many of his contemporaries (Binford, 1964; McPherron, 1967; Brose, 1970). Schiffer instead argued that reliable human behavioural inference relies on a clear understanding of the archaeological context and suggested that the transformations which affect the archaeological record can broadly be grouped into two categories: those related to anthropogenic activity which he labelled *C-transforms*; and those related to geogenic or otherwise environmental processes which he labelled *N-transforms*. While much work in site formation processes throughout the 1980s and 1990s was developed in ethnoarchaeological case studies, the emphasis of formation theory on deposits, as opposed to strictly investigating artefactual assemblages, naturally aligned with the focus and emerging methodological innovations of geoarchaeological studies, in particular soil micromorphology (Goldberg, 1979; Goldberg, 1980; Fedoroff and Goldberg, 1982; Courty et al., 1989; Wattez et al., 1990; Weiner et al., 1995; Simpson and Barrett, 1996). Conceptually, it came to be recognised that sedimentary deposits in archaeological contexts are in themselves artefacts of past human activities, which can be modified and transformed through processes such as trampling, sweeping, burning, or the deliberate importation of exogenous materials for flooring or bedding (Miller et al., 2013). Deposits may also be greatly altered by soil formation (pedogenesis) or chemical diagenesis, for instance through the deposition of bird or bat guano (Karkanas and Goldberg, 2018). In the subsequent two decades, the efficacy of soil micromorphology for elucidating complex site formation processes in a wide range of environments has been well established (Karkanas et al., 2000; Mallol et al., 2009; Mallol et al., 2010; Friesem et al., 2014; Morley et al., 2017; Stahlschmidt et al., 2018; Angelucci et al., 2019; McAdams et al., 2019; Patania et al., 2019; Ward et al., 2019).

A key component for understanding depositional dynamics and site formation is the reconstruction of the local and regional environmental context and how this might have fluctuated in the time since the deposit was formed. Geoarchaeological studies have long emphasised the importance of palaeoenvironmental reconstruction (Laville, 1976; Lynch, 1986; Schuldenrein, 1986). Observation of sediments at the microstratigraphic scale can yield vital clues about local and regional environmental conditions, and palaeoenvironmental data is implicit in most soil micromorphological studies (Courty and Vallverdu, 2001; Stephens et al., 2005; Vallverdú-Poch and Courty, 2012). Soil micromorphology is well suited to the identification of diagnostic horizons and properties indicative of frost action in cold or periglacial climate conditions (Vliet-Lanoë, 2010; Krajcarz and Krajcarz, 2019; Nieuwendam et al., 2020), or past periods of aridity which can be indicated by the presence of gypsic pedofeatures, pseudomorphic voids or calcite pseudomorphs (Lebedeva-Verba and Gerasimova, 2009; Poch et al., 2018). The presence of specific microstructures, fabrics, or post-depositional features linked to wet or waterlogged environments has also been reported (Sedov et al., 2008; Mallol et al., 2009), as well as characteristic pedofeatures related to repeated cycles of wetting and drying, which induce swelling and shrinking of the matrix and deformation of pores (Pires et al., 2008; Stahlschmidt et al., 2018). Environmental and climatic information inferred from micromorphological observations provides a robust qualitative source of data to complement other proxies. One distinct advantage of the soil micromorphological approach is the ability to establish and link contextualised environmental data to specific microfacies, allowing archaeologists to estimate the timing, duration and overall magnitude of climatic processes at the highest possible scale of resolution and construct a robust framework for investigating human-environmental interactions through time.

Several key observations arising from soil micromorphological analyses, such as the rate of sedimentation, mode of deposition, post-depositional disturbances or chemical alteration, have the potential to greatly influence the results of other sedimentary climate proxies, including lipid biomarker characterisation and CSIA. In this thesis, we present the first attempts to deploy these methods in a single integrated workflow, as a step towards providing high-resolution onsite palaeoclimate data against which archaeological records can be compared.

2.2. Lipid biomarkers and *n*-alkane biosynthesis in plants

The term *biomarker*, or biological marker, is used to describe any organic compound which can be traced to a specific biological source (Eglinton et al., 1964; Evershed, 1993). The term can be applied to a wide variety of biomolecules, although lipids have received the most attention in archaeological and palaeoecological research (Evershed et al., 1999). Peters et al. (2005) identify three key features which distinguish lipid biomarkers from most other organic compounds:

I. Structures characterised by repeating subunits which indicate precursors were present in formerly living biological organisms.
II. The parent biomarkers are common to specific biological organisms, normally organisms which occur frequently and are widely distributed.
III. Upon burial, the main structural characteristics which identify the compound remain chemically stable.

Hydrocarbons are among the simpler functional classes of lipid biomarkers, and biogenic hydrocarbons are produced in a number of biotic sources (Peters et al., 2005). For instance, saturated aliphatic hydrocarbons, or *n*-alkanes, are widely distributed in nature. Cyanobacteria and algae are known to produce short-chain (low molecular weight; LMW) branched and unbranched alkanes (typically C_{15} - C_{19}), mid-chain (medium molecular weight; MMW) alkanes are more typical of aquatic macrophytes and bryophytes (C_{21} - C_{25}) (Cranwell et al., 1987; Ficken et al., 2000; Klavina and Kviesis, 2015), while long-chain (high molecular weight; HMW) alkanes are linked with insect cuticular lipids and more commonly plant epicuticular leaf waxes (C_{27} to C_{35}) (Eglinton et al., 1962; Gibbs and Pomonis, 1995; Blomquist et al., 2019).

A plant cuticle can be described as a fine waxy lipophilic film which coats the epidermal surfaces of most leaves, as well as other plant organs such as non-woody stems and flowers (Post-Beittenmiller, 1996). Cuticular leaf waxes play a critical role in moderating functions which are essential for plant survival, these include the restriction of non-stomatal water loss linked to biotic and abiotic stresses, as well as protecting against adverse effects produced by exposure to ultraviolet radiation (Reicosky and Hanover, 1978; Barnes et al., 1994; Riederer and Schreiber, 2001; Cheng et al., 2019). These waxes may also play a role in protecting plants against fungal or bacterial pathogens (Jenks et al., 1994).

Plants biosynthesise the *n*-alkane component of cuticular leaf waxes from precursor saturated very long-chain fatty acids (VLCFA). Most cuticular leaf wax components are derived from VLCFA chains that are 20 to 32 carbons in length (Post-Beittenmiller, 1996). The reactions involved in leaf wax biosynthesis are localised in the epidermal cells (Kolattukudy, 1968; Kunst and Samuels, 2003; Tinto et al., 2017). Initially, de novo fatty acids $C_{16:0}$ and $C_{18:0}$ are synthesised in plastids, membrane-bound organelles located in the cells of plants, through a series of consecutive enzymatic steps produced by soluble enzymes which form the fatty acid synthase complex (FAS) (Ohlrogge et al., 1993; Jaworski et al., 1994). Four basic reactions take place, condensation, reduction, dehydration, and another reduction, which produce a two-carbon elongation of the acyl chain (Post-Beittenmiller, 1996). A series of elongation steps linked to microsomal enzymes subsequently follow which extend the $C_{16:0}$ and $C_{18:0}$ fatty acids producing VLCFA chains in a process which is catalysed by membrane-associated multienzyme complexes referred to as fatty acid elongases (FAE). These reactions are analogous to those involved in the synthesis of de novo fatty acids (von Wettstein-Knowles, 1982). These VLCFA chains are required to synthesise the cuticular wax lipids, and multiple rounds of elongation are necessary to produce the requisite acyl chain lengths. Chain length specificity is governed by interactions between different elongases, though the precise metabolic roles played by specific elongase condensing enzymes is not well understood (Kunst and Samuels, 2003; Tinto et al., 2017). In the vast majority of plant species, wax biosynthesis occurs through two major pathways: an acyl reduction pathway which produces primary alcohols and wax esters, and a decarbonylation pathway which produces aldehydes, alkanes, secondary alcohols and ketones. In many plants, the fatty acid elongation reactions are shared between both the acyl reduction pathway and the decarbonylation pathway, which thus differ only in terms of the enzymes acting on the VLCFA chains and their derivatives (Post-Beittenmiller, 1996).

For the production of *n*-alkanes through the decarbonylation pathway, aldehydes are first produced by a membrane-bound fatty acyl-CoA reductase acting on VLCFA precursors. These aldehydes are subsequently decarbonylated to odd-chain alkanes (C_nH_{2n+2}), with one less carbon atom compared to its fatty acid precursor, in a reaction which is catalysed by an aldehyde decarbonylase (Post-Beittenmiller, 1996; Kunst and Samuels, 2003; Tinto et al., 2017).

2.2.1. Sedimentary n-alkanes in palaeoenvironmental research

Sedimentary *n*-alkanes derived from leaf waxes have emerged in recent years as a robust proxy in palaeoclimatological and palaeoecological research (e.g. Bush and McInerney, 2013; Zhang et al., 2014; Jambrina-Enríquez et al., 2016; Jordan et al., 2017; Jansen and Wiesenberg, 2017). These compounds have particularly high research value in these fields due to their hydrophobic properties and strong resistance to post-depositional degradation. In suitable depositional contexts, *n*-alkanes can preserve over geological timescales (Eglinton et al., 1964; Eglinton and Hamilton, 1967; Cranwell, 1981). Researchers employ a suite of *n*-alkane-specific molecular ratios as proxies for inferring palaeoenvironmental information, including biogenic source (e.g. terrestrial versus aquatic plants), alteration (e.g. microbial reworking) or overprint of organic matter (e.g. through root contribution) (Jansen and Wiesenberg, 2017). The most common molecular ratios for palaeoenvironmental reconstruction are the Carbon Preference Index (CPI) (Bray and Evans, 1961) and the Average Chain Length (ACL) (Poynter et al., 1989; Freeman and Pancost, 2013).

Compound-specific isotope analysis (CSIA), which differs from the bulk isotope analysis more commonly employed in archaeological research by targeting individual compounds, allows researchers to trace the carbon and hydrogen sources of specific lipid biomarkers, adding new layers of information about palaeoclimate and palaeovegetation (Hayes et al., 1990; Burgoyne and Hayes, 1998; Hilkert et al., 1999). The carbon isotopic ratio ($^{13}C/^{12}C$; $\delta^{13}C_{wax}$) of cuticular leaf waxes have been shown to be a sensitive record of perturbations in the carbon cycle, local vegetation dynamics, and climate (Diefendorf et al., 2011; Magill et al., 2013; Diefendorf and Freimuth, 2017), while the stable isotopic ratio of deuterium and hydrogen (D/H; $\delta^{2}H_{wax}$) can record fluctuations in precipitation and the hydrological cycle (Sachse et al., 2006; Sachse et al., 2012). An increasing number of studies in recent years have demonstrated that when appropriate consideration is afforded to the various biological and climatological variables which influence isotopic fractionation in wax lipids, these proxies can be effectively deployed for high-resolution palaeoclimate and palaeoenvironmental reconstructions (Yang and Huang, 2003; Bi et al., 2005; Sachse et al., 2006; Liu and Yang, 2008; Collins et al., 2013; Ladd and Sachs, 2013; Garcin et al., 2014; Gamarra et al., 2016; Wu et al., 2018). Variables may include factors such as vegetation type, evapotranspiration, salinity, aridity, seasonality or temperature (Sachse et al., 2012; Diefendorf and Freimuth, 2017; Liu and An, 2018; Magill et al., 2019). To date, however, few studies have provided robust contextual descriptions of the sedimentary environments sampled for leaf waxes, omitting significant information about depositional and post-depositional processes and potentially hampering interpretations of the molecular data. Bioturbation processes related to soil micro and meso-fauna, often not visible at the macroscopic scale of observation, may significantly disrupt the stratigraphic integrity of the sedimentary sequence. In addition, common anthropogenic activities, such as burning, can potentially alter *n*-alkane molecular ratios and isotopic values. Before these proxies can be reliably applied in archaeological settings, it is critical that the integrity and suitability of the depositional environment are established. We suggest that archaeological soil micromorphology, a well-established method for approaching site formation processes and sedimentary dynamics at the highest possible spatial and temporal resolution, is uniquely well-suited for this task. Observations at the microstratigraphic scale also offer an additional source of environmental and climatic information to complement the molecular data (Courty, 2001; Courty and Vallverdu, 2001; Mallol et al., 2009; Mallol et al., 2010; Stoops et al., 2010; Nicosia and Stoops, 2017).

Chapter 3: A multiproxy record of palaeoenvironmental conditions at the Middle Palaeolithic site of Abric del Pastor (Eastern Iberia)

Rory Connolly [1, 2], Margarita Jambrina-Enríquez [1], Antonio V. Herrera-Herrera [1], Paloma Vidal-Matutano [3, 4], Ana Fagoaga [5, 6], Rafael Marquina-Blasco [5, 6], María Dolores Marin-Monfort [7], Francisco Javier Ruiz-Sánchez [5, 6, 8], César Laplana [9], Salvador Bailon [10, 11], Leopoldo Pérez [12, 13], Lucia Leierer [1, 2], Cristo M. Hernández [2], Bertila Galván [2], Carolina Mallol [1, 2]

1. Instituto Universitario de Bio-Organica Antonio Gonzalez (IUBO), Universidad de La Laguna, 38206, Canary Islands, Spain. rconnoll@ull.es; mjambrin@ull.edu.es; avherrer@ull.edu.es; lleierer@ull.es; cmallol@ull.edu.es
2. Departmento de Geografia e Historia, Universidad de La Laguna, 38200, Canary Islands, Spain. chergomw@gmail.com; bgalvan@ull.es
3. TARHA Research Group, Department of Historical Sciences, Universidad de Las Palmas de Gran Canaria, 35003, Canary Islands, Spain. paloma.vidal@ulpgc.es
4. Université Côte-d'Azur, CEPAM, CNRS, France.
5. Grup d'Investigació en Paleontologia de Vertebrats Cenozoics (PVC-GIUV), Àrea de Paleontologia, Universitat de València, Dr. Moliner, 50, CP 46100, València, Spain. ana.fagoaga@uv.es; rafael.marquina@uv.es; francisco.ruiz@uv.es
6. Museu València d'Història Natural, L'Hort de Feliu, P.O. Box 8460 Alginet, València, 46018, Spain.
7. Museo Nacional de Ciencias Naturales (CSIC), José Gutiérrez Abascal 2, 28006, Madrid, Spain. dores@mncn.csic.es
8. Universidad Estatal Península de Santa Elena, INCYT-UPSE, 7047, Santa Elena, Ecuador.
9. Museo Arqueológico Regional de la Comunidad de Madrid, Pza. Bernardas s/n, 28801, Alcalá de Henares, Spain. cesar.laplana@gmail.com
10. Histoire naturelle de l'Homme préhistorique», UMR 7194, Sorbonne universités, MNHN, CNRS, 1, rue René-Panhard, 75013 Paris, France. salvador.bailon@mnhn.fr
11. Archéozoologie, archéobotanique: sociétés, pratiques, environnements», UMR 7209, Sorbonne universités, MNHN, CNRS, 55, rue Buffon, CP 55, 2175005 Paris, France.
12. Institut Català de Paleoecologia Humana i Evolució Social (IPHES), Zona Educacional 4. Campus Sescelades URV (Edifici W3), 43007 Tarragona, Spain. ljperez@iphes.cat
13. Universitat Rovira i Virgili (URV), Área de Prehistoria, Avinguda de Catalunya, 35, 43002 Tarragona, Spain.

Abstract

This paper presents a multiproxy palaeoenvironmental study from Abric del Pastor (Alcoy, Spain), a rock shelter which has yielded evidence for Middle Palaeolithic human occupation. The sedimentary sequence has been analysed for lipid biomarker *n*-alkane abundances (ACL, CPI), compound-specific leaf wax δ^2H and δ^{13}C, and bulk organic geochemistry (TOC, %N, %S), providing a record of past climate and local vegetation dynamics. Site formation processes have been reconstructed through the application of soil micromorphology. Analyses

of anthracological, microvertebrate and macrofaunal assemblages from selected subunits are also presented here. Our data indicates that a variable climate marked by predominantly cold conditions persisted through most of the sequence and that Neanderthal occupations in stratigraphic unit IVd, assigned to MIS 4 or late MIS 5, occurred in a landscape setting characterised by a mosaic of biotopes. The presence of key resources inside the ravine where the site is located suggests that the occupation of the rock shelter may have been strategically motivated by a subsistence and mobility strategy which focused on zones of localised ecological resilience, such as intra-mountainous valleys or ravines, during periods of global or regional environmental downturn.

3.1. Introduction

Abric del Pastor, Alcoy, Spain (Fig. 3.1) hosts a sequence containing Upper Pleistocene deposits overlain by reworked Holocene sediments. The site has yielded evidence for multiple short-term Neanderthal occupation events (Machado et al., 2013). Archaeological remains recovered from the site include lithic artefacts (Galván Santos et al., 2007; Hernández et al., 2010; Machado et al., 2013), charcoal (Vidal-Matutano et al., 2015, 2017) and faunal remains (Sanchis et al., 2015; Pérez et al., 2017). In addition, at least 17 combustion features have been identified throughout the sequence. Ongoing excavations have produced a sedimentary sequence which has been divided into six primary lithostratigraphic units (S.U. I - VI), with further subdivisions therein. The current chronological framework is based on ESR dates obtained from animal teeth recovered in S.U. IVb (48 kya ± 5000 1σ) and S.U. VI (62 kya ± 12,000 1σ), as well as an OSL date from a quartz grain recovered in S.U. IVd (63 kya ± 5000 1σ) (Mallol et al., 2019) (Fig. 3.2) (further information on the methods used for dating is provided in Appendix 1 Table 1 and 2). Taking into consideration the error ranges, these dates frame the sequence at Abric del Pastor between 43 kya and 72 kya, covering the whole of MIS 4 and potentially extending into late MIS 5 and/or early MIS 3. Although the current dates are stratigraphically coherent, additional samples are required to corroborate the site chronology. With this in mind, our aim here is to provide independent climatic and environmental data, recovered from deposits containing direct evidence for human occupations, against which future hypotheses concerning the chronology of the site and Neanderthal responses to climate change can be further tested.

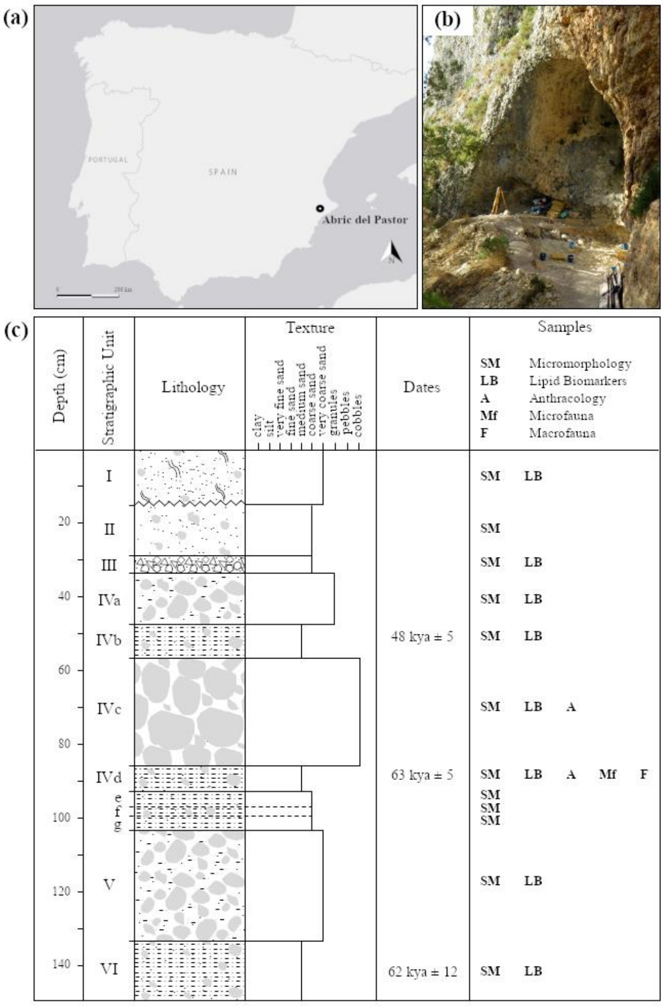

Figure 3.1 Location of site (a), drone image of the rock shelter (b) and stratigraphic log showing the sampling locations for the different proxies used in the current study (c). Dates are reported at the one sigma (1σ) confidence level.

The Iberian Peninsula is widely regarded as crucial for understanding how Neanderthals responded to fluctuations in environmental conditions (Jiménez-Espejo et al., 2007; Wood et al., 2013; Marín-Arroyo et al., 2018), and the prospect of an MIS 4 setting for the occupations recorded in S.U. IVd warrants consideration, as the palaeoenvironmental record for this marine isotope stage in the Iberian Peninsula remains poorly resolved in comparison to MIS 5 (e.g. Blain et al., 2014; Torres et al., 2015; Daura et al., 2015; Ochando et al., 2019) or MIS 3 (e.g. d'Errico and Sánchez Goñi, 2003; Blain et al., 2013; López-García et al., 2014; Sánchez-Hernández et al., 2014; Alcaraz-Castaño et al., 2017; Daura et al., 2017). There is a paucity of long-term continuous terrestrial sequences and site-specific records for the peninsula, although off-shore marine records suggest that rapid global climatic cooling and a significant decrease in sea-surface temperatures (SST) may have driven the development of semi-desert vegetation (Sánchez Goñi et al., 1999; Sánchez Goñi and d'Errico, 2005). The peninsula, owing to its latitudinal range, its diverse topography and the climatic influence of the Atlantic Ocean and Mediterranean Sea, is characterised by considerable climatic diversity in which local environmental conditions change abruptly over relatively short distances (Rivas-Martínez, 1987; López-García et al., 2013). In this context, localised zones of ecological resilience (Holling, 1973; Gunderson, 2000), or vegetation refugia, may have provided conditions favourable to human occupation and subsistence during periods of global climatic deterioration.

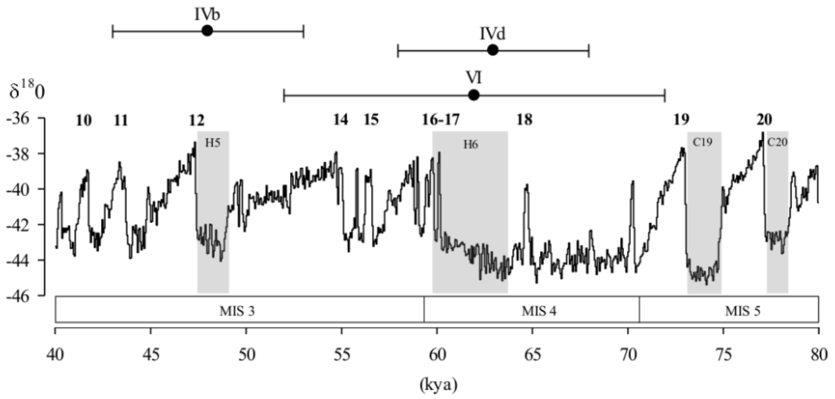

Figure 3.2 Comparing the site chronology from Abric del Pastor (S.U. IVc, IVd and S.U. VI, error bars report the one sigma (1σ) confidence level) with δ18O record of the NGRIP ice core (North Greenland Ice Core Project members, 2004). ESR (IVb and VI) and OSL (IVd).

New evidence and site-specific environmental records are required to improve our understanding of the role which climate may have played in Neanderthal social and cultural evolution. From this perspective, we investigate carbon and hydrogen isotope values of individual lipid biomarkers (*n*-alkanes) to gain insight into hydroclimatic and vegetation dynamics through the stratigraphic sequence at Abric del Pastor (S.U. I – VI; 110cm). These proxies are now widely used for palaeohydrological and palaeoecological reconstructions (Bi et al., 2005; Sachse et al., 2012; Collins et al., 2013, 2017; Diefendorf and Freimuth, 2017; Jordan et al., 2017; Norström et al., 2018; Wu et al., 2018). Sedimentary *n*-alkanes are saturated aliphatic hydrocarbons derived from the epicuticular leaf waxes of vascular plants. Plants usually produce *n*-alkanes with a range of different chain lengths and an odd-over-even predominance (Eglinton et al., 1962; Eglinton and Hamilton, 1967). These compounds have been shown to preserve well in sediments and yield valuable information about their biological source, making them well suited for palaeo-ecosystem reconstructions. Compound-specific $\delta^{13}C$ and $\delta^{2}H$ of individual *n*-alkanes, which record both ecologic (carbon isotope) and hydrologic (hydrogen isotope) information, are also increasingly being utilised in terrestrial palaeoenvironmental research (Yang and Huang, 2003; Collins et al., 2013, 2017; Jambrina-Enríquez et al., 2016; Uno et al., 2016; Wang et al., 2016; Wu et al., 2018). Different processes govern the carbon and hydrogen isotopic compositions of leaf waxes, thus revealing different information about past environmental conditions.

Among other factors, $\delta^{13}C_{wax}$ values are influenced by the ratio between ^{12}C and ^{13}C in the atmosphere ($\delta^{13}C_{atm}$) and isotopic discrimination during photosynthetic carbon fixation ($\triangle\delta^{13}C$). Studies have demonstrated that differences in ^{13}C fractionation among C3 and C4 plants are recorded by leaf wax $\delta^{13}C$ values, making it possible to discriminate between these vegetation types. Other factors such as water availability, taxa, light intensity, nutrient status and canopy effects also influence $\delta^{13}C_{wax}$ values, to various extents (Diefendorf et al., 2010; Kohn 2010; Diefendorf and Freimuth, 2017). $\delta^{2}H_{wax}$ values are determined by the relative abundance of hydrogen (H) and deuterium (D) in the source water used by plants during leaf wax synthesis (Sachse et al., 2012). As leaf water ultimately derives from precipitation, compound-specific isotope analysis of sedimentary *n*-alkanes can yield useful information about the hydrogen isotopic composition of past precipitation ($\delta^{2}H_{p}$). $\delta^{2}H$ values of mean annual precipitation (MAP) have been shown in certain cases to correlate positively with $\delta^{2}H_{wax}$ values (Sachse et al., 2012). The hydrogen isotopic composition of leaf waxes is also, however, influenced by other factors. Liu and An (2018) identify precipitation $\delta^{2}H$, plant type and evapotranspiration as primary controls over $\delta^{2}H_{wax,}$ while additional factors such as aridity, seasonality, temperature and relative humidity can act as second level or third level controls.

Here, we aim to frame our biomolecular data within a broad reconstruction of site formation processes, which are investigated through the application of soil micromorphology. This approach also offers the opportunity to identify features or processes at the microstratigraphic scale which may be indicative of certain environmental conditions (Courty 2001; Courty and

Vallverdu, 2001; Nicosia and Stoops 2017). We also include analyses of anthracological, microvertebrate and macrofaunal assemblages from subunit S.U. IVd. We focus our analyses on S.U. IVd as OSL dating implies a possible MIS 4 setting for the Neanderthal occupations recorded in this subunit.

3.2. Regional setting and site background

3.2.1. Abric del Pastor

Abric del Pastor is a rock shelter situated 820 m a.s.l on a north facing slope of the Barranc del Cinc ravine in the Mariola mountain range, Alcoy, south-eastern Spain. The site is located approximately 30 km from the modern coastline, encompassing an area of *c.* 60 m^2 and occurs in a geological context characterised by Miocene Tortonian formations composed of bioclastic calcirudites. The shelter is adjacent to the Serpis river and was formed through phreatic erosional processes acting on a karstic paleotube. Processes of chemical dissolution and mechanical weathering, for instance through repeated freeze-thaw cycles during climatic cooling episodes, appear to be the primary agents driving the sedimentation at the site through the disintegration of autochthonous limestone.

Mario Brotons led the first excavations at Abric del Pastor in 1953. This work focused on the central area of the modern excavation surface. A considerable number of faunal remains and lithic artefacts were recovered (for instance >2400 lithics), however, poor record keeping has rendered these materials devoid of any reliable contextual information. Brotons' excavations affected only a small area and the uppermost layers of the archaeological deposits (S.U. I, II, III), leaving most of the site intact (Galvan et al., 2007; Molina et al., 2010). Current excavations, directed by the Universidad de La Laguna, Tenerife, are ongoing since 2005.

3.2.2. Sedimentary sequence

S.U. I (13 - 65 cm thickness) is formed by episodic Holocene sedimentation. This unit is composed of heavily bioturbated and reworked humic topsoil yielding Middle Palaeolithic industries alongside diagnostic Neolithic pottery fragments and other modern anthropogenic debris.

S.U. II (08 - 13 cm thickness) is an isolated pocket of matrix-supported dark brown sandy gravelly sediment truncated by S.U. I at the NW corner of the excavation area. Components include faunal remains and a single combustion feature.

S.U. III (03 - 12 cm thickness) is a thin, locally discontinuous, partially cemented carbonate crust composed of calcareous sand and fine to medium gravel. This unit has yielded few archaeological remains.

S.U. IV (55 - 72 cm thickness) is composed of laterally discontinuous, clast-supported, limestone cobble beds (subunits IVa, IVe and IVg) interspersed by loosely compacted, matrix-supported, fine-grained, calcareous sandy-gravelly deposits with frequent limestone cobbles (subunits IVb, IVd and IVf). Subunit IVc, which extends across the whole excavation surface, comprises boulders and large angular cobbles with very little fine material, resulting from one or more significant roof collapse events. S.U. IV has yielded abundant archaeological material including lithics, faunal remains, combustion features and charcoal. Previous archaeostratigraphic analyses of the lithic record incorporating Raw Material Units (RMU's) and refits has identified between 4 and 6 short-term Neanderthal occupation episodes within subunits IVa, IVb and IVc alone (Machado et al., 2013).

S.U. V (15 - 25 cm thickness) is notable for a concentration of large boulders in the SW part of the excavation surface, representing a partial collapse of the shelter roof. The bulk of the deposit is composed of loosely compacted, matrix-supported, fine-grained calcareous sand with fine to medium gravel.

S.U. VI (indeterminate thickness) is composed of moderately compacted sandy-silty sediment with a relatively low proportion of small and medium gravel. Despite excavation of this unit having so far been limited to the 4 m^2 sondage situated at the back of the rock shelter (Appendix 1 Figure 1), a dense concentration of combustion residues, lithics and faunal remains have been recorded.

3.3. Material and methods

Bulk sediment samples representing S.U.'s I, III, IV, V and VI were collected in vertical sequence from the north profile (A7[1], Z7[2], see Appendix 1 Figure 1). S.U. II has not been analysed for lipid biomarkers or lipid biomarkers because this is a discreet unit only present in a small pocket at the NW corner of the excavation surface. All samples were collected using stainless steel spatulas washed with MeOH and dichloromethane (DCM), using Al foil to avoid phthalate contamination from plastic bags. Samples were then stored at -20 °C and subsequently sub-sampled for lipid biomarker analyses and organic geochemistry.

3.3.1. Total Organic Carbon (TOC), % Sulphur (%S), % Nitrogen (%N)

TOC (%) and %S was analysed with a LECO SC 144DR furnace. Measurement accuracy is 1% RSD *or* ± 25 ppm for carbon (RMS 0.053648) and 1% RSD *or* ± 2.5 ppm for sulphur (RMS 0.044829). %N was measured using a VARIO MAX CN elemental analyser. The standard deviation is <0.3% and the rate of recovery >99.5%. Analyses were carried out at the Instituto Pirenaico de Ecología (IPE-CSIC), Spain.

3.3.2. Extraction and analysis of n-alkanes

Extraction and analyses of lipids as well as subsequent isotopic analyses of all samples were carried out at the Archaeological Micromorphology and Biomarkers Laboratory (AMBI), Universidad de La Laguna, Tenerife. 20g sediment samples were dried at 60 °C for 48 hours and subsequently ground and homogenised using an agate pestle and mortar cleaned with MeOH and dichloromethane (DCM). All non-volumetric glassware used for lipid extraction were thoroughly cleaned, solvent washed with MeOH and calcined at 450 °C for 10 hours prior to extraction to eliminate potential contaminants. Lipids from 20g sediment samples were extracted in 150mL dichloromethane/methanol (DCM:MeOH 9:1) by ultrasonic extraction (three cycles of 30 minutes) and centrifugation (three cycles at 4700rpm). The total lipid extract (TLE) was then concentrated under a steady flow of N_2 gas at 40 °C in a rotary evaporator. The TLE was subsequently reconstituted using DCM and separated into fractions of differing polarity by solid phase extraction (SPE) through a silica gel column (1g silica, 70-230 mesh and 0.1g sand 50-70 mesh, both previously calcined at 450 °C for 10 hours).

Here we present results of fraction 1 (F1: *n*-alkanes), which was eluted with $^{3}/_{8}$ of dead volume (DV) in *n*-hexane. F1 was subsequently concentrated under a steady stream of N_2 gas at 40 °C in an Organomation rotary evaporator and stored at -20 °C. Prior to measurement, 3µL of internal standard (IS) 5α-androstane 8mg/L was added and the volume was completed with 150 µL of DCM. F1 was analysed by gas chromatography with a coupled mass-selective detector (GC-Agilent 7890B, MSD Agilent 5977A) equipped with a HP-5MS capillary column (30m, ID: 250 µm, film thickness 0.25 µm). A temperature program was applied with an initial temperature of 70 °C for 2 min and a heating rate of 12 °C/min to 140 °C, and a final temperature of 320 °C with a heating rate of 3 °C/min for 3 min, using a Helium carrier gas

(2mL/min). The PVT injector was held at a split ratio of 5:1 at an initial temperature of 70 °C for 0.85 min and heated to 300 °C at a programmed rate of 720 °C/min.

Compounds were identified by comparison of their retention times and mass spectra to those of reference compounds (mix C_8-C_{40} and 5α-androstane, Supelco) and mass spectral library databases (NIST). Analytes were quantified using calibration curves obtained by plotting the ratio Area/Area$_{IS}$ *versus* the concentration of each reference compound, with correlation coefficients higher than 0.995. The *n*-alkane concentration is expressed as µg of individual compound per gram of dry sample (µg gds^{-1}). Error ranges for individual *n*-alkanes are reported as standard deviation (Appendix 1 Table 3).

To evaluate the distribution of *n*-alkanes we used the average carbon length (ACL) and Carbon Preference Index (CPI). Indices such as ACL and CPI yield important information on the potential sources of sedimentary OM. ACL values, which are broadly structured by phylogenetic relationships, reflect changes in vegetation structure through a sedimentary sequence. Temperature and hydrological controls, however, also play a role in determining ACL values within individual plant communities (Sachse et al., 2006; Diefendorf et al., 2015a). CPI values are related to the odd-over-even predominance (OEP) of *n*-alkanes, where values >5 have typically been associated with epicuticular wax of higher plants and lower values ~1 with bacteria or algae (Cranwell et al., 1987). CPI has also been employed as an indicator of *n*-alkane degradation in sediments, where low temperatures and dry conditions correspond to low diagenetic rates resulting in increased CPI values, and increased temperatures with more humid conditions correspond to higher diagenetic rates and lower CPI values (Kuder and Kruge, 1998; Xie et al., 2004; Ortiz et al., 2010). CPI values vary considerably within and amongst different plant species, however, so a cautious approach should be taken to the use of CPI as a quantitative indicator of *n*-alkane degradation (Bush and McInerney, 2013). CPI values can also be affected by thermal degradation through the incorporation of charred biomass (Eckmeier and Wiesenberg, 2009; Wiesenberg et al., 2009; Diefendorf et al., 2015b; Wang et al., 2017). As such, these values are best interpreted in conjunction with other proxies.

The ACL metric, originally defined by Poynter et al. (1989), was calculated here following the recommendations of Freeman and Pancost (2014) using the C_{18} - C_{35} interval:

$$ACL_{18\text{-}35} = \Sigma(Ci \times [Ci]) / \Sigma[Ci];\ 18 \leq i \leq 35$$

The CPI value (C_{18} to C_{35}) was calculated following the equation set out in Bray and Evans (1961):

$$CPI_{18\text{–}35} = [(\Sigma C_{19\text{–}35odd}/\Sigma C_{18\text{–}34even}) + (\Sigma C_{19\text{-}35odd}/\Sigma C_{20\text{–}36even})] \times 0.5$$

3.3.3. Gas Chromatography – isotope ratio MS (GC-IRMS)

Carbon and hydrogen isotope analysis of individual *n*-alkanes was carried out using a Thermo Scientific Isotope Ratio Mass Spectrometer Delta V Advantage coupled to a GC Trace1310 through a Conflo IV interface with a temperature converter GC Isolink II. The GC was fitted with a Trace Gold 5-MS (Thermo Scientific) fused silica capillary column ((5%-diphenyl)-dimethylpolysiloxane, 30 m length x 0.25 mm i.d., 0.25 μm film thickness). Helium was used as the carrier gas at a flow rate set at 1.5 mL/min. All measurements were repeated three times. Data acquisition and processing were carried out using the Isodat 3.0 software (Thermo Scientific).

Carbon and hydrogen isotope values are reported for *n*-alkanes C_{29} and C_{31} because these compounds were consistently present in sufficient concentrations for isotopic analyses. Samples were injected by means of a Programmed Temperature Vaporising injector (PTV) in splitless mode, with the temperature increasing from 60 °C to 79 °C (held 30 s, rate 10 °C/min), then to 325 ºC (held 3 min) at a rate 10 ºC/s and finally to 350 ºC (held 3 min) at 14 ºC/s. The temperature programme comprised a 2 min isothermal period at 70 ºC increasing to 140 ºC (held 2 min) at a rate of 12 ºC/min, followed by an increase period to 320 ºC (held 15 min) at 3 ºC/min. Combustion reactor temperature was maintained at 1000 °C for carbon isotope analysis. The high temperature conversion (HTC) oven was maintained at 1420 ºC for hydrogen isotope analysis. Obtained values were normalised to the Vienna Pee Dee Belemnite (VPDB) scale ($\delta^{13}C$) and Vienna Standard Mean Ocean Water (VSMOW) scale ($\delta^{2}H$) using a *n*-alkane Schimmelmann type A6 mixture (n-C_{16} to n-C_{30}) of known isotopic composition from Arndt Schimmelmann (Biogeochemical Laboratories, Indiana University). Certificate of analysis indicates that data for *n*-alkane Schimmelmann type A6 mixture have a precision of ±0.05‰ for $\delta^{13}C$ and ±1.5‰ for $\delta^{2}H$. Reproducibility was better than ± 0.5‰ for carbon isotope measurements and better than ± 5.0‰ for hydrogen isotope measurements.

To investigate the processes governing the hydrogen composition of sedimentary *n*-alkanes, a robust dataset of the isotopic signatures of potential sources, such as precipitation, is required. Here we consider monthly precipitation amount and precipitation $\delta^{2}H$ ($\delta^{2}H_{p}$) data available from two GNIP stations near the study area for comparison (Global Network for Isotopes in Precipitation; IAEA/WMO, 2006).

3.3.4. Micromorphology

Intact, oriented blocks of sediment from all stratigraphic units were extracted from selected profiles and from across the excavation surface for micromorphological analyses. The goal of applying this technique was to characterise site formation processes and identify features or processes at the microstratigraphic scale, which could indicate particular climatic or environmental conditions.

Samples were oven dried at 60 °C for 48 hours and subsequently impregnated with a mixture of polyester resin (Palatal strained resin UN1866, TNK composites), styrene (Styrene monomer [CAS: 100-42-5] UN2055, TNK composites) and catalyser (Luperox [CAS: 78-93-3], TNK composites) in a 7:3:0.1 ratio. The hardened blocks were then cut in 1 cm-thick slabs using a Euro-Shatal M31100 radial saw. Samples collected during archaeological field seasons 2010 - 2015 were sent to Spectrum Petrographics (Vancouver, WA, USA) for thin section manufacture (7 cm x 5 cm x 30 µm). Samples collected during the 2016 - 2018 field seasons were processed at the Archaeological Micromorphology and Biomarker Laboratory (AMBI), Universidad de La Laguna, Tenerife. Micromorphological analyses were carried out using a Nikon E200 polarising microscope following the standard guidelines set out in Stoops (2003) and Nicosia and Stoops (2017).

3.3.5. Anthracology

During the archaeological field seasons carried out between 2013 and 2016 the sediment excavated from across the entire excavation surface of S.U. IVc and S.U. IVd was processed by systematic flotation using 1.0 and 0.2 mm sieves. S.U. IVd is subdivided into IVd1, IVd2, IVd3, IVd4 and IVd5, representing distinct, locally discontinuous textural facies assigned during excavation of this unit. In this paper, scattered charcoal from these units are included, excluding the concentrated charcoal from the combustion features. Scattered charcoal spread over human living surfaces, having accumulated from an undefined number of combustion and occupation events, are widely accepted as reflecting conditions within the local environment (Badal and Heinz, 1991; Badal 1992; Chabal, 1997).

For the taxonomic identification of specimens, each fragment of charcoal was fractured manually to provide transversal, tangential and radial sections using a Nikon Optiphot-100 bright/dark field incident light microscope with 50-500x magnification. Botanical identification was performed with specialised plant anatomy atlases (Jacquiot et al., 1973; Schweingruber, 1976, 1990) and the reference collection of modern charred woody taxa from the Department of Prehistory, Archaeology and Ancient History, University of Valencia. Spatial information relating to the current distribution of taxa has been obtained from the database of the Anthos Project (www.anthos.es) and processed using GIS software (Quantum GIS v.2.10.1 "Pisa").

3.3.6. Microvertebrate study (S.U. IVd)

Microvertebrate remains

The small vertebrate fossil remains studied in this work consist of isolated dental and bone fragments collected during the 2013 archaeological field season from S.U. IVd, from across the excavation surface. The fossils were processed, sorted and classified using a Leica MS5 binocular microscope. Photographs were taken with a scanning electron microscope at Central Support Facility for Experimental Research (SCSIE) of the Universitat de València. Vertebrate fossils were identified following the anatomical nomenclature and measurement methods provided by van der Meulen (1973), Rabeder (1981) and Jeannet (2000) for arvicolines, van der Weerd (1976) for murids, Daams (1981) for glirids, Reumer (1984) for soricids, Bailon (1999) for amphibians, Roček (1984), Bailon (1991), Barahona (1996) and Barahona and Barbadillo (1997) for lacertids and Szyndlar (1984) and Blain (2009) for snakes. The taxonomic classification follows Wilson and Reeder (2005) for mammals, Uetz and Hošek (2015) for reptiles and Frost (2015) for amphibians.

Palaeoecological reconstruction (microvertebrates)

To reconstruct the climatic conditions of S.U. IVd, the Mutual Ecogeographic Range (MER) method has been applied to the assemblage (Blain et al., 2009; Blain et al., 2016). This consists of identifying regions where the recorded species are currently found and extrapolating the current mean values of these regions' climatic parameters as representative climate estimations for the studied site. This procedure suggests avoiding those species whose distribution is strongly affected by perturbing parameters, such as human pressure. Hence, *Microtus cabrerae*, taxon registered in S.U. IVd, has not been included in this study because it has suffered a range contraction in modern times and many subpopulations are small, fragmented and subject to major inter-annual fluctuations (Laplana and Sevilla, 2013; Pita et al., 2014). Biogeographic cartography of small mammal species in Spain, recorded as presence/absence of each taxa in a 10 x 10 km UTM square grid, was obtained from Palomo et al. (2007), while amphibians and reptiles came from SIARE (AHE, 2016). Climatic information (MAT, mean annual temperature; MAP, mean annual precipitation; MTW, maximum temperature of warmest month; MTC, minimum temperature of coldest month; PWM, precipitation of wettest month; PDM, precipitation of driest month) for these locations was obtained from the World Clim 1.4 database with a 30 arcseconds resolution grid (Hijmans et al., 2005). The resulting climatic parameters were compared with the current climate data from the nearest weather station to the site (Alcoy). Further details of the microvertebrate study methods and taphonomic remarks on the assemblage are given in Appendix 1.

3.3.7. Macrofaunal study (S.U. IVd)

Zooarchaeological methods

Zooarchaeological and taphonomic analyses of faunal material recovered during the excavation of S.U. IVd were performed using established standard methods (Lyman, 1994; Reitz and Wing, 2008). Where present, material was recorded for all excavation squares across the excavation surface. Remains were taxonomically and anatomically identified, except in specimens with insufficient information. Those remains were classified into three categories (long, flat or articular) and associated with a weight-size category based on bone density, circumference, and cortical surface thickness. Weight-size categories were determined in keeping with archaeological examples (Uerpmann, 1973; Bunn, 1986) and current weight references based on wild male specimens (Palomo et al., 2007): large-sized (> 300 kg), medium-sized (100-300 kg), small-sized (5-100 kg) and very small-sized (< 5 kg). Five abundance measures were employed: number of remains (NR), number of identified specimens (NISP), the minimal number of elements (MNE), the minimal number of individuals (MNI) and the minimal animal units (MAU). To assess the assemblage's integrity, we calculated the fragmentation rate, the relative abundance (%RA) and the standardised MAU (%MAU). The last of these was used to calculate the differential preservation index by weight-size, applying the Pearson's r and Kendall's tau correlation coefficient test with Past 3.12© free software. Published data was referred to for large and medium-sized animals (Kreutzer, 1992; Lam et al., 1999) and for small-sized animals (Lyman, 1984; 1985; 1994). Further information on the methods used for the study of the macrofaunal material is provided in Appendix 1.

Palaeoecological reconstruction (macrofauna)

The formalisation of indicator species according to a bioclimatic classification has been applied here (Hernández-Fernández, 2001; Rodríguez, 2013; Walter, 1973). A table has been constructed with the theoretical distribution of species according to different biomes or Climate Restriction Index (CRI). The distribution in the reference material is established for mammalian species, in our work we have also included the theoretical distribution of other taxa registered in the set, i.e. birds and tortoises. Once the CRI is calculated, the bioclimatic component (BC) of the set for each biome is obtained by means of the formula $BC = (\Sigma CRIi) * 100 / S$, where S is the number of species and CRIi the index of climatic restriction of each of the species. Previously calculated discriminant functions are applied from a wide database of localities and species (Hernández-Fernández, 2001, 2006; Hernández-Fernández and Peláez-Campomanes, 2003, 2005), in order to obtain data such as annual average temperature

(AAT) or precipitation (AAP). From this, it is possible to infer the most probable biome for our faunal assemblage (Pérez et al., 2017).

3.4. Results

3.4.1. Total Organic Carbon (TOC), % Sulphur (%S), % Nitrogen (%N)

TOC ranged from 0.06 to 3.91% with an average of 1.11% (Fig. 3.3). The highest concentration was recorded in the uppermost part of S.U. I, while the lowest concentration of TOC was recorded in S.U. V. Mild fluctuations and a generally decreasing trend is observed down-profile, with the exception of S.U VI, where there is a slight increase of 0.8%. TS values ranged between 0.01% and 0.07%, with an average value of 0.03% (Fig. 3.3). The maximum concentration of TS, 0.07%, is recorded in the uppermost part of S.U I. The lowest values for TS are recorded in S.U. IVc and IVd. TN values ranged from 0.01% to 0.29%, with an average TN value through the sequence of 0.07% (Fig. 3.3). The maximum value of 0.29% is recorded as a sharp increase in the lower part of S.U. I. Mild fluctuations are observed down-profile between 0.01% and 0.03%.

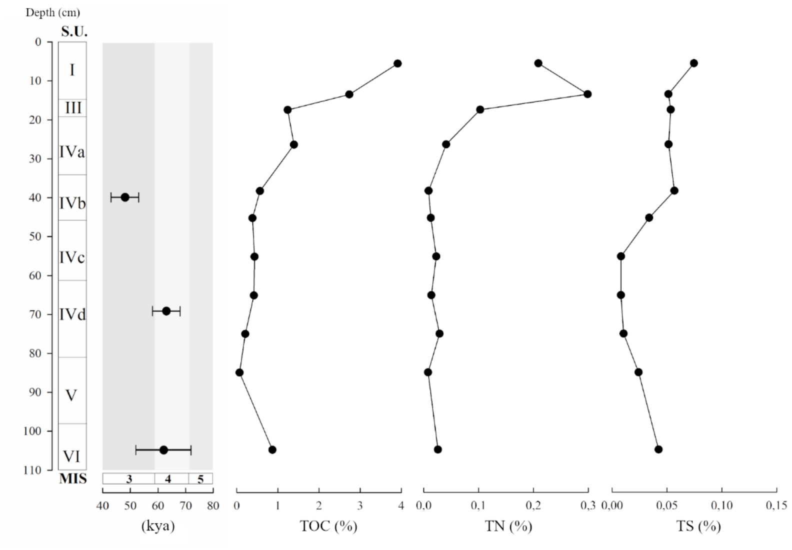

Figure 3.3 Total organic carbon (TOC,%), total nitrogen (TN,%), and total sulphur (TS,%).

3.4.2. Sedimentary leaf waxes

Total *n*-alkane concentration ranged between 0.04 and 1.59 µg/g dry sediment. Most samples through the sequence yielded *n*-alkane distributions with a predominance of long-chain compounds (C_{29}-C_{35}), consistent with higher order vascular terrestrial plants (Fig. 3.4) (Table 3.1), although samples collected from S.U IVc and S.U. IVd also show input from mid-chain length compounds (C_{23}-C_{27}). Even-numbered homologues recorded in S.U. IVb (lower) and S.U. VI were below the limit of quantification, so CPI values for those units are not included here. CPI values through the sequence are generally low, with a minimum of 0.7 (S.U. V) and a maximum of 7.9 (S.U. III) (Fig. 3.5). ACL values ranged between a minimum of 27.2 (S.U. IVd upper) and a maximum of 32.5 (S.U. V), with a notable shift toward lower values in S.U. IVc and S.U. IVd (upper).

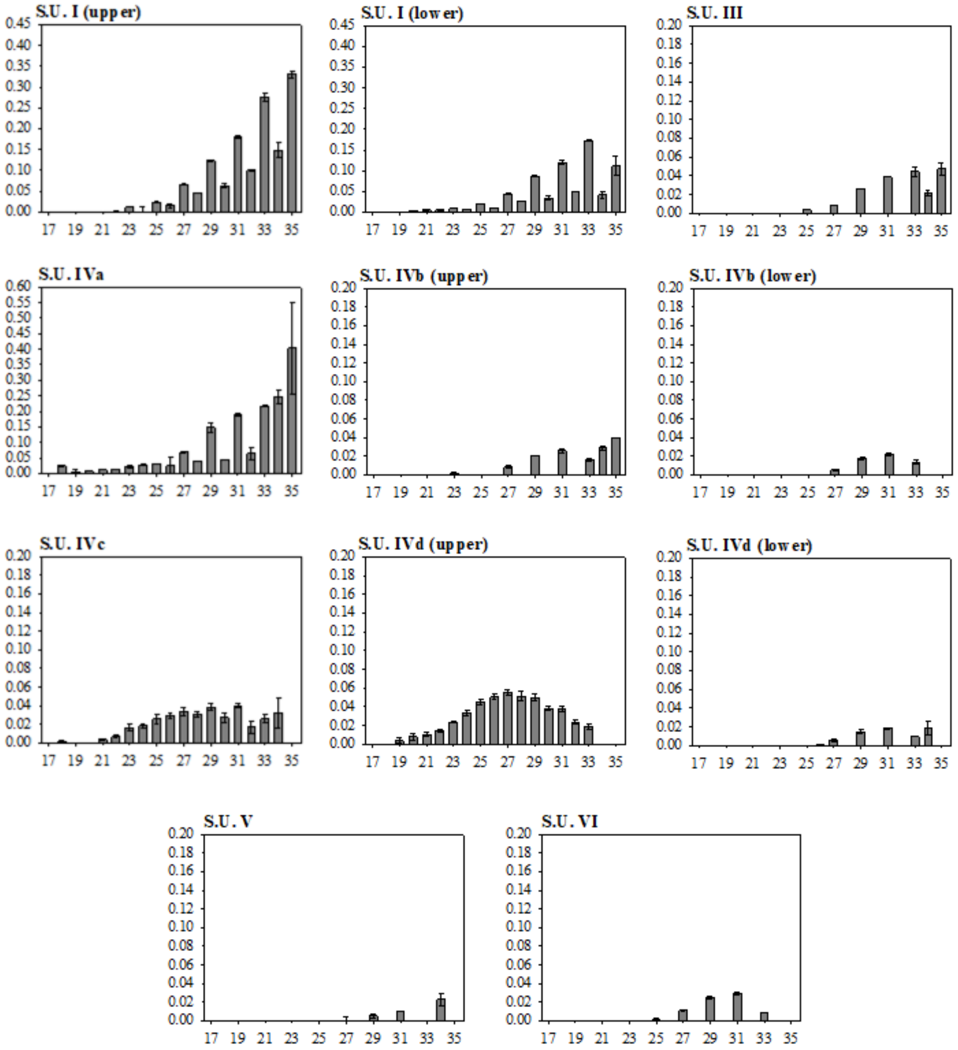

Figure 3.4 Histograms displaying the distribution and concentration of n-alkanes extracted from sediments at Abric del Pastor. IS: 5α-androstane. The x-axis represents the alkane carbon chain length and the y-axis represents the concentrations given in µg per g of dry sediment (µg/g). Note the larger scale for samples from S.U. I and S.U. IVa.

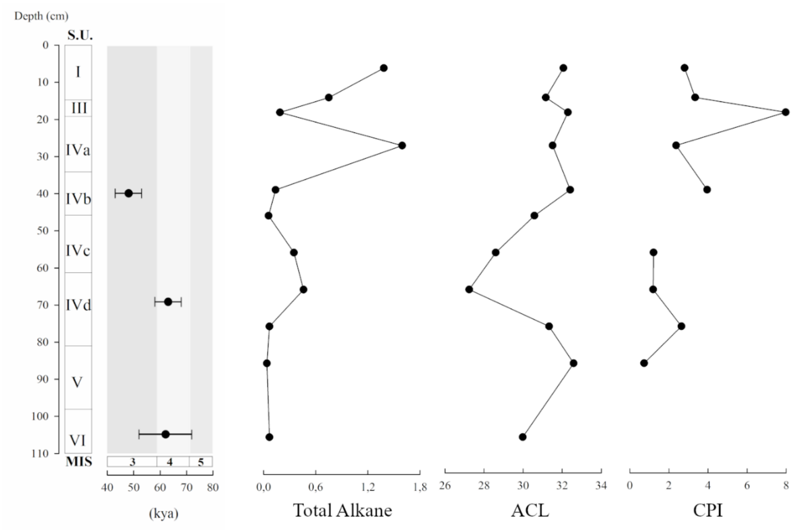

Figure 3.5 Leaf wax lipid biomarkers.Total *n*-alkane concentration, ACL and CPI.

S.U.	**I**	**I**	**III**	**IVa**	**IVb**	**IVb**	**IVc**	**IVd**	**IVd**	**V**	**VI**
TOC%	3.91	2.74	1.24	1.39	0.56	0.43	0.42	0.21	0.07	0.87	0.38
TN%	0.21	0.30	0.10	0.04	0.01	0.01	0.02	0.01	0.03	0.01	0.03
TS%	0.07	0.05	0.05	0.05	0.06	0.03	0.01	0.01	0.01	0.02	0.04
n-Alkanes (µg/g dry sediment)											
C_{17}	*	*	*	*	*	*	*	*	*	*	*
C_{18}	*	*	*	0.025	*	*	0.002	*	*	*	*
C_{19}	*	*	*	0.005	*	*	*	0.004	*	*	*
C_{20}	*	0.003	*	0.007	*	*	*	0.008	*	*	*
C_{21}	0.001	0.006	*	0.013	*	*	0.004	0.01	*	*	*
C_{22}	0.001	0.005	*	0.014	*	*	0.007	0.015	*	*	*
C_{23}	0.012	0.011	*	0.022	0.002	*	0.016	0.023	*	*	*
C_{24}	0.001	0.006	*	0.028	*	*	0.018	0.034	*	*	*
C_{25}	0.024	0.021	0.003	0.032	*	*	0.026	0.045	*	*	0.001
C_{26}	0.015	0.011	*	0.025	*	*	0.029	0.05	0.001	*	*
C_{27}	0.066	0.044	0.009	0.069	0.008	0.005	0.034	0.055	0.006	*	0.011

C_{28}	0.046	0.026	*	0.039	*	*	0.03	0.051	*	*	*
C_{29}	0.123	0.087	0.026	0.148	0.021	0.017	0.038	0.05	0.014	0.005	0.025
C_{30}	0.063	0.035	*	0.044	*	*	0.027	0.038	*	*	*
C_{31}	0.181	0.12	0.039	0.188	0.026	0.022	0.04	0.038	0.018	0.011	0.029
C_{32}	0.101	0.049	*	0.064	*	*	0.017	0.023	*	*	*
C_{33}	0.276	0.172	0.044	0.217	0.016	0.014	0.026	0.019	0.012	*	0.009
C_{34}	0.148	0.042	0.021	0.247	0.029	*	0.032	*	0.018	0.023	*
C_{35}	0.331	0.111	0.047	0.403	0.041	*	*	*	*	*	*
Total	1.38	0.75	0.19	1.59	0.14	0.06	0.35	0.46	0.07	0.04	0.07
ACL	32.0	31.1	32.2	31.4	32.3	30.5	28.6	27.2	31.3	32.5	29.9
CPI	2.7	3.3	7.9	2.3	3.9	-	1.1	1.1	2.6	0.7	-

Table 3.1 Total organic carbon (TOC), total nitrogen (TN) and total sulphur (TS) as well as n-alkane concentrations, ACL and CPI values through the stratigraphic sequence. * denotes compounds which were detected but in quantities below the limit of quantification.

3.4.3. δ^2H_{wax}

In the region around Abric del Pastor, a strong negative correlation between monthly precipitation amount and precipitation δ^2H (δ^2H_p) is recorded at two GNIP (Global Network for Isotopes in Precipitation; IAEA/WMO, 2006) stations in Murcia and Valencia (Fig. 3.6). This suggests some degree of influence by the amount effect (Dansgaard, 1964) on regional δ^2H_p values, which in turn may contribute to variability in our δ^2H_{wax} signal.

δ^2H_{wax} was analysed for C_{29} and C_{31} *n*-alkanes extracted from sediments collected through the sequence (Fig. 3.7) (Table 3.2). For nC_{29}, the δ^2H_{wax} range is -129‰ to -170‰. The lowest values of -170‰ and -164‰ are recorded in the Holocene sediments from S.U. I. A trend towards low values is also recorded in the uppermost part of S.U. IVd and in S.U. IVc, at -152‰ and -153‰ respectively. Through the rest of the sequence values fluctuate between -129‰ and -148‰. δ^2H_{wax} values for nC_{31} are generally lower than those obtained for nC_{29} ranging from -137‰ to -174‰. Overall, however, both sets of values have a similar degree of variation and follow a similar trend.

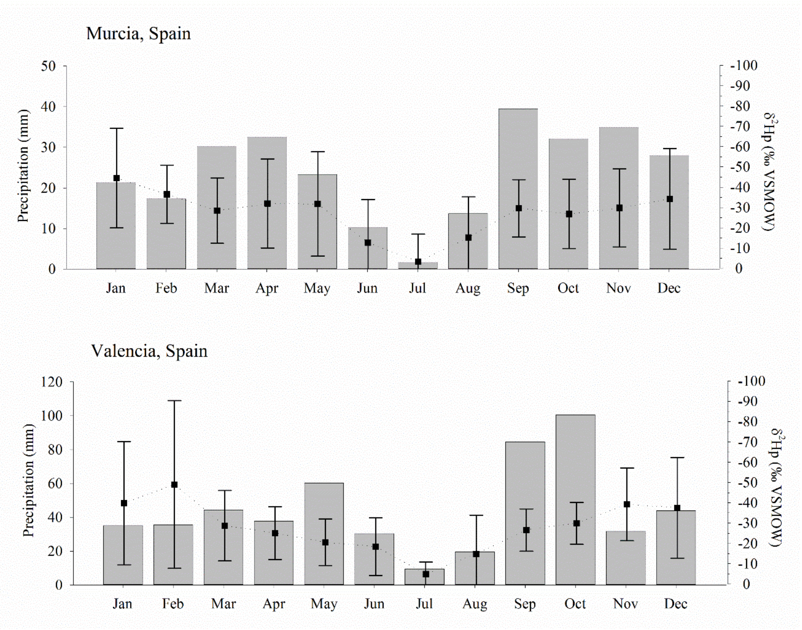

Figure 3.6 Seasonal cycle of precipitation amount (grey bars) and δ^2H_P (black squares) for GNIP stations (IAEA/WMO, 2006) in Murcia (n=11, 2000 – 2010) and Valencia, Spain (n=16, 2000 – 2015).

3.4.4. $\delta^{13}C_{wax}$

$\delta^{13}C_{wax}$ measurements were analysed for C_{29} and C_{31} *n*-alkanes extracted from sediments collected through the sequence (Fig. 3.7) (Table 3.2). $\delta^{13}C_{wax}$ values for *n*C_{29} ranged between -32.4‰ and -38.0‰, with maximum ^{13}C enrichment in S.U. IVb, where values of-32.4‰ and -32.8‰ were obtained. A similarly high value is recorded in the base of S.U. IVd at -32.5‰. The lowest value of -38.0‰ comes from S.U. IVa. $\delta 13C_{wax}$ values for *n*C_{31} are generally lower than those obtained for *n*C_{29}, ranging between -33.6‰ and -40.3‰. Overall, however, both sets of values have a similar degree of variation and follow a similar trend.

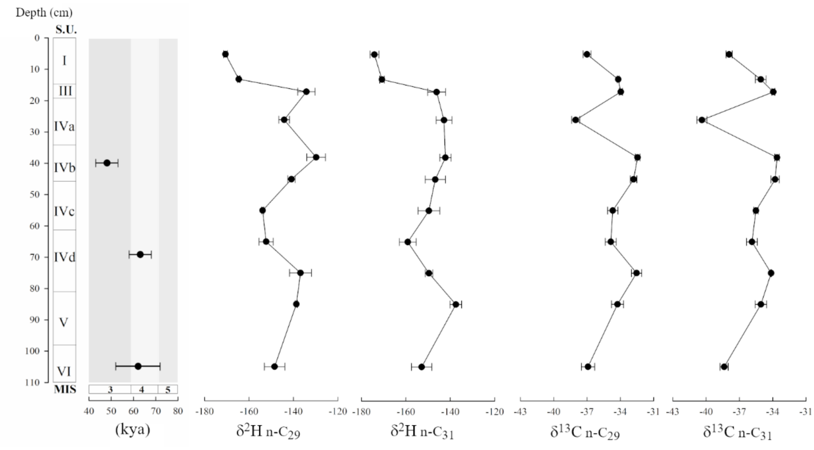

Figure 3.7 δ^2H_{wax} for *n*-alkanes C_{29} and C_{31}, and $\delta^{13}C_{wax}$ for *n*-alkanes C_{29} and C_{31}.

S.U.	I	I	III	IVa	IVb	IVb	IVc	IVd	IVd	V	VI
δ^2H_{wax}											
C_{29}	-170±1	-164±1	-134±4	-144±2	-129±4	-140±2	-153±1	-152±3	-136±5	-138±1	-148±5
C_{31}	-174±2	-170±1	-146±4	-142±4	-142±3	-146±5	-149±5	-159±4	-149±2	-137±3	-152±5
$\delta^{13}C_{wax}$											
C_{29}	-36.9±0.4	-34.2±0.1	-33.9±0.2	-38.0±0.4	-32.4±0.2	-32.8±0.3	-34.7±0.5	-34.9±0.5	-32.5±0.5	-34.3±0.5	-36.9±0.6
C_{31}	-37.9±0.3	-35.1±0.5	-33.9±0.1	-40.3±0.5	-33.6±0.2	-33.8±0.4	-35.5±0.2	-35.9±0.5	-34.1±0.1	-35.1±0.5	-38.4±0.4

Table 3.2 δ^2H_{wax} and $\delta^{13}C_{wax}$ through the stratigraphic sequence. Values are expressed in per mil (‰). Error reports standard deviation.

3.4.5. Micromorphology

The samples analysed are generally composed of the same sedimentological and lithological elements, characterised by a locally reworked sandy sediment, with 5-10% subangular to angular fine and medium sand, ~30% subrounded coarse sand and gravel, resulting principally from the mechanical weathering and decay of the fossiliferous quartz-rich limestone rock shelter. The coarse mineral components frequently appear fissured. The sedimentary matrix is composed of micritic calcite which, with notable exceptions in S.U. IVb and IVd, generally occurs in a good state of preservation with few dissolution features. Clay is present only in small quantities, occurring locally as thin coatings, cappings or infilling the interstitial void space. Detailed descriptions of each thin section sample are provided in Appendix 1 (Table 5).

Microfacies types

Below, we outline the microfacies types identified through micromorphological analyses of thin sections by polarised light microscopy. Brief descriptions are included with a representative photomicrograph of each of the primary microfacies types (Fig. 3.8). Similar features and components are recurrent throughout the sequence (Fig. 3.9 and 3.10) but vary considerably in their degree of abundance, reworking or post-depositional alteration.

1. *Microfacies type 1* This microfacies type is characterised by a crumb to granular microstructure which is quite open, lithologically composed of fine and medium sand-sized grains of quartz alongside micritic and micro-sparitic fossiliferous limestone, which occurs in sizes ranging from fine sand to coarse gravel. Morphologically this fraction appears subrounded to rounded. Frost induced fissuring of larger clasts is observed in addition to the presence of platy coarse grains. Dusty clay coatings occur throughout, as well as clay cappings. Frequent components include burned and unburned angular bone fragments and pieces of both massive and fibrous charcoal, ash

rhombs, occasional fat-derived char which occurs as ~0.5-1.5 mm massive black fragments with a vesicular porosity, and rare coprolites. The internal organisation of the components is unsorted. This microfacies type is associated with good preservation of the calcitic fraction.

(a) *Microfacies type 1a* This microfacies type is similar to MF type 1 but with a higher degree subrounding and rounding of the coarse mineral elements, Fe-Mn segregation and the presence of limpid clay infillings.

(b) *Microfacies type 1b* This microfacies type is similar to MF type 1a but exhibits a poorer preservation of the calcitic matrix.

2. *Microfacies type 2* This microfacies type is characterised by a weakly expressed platy/lenticular microstructure, lithologically very similar to MF type 1. Frost induced fissuring of the coarse mineral fraction is again evident. Components include scattered, unsorted, unburned angular bone fragments and reworked calcitic wood ash. The calcitic fraction is well preserved.

3. *Microfacies type 3* This microfacies type is characterised by a spongy to vughy microstructure dominated by a vesicular or vughy porosity. Lithologically this type is composed of fine and medium sand-sized grains of quartz, although in lower abundance than other MF types, alongside micritic and micro-sparitic fossiliferous limestone ranging from fine sand to coarse gravel. Clasts exhibit a high degree of subrounding and rounding. Components are unsorted and scattered and include reworked charcoal and bone. No calcitic wood ash is observed in this MF type. The calcitic fraction is well preserved.

4. *Microfacies type 4* This microfacies type is characterised by a massive microstructure with low porosity, and a lithology of fine and medium sand-sized grains of quartz alongside micritic and micro-sparitic fossiliferous limestone ranging in size from fine sand to coarse gravel. Clasts occur as sub-angular to angular. Cryofeatures observed in the other MF types are not as evident here. Components include reworked calcitic ash rhombs and angular unburned bone fragments. The calcitic fraction is well preserved.

    (a) *Microfacies type 4a* This microfacies type is similar to MF type 4 but with subrounded to rounded coarse mineral elements and frost induced fissuring of the coarse grains.

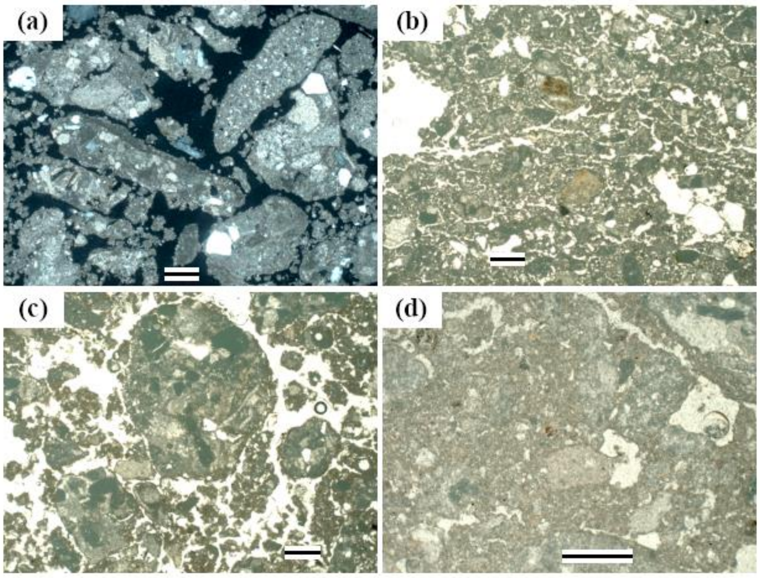

Figure 3.8 Photomicrographs of primary microfacies types (scale 500µm) (a) MF type 1 (b) MF type 2 (c) MF Type 3 (d) MF Type 4.

Stratigraphic description

S.U. I

This unit is characterised microscopically by MF type 1. The microstructure is crumb to granular with coarse sand and gravel occurring as subrounded to rounded. Organisation of the components is unsorted with a high porosity generated by channels due to root bioturbation. The matrix has a dusty appearance owing to the presence of silt-sized organic matter (humified or carbonised plant cells). Terrestrial snail shell, charcoal, bone fragments and coprolites were identified throughout. Abundant dispersed faecal spherulites were also identified in the uppermost part of this unit.

S.U. II

This unit is characterised mainly by MF type 4 but with isolated zones more closely resembling MF type 1. It exhibits a slight increase in the relative proportion of fine and medium sized quartz sand. Medium and coarse limestone gravel is in a poorer state of preservation than in other units. Gravel-sized clasts frequently exhibit dissolution cavities with rounded edges and dusty clay coatings. Components include angular bone fragments, both burned and unburned, and calcitic wood ash likely resulting from a reworked combustion feature in this unit.

S.U. III

This unit, which is composed of a thin cemented carbonate crust yielding very few archaeological remains, was represented in a single thin section, characterised by MF type 1. Components include bone fragments and rare faecal spherulites.

S.U. IVa-g

Subunit IVa is captured in two thin section samples and is predominantly characterised by the massive microstructure exhibited by MF type 4a, but also containing MF type 1a and MF type

2. The coarse mineral fraction generally occurs as subrounded to rounded and frequently fissured. Components include ash and frequent bone fragments.

Subunit IVb comprises MF type 1b and MF type 3 with a crumb/granular to vughy microstructure. The calcitic matrix within this subunit shows slight dissolution and a porosity with a horizontal arrangement, indicative of cryoturbation. This subunit also contains a lower proportion of gravel relative to the other subunits within S.U IV. The medium and coarse gravel in subunit IVb is also more notably angular, regularly occurring with a lenticular or platy morphology, typical of frost affected sediments. Impregnation of iron oxides is also frequent and occurs both in the matrix and as fine silt sized nodules. The components are very similar to IVa.

Subunit IVc, which is a roof collapse deposit composed of boulders and large angular cobbles, due to the absence of fine material has not been included in the micromorphological study.

Subunit IVd is characterised microscopically by MF type 1a and MF type 3, with a crumb/granular to spongy microstructure. A slightly higher proportion of gravel is recorded in this subunit relative to the other subunits within S.U IV. Again, clasts with a platy morphology are frequent. Dusty clay cappings and fissuring of clasts may be further evidence of mild cryoturbation. Components are similar to IVa and IVb but occur in higher abundances.

Subunits IVe and IVf are represented in two thin sections, characterised by MF type 1 and MF type 1a, with an open crumb to granular microstructure. Well-rounded clasts, fissuring and clay cappings are frequent. Similar to the other subunits in S.U. IV, components include bone fragments, reworked ash and charcoal.

Subunit IVg is represented in three thin sections and is characterised by MF type 1 with an open crumb to granular microstructure. A higher proportion of gravel occurs in this subunit relative to the overlying subunits. Fe and Mn impregnation features were also identified. Anthropogenic components, such as ash or charcoal, are greatly reduced in quantity within this subunit.

S.U. V

This unit is represented in a single thin section characterised by MF type 1. Lithologically this unit is very similar to S.U IVa with a calcitic matrix and an open crumb to granular microstructure. The matrix is slightly permeated by iron oxides and clay coatings. Components include rare charcoal and bone fragments.

S.U. VI

This unit is characterised by MF type 1 with an open crumb to granular microstructure which is locally compacted. Corroded and fissured clasts in this unit are similar to those recorded in S.U II. Anthropogenic components include burned bone, charcoal, calcitic wood ash and fat-derived char. These occur in much greater abundances than other units. Faecal spherulites are recorded here mixed with reworked combustion residues. Dusty clay coatings and infillings are common. Needle fibre calcite is also recorded here in-filling the interstitial pore space.

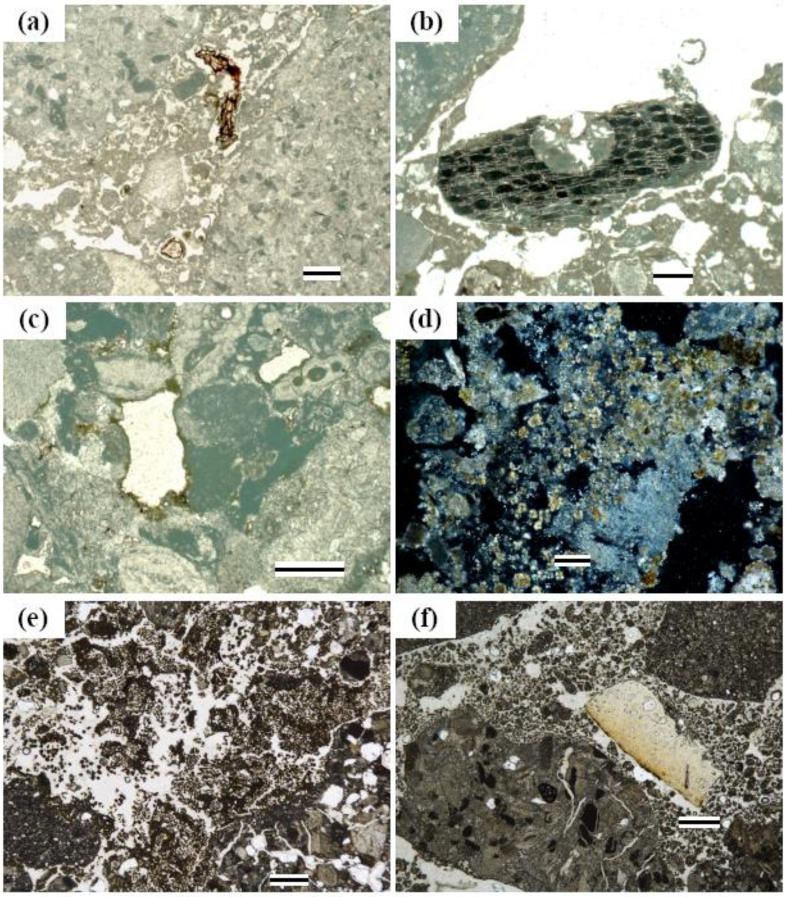

Figure 3.9 Micromorphological components and features observed at Abric del Pastor (a) Fresh organic vegetal matter associated with root bioturbation (PPL, S.U. IVa, scale 500 µm) (b) Fragment of carbonised vegetal matter (PPL, S.U. II, scale 500 µm) (c) Dissolution well with fine dusty clay coating in limestone clast (PPL, S.U. II, scale 500 µm) (d) Faecal spherulites associated with reworked ashy aggregate (XPL, S.U. VI, 100 µm) (e) Bioturbated matrix with soil fauna excrements (PPL, S.U. IVd, 1000 µm) (f) Burnt bone in loose sandy sediment with crumb to granular microstructure, note the fissured clast (PPL, S.U. IVd, scale 1000 µm).

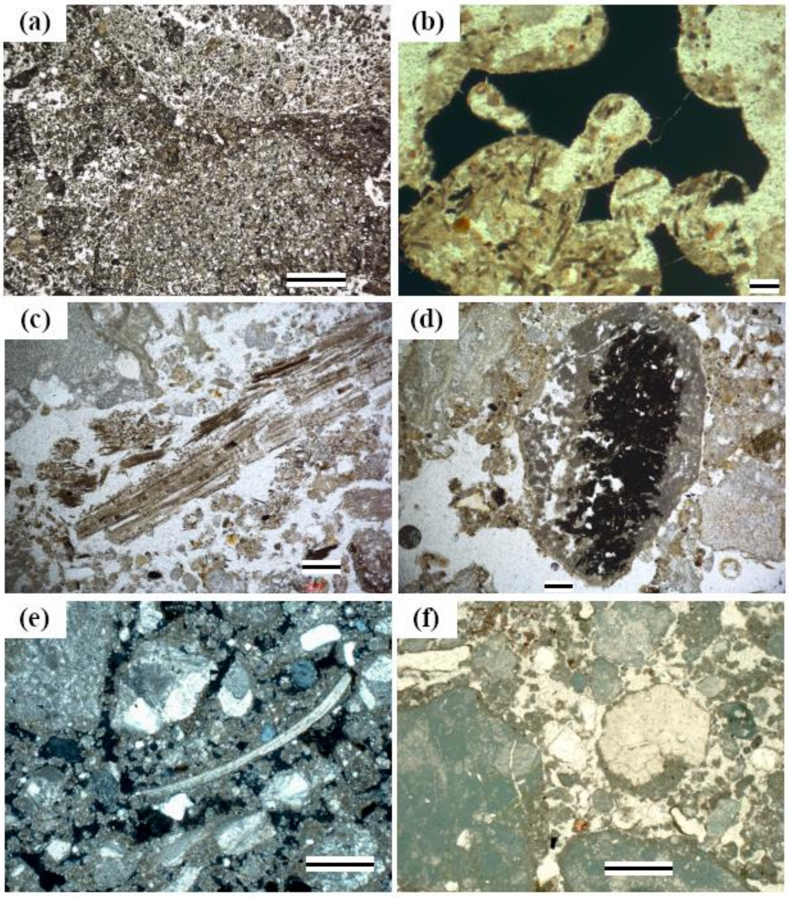

Figure 3.10 Micromorphological components and features observed at Abric del Pastor (a) Soil crust (PPL, S.U. IVd, scale 1000 µm) (b) Fragment of fat-derived char (PPL, S.U. VI, scale 1000 µm) (c) Partially carbonised and ashed plant material (PPL, S.U. VI, scale 100 µm) (d) Reworked ashy aggregate (XPL, S.U. VI, scale 1000 µm) (e) Fragment of terrestrial snail shell (XPL, S.U. I, scale 500 µm) (f) Massive coprolite (PPL, S.U. I, scale 500 µm).

3.4.6. Anthracological remains

Anthracological data from Abric del Pastor has been partially published in previous works. Here, anthracological data from S.U. IVc, IVd1, IVd2 (Vidal-Matutano et al., 2015) and S.U. IVd3 (Vidal-Matutano et al., 2017) is presented together with new anthracological data from S.U IVd4 and S.U. IVd5 (Table 3.3). The scattered charcoal assemblages analysed from units IVc and IVd (IVd1-5) at Abric del Pastor include a total of 957 charcoal fragments and at least

19 taxa have been identified. Despite the small size of most of the wood charcoal remains (1 – 2 mm) and its scarcity in some units, a high variety of taxa indicating the presence of several plant formations in the surroundings can be inferred. Charcoal data from IVd2 and IVd3 has been unified here as data for each unit was not statistically representative (< 100 remains).

Stratigraphic Unit	**IV c**		**IV d 1**		**IV d 2**	**IV d 3**		**IV d 4**		**IV d 5**	
Taxa	**n**	**%**	**n**	**%**	**n**	**n**	**%**	**n**	**%**	**n**	**%**
Cistaceae	1	0.37	1	0.58	*	*	*	*	*	*	*
Ephedra sp.	5	1.84	*	*	*	*	*	*	*	*	*
Euphorbiaceae	4	1.47	1	0.58	*	*	*	*	*	*	*
Fabaceae	5	1.84	8	4.62	4	7	7.78	6	3.13	*	*
Fraxinus sp.	1	0.37	*	*	*	5	5.56			*	*
Juniperus sp.	145	53.31	93	53.76	28	28	31.11	65	33.85	90	54.55
Labiatae	7	2.57	*	*	*	*	*	1	0.52	*	*
Maloideae	3	1.10	13	7.51	*	*	*	1	0.52	*	*
Monocotyledoneae tp. Poaceae	1	0.37	*	*	*	*	*	*	*	*	*
Pinus nigra-sylvestris	4	1.47	8	4.62	3	8	8.89	38	19.79	44	26.67
Pistacia sp.	39	14.34	20	11.56	23	8	25.56	5	2.60	3	1.82
Prunus sp.	*	*	*	*	*	*	*	2	1.04	*	*
Quercus sp.	10	3.68	11	6.36	6	9	10.00	41	21.35	12	7.27
Quercus sp. deciduous	*	*	*	*	*	*	*	5	2.60	*	*
Quercus sp. evergreen	41	15.07	12	6.94	1	14	15.56	14	7.29	5	3.03
Rhamnus-Phillyrea	*	*	*	*	*	*	*	7	3.65	*	*
Rosa sp.	*	*	2	1.16	*	*	*	*	*	*	*
Salix-Populus	2	0.74	2	1.16	*	7	7.78	3	1.56	9	5.45
Taxus baccata	*	*	2	1.16	*	4	4.44	4	2.08	1	0.61
Ulmaceae	4	1.47	*	*	*	*	*	*	*	1	0.61
Total fragments	**272**	100	**173**	100	**65**	**90**	100	**192**	100	**165**	100
Total taxa	**14**		**11**		**6**	**9**		**13**		**7**	

Table 3.3 New charcoal data from Abric del Pastor (IVd 4 and IVd5), presented here with S.U. IVc, IVd1, IVd2 (Vidal-Matutano et al., 2015) and S.U. IVd3 (Vidal-Matutano et al., 2017). Note that data from IVd2 and IVd3 are joined here because the total number of wood charcoal fragments for each unit is not statistically representative.

The most representative taxa throughout S.U IV from Abric del Pastor is *Juniperus* sp. (juniper) together with xeric taxa (Euphorbiaceae, *Ephedra* sp., Cistaceae) (Fig. 3.11). This overall pattern is seen throughout S.U. IVd and IVc (values of 36 – 58%). Values from *Pinus nigra-sylvestris* (black-scots pine) suggest a clear trend decreasing from 29% (S.U. IVd5) to 1% (S.U. IVc). In addition to this, Mediterranean mixed forest taxa including evergreen and deciduous

Quercus (oaks), *Pistacia* sp. (terebinth), *Rosa* sp. (rose), *Prunus* sp. or Maloideae (Rosaceae family) are abundant throughout IVd4 - IVc (38 – 49%). Notably lower proportions of these taxa are, however, recorded in IVd5 (12%). Finally, riverine taxa such as Ulmaceae (the elm family), *Salix-Populus* (willow-poplar) and *Fraxinus* sp. (ash) are present in small amounts (values < 7%). We infer two distinct anthracological phases from the analysed remains (AP-1 and AP-2). Phasing is a preliminary assessment of the data which relies on grouping analytical units to infer periods of distinct environmental conditions.

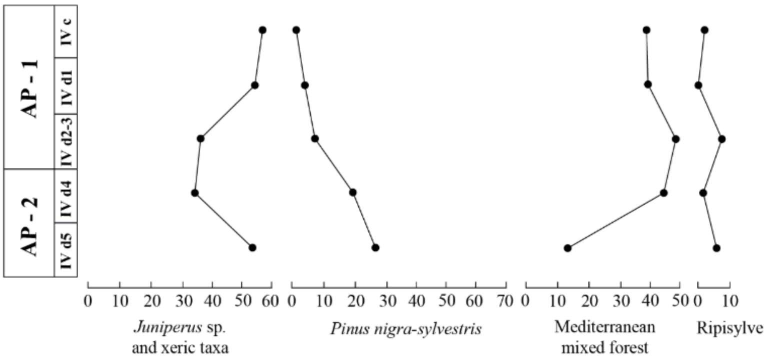

Figure 3.11 Anthracological data (main plant formations) from Abric del Pastor (IVc – IVd5).

3.4.7. Microvertebrate study (S.U.IVd)

The small vertebrate assemblage from the S.U. IVd contains 295 dental and bone remains that correspond to 33 individuals. The faunal list of this unit contains 3 rodents (*Microtus cabrerae*, *Eliomys quercinus* and *Apodemus sylvaticus*), 1 insectivore (*Crocidura* gr. *russula-gueldenstaedtii*), 1 anuran (*Pelodytes* sp.), 2 lizards (cf. *Timon lepidus* s. l. and cf. *Podarcis* sp.) and 3 snakes (Colubridae indet., *Coronella girondica* and Viperidaea indet.) (Appendix 1 Figure 2). The studied assemblage is characterised by the dominance of *Apodemus sylvaticus* (MNI=15), followed by cf. *Podarcis* sp. (MNI=8), *Eliomys quercinus* (MNI=3) and *Microtus cabrerae*, *Crocidura* gr. *russula-gueldenstaedtii*, *Pelodytes* sp., cf. *Timon Lepidus* s. l., Colubridae indet., *Coronella girondica* and Viperidae indet. (MNI=1) (Table 3.4).

Taxon	NISP	NMI	%	OD	OH	OWo	Wo	R	W
Microtus cabrerae	6	1	3.03	0	0.50	0.50	0.00	0.00	0.00
Eliomys quercinus	9	3	9.09	0	0.10	0.40	0.30	0.20	0.00
Apodemus sylvaticus	125	15	45.45	0	0.25	0.50	0.25	0.00	0.00
Crocidura russula-gueldenstaedtii	2	1	3.03	0.40	0.10	0.40	0.10	0.00	0.00
Pelodytes sp.	1	1	3.03	0.33	0.16	0.25	0.08	0.16	0.00
Lacertidae indet.	21	-	-	-	-	-	-	-	-
cf. *Timon lepidus* s.l.	5	1	3.03	-	-	-	-	-	-
cf. *Podarcis* sp.	16	8	24.24	-	-	-	-	-	-
Serpentes indet.	2	-	-	-	-	-	-	-	-
Colubridae indet.	5	1	3.03	-	-	-	-	-	-
Coronella girondica	7	1	3.03	0.25	0.05	0.35	0.20	0.15	0.00
Viperidae indet.	1	1	3.03	-	-	-	-	-	-
Total	**200**	**33**	**100**	**4**	**22**	**47**	**23**	**4**	**0**

Table 3.4 Number of Identified Specimens (NISP), Minimum Number of Individuals (MNI) and percentage of representation (%) of small vertebrates from the Unit IVd from Abric del Pastor. Distribution by habitat: **OWo**: Open Woodland, **Wo**: Woodland/Edge-woodland, **OD**: Open Dry, **OH**: Open Humid, **Wa**: Water and **R**: Rocky. Those species in open nomenclature indicate that these taxa could not be classified to the specific habitat level (dashes).

Palaeoecological reconstruction using the MER method indicates a MAT slightly lower than present conditions (-1.48 ºC) (Table 3.5). Other climatic parameters such as MTC (-1.05 ºC) and MTW (-0.78 ºC) point to a cooler climate with precipitation values ranging from 411 mm to 837 mm (MAP 624.13 mm). As only generalist species have been included in the reconstruction, the entire range of possible values should be considered.

	Mean	SD	Max.	Min.	Δ	Alcoy
MAT	12.22	2.85	18.3	-0.2	-1.48	13.7
MTC	0.65	2.88	8.4	-11.4	-1.05	1.7
MTW	27.72	3.47	35.9	11.8	-0.78	28.5
MAP	624.13	212.92	1586	220	81.83	542.3
PWM	77.72	26.25	251	32	3.42	74.3
PDM	23.02	16.09	101.0	0.0	7.82	15.2

Table 3.5 Values of climatic parameters in the region around Alcoy today based on Hijmans et al. (2005) and those obtained through the MER method from the microvertebrate assemblage of S.U. IVd. SD= standard deviation; Max.= maximum; Min.= minimum; Δ= difference with present day conditions. MAT= mean annual temperature; MTC= minimum temperature of the coldest month; MTW= maximum temperature of the warmest month; MAP= mean annual precipitation; PWM= precipitation of wettest month; PDM= precipitation of driest month.

3.4.8. Macrofaunal study (S.U. IVd)

A total of 476 faunal remains has been analysed for this study, 46% of which have been taxonomically determined. Artiodactyls, composed at species level by *Bos primigenius*, *Capra pyrenaica* and *Cervus elaphus*, are the most frequent group among ungulates (73 NR), while perissodactyls are represented only by *Equus ferus* (1 NR). Testudines are the taxonomic category with the greatest number of identified remains in the assemblage (129 NR), all attributed to *Testudo hermanni*. Few remains of rabbit (*Oryctolagus cuniculus*, 8 NR), undetermined birds (2 NR) and small carnivore (1 NR) have also been recorded. The remaining 54% of the assemblage has not been determined taxonomically but can be associated with a weight size category. Medium size is the most abundant category (76 NR), followed by mall (23 NR), very small (5 NR) and large (2). A total of 142 NR could not be determined (Table 3.6).

Taxa	NISP / NR	MNE	MNI
Artiodactyla	8	7	-
Bos primigenius	2	2	1
Caprinae	16	16	2
Capra pyrenaica	28	23	2
Cervidae	5	2	1
Cervus elaphus	14	9	3
Equus ferus	1	1	1
Oryctolagus cuniculus	8	8	2
Testudinidae	5	5	1
Testudo hermanni	100	78	4
Testudo sp.	29	29	2
Small carnivore	1	1	1
Birds	2	2	1
Total NISP	**219**	**183**	**21**
Large size	2	-	-
Medium size	76	-	-
Small size	32	-	-
Very small size	5	-	-
Undetermined	142	-	-
Total NR	**257**	**-**	**-**

Table 3.6 Faunal remains from S.U. IVd at Abric del Pastor.

The fragmentation rate is high, with most of the remains measuring < 2 cm in length. Diagenetic alterations were observed throughout the assemblage, with a total of 574 surface damage features identified: concretions (42%), manganese oxide staining (29%), root-marks (15%), corrosion (8%), weathering (5%) and gnaw marks (1%). The skeletal material contains a high quantity of cranial remains, mainly in the form of isolated teeth of *Bos primigenius* and *Capra pyrenaica*, while long bone fragments occur more frequently among *Cervus elaphus*. In the case of tortoise, backplate fragments and plastron are relatively abundant. Conservation analysis by bone density shows a statistically significant positive correlation ($p < 0.05$) in wild goat (0.66) and cervids (0.45), demonstrating an important bias in part of the assemblage. For this reason, utility indices were not applied.

A total of 184 old fractures (fresh and dry) have been identified. They are mainly present in the long bones of ungulates, in the medium-weight size category and to a minor extent in cranial and coxal fragments, scapulae ribs, and a small quantity of tortoise plates. A large proportion of fresh fractures can be clearly linked to anthropogenic activity. See Appendix 1 for additional taphonomic data and information on anthropogenic surface alterations.

Our bioclimatic component calculations (Appendix 1 Figure 4) suggest that the most probable biome for the Abric del Pastor Unit IVd faunal assemblage is Type IV (Mediterranean) (Table 3.7).

Species	**I**	**II**	**II/III**	**III**	**IV**	**V**	**VI**	**VII**	**VIII**	**IX**	**Total**
Capra hircus	0.000	0.000	0.000	0.000	1.000	0.000	0.000	0.000	0.000	0.000	1.000
Cervus elaphus	0.000	0.000	0.000	0.000	0.333	0.000	0.333	0.333	0.000	0.000	0.999
Bos frontalis	0.000	0.000	0.000	0.000	0.333	0.333	0.333	0.000	0.000	0.000	0.999
Equus onager	0.000	0.000	0.000	0.333	0.333	0.000	0.000	0.333	0.000	0.000	0.999
Vulpes vulpes	0.000	0.000	0.000	0.143	0.143	0.143	0.143	0.143	0.143	0.143	1.001
O. cuniculus	0.000	0.000	0.000	0.000	1.000	0.000	0.000	0.000	0.000	0.000	1.000
Testudo hermanni	0.000	0.000	0.000	0.000	0.500	0.500	0.000	0.000	0.000	0.000	1.000
P. pyrrhocorax	0.000	0.000	0.000	0.333	0.333	0.333	0.000	0.000	0.000	0.000	0.999
CRI	**0.000**	**0.000**	**0.000**	**0.809**	**3.975**	**1.309**	**0.809**	**0.809**	**0.143**	**0.143**	**7.997**

BC	**0.000**	**0.000**	**0.000**	**10.116**	**49.706**	**16.368**	**10.116**	**10.116**	**1.788**	**1.788**	**100**
AAT	**17.711**										
SD	**3.751**										
AAP	**268.349**										
SD	**558.709**										

Table 3.7 Climate restriction index (CRI), bioclimatic component (BC), annual average temperature (AAT) and precipitation index (AAP).

3.5. Discussion

Leaf waxes derived from terrestrial higher plants are the predominant source of long-chain length *n*-alkanes (nC_{27}– nC_{35}) at Abric del Pastor. Although long-chain homologues (nC_{27}–nC_{35}) derived from higher plants dominate through most of the sequence, sediment samples collected from S.U IVd and S.U. IVc yielded *n*-alkane distributions with proportionally increased concentrations of mid-chain length homologues (nC_{18} to C_{26}) which do not display a strong odd-over-even predominance. Although microbial degradation can alter the chain length distribution of *n*-alkanes (Brittingham et al., 2017), a more likely explanation here may be the incorporation of charred biomass related to anthropogenic combustion activities. Although care was taken during sampling to avoid thermally altered sediments, dispersed ash, charcoal and burned bone are recorded elsewhere in these units at the microstratigraphic scale. Furthermore, at least eight discreet combustion features have been recorded during the excavation S.U. IVd, more than in any other unit (Mallol et al., 2019). Studies elsewhere have demonstrated the effects of thermal degradation on *n*-alkane preservation and distributions (Eckmeier and Wiesenberg, 2009; Wiesenberg et al., 2009; Diefendorf et al., 2015b; Wang et al., 2017; Jambrina-Enríquez et al., 2018). With increasing temperatures, there is a decrease in chain length and a modification of the carbon preference from odd to even homologues, lowering ACL and CPI values. The *n*-alkane distributions and observed co-variance of ACL and CPI in S.U. IVd and IVc could therefore be explained by the effects of anthropogenic fire.

$\delta^{13}C_{wax}$ values are within the expected limits for a predominant contribution from C3 plants (Ficken et al., 1998). Through the entire sequence, there is a range of up to 5.6‰ (nC_{29}) and 6.7‰ (nC_{31}) for carbon isotope values, and up to 41‰ (nC_{29}) and 37‰ (nC_{31}) for hydrogen isotope values. $\delta^{13}C_{wax}$ decreases from -32.5‰ to -34.9‰ (nC_{29}) and -34.1‰ to -35.9‰ (nC_{31}) between the base and the uppermost part of S.U. IVd, while $\delta^{2}H_{wax}$ decreases from -136‰ to -152‰ (nC_{29}), and from -149‰ to -159‰ (nC_{31}). Although thermal alteration may have contributed to the observed variability (Weisenberg et al., 2009), notably in S.U. Numerous factors likely influence IVd and IVc, δ^{13}Cwax and δ^{2}Hwax values through the sequence. Water availability, temperature changes and specific plant attributes can affect fractionation of carbon isotopes by plants during CO_2 uptake and fixation (Δ_{leaf}) (Kaplan et al., 2002; Diefendorf and Freimuth, 2017). Diefendorf et al. (2010) have demonstrated that MAP is a strong predictor of Δ_{leaf}, although microclimate and ecosystem structure factors are also likely to influence $\delta^{13}C_{wax}$. Precipitation δ^{2}H, evapotranspiration and vegetation type are considered direct controls $\delta^{2}H_{wax}$ values, although other environmental and physiological variables can exert secondary controls (Sachse et al., 2006, 2009, 2012; Liu and Yang, 2008; Liu and An, 2018). Changes in moisture source (Z. Liu et al., 2008; Tipple et al., 2015) or fluctuations in the intensity of the North Atlantic Oscillation (NAO) could play a role in determining precipitation patterns and δ^{2}H values (Muñoz-Díaz and Rodrigo, 2004; Brittingham et al., 2019), explaining some of the variability observed through the sequence at Abric del Pastor. North Atlantic dynamics have been shown to play a significant role in the isotopic composition and variability of precipitation (Benetti et al., 2017). These effects have been recorded elsewhere in the Iberian Peninsula (Jambrina-Enríquez et al., 2017).

A negative correlation between monthly precipitation amount and precipitation δ^{2}H recorded at GNIP (Global Network for Isotopes in Precipitation; IAEA/WMO 2006) stations in Murcia and Valencia suggests that regional $\delta^{2}H_{p}$ values may be influenced to some extent by precipitation amount. Temperature is also likely to have been a significant factor, however, as this plays a role in governing soil water evaporation and leaf transpiration, which in turn affects the primary signal (Sachse et al., 2012; Kahmen et al., 2013; Wang et al., 2016). Water availability is an important control on $\delta^{13}C$ in C3 plants, which has also previously been shown in certain cases to positively correlate with MAP and relative humidity (RH) (Farquhar et al., 1989; Diefendorf et al., 2010; Garcin et al., 2014; Diefendorf and Freimuth, 2017). Co-varying trends between δ^2H_{wax} and $\delta^{13}C_{wax}$ through the sequence at Abric del Pastor could therefore be linked to the combined effects of changes in moisture source, precipitation amount and fluctuations in temperature and evaporative stress.

Evidence of generally cool conditions throughout the sequence are recorded at the microstratigraphic level by the occurrence of weakly lenticular and granular microstructures, in addition to features such as soil cappings, and frequent platy or fissured clasts characteristic of cyclical freeze-thaw processes (Vliet-Lanoë, 2010). The sequence is generally composed of laterally discontinuous sands and gravels derived from the collapse and disintegration of the limestone conglomerate which makes up the rock shelter. Faecal spherulites recorded in S.U. I may be linked to the presence of goats at the site in relatively recent times. In addition to input of fresh leaves from the modern trees and vegetation immediately adjacent to the site, this probably contributes to the elevated TOC values in S.U. I. Other sources may include the frequent occurrence of fresh root-derived OM which has been observed in several thin sections. This highlights the effects of active bioturbation, although, it should be noted that this does not uniformly affect entire the sequence, being more intense in the uppermost units (S.U. I - IVa). Good preservation of the calcitic matrix, sedimentary components, and anthropogenic material throughout most of the sequence signal generally high rates of sedimentation. Indicators of slower sedimentation rates, increased surface exposure and the presence of moisture also occur, however, in the form of redoximorphic features and instances where it is evident that the calcitic matrix has been affected by dissolution processes. This is observed in S.U. IVd, for instance, and might partially explain the degree of thermal degradation affecting *n*-alkane distributions as slower sedimentary rates produce a palimpsest effect with the concentration and superimposition of materials related to successive combustion events (Bailey, 2007; Machado et al., 2015). The occurrence of textural contrasts and sharp contacts between depositional facies suggest sedimentary accretion at the site is dynamic and responsive to external processes, most likely linked to shifting environmental conditions.

Cool temperatures are also implied by the charcoal assemblage from S.U. IVc and IVd which shows a predominance of juniper (> 50% in some subunits) relative to pine, coherent with the establishment of a cold climate during which heliophilous, dought-tolerant plants progressively developed, accompanied by a decrease in temperatures throughout the Iberian Peninsula (Sánchez-Goñi et al., 1999). Our reconstruction points to dry or semi-arid supramediterranean conditions (MAT of 8 – 13 ºC, -4 ºC and MAP of 200 – 600 mm, -80 mm), which is congruent with the observed δ^2H_{wax} and $\delta^{13}C_{wax}$ values if we accept that temperature and evaporative stress are the dominant controls. Indeed, juniper species show great resistance to changes in temperature and humidity, being physiologically adapted to stress tolerance with low demands in terms of soil (Costa et al., 2005). The homogenous anatomical structure of *Juniperus* does not allow for the discrimination of the species gathered, which could hypothetically include thermophilous species (*J. oxucedrus, J. phoenicea*) or cryophilous ones (*J. communis, J. thurifera, J. sabina*), whose present-day range covers from thermo-Mediterranean to supra-Mediterranean bioclimatic belts together with dry or semi-arid conditions (Costa et al. 2005). However, carpological data from El Salt, a Middle Palaeolithic site located 4 km away from Abric del Pastor, indicate the presence of *Juniperus sabina* (savin juniper) in the region (units VIII – Xa), at least during MIS 3 (Vidal-Matutano et al. 2018a). This taxon is currently abundant in the supra-Mediterranean and oro-Mediterranean bioclimatic belts, above 1100 –

1200 m a.s.l., occurring together with other species of the same genus (*J. communis, J. thurifera*) (Rivas-Martínez, 1987; Costa et al. 2005). The absence of thermophilous juniper at Abric del Pastor would be consistent with an anthracological assemblage reflecting a temperature range which is lower than present conditions. The appreciable percentage of mixed forest taxa in those units coinciding with decreasing values of juniper might be explained by the location of the rock shelter in a narrow ravine, where access to several plant formations is possible within a short distance (< 1 km). The presence of these plant formations, with different ecological requirements to juniper, point to the existence of a local vegetation refugium, composed of several biotopes, facilitated by the orography of the narrow ravine.

The current spatial distribution of plant taxa recorded in S.U. IV has been obtained for the Iberian Peninsula, taking into account *Juniperus communis, Juniperus ocycedrus, Juniperus phoenicea, Juniperus thurifera, Juniperus sabina, Pinus nigra* subsp. *salzmanii, Pinus nigra* subsp. *Arnold, Taxus baccata, Pistacia terebinthus, Quercus ilex ballota* and *Quercus faginea*. This is presented here alongside the distribution of the microfaunal species recorded in S.U. IVd (Fig. 3.12). The Javalambre and Gúdar mountain ranges (Teruel) and the eastern Iberian mountain system show the highest proportions of overlapping plant taxa. This mountainous region (1000 – 1500 m a.s.l.) is located at the supramediterranean bioclimatic belt with a MAT of 8 – 10 ºC and a MAP of 400 – 600 mm (Rivas-Martínez, 1987). Isolated locations are also highlighted in the Pyrenees and the Central and Betic mountain systems.

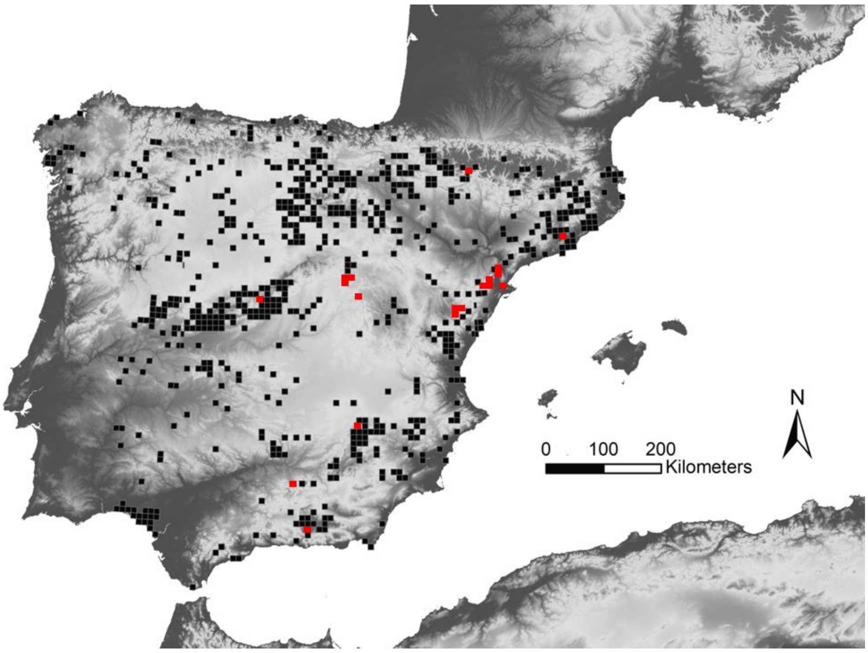

Figure 3.12 10 x 10 UTM squares obtained overlapping the distribution areas of the main plant (red squares) and small mammal, reptile and amphibian (black squares) species analysed in this study.

Our palaeoecological reconstruction based on the the microfauna suggests a similar scenario, with generally cooler (MAT -1.48 ºC) and possibly drier (411 mm to 837 mm) conditions than present. The Habitat Weighting Method indicates a predominance of open woodland environments (47%) (Appendix 1 Figure 3), which includes woodland margins and forest patches with moderate ground cover, evidenced by the abundance of *Apodemus sylvaticus*. This species is ubiquitous throughout Spain, normally occupying areas with a good shrub or tree cover (Palomo et al., 2007). Woodlands and Open Humid habitats are next most-commonly represented habitat types in S.U. IVd, although values are only approximately half those obtained for Open Woodland habitats, at 23% and 22% respectively. Species linked to rocky environments such as *Eliomys quercinus*, *Pelodytes* sp., *Coronella girondica* and Viperidae indet. are probably explained by the topographic context of the site, near a cliff. The presence of temporary water bodies is indicated by the remains of *Pelodytes* sp., despite appearing in lower proportions. The probable agent responsible for the accumulation of the assemblage, *Bubo bubo*, is a nocturnal raptor widespread throughout Europe and Asia (see Appendix 1). This species depends on a wide range of prey and its associated prey assemblages are taxonomically diverse with a high degree of equitability.

The macrofaunal assemblage from S.U. IVd is characteristic of Mediterranean conditions. Climatic reconstruction based on the CRI model yielded an AAP value of 268 mm, which is consistent with ranges obtained from other proxies. Variation in the proposed temperature values between the different datasets probably reflect the disparate depositional agents responsible for their accumulation and the differing spatial resolutions of the proxies. The taxonomic composition of the assemblage is potentially congruent with either an MIS 5 setting, or a phase of climatic amelioration during MIS 4. As such, the frequent occurrence of Mediterranean tortoise (*Testudo hermanni*) in S.U. IVd is notable. In Pleistocene chronologies, there are few archaeological deposits in the Mediterranean area where *Testudo hermanni* is present during MIS 4, limited to Cova Dalt del Tossal de la Font (MIS5d-4) and Abric del Pastor (Morales and Sanchis, 2009; Sanchis et al., 2015; Mallol et al., 2019). In fact, a recent review of Neanderthal consumption of *Testudo hermanni* in the Iberian Peninsula by Nabais and Zilhão (2019) suggests that the species may have almost completely disappeared from the peninsula at the onset of MIS 4 as a result of over-exploitation. It’s presence at Abric del Pastor is in agreement with the anthracological data which suggests that the ravine where the site is located probably acted as a vegetation refugium, providing sufficient tree and shrub cover for this species to thrive, as well as an abundant and diverse source of woody biomass which could be exploited as fuel by Neanderthal groups.

The resolution of the current chronological framework at Abric del Pastor limits the direct comparisons which can be drawn between our sequence and other regional palaeoclimate records. Nevertheless, our most complete dataset comes from S.U. IVd, which corresponds with an OSL date of 63 kya ± 5000, implying an MIS 4 or possible late MIS 5 setting. During the period in question, evidence from the upper Tagus Basin suggests the accumulation of significant loess deposits are linked to cool and dry conditions through MIS 4, but perhaps began accumulating as early as late MIS 5 (Wolf et al., 2018). This might point to the development of adverse environmental conditions in the Iberian interior, with decreasing vegetation cover limiting the availability of important resources. In such a scenario, peripheral regions along the Iberian coastline may have been more climatically favourable for Neanderthal groups. Pollen records from Area Longa (Galicia) in the north-west of the peninsula record a stadial vegetation with grassland and heathland through the earliest stages of MIS 4 (Gómez-Orellana et al., 2007; Fletcher et al., 2010), while palynological records from Abric Romaní, in the north-east, record a predominance of steppe vegetation (*Artemisia*) characteristic of generally dry and cold conditions, interspersed by rapid episodic shifts in vegetation structure which led to an increase in grasses (Poaceae) followed by a decline in pines and deciduous oaks (*Quercus*). The presence of *Betula* with *Corylus*, *Viburnum* and Mediterranean taxa, suggest that localised glacial refugia persisted during MIS 4 (Burjachs and Julià, 1994; Biltekin et al., 2019). This is in keeping with the data presented here from Abric del Pastor and taken together could predict similar conditions for MIS 4 throughout the Eastern Iberian Peninsula, pointing to a mosaic scenario with different biotopes shaped by local geographic factors.

3.6. Concluding remarks

Drawing on multiple lines of evidence, we have investigated climatic variability through the sequence at Abric del Pastor. Our data points to a generally cold but variable climate through the Pleistocene part of the sequence, as evidenced by the persistent presence of cryoturbation features in our micromorphological samples. *n*-Alkane distributions and co-varying CPI and

ACL values in S.U. IVc and IVd reflect degradation linked to the probable incorporation of charred biomass associated with anthropogenic burning events. This is supported by the archaeological evidence at the macroscopic scale where eight combustion features are recorded in S.U. IVd, as well as at the microstratigraphic scale where combustion residues are linked to microfacies which show signs of slower sedimentary rates. Fluctuations in δ^2H_{wax} and $\delta^{13}C_{wax}$ through the sequence can be explained as the combined effects of moisture source changes, regional precipitation amount and changes in atmospheric temperatures. This is consistent with our anthracological analysis of S.U. IVc and IVd which indicates a prevalence of dry to semi-arid supramediterranean conditions (MAT -4 ºC and MAP of 200 – 600 mm, -80 mm) and our reconstruction based on the small-mammal assemblage (MAT -1.48 ºC, MAP 411 mm to 837 mm). At this part of the sequence, which corresponds with an OSL date of 63 kya (± 5000 1σ), we propose a scenario where open dry woodland formations extended throughout the upper reaches of the valley, while Mediterranean mixed forest taxa and riverine species survived within the Barranc del Cinc ravine, a vegetation refugium providing adequate tree cover and ground shrubs to support species such as *Testudo hermanni,* which were exploited for subsistence by Neanderthal groups. The ravine also provided an abundant fuel source in the form of woody biomass. The occupation of the rock shelter may have formed part of a broad subsistence and mobility strategy focused on intra-mountainous valleys or ravines, like the Barranc del Cinc, which are zones of ecological resilience and biodiversity that provide opportunities for the construction of crucial econiches.

Finally, our results demonstrate the utility of a coupled biomolecular and geoarchaeological approach, however, encourage caution for future studies in archaeological contexts where microscopic residues, related to anthropogenic fire for instance, can potentially influence the molecular or isotopic signal. In such cases, soil micromorphology is a powerful tool for determining the extent of anthropogenic impact on sediments and establishing vital constraints for the interpretation of biomolecular data.

Chapter 4: Investigating the palaeoenvironmental context for the disappearance of Neanderthals in Eastern Iberia: a multiproxy study of Stratigraphic Units VIII – V (upper) at El Salt (Alcoy)

Rory Connolly [1, 2], Cristina Val-Peón [3], Antonio V. Herrera-Herrera [1], Margarita Jambrina-Enriquez [1, 4], Lucia Leierer [1, 2], Carolina Mallol [1, 2]

1. Instituto Universitario de Bio-Organica Antonio Gonzalez (IUBO), Universidad de La Laguna, 38206, Canary Islands, Spain. rconnoll@ull.es; mjambrin@ull.edu.es; avherrer@ull.edu.es; lucia.leierer@gmail.com; cmallol@ull.edu.es
2. Departmento de Geografia e Historia, Universidad de La Laguna, 38200, Canary Islands, Spain.
3. Institute of Neotectonics and Natural Hazards, RWTH Aachen University, Lochnerstrasse 4-20, 52056 Aachen, Germany
4. Departamento de Biología Animal, Edafología y Geología, Facultad de Ciencias, Universidad de La Laguna, 38200, Canary Islands, Spain.

Abstract

Here we present a multiproxy palaeoenvironmental study from Stratigraphic Units VIII – V (upper) at the Middle Palaeolithic site of El Salt (Alcoy, Spain), which hosts a long sequence of Late Pleistocene deposits yielding abundant evidence for recurrent Neanderthal occupations through the course of Marine Isotope Stage 3 (MIS 3). Site formation processes have been reconstructed through the application of soil micromorphology and the sedimentary sequence has been analysed for lipid biomarker *n*-alkane abundances (CPI, ACL, VPD, LAR, P*aq*), compound-specific isotope analysis (δ^2H_{wax} and $\delta^{13}C_{wax}$), bulk organic geochemistry (TOC), and pollen/non-pollen palynomorphs. Our results are in line with other regional studies and support previous palaeoecological research at this site which suggests that the cessation of Neanderthal activity in Eastern Iberia *c.* 45 kya coincides with a scenario of widespread aridification.

4.1. Introduction

The disappearance of Neanderthals from the archaeological record *c.* 40 kya, and their subsequent placement by anatomically modern humans (AMH) across Europe, is a defining characteristic of the Middle to Upper Palaeolithic transition (MUPT), a process widely regarded as amongst the most significant cultural transitions to have occurred in the course of human evolution (Blockley et al., 2008; d'Errico and Sánchez Goñi, 2003; Finlayson et al., 2007; Greenbaum et al., 2018; Mellars, 2004; Morley, 2012; Villa et al., 2018; Villa and Roebroeks, 2014; Zilhao, 2006). There remains, however, considerable debate regarding the extent to which climatic change should be considered a driving factor in this process (Blain et al., 2013; Burke et al., 2014; Defleur and Desclaux, 2019; Finlayson, 2004; Finlayson and Carrión, 2007; Jiménez-Espejo et al., 2007; Müller et al., 2011; Roberts and Bricher, 2018; Sepulchre et al., 2007; Staubwasser et al., 2018; Wakano et al., 2018; Wolf et al., 2018). Owing to its geographical situation and the possible late survival of Neanderthals in this region, the Iberian Peninsula has long been considered a key location for understanding Neanderthal adaptation to climate. It has been suggested that the southern and eastern margins of the peninsula may have provided local refugia with conditions favourable to Neanderthal survival during periods of wider global climatic deterioration (Finlayson et al., 2007; Jennings et al., 2011; Ochando et al., 2019).

The climatic and environmental framework for Iberia during Marine Isotope Stage 3 (MIS 3) (57-29 kya) is largely drawn from off-shore marine cores, peat deposits, and speleothems, while palynological, palaeobotanical and palaeontological material recovered from archaeological contexts has provided an additional source of information (Burjachs et al., 2012; Daura et al., 2017; Esteban et al., 2017; López-García et al., 2014, 2012; Ochando et al., 2019). These records indicate highly variable conditions which fluctuated between extremely cold episodes with occasionally short-lived warm intervals linked to globally significant Heinrich events and Dansgaard-Oeschger (D/O) oscillations (Fletcher et al., 2010; Naughton et al., 2009; Roucoux et al., 2001, 2005; Sánchez Goñi et al., 2008; Sanchez Goñi and Harrison, 2010). Throughout Heinrich events, mean annual precipitation (MAP) in Iberia is estimated to have been approximately 400 mm less than current values, with winter temperatures between 6 - 13 °C lower. More temperate climate phases, on the other hand, are marked by MAP values between 600 - 800 mm and winter temperatures between 5 - 10 °C, similar to conditions experienced throughout the peninsula today (Cacho et al., 1999; d'Errico and Sánchez Goñi, 2003; Sánchez Goñi et al., 2008). Cold phases with low MAP values resulted in the development of large areas dominated by desert-steppe vegetation which saw a reduction in vegetation cover to less than 25 % of present-day values (d'Errico and Sánchez Goñi, 2003; Sepulchre et al., 2007).

The final phase of Neanderthal demographic collapse has been attributed by some to an episode of abrupt aridification and climatic cooling during Heinrich Event 4 (HE 4) between 39 - 40 kya (Bradtmöller et al., 2012; e.g. d'Errico and Sánchez Goñi, 2003; Mellars, 2006). There is, however, mounting evidence that in several locations the disappearance of Neanderthal groups occurred prior to the onset of HE 4 (Higham et al., 2014; Wood et al., 2013). Here, we combine a range of palaeoenvironmental techniques to investigate a sedimentary sequence from Stratigraphic Units (S.U.) VIII - V (upper) at the Middle Palaeolithic site of El Salt in Eastern Iberia, where a recent TL and OSL dating program has indicated the disappearance of the local Neanderthal population c. 45 kya (Galván et al., 2014).

4.2. Materials and methods

4.2.1. Site background

El Salt (38˚41'14" N, 0˚30'32" W, 680 a.s.l.) is an open-air Middle Palaeolithic site situated *c.* 3 km outside the city of Alcoy, immediately south-east of the Sierra de Mariola in a mountainous region of Eastern Iberia's central Mediterranean coast, close to the Serpis and Barxell rivers (Fig. 4.1). Archaeological excavations, which are ongoing since 1986 and led by a multidisciplinary team from the Universidad de La Laguna, have yielded abundant evidence for recurrent Neanderthal occupation activity between 60.7 ± 8.9 and 45.2 ± 3.4 ka BP (Fagoaga et al., 2018; Galván et al., 2014, 2001; Garralda et al., 2014; Gómez de la Rua et al., 2010; Leierer et al., 2019; Machado et al., 2017, 2015; Mallol et al., 2013; Rodríguez-Cintas and Cabanes, 2017; Sistiaga et al., 2014; Vidal-Matutano et al., 2018b). Activity areas at the site are concentrated at the base of a 38 m high Palaeocene limestone cliff which is covered by partially active tufa/travertine formation and formed along a thrust fault. Tufa formation is driven by an 80 m episodic waterfall which is fed by the Barxell River and Pou del Barxell spring (806 m a.s.l.), located 3.6 km upstream (Ordóñez et al., 2016). El Salt is today situated in a mesomediterranean bioclimatic belt with MAP values >500 mm and a mean annual temperature (MAT) of 14 °C (Rivas-Martınez, 1987).

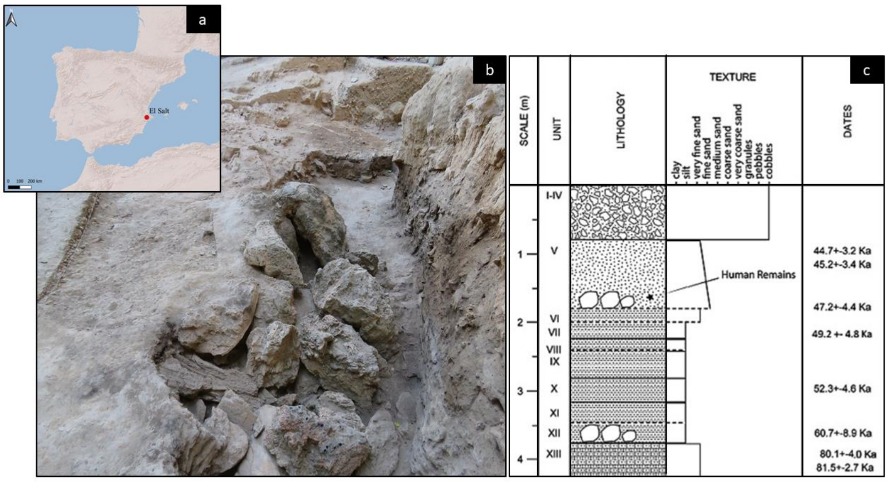

Figure 4.1 El Salt Middle Palaeolithic site: (a) Map showing location of the site on the Iberian Central Mediterranean coast; (b) Photograph of site excavation surface. Note the large limestone blocks from the roof collapse; (c) Stratigraphic log showing the position of the recovered human remains and absolute dates (after Galván et al., 2014).

The sequence hosts a 6.3 m thick deposit which has been divided into thirteen primary stratigraphic units (S.U. XIII - S.U. I), broadly grouped according to their macroscopic textural characteristics and their archaeological content (Galván et al., 2014): S.U. XIII at the base of the sequence is an archaeologically sterile travertine platform. Dating by U-Th places this between 81.5 ± 2.7 kya and 80.1 ± 4 kya (Fumanal, 1994). S.U. XII - S.U. IX (~1.5m) is formed by horizontally bedded fine geogenic sands overlaying a clastic facies at the base of this segment, which contains a number of considerably large blocks, pointing to a significant collapse event. Archaeological material is abundant in this part of the sequence, being particularly concentrated in S.U. X, which yielded a large number of simple flat combustion structures with associated faunal and lithic assemblages (Leierer et al., 2019; Machado and Pérez, 2015; Mallol et al., 2013). S.U. VIII to S.U V (lower) (1.5 - 2.8 m) is composed of horizontally bedded geogenic sands, S.U. VI is sealed by large blocks which suggest another significant collapse event. The concentration of archaeological material in this part of the sequence is marked by a notable decrease both laterally and vertically. S.U. V (upper) (~0.5 m) is characterised by sandy silt with medium to large gravel in the top 20 cm. Archaeologically only two small flint blades, occasional debitage and a single combustion feature are recorded here. S.U. IV - S.U. I (~1.3 m) consist of irregular beds of gravel and cobbles within a silty clayey matrix. Stratification is evidently quite disturbed with Neolithic pottery having been recovered commingled with late Upper Palaeolithic, Epipalaeolithic and Mesolithic materials.

A previous study of the small mammal assemblage recovered from S.U. Xb (52.3 ± 4.6 ka) indicated relatively cold and humid conditions in an environment composed predominantly of open woodlands and a patchwork of dry and humid meadows (Fagoaga et al., 2018), while anthracological and carpological analyses of plant remains recovered from S.U. Xb, Xa, IX, and XIII (52.3 ± 4.6 ka to 49.2 ± 4.8 ka) pointed to a predominance of sub-humid supra-Mediterranean conditions (MAT 8–13 °C and MAP 600–1000 mm) (Vidal-Matutano et al., 2018b). A more recent study of the small mammal assemblage recovered from S.U. V (upper) (45.2 ± 3.4 ka to 44.7 ± 3.2 ka) suggests an arid climatic setting at this part of the sequence, around the time of the final Neanderthal occupations at the site (Fagoaga et al., 2019). Here, we focus on S.U's VIII – V (upper) (Fig. 4.2).

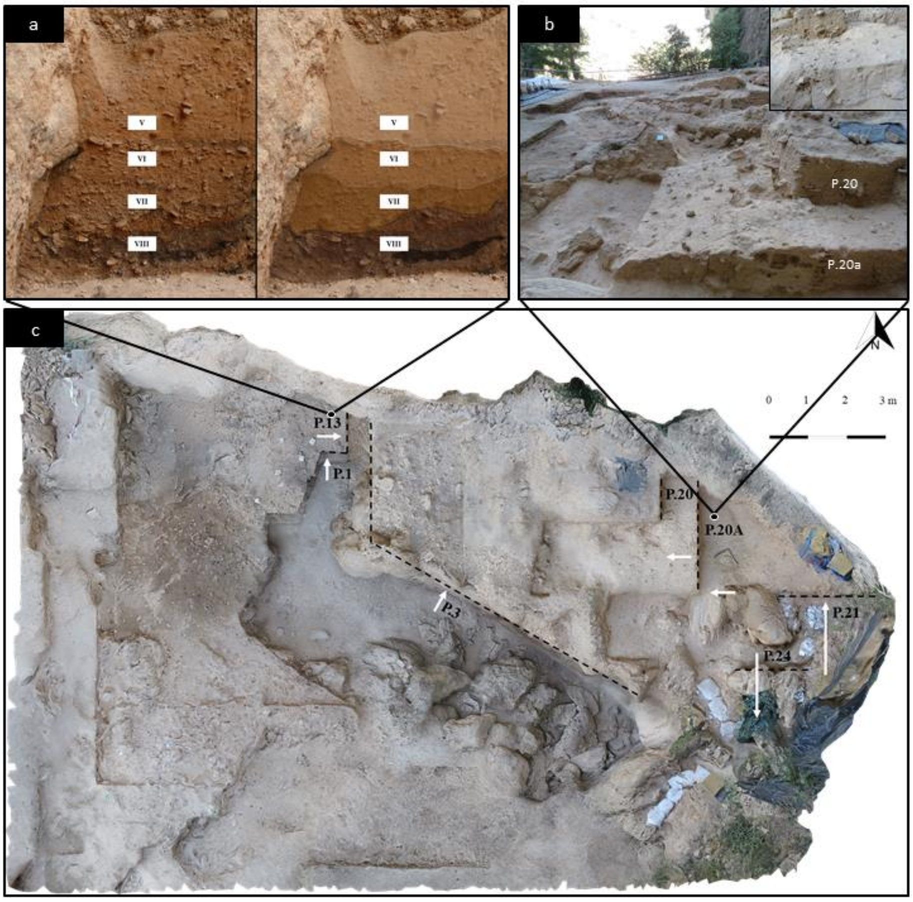

Figure 4.2 Sediment profiles mentioned in this study: (a) Photograph of P.13 with stratigraphic units highlighted and labelled; (b) Photograph of P.20 and P.20a which comprise S.U. V (upper). Inset shows a close-up of the fine sediments recorded at this part of the sequence; (c) Site orthophotograph with profiles highlighted and numbered.

4.2.2. Soil micromorphology

Intact, oriented blocks of sediment from S.U. VIII - S.U. V (upper) were extracted from selected profiles (P.1, P.3, P.13, P.21 and P.24) for micromorphological analysis. The goal of applying this technique was to characterise site formation processes and the local sedimentary context, identifying features at the microstratigraphic scale which may be linked to particular environmental conditions.

Samples were oven-dried at 60 °C for 48 hours and subsequently impregnated with a mixture of polyester resin (Palatal strained resin UN1866, TNK composites), styrene (Styrene monomer [CAS: 100-42-5] UN2055, TNK composites) and catalyser (Luperox [CAS: 78-93-3], TNK composites) in a 7:3:0.1 ratio. After hardening, a Euro-Shatal M31100 radial saw was used to cut the blocks into 1 cm-thick slabs. Samples were sent to Spectrum Petrographics (Vancouver, WA, USA) for thin section manufacture (7 cm x 5 cm x 30 µm) and micromorphological analyses were carried out using a Nikon E200 polarising microscope. Descriptions follow the standard guidelines set out in Stoops (2003) and Nicosia and Stoops (2017).

4.2.3. Total Organic Carbon (TOC)

TOC (%) was analysed with a LECO SC 144DR furnace at the Instituto Pirenaico de Ecología (IPE-CSIC), Spain.

4.2.4. Lipid biomarker analysis (n-alkanes)

Sediment samples (5-10 g) from S.U. VIII – V (upper) were collected from P.13, P.20, P.20a, and P.21 at a 1-5 cm interval. The black layers (BL) at the base of S.U. VIII were not sampled for lipids to avoid anthropogenic combustion residues. Lipid biomarker analyses were conducted at the Archaeological Micromorphology and Biomarkers Laboratory (AMBI), Universidad de La Laguna, Tenerife.

Samples were oven-dried at a temperature of 60 ºC for 24 h prior to extraction. Extraction of the target alkanes from sediments was carried out following the optimised QuEChERS method set out by Herrera-Herrera et al. (2020) based on the original methodology proposed by Anastassiades et al. (2003). 5 g of sediment was transferred to a 50 mL PTFE tube and one spherical glass ball was included. 10 mL of DCM as extraction solvent was added and the mixture was manually shaken for 1 min. IS was added (1 µL 400 mg/L) and the tube was again manually agitated for 30 s. 4 g of $MgSO_4$ and 1 g of NaCl were subsequently added. Manual agitation was again carried out for a duration of 1 min and the mixture was centrifuged at 4700 r.p.m. for 5 min using a Mega Star 1.6 from VWR International (Barcelona, Spain). The supernatant (approx. 6 mL) was then transferred to another 50 mL PTFE tube containing 150 mg of MgSO4 and 25 mg of PSA (clean-up sorbent). This was manually agitated for 30 s and centrifuged at 4700 r.p.m. for 5 min. The supernatant was collected and evaporated under a nitrogen flow using an Organomation evaporator (Massachusetts, USA). The residue was reconstituted in 50 µL of hexane prior to injection in the GC-MS system.

Identification of individual compounds was carried out by comparison of retention times and mass spectra to those of reference compounds (mix C_8-C_{40} and 5α-androstane, Supelco) and mass spectral library databases (NIST). Quantification of concentrations was achieved using calibration curves obtained which plot the ratio Area/Area$_{IS}$ versus the concentration of reference compounds. Correlation coefficients for each sample were higher than 0.995. Concentration is expressed here in terms of µg of individual compound per gram of dry sample (µg gds^{-1}). Concentration of *n*-alkanes are calculated using calibration curves following the recommendations of Herrera-Herrera et al. (2020).

The Average Chain Length (ACL) was calculated following Poynter et al. (1989) and Freeman and Pancost (2013) using the C_{18} - C_{35} interval: $ACL_{18\text{-}35} = \Sigma(Ci \times [Ci]) / \Sigma[Ci]; 18 \leq i \leq 35$
The mean annual Vapour Pressure Deficit (VPD$_{av}$) was calculated following Eley and Hren (2018): $VPD = 1.3125 - \sqrt{14.1208 - 0.4629 \text{ x } ACL}$

The Carbon Preference Index (CPI) value (C_{18} to C_{35}) follows the equation set out in Bray and Evans (1961) and Cooper and Bray (1963): $CPI_{25–33} = [(\Sigma C_{25–33odd}/\Sigma C24–32_{even}) + (\Sigma C_{25\text{-}33odd}/\Sigma C_{26–34even})] \times 0.5$

Values > 1 denote an odd over even preference (OEP) while values < 1 are indicative of an even over odd preference (EOP).

The Paq index was calculated following Ficken et al. (2000): Paq = $(C_{23} + C_{25})/(C_{23} + C_{25} + C_{29} + C_{31})$

The value [Ci] represents the *n*-alkane concentration where i is the number of carbon atoms. The relative contribution of *n*-alkanes C_{29} and C_{31} through the sequence was assessed using long-chain n-alkane ratios (LARs): $C_{29} / (C_{29} + C_{31})$

4.2.5. Compound specific isotope analysis (CSIA)

Isotope analysis of individual *n*-alkanes was carried out using a Thermo Scientific Isotope Ratio Mass Spectrometer Delta V Advantage coupled to a GC Trace1310 through a Conflo IV interface with a temperature converter GC Isolink II. A Trace Gold 5-MS (Thermo Scientific) fused silica capillary column ((5%-diphenyl)-dimethylpolysiloxane, 30 m length x 0.25 mm i.d., 0.25 μm film thickness) was used. The helium carrier gas flow rate set was set at 1.5 mL/min. All measurements were carried out in triplicate. Isodat 3.0 software (Thermo Scientific) was employed for data acquisition and processing.

Here, carbon ($\delta^{13}C$) and hydrogen ($\delta^{2}H$) isotope values are reported for n-alkanes C_{29} and C_{31}. Samples were injected using a Programmed Temperature Vaporising injector (PTV) in splitless mode. Temperatures initially increased from 60 °C to 79 °C (held 30 s, rate 10 °C/min) and then to 325 ºC (held 3 min, rate 10 ºC/s) and finally to 350 ºC (held 3 min, rate 14 ºC/s). For the GC oven, a 2 min isothermal period at 70 ºC increasing to 140 ºC (held 2 min, rate 12 ºC/min) was followed by an increase to 320 ºC (held 15 min, rate 3 ºC/min). The high-temperature conversion (HTC) oven was maintained at 1000 ºC during carbon isotope analysis and 1420 ºC during hydrogen isotope analysis. Values were normalised to the Vienna Pee Dee

Belemnite (VPDB) scale ($\delta^{13}C$) and Vienna Standard Mean Ocean Water (VSMOW) scale (δ^2H) using an *n*-alkane Schimmelmann type A6 mixture (nC_{16} to nC_{30}) of known isotopic composition (Arndt Schimmelmann; Biogeochemical Laboratories, Indiana University). Reproducibility was greater than ± 0.5‰ for carbon isotope measurements and ± 5.0‰ for hydrogen isotope measurements.

4.2.6. Pollen

A total of 42 samples were collected from four different profiles: 28 from P.13, 5 from P.20, 6 from P.20a, and 4 from P.21. P.13 was sampled at 1-5 cm interval, while the other profiles were sampled every 10 cm.

Samples were chemically treated according to the modified Goeury and de Beaulieu (1979) methodology described by Burjachs et al. (2003). The treatment includes hydrochloric acid (HCl) to remove carbonates, NaOH digestion to remove humic acids, Thoulet heavy liquid (2–2.1 cm3/g) for densimetric extraction of palynomorphs, and hydrofluoric acid (HF) to destroy glass-fibre filters. Palynomorphs were counted in an optical microscope at 40x and 1000x to a minimum pollen sum of 150 terrestrial pollen grains. They were identified using published keys (e.g. Moore et al., 1991; Reille, 1992, 1995) and a modern pollen reference collection.
Palynological diagrams were plotted using TiliaIT software, version 2.0.41 (Grimm, 1991–2015). General pollen results are expressed in percentages, as well as taxonomic variability. They are divided into arboreal pollen (AP) and non-arboreal pollen (NAP) to conform to the European Pollen Database (EPD) standard (http://www.europeanpollendatabase.net/). Different pollen zones are defined using a stratigraphically constrained cluster analysis (CONISS) (Grimm, 1987). Although cluster was included, zones were not highlighted in the diagram to focus instead on the differences between the different stratigraphic units.

To plot a diagram, it was necessary to sum some components. The basis sum includes the arboreal and non-arboreal elements (AP/NAP). Some taxa are usually excluded from this sum because, due to factors in their production and dispersion, they are overrepresented and can distort our results. In archaeological deposits, and more specifically in caves and rock-shelters, the presence of entomophilous pollen grains can be related to human or animal activity (González Sampériz, 1998); one well-known example is Asteraceae (Bottema, 1975; Carrión, 1992; Carrión and Munuera, 1997). Sometimes, taxa may occur in lumps, and it is considered that a significant portion of these pollen grains may be buried by insects (Bottema, 1975; Davis and Buchmann, 1994). For these reasons, the following taxa were excluded from our basis sum and included in the total pollen sum: Cyperaceae, Asteraceae (Cardueae, Asteroideae, Liguliflorae type, and *Centaurea*) Apiaceae, and Liliaceae.

4.2.7. Non-Pollen Palynomorphs (NPPs)

Non-pollen palynomorphs (NPPs) are microfossils included in sediments that are processed for palynological analysis. They are sub-fossil remains of a great variety of organisms that can be sensitive to various ecological parameters or to human presence (Miola, 2012). Although some NPPs have been identified and related to specific conditions, the origins of most of them remain unknown. NPPs were counted under the microscope alongside the identification of pollen grains. Diagrams were plotted using TiliaIT software, version 2.0.41 (Grimm, 1991–2015). Different zones were defined using a stratigraphically constrained cluster analysis (CONISS) (Grimm, 1987). As before, zones were not marked in the diagram to better highlight the differences between archaeological levels.

4.3. Results

4.3.1. Soil micromorphology

Samples are generally composed of similar sedimentological and lithological components, although abundances and degree of weathering vary considerably within and between different stratigraphic units. This is represented by an organic-rich heterometric mix of quartz sand, detritic tufa and travertine from an Upper Pleistocene freshwater spring system, as well as micritic peloids and fossiliferous micritic to microsparitic limestone derived from the physical weathering and disaggregation of the local bedrock. Here, we have arranged the lithological fraction into lithology types A, B, B*, C, D and E (Table 4.1) according to the distribution of lithological elements and textural classes. The fine mass throughout the sequence is composed of calcitic-crystallitic clayey silt which is locally decalcified (Fig. 4.3) or undifferentiated and the predominant microstructure throughout is described here as intergrain microaggregate, although locally massive, granular and vughy microstructures are also recorded. The same organic components are ubiquitous throughout the sequence; this includes *Celtis sp.* seed coatings, coprolites (massive and fibrous), guano accumulations, bone fragments, charcoal, flint debitage, calcitic wood ash, fat-derived char, and microfaunal remains (Table 4.2). Detailed descriptions of each thin section sample are provided in Appendix 2.

LT	QUARTZ s	vfs	fs	ms	cs	vcs	g	MICRITIC PELOIDS s	vfs	fs	ms	cs	vcs	g	TUFA & TRAVERTINE s	vfs	fs	ms	cs	vcs	g	FOSSILIFEROUS QUARTZ RICH LIMESTONE s	vfs	fs	ms	cs	vcs	g	FOSSILIFEROUS MARL s	vfs	fs	ms	cs	vcs	g
A	1A	1A	1A	1S					1R	1R	1R				2S	2S	2S	2S	2R	2R	2S			2S	2S	2S	2S	2S			1S	1S	1S	1S	
B	2A	2A	2A	2S					3R	3R	3R				1S	1S	1S	1S	1S	1S				1S	1S	1S									
B*	2A	2A	2A	2S					3R	3R	3R				1S	1S	1S	1S	1S	1S				1S	1S	1S	1S	2A							
C	1A	1A	2A	2A					1R	1R	1R				2S	2S	2S	2S	2R	2R	2S					1S	1S								
D	1A	1A	1A	1S					1R	1R	1R				1S	1S	1S	1S	1S	1S															
E	1A	2A	2A	1S					1R	1R	1R							1S	1S	1S				1S	1S	1S									

Table 4.1 Lithology types (LT) present through the sedimentary sequence at El Salt. Textural classes follow the Wentworth scale used for the classification of fine sediment: silt (s, 50 – 2 µm), very fine sand (vfs, 125 – 50 µm), fine sand (fs, 250 – 125 µm), medium sand (ms, 500 - 250 µm), coarse sand (cs, 1000 - 500 µm), very coarse sand (vcs, 2000 – 1000 µm), gravel (g, >2000 µm). Key: 1 = rare/few (0 – 15 %), 2 = common (15 – 50 %), abundant/dominant (>50 %), angular (A), subangular/subrounded (S), rounded (R).

COMPONENT	DESCRIPTION	VIII	VII	VI	V (LOWER)	V (UPPER)
SEED COATINGS	Seed coatings from the *Celtis sp.* plant are ubiquitous throughout the sequence, ranging from fragments of *c.* 150 µm to more complete examples over 1 cm. Occasionally fragmented or bumed examples occur in association with combustion residues. Previously reported in El Salt S.U. Xb by Mallol et al. (2013), Rodríguez-Cintas et al. (2017), and Vidal-Matutano et al. (2018b).	2S	3S	2S	1S	1 S
COPROLITES	Phosphate-rich massive and fibrous coprolites of herbivore origin are recorded in several units through the sequence. Frequently exhibit micrometre-sized plant pseudomorphs. Previously reported in El Salt S.U. Xb by Leierer et al. (2019).	2S	2S	2S	1S	1S
PHOSPHATE	Phosphatic features of the El Salt sequence are predominantly associated with guano (from birds or bats), which is isotropic in XPL and appears in PPL as pale yellow to yellow amorphous concentrations which exhibit a bedded spongy microstructure and vughy porosity. Phosphatic crusts are also recorded in several units and may indicate prolonged surface exposure and human site abandonment (Karkanas et al., 2017).	3	3	3	2	2
GYPSUM	Authigenic mm-sized gypsum nodules/crystals occur throughout the El Salt sequence but seem to be particularly prevalent in S.U. V (lower and upper). These appear as infillings within the interstitial void space, although a few gypsic coatings have been recorded. Their presence is consistent with secondary mineral formation linked to repeated cycles of post-depositional dissolution and re-precipitation (Poch et al., 2018), although the diagenetic alteration of guano may account for a small amount of the observed gypsum (Goldberg et al., 2009; Shahack-Gross et al., 2004)	1	2	2	3	3
CHARCOAL	Charcoal fragments, typically < 500 µm, are ubiquitous throughout the El Salt sequence, although there is considerable variation in the proportions and spatial organisation both within and between units. In some samples, local concentrations of charcoal fragments appear angular, these are generally associated with anthropogenic combustion features, whereas in other samples, diffusely bedded charcoal fragments interspersed throughout the matrix appear sub-rounded to rounded. Both woody and fibrous charcoal are recorded, although woody charcoal predominates. Though few, the presence of	3A	3A	3A	1S	1S

	finely laminated fibrous charcoal may indicate monocotyledonous plants (Miller and Sievers, 2012; Miller et al., 2013). This is consistent with anthracological analysis conducted on S.U. Xb - VIII by Vidal-Matutano et al. (2018b).					
CHAR	Small fragments, < 300 µm, of char are rare. Where present, these occur as sub-rounded isotropic fragments of massive black glassy material with a vesicular texture. These have previously been recorded in micromorphological samples from El Salt as well as other archaeological contexts containing combustion residues (Leierer et al., 2019; Goldberg et al., 2009), and are most likely linked to the combustion of animal and plant fats.	-	1S	-	-	-
PHYTOLITHS	Some of the units from El Salt contain numerous phytoliths. These are identified as elongate psilate morphotypes and often appear as clusters, both in anatomical connection and loose. Phytoliths from El Salt have previously been described for S.U. Xb by Rodríguez-Cintas et al. (2017).	2	1	2	1	1
BONE	Bone fragments occur in all samples from the El Salt sequence. These are generally sand to cm-sized pieces predominantly derived from small mammals. Appear as angular to sub-angular/sub-rounded fragments, yellow to white in colour (PPL). In some samples associated with anthropogenic combustion activities, fragments appear burned or calcined. Spatial distribution varies between units, with fragments sometimes appearing to be interspersed chaotically throughout the matrix, and other times appearing to be diffusely bedded.	3S	3S	2S	2S	2S
FLINT MICROFLAKES	Cryptocrystalline flint microflakes of anthropogenic origin are recorded in several units at El Salt. These appear as angular fragments ranging in size from 500 µm to 1 cm,and are pale yellow in colour (PPL). Some fragments show moderate weathering and signs of fissuring, which may be related to heating. Similar microflakes have been recorded from El Salt S.U. Xb in association with combustion features, as well as a wide range of other sites (Angelucci, 2010; Leierer et al., 2019).	-	2A	2A	-	-
ROOF SPALL	In addition to the large limestone boulders that seal S.U. VI, elongated sub-angular to sub-rounded fragments derived from the spalling of material from the Palaeocene limestone cliff and shelter roof are found throughout the sequence. These include fossiliferous limestone, recrystallised tufa, and travertine, and have previously been reported by Mallol et al., (2013) and Leierer et al., (2019) in S.U. Xb.	2S	2S	2S	1A	1A
ORGANIC PARTICLES (BLACK OM)	Silt to sand-sized particles of finely comminuted, humified organic matter and fibrous organic material is recorded in several units at El Salt, although the abundance varies considerably between units. In all likelihood these materials are the product of natural agents and reflect the remains of decayed plants. Their deposition can be linked to the presence of leaf litter from surrounding vegetation, or alternatively to faunal activity such as nesting birds (Miller et al., 2013). Anthropogenic activity may also account for some of the accumulation of organic particles.	3	2	2	1	1

Table 4.2 Components identified in thin section from micromorphological samples from El Salt. Key: 1 = rare/few (0 – 15 %), 2 = common (15 – 50 %), abundant/dominant (>50 %), angular (A), subangular/subrounded (S), rounded (R).

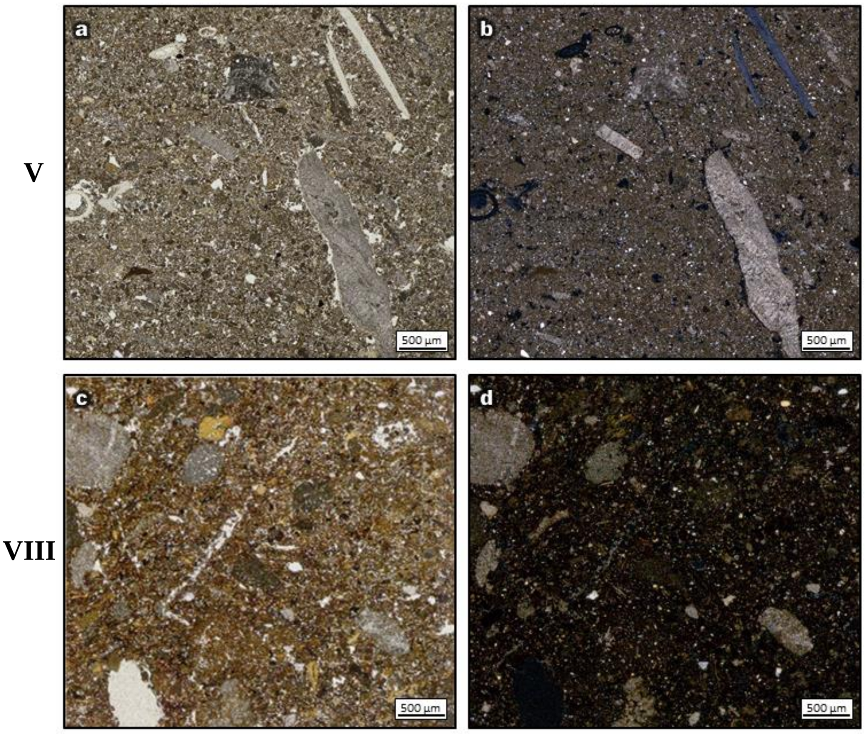

Figure 4.3 Photomicrographs (XPL, cross-polarised; PPL, plane-polarised) of a sedimentary matrix showing the calcified (a. PPL; b. XPL) and decalcified (c. PPL; d. XPL) groundmass typical of S.U. V and S.U. VIII respectively.

S.U. VIII

S.U. VIII is characterised by lithology types A and C, composed of diffusely bedded, moderately sorted, detrital sand and gravel and decalcified groundmass. The presence of intact and fragmented guano crusts is a recurrent feature in this unit. A thin layer of anatomically connected phytoliths is also identified here, as well as disarticulated phytoliths scattered throughout. Their presence at this part of the sequence is noteworthy as they are typically absent or poorly represented in S.U. V, though it is worth noting that a previous study has shown that phytoliths are a common feature of unit Xb (Rodríguez-Cintas et al., 2017). Charcoal fragments and silt to sand-sized organic particles (black OM) are abundant throughout this unit. Pockets of phosphate, massive and fibrous coprolites, authigenic gypsum infillings, fragments of bone and shell, *Celtis sp.* seed coatings and flint debitage also occur.

S.U. VII

S.U. VII is lithologically very similar to S.U. VIII, being composed of lithology types A and C. Here, however, the diffusely bedded detrital sand and gravel appears more poorly sorted. This unit is locally bioturbated, as evidenced by the presence of channels and chambers infilled by faecal excrements produced by endogeic earthworms or another soil mesofauna. There is a reduction in the abundance of organic particles (black OM) relative to S.U. VIII, however, biogenic components are also marked by a significant increase in the number of seed coatings, charcoal, and large bone fragments (burned and unburned) as well as the presence of calcitic wood ash. A black anthropogenic combustion layer is recorded in samples from P.3. Diagenetic alteration of this unit is also evidenced by the presence of yellowish phosphatic hypocoatings (reaction rims) affecting limestone and travertine gravel, and gypsum is more abundant than S.U. VIII.

S.U. VI

Lithology type A predominates throughout this stratigraphic unit, which is characterised by poorly sorted detrital sands and gravel, dominated by tufa grains showing signs of physicochemical weathering. Phosphatic clay, phosphatic grains and guano are recorded throughout. The abundance of organic particles, gypsum infillings and biogenic components are largely similar to S.U. VII although seed coatings are notably less abundant in samples from P.3. Post-depositional bioturbation is very evident in this unit, evidenced by the presence of faecal pellets and anorthic clay nodules. A thin black lens linked to anthropogenic combustion is recorded in thin sections from P.21, with an abundance of charcoal and burned bone. Clusters of articulated phytoliths are also recorded here. A relatively intact guano crust is recorded in the upper part of this unit from P.24.

S.U. V (lower and upper)

The transition from S.U. VI to S.U. V (lower) is marked by a notable change in the style of sedimentation (Fig. 4.4). At the macroscopic scale, this is observed in the field as a shift to much finer reddish sediments. At the microstratigraphic scale, this unit is characterised by lithology type B, being predominantly composed of diffusely bedded, moderate to well-sorted, fine calcitic sand. There is a notable reduction in the abundance of fine organic particles throughout these units. An increase in the abundance of gravel is recorded in S.U. V (upper) relative to S.U. V (lower). The fresh state of the coarse fraction points to relatively high rates of sedimentation, and the abundance of gypsum infillings is markedly increased relative to the underlying units. Anthropogenic material, such as charcoal, is relatively rare, and there is an observed decrease in the occurrence of *Celtis sp.* seed coatings. This is detected in samples from P.1, P.3 and P.21, suggesting this is not a localised effect and likely reflects a reduction in the presence of *Celtis sp.* in the vicinity of the site.

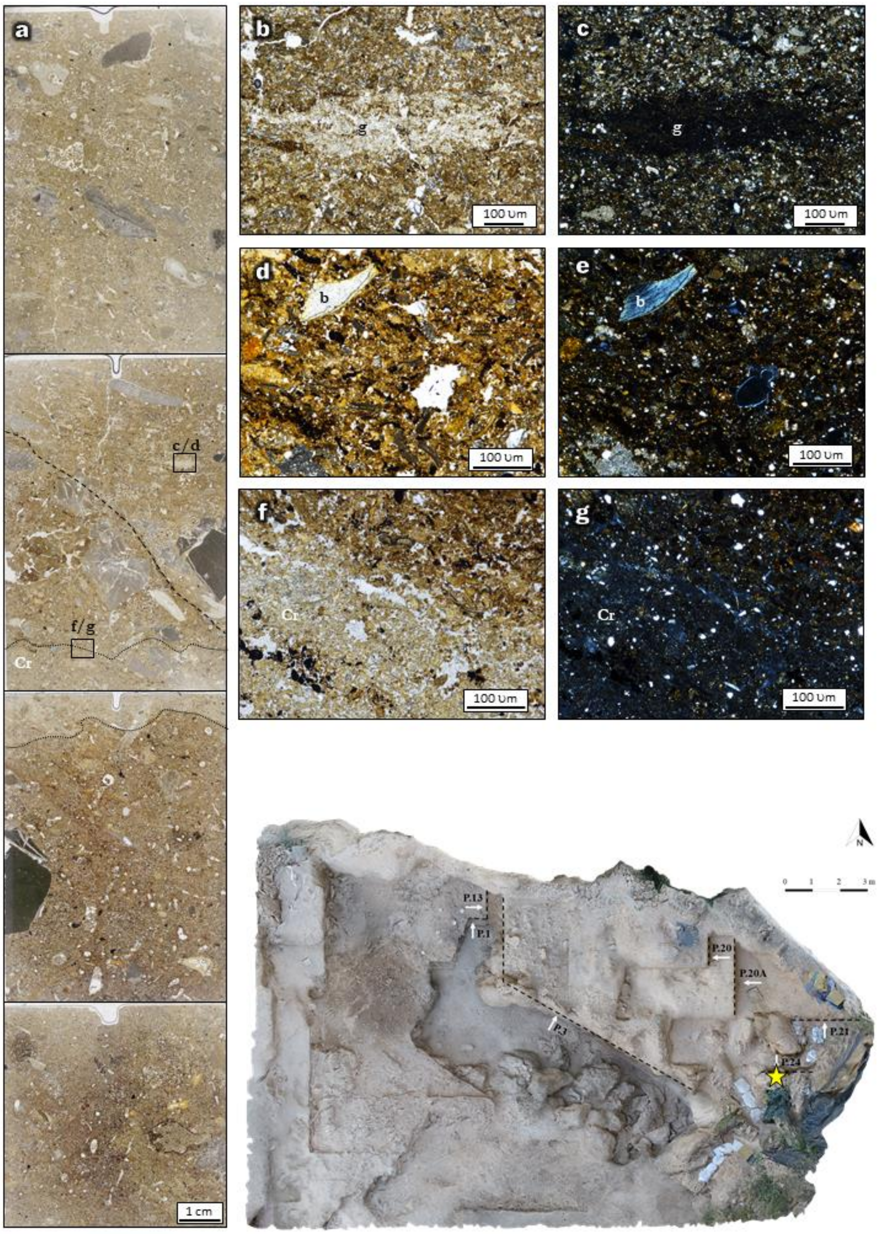

Figure 4.4 Flatbed scan of block sample from P.24 of a sedimentary matrix showing the stratigraphic contact between S.U. VI and S.U. V (lower) overlying. Note the presence of a phosphatic crust [Cr] below the level of the contact (a); decayed guano [g] mixed with sandy coarse fraction in PPL (b) and XPL (c); Organic and phosphate-rich matrix with abundant seed coatings and bone [b] fragments in PPL (d) and XPL (e); Phosphatic crust [Cr] indicating periods of surface stabilisation in PPL (f) and XPL (g). Orthophotograph indicates the position of P.24 within the site.

4.3.2. TOC (%) and sedimentary n-alkanes

The results from TOC (%) and analysis of sedimentary *n*-alkanes are presented in Figure 4.5 and Table 4.2. TOC ranged from 0.02 to 1.77%, with an average of 0.74%. The highest concentration was recorded in S.U. VIII, while the lowest concentration comes from S.U. V.

The sequence has an average total *n*-alkane concentration of 0.25 μg/g of dry sediment. Quantified samples range between 0.04 and 0.97 μg/g, with higher concentrations generally coming from the uppermost part of S.U. V. It was possible to identify *n*-alkanes in their individual chromatograms for two samples from S.U. VII but these occur at concentrations below the limit of quantification and so have been excluded. The dominance of odd over even long-chain homologues (OEP), typical of terrestrial leaf waxes, is quantified and assessed by CPI values which range from a minimum of 2.1 to a maximum of 14.1, with a mean of 5.4, indicating that lipids were not subject to significant microbial degradation. The best preservation is recorded in S.U. V (upper) (P.21).

P*aq* values throughout the sequence generally vary between 0–0.4, which is within the expected range for higher order terrestrial plants, except for one sample from S.U. VI which recorded a value of 0.5, indicating a mix of terrestrial and aquatic plant input at this part of the sequence. ACL values, which reflect broad changes in plant community composition, ranged between a minimum of 25.94 and a maximum of 30.10, with higher values also generally recorded through S.U. V. ACL values correspond with VPD, which has a mean value of 0.3 kPa through the full sequence. VPD reaches its maximum value (0.9 kPa) in S.U. V (upper), with a mean value of 0.5 kPa through this unit.

4.3.3. Compound specific isotope analysis (CSIA)

$\delta^{13}C_{wax}$

C_{29} and C_{31} *n*-alkanes were analysed for $\delta^{13}C_{wax}$ through the sequence (n=32). Reliable values (reproducibility greater than ± 0.5‰) were obtained in 28 samples. We have opted to include two samples where the standard deviation between replicates was 0.6‰ for $\delta^{13}C_{wax}$ of alkane nC_{29} when the corresponding values from the same sample for nC_{31} were greater than ± 0.5‰. Values for both C_{29} and C_{31} *n*-alkanes displayed a broad fluctuating trend through the sequence. For nC_{29}, $\delta^{13}C_{wax}$ ranges from -32.0‰ to -24.3‰, with a mean of -28.2‰, while nC_{31} values fluctuate between a minimum of -32.0‰ and a maximum of -23.4‰, with a mean of -28.7‰.

$\delta^{2}H_{wax}$

C_{29} and C_{31} *n*-alkanes were analysed for $\delta^{2}H_{wax}$ through the sequence (N=32), and reliable values (reproducibility greater than ± 5.0‰) were obtained for ten samples. Nine of these come from S.U. V (lower and upper) and one from S.U. VIII. The remaining samples did not yield sufficient concentrations for obtaining reliable isotope values; therefore, $\delta^{2}H_{wax}$ values are not presented for S.U. VII or S.U. VI. For nC_{29}, $\delta^{2}H_{wax}$ ranges from -176‰ to -124‰. The lowest values, -176‰ and -166‰, are recorded in the uppermost part of S.U. V (P.21). For nC_{31}, $\delta^{2}H_{wax}$ follows a similar trend, although with more variation. Values range from -171‰ to -88‰, with the lowest values again clustered in the uppermost part of S.U. V (P.21).

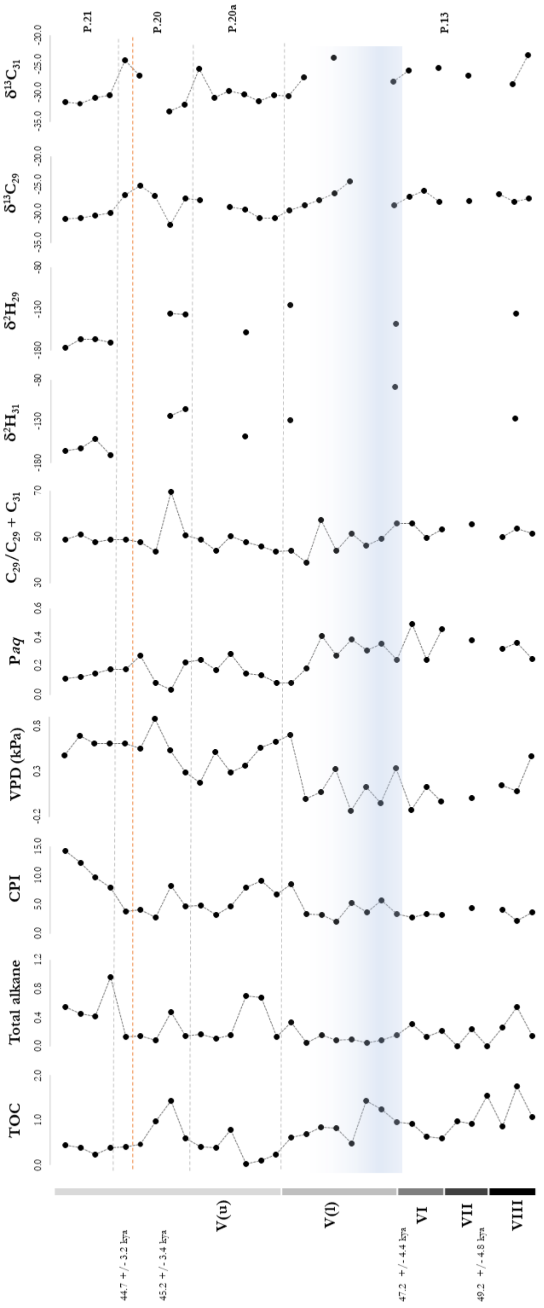

Figure 4.5 Results of TOC (%); Total *n*-alkane (μg/g dry sediment); Carbon preference index (CPI); Vapour Pressure Deficit (VPD) (kPa); proportion of aquatic plants (Paq); Long alkane ratio (LAR) $nC_{29}/nC_{29}+nC_{31}$); δ^2H_{wax} (nC_{29} and nC_{31}); $\delta^{13}C_{wax}$ (nC_{29} and nC_{31}). Grey dotted lines indicate the profile where samples were collected. The red dotted line indicates the position in the sequence after which evidence for human occupation ceases to be recorded. The blue gradient bar indicates the proposed timing for the Heinrich 5 event (HE5) within the sequence.

	Sample ID	***TOC (%)***	***Total alkane***	***CPI*** $_{(25-35)}$	***ACL*** $_{(17-35)}$	***VPD (kPa)***	***Paq***	***LAR*** $(nC29/(nC29+nC31)$	δ^2H_{29}	±	δ^2H_{31}	±	$\delta^{13}C_{29}$	±	$\delta^{13}C_{31}$	±
V (upper)	BM22	0.45	0.55	14.1	29.0	0.5	0.1	48.9	-176	5	-165	4	-30.9	0.1	-31.6	0.3
	BM23	0.39	0.45	12.1	29.7	0.7	0.1	51.0	-166	3	-162	0	-30.7	0.1	-31.8	0.5
	BM24	0.23	0.42	9.7	29.4	0.6	0.1	47.8	-166	5	-151	4	-30.2	0.1	-30.9	0.3
	BM25	0.40	0.97	7.9	29.4	0.6	0.2	48.8	-170	3	-171	1	-29.8	0.1	-30.5	0.2
	BM26	0.40	0.12	3.8	29.4	0.6	0.2	49.0	*	*	*	*	-26.7	0.2	-24.3	0.0
	BM27	0.47	0.15	4.1	29.2	0.5	0.3	47.9	*	*	*	*	-25.1	0.6	-26.9	0.2
	BM28	0.98	0.08	2.7	30.1	0.9	0.1	43.7	*	*	*	*	-26.9	0.4	*	*
	BM29	1.44	0.47	8.1	29.2	0.5	0.0	69.8	-135	1	-123	5	-32.0	0.2	-33.2	0.1
	BM30	0.60	0.14	4.7	28.2	0.3	0.2	50.8	-136	4	-115	2	-27.3	0.2	-32.0	0.2
	BM31	0.41	0.16	4.8	27.7	0.2	0.2	49.1	*	*	*	*	-27.7	0.3	-25.7	0.3
	BM32	0.38	0.11	3.1	29.1	0.5	0.2	43.9	*	*	*	*	*	*	-30.9	0.4
	BM33	0.78	0.15	4.7	28.2	0.3	0.3	50.5	*	*	*	*	-28.9	0.4	-29.7	0.1
	BM34	0.02	0.70	7.8	28.6	0.4	0.1	47.6	-158	2	-148	4	-29.3	0.5	-30.2	0.2
	BM35	0.10	0.68	9.1	29.3	0.6	0.1	46.0	*	*	*	*	-30.7	0.2	-31.4	0.4
	BM36	0.23	0.13	6.7	29.5	0.6	0.1	43.6	*	*	*	*	-30.7	0.1	-30.4	0.1
V (lower)	BM37	0.62	0.34	8.5	29.7	0.7	0.1	44.0	-124	0	-128	1	-29.4	0.2	-30.5	0.3
	BM38	0.70	0.04	3.4	26.7	0.0	0.2	39.0	*	*	*	*	-28.5	0.2	-27.2	0.1
	BM39	0.84	0.15	3.3	27.2	0.1	0.4	57.4	*	*	*	*	-27.6	0.2	*	*
	BM40	0.82	0.09	2.1	28.4	0.3	0.3	43.9	*	*	*	*	-26.5	0.4	-23.9	0.4
	BM41	0.49	0.09	5.3	25.9	-0.1	0.4	51.5	*	*	*	*	-24.3	0.4	*	*
	BM42	1.44	0.05	3.7	27.5	0.1	0.3	46.3	*	*	*	*	*	*	*	*
	BM43	1.25	0.08	5.7	26.5	-0.1	0.4	49.2	*	*	*	*	*	*	*	*
	BM44	0.97	0.15	3.4	28.4	0.3	0.2	55.8	-147	3	-89	4	-28.5	0.5	-28.0	0.0
VI	BM45	0.93	0.31	2.7	26.0	-0.1	0.5	56.0	*	*	*	*	-27.1	0.4	-26.1	0.2
	BM46	0.64	0.13	3.4	27.5	0.1	0.2	49.7	*	*	*	*	-25.9	0.3	*	*
	BM47	0.59	0.21	3.2	26.6	0.0	0.5	53.4	*	*	*	*	-28.0	0.1	-25.7	0.2

VII	BM48	0.98	*	*	*	*	*	*	*	*	*	*	*	*	*	*
	BM49	0.93	0.24	4.4	26.8	0.0	0.4	55.6	*	*	*	*	-27.8	0.2	-27.0	0.5
	BM50	1.55	*	*	*	*	*	*	*	*	*	*	*	*	*	*
VIII	BM51	0.87	0.26	4.1	27.5	0.1	0.3	48.4	*	*	*	*	-26.6	0.1	*	*
	BM52	1.77	0.55	2.2	27.2	0.1	0.4	53.7	-135	5	-126	2	-27.9	0.6	-28.5	0.2
	BM53	1.08	0.14	3.7	29.0	0.5	0.2	51.4	*	*	*	*	-27.3	0.5	-23.4	0.4

Table 4.3 Results of TOC (%); Total *n*-alkane concentration (µg/g dry sediment); Carbon preference index (CPI); Average chain length (ACL); Vapour pressure déficit (VPD) (kPa); proportion of aquatic plants (Paq); LAR $nC_{29}/nC_{29}+nC_{31}$); δ^2H_{wax} (nC_{29} and nC_{31}) and associated ± error; $\delta^{13}C_{wax}$ (nC_{29} and nC_{31}) and ± error. Isotope values are expressed in per mil (‰). Error reports the standard deviation. * denotes samples where analyte was not present or below the limit of detection.

4.3.4. Pollen

Of the 28 samples analysed from S.U. VIII - V (lower) (P.13), 14 were sterile and thus discarded. As a result, S.U. V (lower) is not represented in the palynological results. The remaining 14 samples (S.U. VIII - VI) yielded a total of 41 taxa (Fig. 4.6).

S.U. VIII

This unit is composed of 8 samples in total, from which the three uppermost samples (38-40, 44-47 and 51-54 cm) were found to be sterile and discarded. Arboreal elements are predominant, consistently above 66%, although with notable variability. One remarkable aspect is the internal variation of *Pinus nigra-sylvestris*, from values close to 33% (26-27 cm) to values below 8% in the subsequent sample (27-30 cm). Mesic elements, such as *Salix, Fraxinus, Corylus, Castanea* type, *Betula,* and *Celtis,* vary from 8.2% (26-27 cm) to 23.8% (27-30 cm). Some other Mediterranean taxa are primarily composed of *Oleae* and *Phillyrea*, with the punctual presence of Cistaceae and *Juniperus*. The total sum of these components is always below 10%, except between 26-27 cm, which is instead closer to 20%. The main non-arboreal taxon is always A. asteroideae, with values around 48% in samples from 32 to 35 cm and 18 to 20 cm, to values near 20% in the other three samples. The sample from 27 to 30 cm presents remarkable peaks of Liliaceae (31.9%) and Asteraceae cardueae (16.5%), sometimes appearing in lumps. Within the NAP, some other herbs are worth mentioning. Amaranthaceae appears between 2% (22-25 cm) and 15% (18-20 and 27-30 cm) and Poaceae ranges from 2.2% (27-30 cm) to 8.3% (32-35%). Erica is always present, varying from 1.5% (18-20 cm) to 6.5% (27-30 cm), while the presence of Artemisia is intermittent, from being absent (samples between 26 and 30 cm) to be *c*. 7% (the first and last sample of the unit). Cyperaceae shows values of 0.7% (27-30 cm) to 4.4% (22-25 cm).

S.U. VII

S.U. VII is composed of four samples. This unit is characterised by an abrupt decrease in arboreal pollen, which shows a progressive recovery from 45% in the lower sample to 71% in the uppermost part of the unit. The three lower samples are marked by a predominance of evergreen *Quercus* in the arboreal strata (18%, 25%, and 17%), followed by *Pinus sylvestris-nigra* (12-14%). *Cedrus* appears in low percentages *c*. 2% and deciduous *Quercus* shows similar values in each of the three samples (6%-8%). Other broad-leaf trees disappear in samples between 56 and 63 cm, and their values are low (below 2.2%) in samples between 66 and 73 cm. Other Mediterranean elements are scarce throughout this unit, with the sole exception of one sample between 66 and 69 cm. It presents values below 14% but the greatest variety of taxa: *Oleae, Phillyrea, Ligustrum, Myrtus*, and Cistaceae. The most remarkable aspect is the presence of Amaranthaceae within the non-arboreal elements, with a maximum of 45% (56-59 cm), and percentages of 21% and 31% in the other samples. Some other herbs, such as *Artemisia* (3.3% to 8.9%), Poaceae (1.2% to 8.9%), Caryophyllaceae (below 4%), and *Erica* type (1% to 5.4%) appear in low amounts. The inflexion point is constituted by the upper sample (70-73 cm), in which the AP is mainly composed of *Pinus sylvestris-nigra* (30.4%). Evergreen *Quercus* decreases (21.7%), while deciduous *Quercus* increases (11%). Other mesic trees slightly increase (*Betula*, 2%) and other Mediterranean components decrease (6%) in relation to the previous sample (12%). Within the non-arboreal pollen, Amaranthaceae decreases (9%) in favour of Asteraceae Liguliflorae type (54%).

S.U. VI

S.U. VI is composed of four samples, although one sample was found to be sterile (79-84 cm). All of the other samples in this unit exhibit arboreal pollen values above 90%. An abrupt increase of *Pinus nigra-sylvestris* (consistently above 50%) to the detriment of evergreen

Quercus (5%-17%) is noteworthy. *Pinus pinaster* appears, although in low percentages (3%-6%), as well as *Cedrus* (1%-3%). Deciduous taxa are present in low amounts, e.g. deciduous *Quercus* (4%-7%), *Betula, Castanea* type, *Corylus*, and *Salix* (all under 3%). Between 76 and 79 cm, there is a peak in some Mediterranean taxa (*Oleae* and *Phillyrea*, 9% and 8%, respectively), but they are generally scarce throughout this unit. Non-arboreal values are rather low, and their main components are Caryophyllaceae (76-79 cm, 4%), A. asteroideae (84-87 cm, 28%), and A. Liguliflorae type (89-92 cm, 33%).

S.U. V (upper)

A total of 15 samples from S.U. V (upper) were processed (4 from P.21, 5 from P.20, and 6 from P.20a). All the samples are sterile in terms of their pollen content, with the exception of one sample from P.20a. Figure 4.7 presents the palynological results of this sample expressed in percentages, together with the percentages of arboreal/non-arboreal pollen. A synthesis of the main taxa and ecological groups is presented in Figure 4.8. Arboreal pollen (50.9%) and non-arboreal pollen (49.1%) exhibit similar percentages. Evergreen *Quercus* (14.2%) is the most abundant tree, together with *Pinus nigra-sylvestris* (11.3%). Broad-leaf elements, such as deciduous *Quercus* and *Celtis,* are close to 10%, while other Mediterranean taxa, mainly represented by *Phillyrea* reach 12%. *Cedrus* and *Erica* type appear below 1% each. The most abundant herbs are Asteroideae (37.2%), Amaranthaceae (32%), and Caryophyllaceae (11.3%). It is possible to infer a patchy/semi-opened landscape alternating with open areas and mixed forests, with the punctual presence of deciduous elements. Mediterranean components are better represented than the mesic, indicating a temperate climate. The presence of xerophytic elements implies increased aridity, reinforced by the presence, albeit slight, of *Cedrus*.

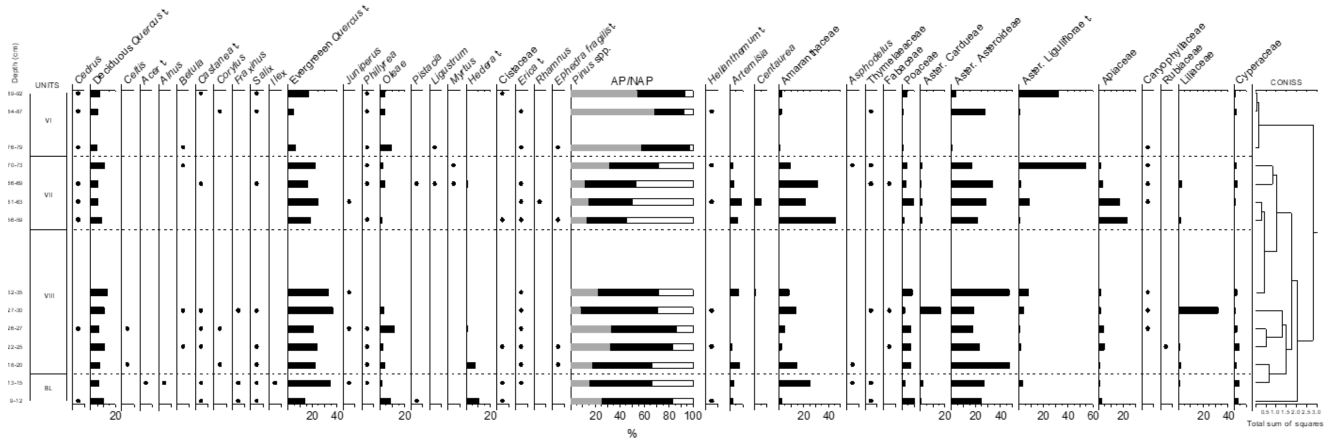

Figure 4.6 Diagram presenting palynological results from P.13 expressed in percentages. BL denotes anthropogenic combustion layer at base of S.U. VIII.

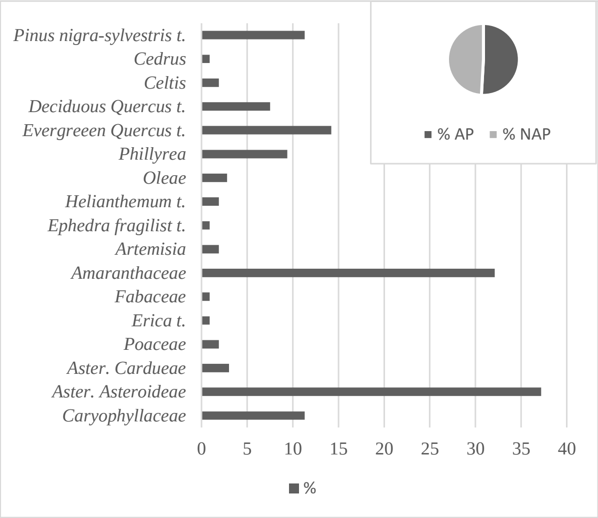

Figure 4.7 Graph which illustrates the palynological remains recorded in a single sample from P.20a. Results are expressed in percentages of taxa and the relative contribution of arboreal/non-arboreal pollen is presented (inset).

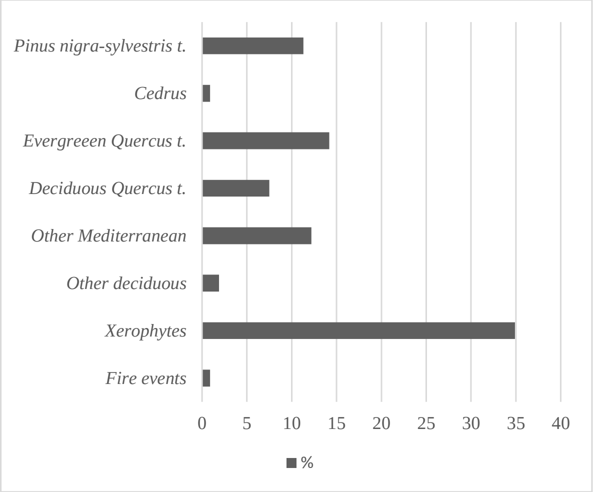

Figure 4.8 Histogram presenting the most representative taxa and vegetation groups recorded in a single sample from P.20a.

4.3.5. Non-pollen palynomorphs

S.U. VIII – S.U. V (upper)

Figure 4.9 presents the general results of the non-pollen palynomorphs from S.U. VIII - V (lower) (P.13), expressed in percentages, as well as the taxonomic variability. This includes the following categories. Pteridophyta-Bryophyta: monolet and trilete spores of mosses and ferns; Algae: *Spirogyra*, *Cosmarium*, and the cyanobacteria *Gloeotrichia*; Fungi: *Glomus* sp., HdV 79, Sordariaceae, HdV 200, HdV 462, HdV 463, TM 330 C; Animalia: HdV 52, HdV 36, HdV 36c, zoo remains, coleoptera; Planta: phytoclasts and phytoclasts/panal. *Pseudoschizaeae* is of unknown origin and cannot be included in any category. *Glomus* sp. and HdV 200 are plotted against the total sum of fungi to highlight their presence within this category.

The synthetic diagram (Fig. 4.10) presents the main groups and the most representative taxa with known palaeoecological significance. These groups are divided into Pteridophyta, Bryophyta, Algae, Fungi, Animalia, and Planta, and conform with different works included in van Hoeve and Hendrikse (1998) and the Non-Pollen Palynomorphs Database (http://nonpollenpalynomorphs.tsu.ru).

A synthetic diagram with the most representative taxa and categories of palynomorphs was also plotted (Fig. 4.11). It includes the groups presented in both synthetic diagrams of pollen and NPPs. Concentrations of pollen, NPPs, and microcharcoal particles were also included. They were calculated following the volumetric method described in Loublier (1978) and Burjachs (1990). Results are expressed in grains/gr (pollen), palynomorphs/gr (NPPs), and particles/gr (microcharcoal) of dry sediment.

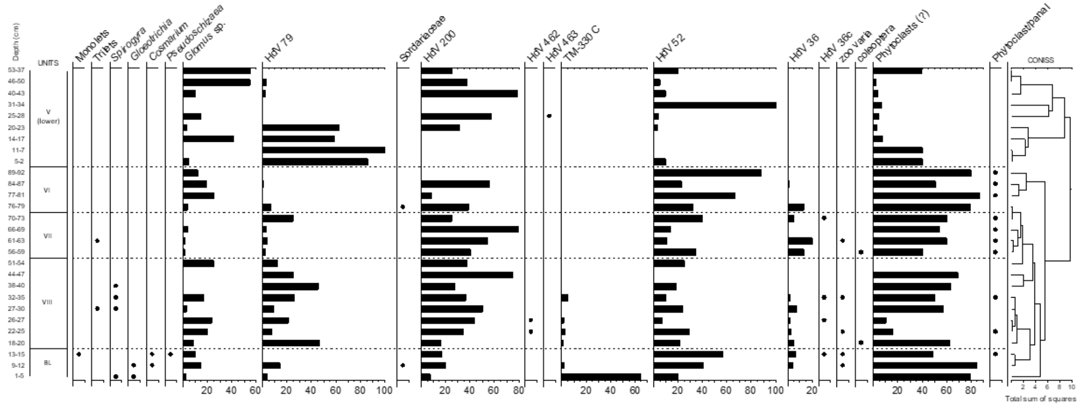

Figure 4.9 Graph presenting non-pollen palynomorphs from P.13 in percentages. BL denotes anthropogenic combustion layer at base of S.U. VIII.

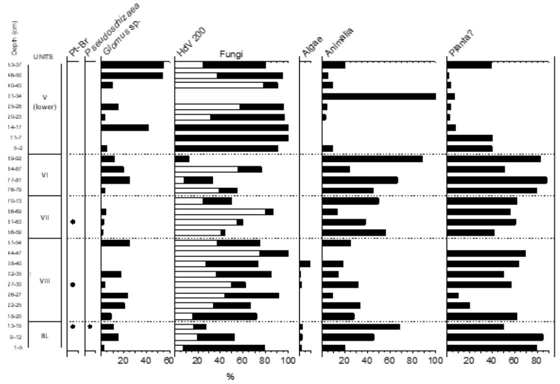

Figure 4.10 Main groups and most representative taxa from P.13 with known palaeoecological significance. BL denotes anthropogenic combustion layer at base of S.U. VIII.

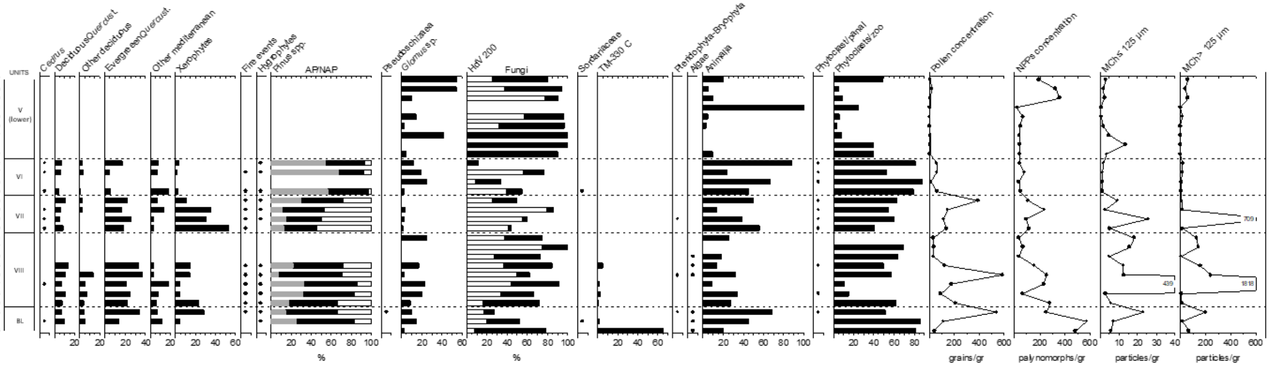

Figure 4.11 Different taxa and categories of pollen and NPPs from P.13. Line graphs represent pollen, NPPs, and microcharcoal (MCh) expressed in concentrations. BL denotes anthropogenic combustion layer at base of S.U. VIII.

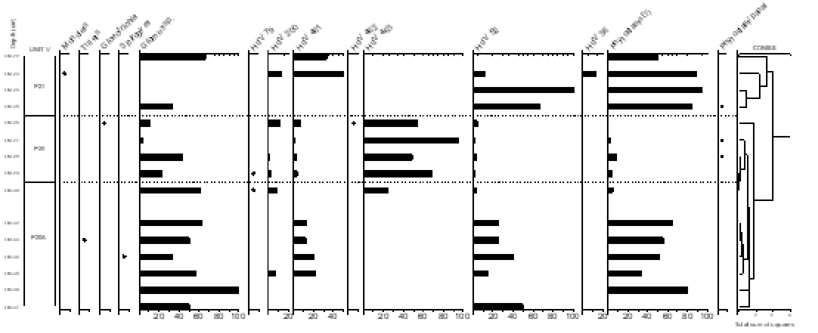

Figure 4.12 Synthetic diagram dsiplaying the abundances of NPPs from S.U. V (upper) (P.20, P.20a, P.21), expressed in percentages, as well as the taxonomic variability. The dashed lines indicate subdivisions between profiles.

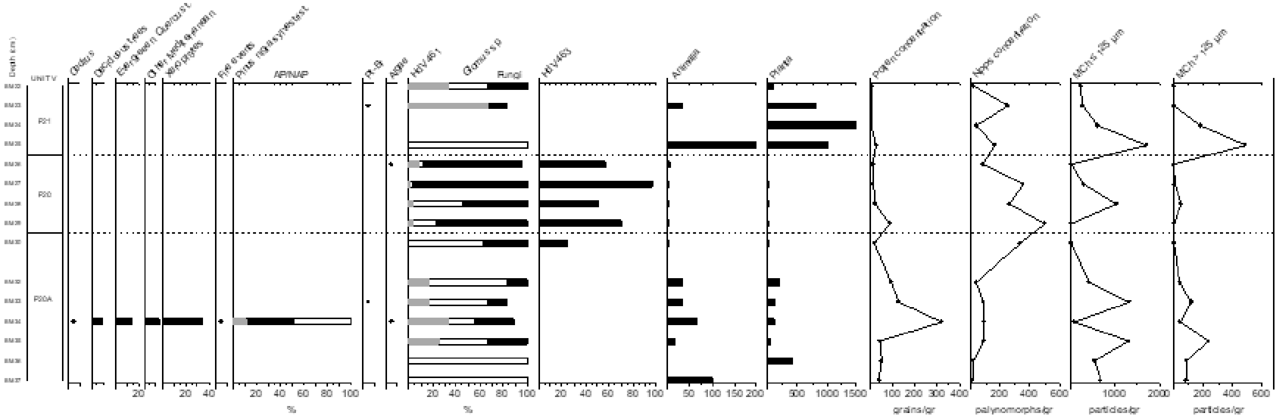

Figure 4.13 Synthetic diagram displaying the different taxa and categories of pollen and NPPs from S.U. V (upper) (P.20, P.20a, P.21). Line graphs represent pollen, NPPs, and microcharcoal (MCh) expressed in concentrations. The dashed lines indicate subdivisions between profiles.

4.4. Discussion

4.4.1. Site-formation at El Salt S.U VIII - S.U. V (upper)

The coarse lithological fraction observed through the El Salt sequence is largely derived from the mechanical weathering and disintegration of the local geology, particularly tufa and travertine linked to the nearby spring system and the Palaeocene limestone cliff which overlooks the site. The large limestone blocks at the base of S.U. V (lower), which seals the lower units, would once have formed the overhanging roof of a substantial rock shelter. The collapse of the roof structure corresponds with a notable change in the style of sedimentation and an abrupt decrease in evidence for human occupation. Two main phases of site formation can therefore be defined: the first phase comprises S.U. VIII - S.U. VI and predates the collapse event; and a second phase comprising S.U. V (lower and upper) which post-dates the opening up of the shelter. Differences in sediment composition and fabric between phases one and two, observable both in the field and at the microstratigraphic level, reflect the interplay of different climatic, environmental, transport, and deposition processes.

Post-depositional diagenetic alteration is reflected by the presence of gypsic features observed through soil micromorphology. This is notably more frequent in the second phase of site formation, gradually decreasing down-profile. Gypsum formation is typically linked to evaporative processes in soils under arid or semi-arid climates (Poch et al. 2018). Here, the repeated occurrence of gypsum infilling interstitial void space suggests that this is likely a secondary and sub-recent process. Decalcification of the groundmass during phase one (S.U. VIII - S.U. VI) reflects soil phosphate accumulation related to elevated input of guano. Although guano is recorded in S.U. V, it is much less abundant, and the matrix appears more calcitic.

4.4.2. Environmental and climatic context

Phase one (VIII - VI)

Soil micromorphological, palynological and our *n*-alkane evidence is consistent with other regional palaeoclimatic datasets in pointing to broad fluctuations in humidity and aridity through the course of MIS 3 (Sánchez Goñi et al. 2008; Daura et al. 2017). All samples recorded similar *n*-alkane distributions dominated by long-chain (C_{29}-C_{31}) homologues and an OEP characteristic of terrigenous higher plant input. The $\delta^{13}C_{wax}$ values across the whole range, with a mean of 28.2‰ (nC_{29}) and 28.7‰ (nC_{31}), indicate a predominant contribution from C3 plants (Diefendorf and Freimuth 2017).

The presence of guano crusts in soil micromorphology samples from S.U. VIII and S.U. VI points to recurrent intervals of stable surface exposure with relatively slow rates of sedimentation (Karkanas and Goldberg 2018). It is notable that these crusts were formed prior to the collapse of the shelter roof and similar crusts have also been recorded in other rock shelter and cave settings such as Blombos Cave (South Africa) and Liang Bua Cave (Indonesia) (Haaland et al., 2020; Morley et al., 2017). It has been suggested that the presence of guano crusts may be a good indicator of human site abandonment (Karkanas 2017). It is also interesting to note that fibrous and massive coprolites are a common component in thin sections from units deposited during phase one, although these are not as prevalent in samples reported by Leierer et al. (2019) for S.U. Xb, who describes a coprolitic matrix for that unit.

Changeable environmental conditions during phase one are reflected by variability in arboreal coverture recorded in the pollen data. Internal variation in the presence of *Pinus nigra* is particularly notable in S.U. VIII and has previously been recorded in a study of scattered charcoal from this unit by Vidal-Matutano et al. (2018b). The observed fluctuations in *Pinus nigra* may be explained by relatively short and alternating periods of higher humidity. Corresponding fluctuations in $\delta^{13}C_{wax}$ therefore likely reflect the combined effects of changes in phylogeny *and* humidity on $\delta^{13}C$ isotopic fractionation, which has been shown to record plant water stress in semi-arid and arid environments (Struck et al., 2020). Several major parameters drive variability of $\delta^{2}H_{wax}$; these include phylogeny; precipitation amount; atmospheric temperature; evapotranspiration; and precipitation source (Sachse et al., 2012; Wirth and Sessions, 2016). Like $\delta^{13}C_{wax}$, fluctuations in $\delta^{2}H_{wax}$ observed in the El Salt sequence reflect a response to phylogeny and wáter stress changes. It is known that regional $\delta^{2}H_{precipitation}$ values are influenced by seasonal or longer-term changes in precipitation amount, based on measurements taken at nearby GNIP stations (Connolly et al., 2019), although it is important to note that several studies have highlighted the importance of precipitation source on $\delta^{2}H$ values in the Iberian Peninsula, where low values are associated with an increased Atlantic precipitation origin, and higher values indicative of a Mediterranean source (Schäfer et al., 2018; Schirrmacher et al., 2020; Toney et al., 2020). VPD is an absolute measure of past atmospheric moisture relative to the air saturation vapour pressure at a given temperature (Eley and Hren, 2018). It is an indicator of the extent to which the atmosphere can extract moisture from land surfaces and a robust proxy for investigating evaporative demands on vegetation. Higher VPD values correspond with periods associated with increased atmospheric demands for water. Where high VPD values correspond with high $\delta^{2}H$ values, it is reasonable to infer aridity as the primary control on $\delta^{2}H$. Where these proxies are decoupled through the sequence, we interpret this as evidence of a change in precipitation moisture source or plant phylogeny.

The main component within the arboreal pollen (AP) is evergreen *Quercus* (Q. *ilex-coccifera* type), followed by *Pinus nigra-sylvestris*. This mixed forest exhibits episodic competitive displacements, probably related to changes in water availability, soil moisture, solar radiation levels, or fire. (Sheffer, 2012). Mediterranean elements generally appear in low percentages. This could be considered an indicator of a temperate climate at this part of the sequence. The presence of deciduous *Quercus* is low but constant, as well as some other deciduous taxa and hygrophytes, which imply some moisture. Humid conditions during phase one are also indicated by Pteridophyta and Bryophyta's presence in samples from S.U. VIII and VII. Our *n*-alkane data also recorded a P*aq* value of 0.5 in S.U. VI, which implies sedimentary input from a mix of terrestrial and aquatic plant sources. The presence of mosses or macrophytes growing in a moist environment may account for this. In S.U VIII, the presence of Spirogyra, although in low percentages, indicates a meso-eutrophic nutrient-rich environment. A reduction in fine organic particles from S.U VIII through VII corresponds with an increase in *Celtis sp.* seed coatings in the micromorphological samples and a decrease in arboreal pollen, with the three lowest pollen samples from S.U. VII presenting high values of xerophytic elements. The decrease and disappearance of hygrophytic elements and some deciduous taxa within this unit point to an opening up of the landscape at certain intervals. This is supported by the presence of *Cedrus*, although it appears in low amounts. Some pollen records show that *Cedrus* is occasionally found during abrupt deforestation events in the forest-dominated periods of the interglacials (Margari, 2002). The fact that Mediterranean elements are few may suggest increasing aridity and a decrease in regional temperatures. Although characteristic soil frost features are generally absent at the microstratigraphic level, it is worth noting that ice-segregation and related soil microstructures depend on water supply and may not develop during exceedingly dry and cold periods (Vliet-Lanoë, 2010).

Taxa associated with fire events and increased burning, mainly pyrophytic shrubs that sprout after fires, are generally present through the sequence in samples with high microcharcoal concentrations. The highest microcharcoal concentrations were identified during site formation phase one in S.U. VIII. Although the occurrence of regional fires cannot be ruled out, it is logical that the microcharcoal input here is due to anthropogenic combustion features recorded during excavation. Abundant black silt-sized particles observed in micromorphology samples from S.U. VIII, and to a lesser degree S.U. VII and VI, represent partially humified plant-derived OM but may also include small amounts of charred particles associated with combustion layers and dispersed residues recorded in S.U. VII and VI. It is notable that these features do not include an ash-rich lens overlying the charcoal-rich layer, the typical microstratigraphy for undisturbed fires recorded by Leierer et al. (2019) in S.U. Xb. This could indicate post-depositional reworking of the original fire context by wind or bioturbation; however, ash dissolution is also a likely biasing factor given the decalcification recorded in these units.

S.U. VII and S. U. VI have been dated to 49.2 ± 4.8 kya and 47.2 ± 4.4 kya, respectively. We suggest that the roof collapse blocks which seal the units of phase one correspond with GS-13 and the onset of HE 5 (*c.* 50 - 47 kya) (Rasmussen et al. 2014). Therefore, samples from S.U. VI, immediately before this event and composed by high percentages of arboreal pollen, likely correspond to GI-13.

Phase two (V lower - V upper)

S.U. V (lower and upper) is a polygenetic deposit characterised by a mix of windblown very fine sands and silts with coarser well-sorted fine to medium calcitic sands and micritic peloids derived from the breakdown of the Palaeocene cliff overlooking the site. These sediments are locally reworked and deposited by low-energy processes such as surface runoff, and there is a notable reduction in the presence of tufa and travertine (lithology type B) relative to units deposited during phase one. This shift in sedimentary dynamics was undoubtedly influenced by the geomorphological restructuring of the shelter following the roof collapse, but also reflects changes in regional climatic and environmental conditions. For instance, the effects of a reduction in regional vegetation cover combined with the opening of the shelter likely account for the observed increase in windblown sediments. There is also a marked reduction at the microstratigraphic scale in the occurrence of anthropogenic materials such as charcoal or flint microflakes, mirroring the reduction in artefactual evidence noted during the excavation of these units. Sediment samples collected for pollen analysis from S.U. V (lower) were determined to be sterile, however, $\delta^{13}C_{wax}$ confirm the presence of local vegetation cover with a predominant contribution from C3 plants during the deposition of this unit.

Although chronological uncertainties make it difficult to draw robust conclusions from comparison in isotopic data between different sites, it is notable that $\delta^{2}H_{wax}$ values for nC_{29} of -135‰ ± 1 and -136‰ ± 4, recorded in S.U. V (upper), are broadly consistent with $\delta^{2}H_{wax}$ from S.U. IVb (-129‰ ± 4) at the nearby site of Abric del Pastor, which has been dated to around the same time (El Salt S.U. V upper: 45 kya ± 3; Abric del Pastor S.U. Vb: 48 kya ± 5) (Connolly et al., 2019). Recurring oscillations observed in VPD during the deposition of S.U. V (lower) reflect fluctuations in the hydroclimatic regime. Notably, the highest VPD values are recorded in S.U. V (upper), pointing toward increased aridification. VPD correlates to ACL, which has also been found to record regional aridity under certain conditions, including in Mediterranean settings (Bush and McInerney, 2013; Norström et al., 2017). Fluctuating aridity is also indicated by the presence of *Glomus* sp, which varies in abundance throughout the sequence but reaches the highest values in S.U. V, particularly toward the top of the unit. This palynomorph is associated with erosive processes affecting soils in dry or desiccated areas, as well as root activity (Anderson et al., 1984; van Geel et al., 1989; López-Sáez et al., 2000). It is notable that δ^2H_{wax} values are more ^2H depleted at the top of S.U. V, which we interpret as evidence of a probable change in precipitation moisture source. Taken together, our results support the chronostratigraphic model for El Salt put forward by Galván et al. (2014) which indicates that the roof collapse corresponds to HE 5, which has been widely linked to the onset of regional aridification (Müller et al., 2011; Sánchez Goñi et al., 2008). Our interpretation also chimes well with previous findings from a recent small mammal study of S.U. V (upper) which calculated an average MAP value of 13.13 mm less than present-day conditions and point to a transition from a woodland dominated environment to more open and arid conditions (Fagoaga et al., 2019). Evidence for similar shifts in regional conditions to more open and arid landscapes coincident with Neanderthal disappearance have also recently been reported in Central Iberia and the Cantabrian region (Wolf et al., 2018; Jones et al., 2018).

4.5. Concluding remarks

In order to investigate the palaeoclimatic context for the final Neanderthal occupations at the Middle Palaeolithic site of El Salt, the sedimentary sequence has been analysed using soil micromorphology, lipid biomarker *n*-alkane abundances (CPI, ACL, VPD, LAR, Paq), compound-specific hydrogen and carbon isotopic records from fossil leaf waxes (δ^2H_{wax} and $\delta^{13}C_{wax}$), bulk organic geochemistry (TOC), pollen, and non-pollen palynomorphs. Our multiproxy palaeoenvironmental study of S.U. VIII – S.U. V (upper) has allowed us to draw the following conclusions:

- Two distinct phases of site formation can be distinguished. Phase one, which comprises S.U. VIII – S.U. VI, precedes the collapse of the rock shelter roof and is characterised at the microstratigraphic scale by lithological coarse fraction dominated by tufa and travertine related to the nearby relict Upper Pleistocene freshwater spring system. The palaeoenvironmental setting during this phase is characterised by mixed forest vegetation and episodic fluctuations in humidity and periods of extended soil surface exposure. Deposits laid down during this phase of site formation yield abundant evidence for Neanderthal occupation activities, including hearth construction and flint knapping.

- Phase two, which comprises S.U. V (lower) – S.U. V (upper), immediately follows the collapse of the shelter roof. A distinct change in sedimentation style characterises this phase with a strong component of wind-blown sediments, a marked reduction in fine organic particles, the occurrence of tufa and travertine, and anthropogenic components. Our palaeoenvironmental data points to a scenario of increasing aridity at this time, between HE 5 and HE 4.
- This study contributes to a better understanding of the diachronous and regional nature of Neanderthal disappearance from the Iberian Peninsula and adds new lines of evidence for exploring the role of climate and environmental change in driving Neanderthal demographic collapse.

Chapter 5: Investigating hydrogen isotope variation during heating of *n*-alkanes under limited oxygen conditions - implications for palaeoclimate reconstruction in archaeological settings

Rory Connolly [1, 2], Margarita Jambrina-Enríquez [1, 3], Antonio V. Herrera-Herrera [1], Carolina Mallol [1, 2]

1. Instituto Universitario de Bio-Organica Antonio Gonzalez (IUBO), Universidad de La Laguna, 38206, Canary Islands, Spain. rconnoll@ull.es; mjambrin@ull.edu.es; avherrer@ull.edu.es; cmallol@ull.edu.es
2. Departmento de Geografia e Historia, Universidad de La Laguna, 38200, Canary Islands, Spain.
3. Departamento de Biología Animal, Edafología y Geología, Facultad de Ciencias, Universidad de La Laguna, 38200, Canary Islands, Spain.

Abstract

This paper reports on a series of heating experiments that focus on *n*-alkanes extracted from leaf, bark, and xylem tissues of the *Celtis australis* plant. These lipid biomarkers were analysed for their compound-specific hydrogen isotopic composition (δ^2H_{wax}) under limited oxygen conditions at 150 °C, 250 °C, 350 °C and 450 °C. Our results reveal isotopic variations in wax lipids of different plant organs during short-term low-temperature combustion. We conclude that, in the absence of a detailed characterisation of the depositional environment in advance of sampling, δ^2H_{wax} values in archaeological or otherwise highly anthropogenic environments should be interpreted cautiously. In addition, we observed that variation is δ^2H_{wax} of leaves is minimal at temperatures ≤ 350 °C, highlighting the potential for δ^2H_{wax} in thermally altered combustion substrates to yield palaeoclimate information, which could allow researchers to investigate links between archaeological and climatic records at a high spatial and temporal resolution.

5.1. Introduction

5.1.1. Hydrogen isotope composition of plant waxes

Lipid biomarkers are organic molecules which can be traced to a specific biological source (Cranwell et al., 1987; Eglinton and Hamilton, 1967; Evershed, 1993; Evershed et al., 1999; Ficken et al., 2000). Compound-specific hydrogen isotope analysis of *n*-alkanes (δ^2H_{wax}) derived from terrestrial and aquatic plant waxes has been shown to record plant source water's isotopic composition, most commonly precipitation (Sachse et al., 2012). The hydrogen isotopic composition of sedimentary *n*-alkanes has thus emerged as a robust proxy for palaeohydrological reconstruction and in the last decade has been increasingly employed in archaeological settings (Brittingham et al., 2019; Diefendorf et al., 2010; Diefendorf and Freimuth, 2017; Glauberman et al., 2020; Jordan et al., 2017; Magill et al., 2016). Numerous studies have reported on the wide range of environmental factors which govern hydrogen isotopic fractionation in plant waxes, which include precipitation δ^2H, precipitation amount, plant type, plant physiology, temperature, aridity, seasonality, and humidity (Gamarra et al., 2016; Liu and An, 2018; Niedermeyer et al., 2016; Sachse et al., 2012). However, it is notable that despite the recent upsurge in the application of this proxy in archaeological settings, little attention has been afforded to the potential impacts of human activities on δ^2H_{wax}. Anthropogenic combustion features and their associated residues, which are chronologically and geographically ubiquitous in archaeological contexts, particularly stand out as an important source of potential bias and the effects of short-term low temperature (< 450 °C) combustion on δ^2H_{wax} values are not well understood.

5.1.2. Anthropogenic combustion features

Anthropogenic combustion features, or hearths, have been the focus of a considerable body of archaeological research in recent years using an array of high-resolution analytical techniques (Butler et al., 2019; Fernández Peris et al., 2012; Haaland et al., 2017; Henry, 2012; Mallol and Henry, 2017; Urban et al., 2019; Whitau et al., 2018). The processes involved in forming anthropogenic combustion features are complex and subject to a considerable range of culturally and environmentally mediated variables. However, at the most basic level, these features are composed of a thermally altered substrate overlain by a black combustion layer resulting from the deliberate exploitation and management of fire by one or more humans in the past. Experimental studies suggest that the occupation surface or substrate on which the fire is lit do not typically exceed temperatures of 300 °C and may provide preferential conditions for the preservation of lipid biomarkers (Mallol et al., 2013; March et al., 2014). The most rudimentary form of anthropogenic combustion feature is a *simple hearth* in which combustion is carried out on a horizontal surface. Other common forms include *cuvette* fires, or *pit hearths*, in which the combustion is carried out in a bowl-like depression. In some instances, pebbles or flagstones may be placed around the fire in a horizontal or vertical position and act as heat retainers, altering the combustion's archaeological and sedimentary signature (Aldeias, 2017; Leierer et al., 2020; March et al., 2014).

Traditionally, palaeoenvironmental information from combustion features has been derived from analyses of the associated charcoal assemblages (e.g. Braadbaart and Poole, 2008; Vidal-Matutano, 2018a; Vidal-Matutano et al., 2015; Whitau et al., 2018) or phytoliths (e.g. Albert and Cabanes, 2007; Allué et al., 2012; Toffolo et al., 2019; Wroth et al., 2019), both of which are the product of human activities related to fire. The application of lipid biomarker analyses, despite being first approached as early as the

1980s (Cliquet et al., 1989; March et al., 1989; Rottlander 1989, 1990), is still, however, not widely employed for the study of combustion features. In recent years, decreasing costs and improved access to instrumental analyses has led to a modest increase in the number of studies that have sought to exploit lipid biomarkers' potential and their associated compound-specific isotope ratios to investigate both experimentally derived and archaeological datasets. To date, however, most of these studies have focused on questions related to cooking activities and the identification of potential fuel sources (Buonasera et al., 2019; Choy et al., 2016; Crass et al., 2011; Jambrina-Enríquez et al., 2019; Kedrowski et al., 2009; Lejay et al., 2016; March, 2013).

Here, we conducted a series of heating experiments to evaluate molecular and isotopic changes to plant-derived wax lipids during short duration combustion events under limited oxygen conditions using leaves, bark and xylem tissues of *Celtis australis*. These plant organs represent common fuel sources in archaeological settings and are likely to be an important source of organic residues in archaeological combustion features. In addition, fine charred particles produced during the combustion of these fuel sources are likely to be locally dispersed in surrounding sediments and may impact isotopic values, leading to incorrect palaeoenvironmental reconstructions. We aimed to assess the degree of preservation of climatic signals in δ^2H_{wax} in anthropogenic combustion features and account for potential biases that could arise due to the mixing of microscopic fine charred particles in the surrounding sediments.

5.2. Materials and methods

5.2.1. Sample collection, preparation, and combustion

Leaf and branch samples of *Celtis australis* were collected in July 2015 and April 2016 from the area surrounding the Middle Palaeolithic site of El Salt in Alcoy, Spain (726 m asl). All samples were rinsed with distilled water to remove potential contaminants and oven-dried at 60 °C for 24 h at the Archaeological Micromorphology and Biomarker Laboratory (AMBI), Universidad de La Laguna, Tenerife.

Leaf (4 g; 1 cm length) and branch (20 g; 2 cm diameter) samples were placed in ceramic crucibles (4.2 cm x 2.5 cm) and covered with Al foil to limit the supply of O_2 during the heating process. All samples were heated in a muffle furnace with a ramp rate of 26 °C/min for a duration of 1 h to temperatures of 150 °C; 250 °C; 350 °C; 450 °C. Following this, samples remained in the closed furnace to cool overnight before being homogenised into a fine powder using a pestle and mortar.

5.2.2. Lipid extraction, analysis, and quantification

All non-volumetric materials were calcined at 450 °C for a duration of 10 h to eliminate potential contaminants. Lipids extraction was carried out with dichloromethane/methanol (DCM:MeOH, 9:1) (10–20 mL) by ultrasonic extraction (3 × 30 min) at controlled temperatures < 30 °C. Samples were subsequently centrifuged (3 × 10 min at 4700 rpm) and filtered through annealed glass wool. Solid-phase column chromatography (2 mL column with glass wool, 0.1 g quartz sand (50–70 mesh) and 1 g of activated silica (70–230 mesh) was used to separate the lipid extract into fractions of differing polarity. Alkanes were eluted with ⅜ dead volume (DV) *n*-hexane (DV 1.5 mL, ⅜ DV 562 µL). Samples were subsequently dried under a steady stream of N_2 in an Organomation evaporator, internal standard (IS) 5α-androstane (2000 mg/L in DCM, purity ≥ 99.9%, Sigma-Aldrich) 8 mg/L was then added. The compounds were analysed by gas chromatography (GC) with a coupled mass-selective detector (GC-Agilent 7890B, MSD Agilent 5977A) which was equipped with a HP-5MS capillary column ((5%-phenyl)-methylpolysiloxane, length: 30m, ID: 250 µm, film thickness 0.25 µm). A temperature program with an initial temperature of 70 °C for 2 min and a heating rate of 12 °C/min to 140 °C and a final temperature of 320 °C was applied with a heating rate of 3 °C/min for 3 min and a total run time of 82.83 min, using a Helium carrier gas (2mL/min). The multimode injector was held at a split ratio of 5:1 at an initial temperature of 70 °C for 0.85 min and heated to 300 °C at a programmed rate of 720 °C/min.

Identification of individual compounds was carried out by comparing retention times and mass spectra to those of reference compounds (mix C_8-C_{40} and 5α-androstane, Supelco) and mass spectral library databases (NIST). Quantification of concentrations was achieved using calibration curves that plot the ratio Area/Area$_{IS}$ versus the reference compounds' concentration. Correlation coefficients for each sample were higher than 0.995. Concentration is expressed here in terms of µg of individual compound per gram of dry sample (µg gds^{-1}).

5.2.3. Compound-specific hydrogen isotope analysis

Compound-specific hydrogen isotope analysis was performed using a Thermo Scientific Isotope Ratio Mass Spectrometer (IRMS) Delta V Advantage. The IRMS was coupled to a GC Trace1310 through a Conflo IV interface with a temperature converter GC Isolink II, with a Trace Gold 5-MS (Thermo Scientific) fused silica capillary column ((5%-diphenyl)-dimethylpolysiloxane, 30 m length x 0.25 mm i.d., 0.25 µm film thickness). A helium flow rate of 1.5 mL/min was employed for all measurements carried out in triplicate. Data acquisition and processing were carried out using Isodat 3.0 software (Thermo Scientific). Hydrogen (δ^2H) isotope values are reported for *n*-alkanes C_{29} and C_{31}. Samples were injected using a Programmed Temperature Vaporising injector (PTV) in splitless mode. Temperatures initially increased from 60 °C to 79 °C (held 30 s, rate 10 °C/min) and then to 325 ºC (held 3 min, rate 10 ºC/s) and finally to 350 ºC (held 3 min, rate 14 ºC/s). For the GC oven, a 2 min isothermal period at 70 ºC increasing to 140 ºC (held 2 min, rate 12 ºC/min) was followed by an increase to 320 ºC (held 15 min, rate 3 ºC/min). The high-temperature conversion (HTC) oven was maintained at 1420 ºC for all samples. Values were normalised to the Vienna Standard Mean Ocean Water (VSMOW) scale using an *n*-alkane Schimmelmann type A6 mixture (*n*-C_{16} to *n*-C_{31}) of known isotopic composition (Arndt Schimmelmann; Biogeochemical Laboratories, Indiana University). Reproducibility greater than ± 5.0‰ was attained for most samples, where reproducibility was less than ± 5.0‰, this is clearly stated.

5.3. Results and discussion

5.3.1. Concentration and molecular ratios of n-alkanes

Fossil leaf waxes ranging from nC_{18} – nC_{33} were detected in the leaf samples, and from nC_{16} – nC_{31} in the bark samples and xylem samples. Total *n*-alkane concentration (µg/g dried sample), Carbon Preference Index (CPI_{25-33}) (Bray and Evans, 1961), and Average Chain Length (ACL_{25-33}) (Freeman and Pancost, 2013) have previously been reported in Jambrina-Enriquez et al. (2018) and are outlined for comparison in Table 5.1 below.

***Celtis* leaves**

	Ref	**150 °C**	**250 °C**	**350 °C**	**450 °C**
Total *n*-alkane (µg/g)	459.1	484.0	360.6	97.0	28.8
CPI_{25-33}	2.7	3.3	5.6	4.3	1.1
ACL_{25-33}	30.3	30.4	30.5	30.1	29.7

***Celtis* branch int. (xylem)**

	Ref	**150 °C**	**250 °C**	**350 °C**	**450 °C**
Total *n*-alkane (µg/g)	0.9	0.9	1.2	1.6	0.1
CPI_{25-33}	1.3	1.3	1.3	1.5	-
ACL_{25-33}	26.9	26.9	27.1	26.0	25.0

***Celtis* branch ext. (bark)**

	Ref	150 °C	250 °C	350 °C	450 °C
Total *n*-alkane (µg/g)	18.5	4.2	3.5	8.5	0.1
$CPI_{25\text{-}33}$	3.1	3.4	1.6	1.1	-
$ACL_{25\text{-}33}$	26.5	26.9	27.9	26.6	-

Table 5.1 Quantitative results for total *n*-alkane concentration, Carbon Preference Index (CPI), and Average Chain Length (ACL) (table modified after Jambrina-Enríquez et al. 2018).

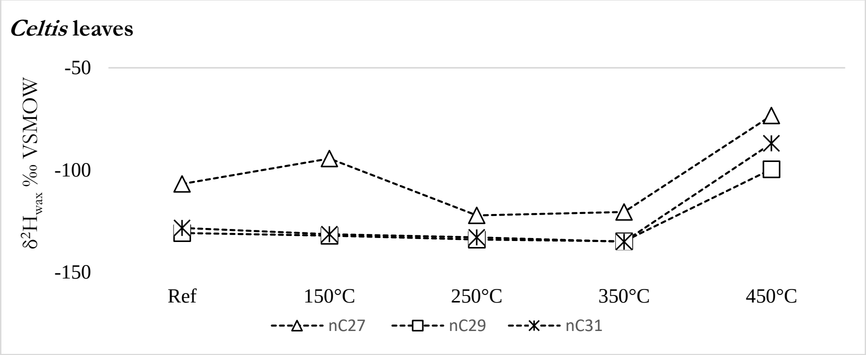

Figure 5.1 Compound-specific hydrogen isotope values of individual long-chain n-alkanes in thermally unaltered reference samples and heated samples of *Celtis australis* leaf. δ^2H_{wax} values (y-axis) are expressed in per mil (‰) and normalised to the Vienna Standard Mean Ocean Water (VSMOW) standard.

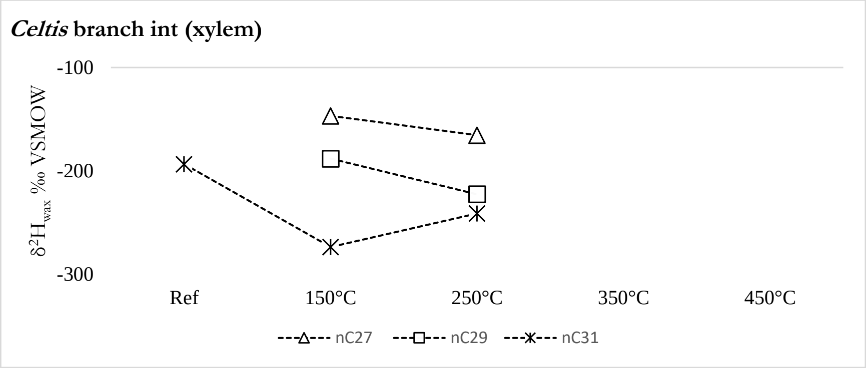

Figure 5.2 Compound-specific hydrogen isotope values of individual long-chain *n*-alkanes in fresh and charred samples of *Celtis australis* branch internal tissue (xylem). δ^2H_{wax} values (y-axis) are expressed in per mil (‰) and normalised to the Vienna Standard Mean Ocean Water (VSMOW) standard.

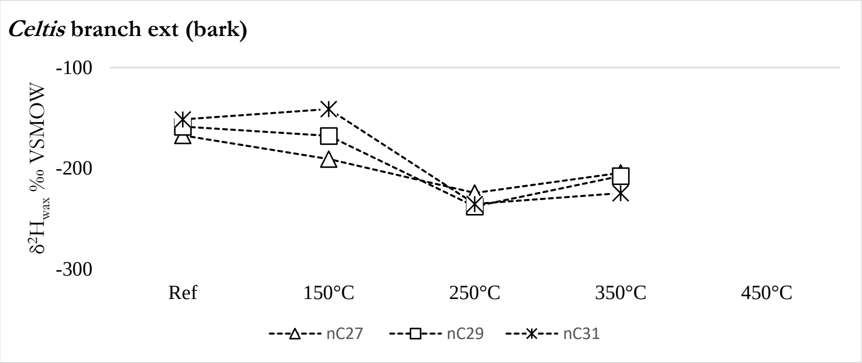

Figure 5. 3 Compound-specific hydrogen isotope values of individual long-chain n-alkanes in in fresh and charred samples of *Celtis australis* branch external tissue (bark). δ^2H_{wax} values (y-axis) are expressed in per mil (‰) and normalised to the Vienna Standard Mean Ocean Water (VSMOW) standard.

***Celtis* leaves**

	Ref	**σ**	**150°C**	**σ**	**250°C**	**σ**	**350°C**	**σ**	**450°C**	**σ**
$\mathbf{C_{27}}$	-106.7	1.2	-94.3	4.3	-122.1	3.2	-120.5	2.9	-73.3	2.1
$\mathbf{C_{29}}$	-130.7	1.0	-132.0	1.4	-133.9	3.7	-134.8	0.6	-99.5	1.0
$\mathbf{C_{31}}$	-128.2	0.6	-131.3	0.9	-132.8	3.0	-135.0	1.7	-87.0	6.1*

***Celtis* branch int. (xylem)**

	Ref	**σ**	**150°C**	**σ**	**250°C**	**σ**	**350°C**	**σ**	**450°C**	**σ**
$\mathbf{C_{27}}$	-	-	-146.8	1.8	-165.4	2.7	-	-	-	-
$\mathbf{C_{29}}$	-	-	-188.2	3.5	-222.7	1.3	-	-	-	-
$\mathbf{C_{31}}$	-193.4	1.1	-273.7	2.4	-241.2	2.2	-	-	-	-

***Celtis* branch ext. (bark)**

	Ref	**σ**	**150°C**	**σ**	**250°C**	**σ**	**350°C**	**σ**	**450°C**	**σ**
$\mathbf{C_{27}}$	-167.3	0.8	-190.8	2.3	-224.3	3.0	-204.5	0.8	-	-
$\mathbf{C_{29}}$	-158.5	4.0	-167.7	1.5	-237.8	5.2*	-207.5	4.1	-	-
$\mathbf{C_{31}}$	-151.4	1.3	-141.2	4.2	-235.2	3.3	-224.5	0.9	-	-

Table 5. 2 Hydrogen isotope values of individual long-chain n-alkanes in thermally unaltered reference samples and heated samples of *Celtis australis* leaf, branch interior (xylem) and exterior (bark). The δ^2H_{wax} values are normalised to the Vienna Standard Mean Ocean Water (VSMOW) standard. Values are expressed in per mil (‰) with one standard deviation. * denotes samples where reproducibility was less than ± 5.0‰ following three replicates.

5.3.2. Variation in δ^2H_{wax} of thermally unaltered reference samples and heated samples of Celtis australis

Here we measured the hydrogen isotope composition of different plant organs of *Celtis australis* during short-term combustions (1 h) at temperatures of 150 °C, 250 °C, 350 °C and 450 °C under limited oxygen conditions (Fig. 5.1-3). We report only the δ^2H_{wax} of nC_{27}, nC_{29} and nC_{31} because these long-chain homologues were recovered in sufficient concentrations for isotopic determination and because these are the most common homologues employed for palaeoecological reconstruction. This data is presented in Table 5.2.

The maximum variation in hydrogen isotope composition observed for each of the sample sets was ~49‰ (nC_{27}), ~80‰ (nC_{31}), and ~94‰ (nC_{31}) for leaves, xylem, and bark, respectively. Based on the nC_{31} homologue, for which isotopic determinations could be made using unaltered reference samples in all three sample sets, leaves are enriched in ^2H (-128.2‰) by ~65‰ relative to xylem (-193.4‰) and ~23‰ relative to bark (-151.4‰). This variation can be explained by physiological and chemical differences which affect alkane biosynthesis and isotopic fractionation in different plant tissues (Post-Beittenmiller, 1996). Although it has been demonstrated that isotopic fractionation of plant xylem water does not occur during root uptake and transport to the leaf, thereby ensuring xylem carries the isotopic signature of the source water, significant differences in δ^2H values have been reported between xylem sap, twigs, roots and wood core (Zhao et al., 2016). Sanchez-Bragado et al. (2019) have also demonstrated that hydrogen isotopic fractionation is affected by photosynthetic processes, with significant differences in δ^2H values observed between plant photosynthetic organs and heterotrophic organs. δ^2H values were beyond the detection limit in unaltered xylem samples for nC_{27} and nC_{29} and corresponding samples heated to temperatures > 350 °C for those homologues. For nC_{29} and nC_{31}, the most common homologues targeted for terrestrial palaeoenvironmental reconstruction, δ^2H values in leaves was generally minimal at temperatures up to 350 °C, with a maximum variation of ~4‰ and ~7‰ respectively, ranging from -131‰ to -135‰ and -128‰ to -135‰. This is followed by an increasing trend in ^2H values at 450 °C. In xylem samples, there is a decreasing trend toward ^{2}H depleted values between 150 °C and 250 °C of ~19‰ (nC_{27}) and ~35‰ (nC_{29}) despite an increase in total *n*-alkane concentration in these samples. Although reliable δ^2H values were not obtained for the unaltered xylem samples for nC_{27} and nC_{29}, making it difficult to meaningfully compare that sample set, a general decreasing trend is observed for nC_{31} between the reference samples and those heated to 250°C. It is also notable that bark samples followed a similar trend to leaves with more depleted values at 250 °C, followed by a slight increase in δ^2H values at 350 °C. Total variation in hydrogen isotope composition of the heated bark samples was in the range of ~57‰ (nC_{27}), ~79‰ (nC_{29}), and ~94‰ (nC_{31}).

To summarise, δ^2H values in *n*-alkanes from leaf waxes were unaltered up to 350 °C with an increasing trend toward ^{2}H enriched values occurring at 450°C. In contrast, in wood tissues (bark and xylem) the original unaltered δ^2H signal was lost at 250 – 350 °C. The observed variations are similar to those described by Jambrina-Enríquez et al. (2018).

5.3.3. Implications for the application of compound-specific hydrogen isotope analysis of fossil leaf waxes in archaeological settings

It is widely accepted that long-chain *n*-alkanes (nC_{27}-nC_{33}), derived from epicuticular leaf waxes, represent the dominant source of *n*-alkanes in sediments (Eglinton and Hamilton, 1967). However, in archaeological contexts or other anthropogenic settings we should not discount the possibility that other plant organs may represent a source of sedimentary *n*-alkanes. Well preserved charred plant tissues and fragments of microcharcoal, which are not visible at the macroscopic scale of excavation, are frequently observed in soil micromorphological samples collected from archaeological sites (Friesem et al., 2014; Goldberg et al., 2009; Leierer et al., 2019; Mallol et al., 2013). In occupation horizons, these materials may represent fuel residues directly linked to combustion features, or alternatively, they may have been deposited through natural agents. For instance, microcharcoal is commonly registered in palynological datasets and has been utilised to study the frequency of natural fires linked to climate shifts (Clark, 1988; Swain, 1973; Val-Peón et al., 2019). Our findings emphasise the need to carefully consider the depositional setting, particularly relating to anthropogenic combustion activities, when interpreting molecular or isotopic information from sedimentary *n*-alkanes in archaeological contexts. The unintentional incorporation of fine charred particles within sediment samples, which has been subjected to temperatures of 450 °C or greater, could lead to misinterpretations of leaf wax δ^2H values and molecular ratios such as CPI and ACL, with significant implications for palaeoclimatic reconstruction. The application of complementary techniques, such as soil micromorphology, can identify charred particles' presence and help eliminate potential biases in the molecular and geochemical datasets. This approach has already effectively been demonstrated at the Middle Palaeolithic site of Abric del Pastor (Alcoy, Spain) (Chapter 4), where abrupt fluctuations in *n*-alkane distribution and compound-specific carbon and hydrogen isotope values through stratigraphic units IVd and IVc were interpreted as resulting from the presence of microscopic charred fuel residues in the lipid biomarker sediment samples (Connolly et al., 2019).

On the other hand, our results here demonstrate that the change in δ^2H values in leaves was generally minimal at temperatures up to 350 °C, with a maximum difference of ~4‰ and ~7‰ for nC_{29} and nC_{31} respectively, ranging from -131‰ to -135‰ and -128‰ to -135‰. This relatively minor ^{2}H depletion is despite a dramatic decrease (~79%) in total *n*-alkane concentration within this temperature range, from 459.1 µg/g to 97 µg/g. Although the effects of short-term low-temperature combustion on *n*-alkane δ^2H values have not been widely investigated, our results are broadly consistent with Wang et al.

(2017), who observed a maximum difference of ~10‰ in δ^2H values of a pure *n*-alkane mixture (nC$_{15}$ to n-C$_{38}$) heated at 100–300 °C. However, it is worth noting that their study was based on a heating duration of 24 h under oxygen-free conditions. As these do not reflect real conditions in the archaeological record, and anthropogenic combustion processes are not produced in the total absence of oxygen, there is a need for more studies like ours which seek to replicate field conditions in so far as is possible in controlled laboratory settings.

The result from our *Celtis australis* leaf samples is potentially significant, as it implies that low-temperature alteration of fossil leaf waxes within sediments (<350 °C) may not eradicate the hydrogen isotope climate signature, opening the door to high-precision onsite palaeoclimate records from lipid biomarkers recovered from archaeological combustion features. In their microstratigraphic study, Mallol et al. (2013) have drawn attention to the potential for thermally altered sedimentary substrates, which underly the black layer of flat combustion features, to yield archaeological information about human activity preceding the combustion event. These sediments, which represent occupation surfaces on which fires were built, do not typically exceed temperatures of 350 °C and may therefore be suitable for compound-specific hydrogen isotope analysis. Such an approach would allow for well-dated palaeoclimate records directly associated with human activities and create a new avenue for exploring human responses to climate change at the site-specific scale. A similar approach has recently been developed by Roffet-Salque et al. (2018) who demonstrated that δ^2H values of lipid residues preserved in pottery from Late Neolithic levels at Çatalhöyük carried the climatic signature of the North Atlantic abrupt climate event which occurred 8.2 kya.

Notwithstanding the relatively small number of samples analysed here, our results provide the initial steps toward establishing boundary conditions for constraining the maximum potential alteration of fossil leaf waxes in thermally altered sediments. Our results are well complemented by Jambrina-Enríquez et al. (2018), who demonstrated that the $\delta^{13}C_{alkane}$ signature of *Celtis australis* leaves also remains constant up to 350 °C under limited oxygen conditions, which suggests that the thermally altered combustion substrates could be targeted for both hydrogen and carbon isotope analysis of individual *n*-alkanes. These isotope signatures respond to different environmental controls and when deployed in tandem allow for more robust conclusions than single isotopic analysis (Bi et al., 2005; Collins et al., 2017; Wu et al., 2018).

5.4. Concluding remarks

Here we investigated the hydrogen isotope composition of thermally unaltered and charred *Celtis australis* leaves, xylem, and bark during short-term combustions (1 h) under limited oxygen conditions in a laboratory-controlled setting, at temperatures up to 450 °C. Our results demonstrate that although significant variation is $\delta^{2}H_{wax}$ is observed in the xylem and bark samples, changes in $\delta^{2}H_{wax}$ of leaf samples are generally minimal up to 350 °C, however, at temperatures exceeding this, considerable changes in hydrogen isotopic composition occur. Our results sound a cautionary note on the application of $\delta^{2}H_{wax}$ as a palaeoclimate proxy in archaeological contexts where the depositional environment is not well understood. We propose that this proxy be enhanced by a detailed characterisation of soil microstratigraphy, which can help eliminate potential isotopic biases that arise due to the mixing of charred microscopic particles ($\geq$ 450 °C) in sediment samples. Nevertheless, our observations highlight the potential for $\delta^{2}H_{wax}$ to record and retain palaeoclimate information at temperatures $\leq$ 350 °C and could be employed to target thermally altered archaeological combustion substrates and link climatic and archaeological datasets at a high spatial and temporal resolution.

Chapter 6: General discussion and conclusion

6.1. Discussion

In this thesis, open questions regarding the application of microscopic and molecular methods for providing new sources of information to approach the relationship between past peoples and their environments have been addressed, with particular reference to the role of climate in Neanderthal social and cultural evolution in Eastern Iberia. Previous studies have demonstrated the potential of archaeological soil micromorphology (Aldeias and Bicho, 2016; Goldberg et al., 2009; Haaland et al., 2020; Mallol, 2006; Stahlschmidt et al., 2018) and compound-specific isotope analysis (Brittingham et al., 2019; Carr et al., 2014; Collins et al., 2017, 2013; Diefendorf et al., 2008; Wang et al., 2016) to yield high-resolution site formation and palaeoenvironmental information across multiple spatial and temporal scales, however, no study has previously deployed these techniques systematically and in tandem for palaeoenvironmental reconstruction in an archaeological setting, nor sought to integrate these approaches with traditional palaeoenvironmental proxies for archaeological research.

The preceding chapters have demonstrated that the combined use of archaeological soil micromorphology and compound-specific carbon and hydrogen isotope analysis of sedimentary fossil leaf waxes can provide additional and complementary information for investigating the relationships between past peoples and their environment. In the third chapter of this thesis, we applied these techniques to investigate climatic variability through Abric del Pastor's sedimentary sequence. This Middle Palaeolithic rock shelter has previously been dated between 43 kya and 72 kya, a key chronological interval for understanding the potential detrimental role of deteriorating MIS 4 global climate conditions on regional Neanderthal populations. Our combined microscopic and molecular approach was complemented by supplementary palaeoenvironmental data from other proxy sources, which included anthracology, micro-vertebrate, and macro-faunal analyses, offering an opportunity to explore the complementarity of our novel approach with more traditional archaeological datasets, one of the key objectives (iii) set out in chapter 1. The results of this study showed that, at the microstratigraphic scale, evidence for cold climate conditions were present in the form of characteristic cryoturbation features, which included platy and granular soil microstructures, soil cappings, and fissured clasts typical of soils and sediments affected by cyclical freeze-thaw processes (Vliet-Lanoë et al., 2004; Vliet-Lanoë, 2010). We also observed micromorphological evidence for localised variation in sedimentary rates, where redoximorphic features and dissolution of the calcitic matrix was interpreted as evidence of more prolonged surface exposures. These processes were particularly notable in S.U. IVd and was key for interpreting trends in the lipid molecular data at that part of the sequence.

Our results confirmed that compound-specific carbon and hydrogen isotope values of *n*-alkanes recovered from Pleistocene sediments at Abric del Pastor record a local vegetation and regional climate signal with high fidelity, and we interpret co-varying δ^2H_{wax} and $\delta^{13}C_{wax}$ values as primarily responding to the combined effects of changes in regional moisture source (i.e. Mediterranean versus Atlantic), precipitation amount and fluctuations in temperature and evaporative stress. With the available evidence, it is not possible to meaningfully disentangle these processes, however, our interpretation is broadly in line with other regional studies in the Iberian Peninsula (Jambrina-Enríquez et al., 2017; Muñoz-Díaz and Rodrigo, 2004; Schirrmacher et al., 2020; Toney et al., 2020). Co-varying trends in the molecular ratios CPI and ACL in S.U. IVc and IVd were interpreted as the result of contamination due to fine charred particles from anthropogenic combustion features being locally dispersed in sediments sampled for lipid biomarkers. The accumulation of these fine particles was undoubtedly accentuated by the slowdown in sedimentary rates observed at the microstratigraphic scale. These observations urge a significant degree of caution in interpreting the lipid molecular and geochemical data at this part of the sequence and motivated the experimental study described in chapter 5. Supplementary palaeoenvironmental data obtained from anthracological, micro-vertebrate and macro-faunal analyses allowed us to 'plug the gap' left by the lipid molecular data in S.U. IVc and IVd, which demonstrates the clear advantage of investigating multiple lines of evidence in parallel. These indicated dry to semi-arid supramediterranean conditions where open dry woodland formations characterise the upper parts of the Barranc del Cinc. Within the ravine where the site is located, Mediterranean mixed forest taxa and riverine species were present in sufficient abundance to provide vital resources for local Neanderthal groups in the form of woody fuel and a habitat for species such as *Testudo hermanni*, which were an important subsistence source. Notwithstanding archaeological evidence from across Europe through MIS 4 which indicates that climatic cooling had detrimental effects on Neanderthal populations, leading to population shrinkage or redistribution (van Andel and Davies, 2003), our results from Abric del Pastor suggest that a mosaic of biotopes likely characterised local conditions along the Central Mediterranean coast of Eastern Iberia. Even across short distances, local variation in conditions was likely influenced significantly by local topographic factors. We have provided evidence for continued Neanderthal occupation at Abric del Pastor despite fluctuations in regional climate conditions. We propose that *c.* 63 kya ± 5 the Barranc del Cinc acted as a vegetation refugium which may have been crucial for the survival of regional Neanderthal populations. Our results highlight the potential for regional and local environmental variability to be masked within large global climatic datasets and call attention to the need for more onsite climate records directly correlated with archaeological data.

In the fourth chapter of this thesis, we provide new insights into site formation and palaeoenvironmental conditions during the deposition of stratigraphic units VIII – V (upper) from the Middle Palaeolithic site of El Salt, which help establish the palaeoclimatic context for the final Neanderthal occupations recorded in the Alcoy region of Eastern Iberia c. 45 kya during MIS 3. Here we combined our novel microscopic and molecular approach with palaeoenvironmental data derived from a detailed study of pollen and non-pollen palynomorphs. We identified two distinct phases of site formation: phase one comprised stratigraphic units VIII – VI and precede the collapse of the rock shelter roof; phase two is represented by stratigraphic unit V (lower and upper). The depositional units of phase one were characterised at the microstratigraphic scale by lithological coarse fraction dominated by tufa and travertine related to the nearby relict Upper Pleistocene freshwater spring system. The presence of guano crusts in our soil thin sections indicates intermittent periods of surface stabilisation of unknown duration, which may correspond with the establishment of vegetation and broad fluctuations in regional environmental conditions. Our pollen data revealed local vegetation dominated by mixed forest taxa which underwent episodic competitive displacements, likely linked to water availability changes.

Our lipid data from phase one shows that *n*-alkanes were not subject to significant microbial degradation. Although $\delta^{13}C_{wax}$ and $\delta^{2}H_{wax}$ results from this phase are too few to draw wholesale conclusions from the isotope data, the general "saw-toothed" pattern observed in total alkane concentration, as well as in VPD, reflect the same changes in vegetation and moisture indicated by the other proxies. The high frequency of anthropogenic materials such as charcoal, burned bones, and flint microflakes in our thin section samples from units VIII – VI, in addition to evidence recovered during excavation, suggest that Neanderthal occupations during phase one at El Salt were recurrent irrespective of persistent environmental oscillations. We propose that S.U. VI (47.2 ± 4.4 ka BP) corresponds with GS-13, just before the onset of HE 5. The collapse of the rock shelter roof marked the beginning of site formation phase two through stratigraphic unit V (lower and upper) and the large limestone blocks from this event seal the underlying units deposited during phase one. Our data supports the argument put forward by Galván et al. (2014) who suggest that the shelter's destabilisation and the roof collapse event correspond to changes in regional environmental conditions provoked by HE 5. Our microstratigraphic study confirms that phase two is characterised by further complexification of the local depositional mechanisms, with a mix of windblown very fine sand and silt with coarser (fine and medium sand) sediments derived from the breakdown of the Palaeocene cliff overlooking the site, all of it locally and syndepositionally reworked and deposited by low-energy processes (runoff). A reduction in regional vegetation cover may account for this increase in windblown sand and silt. A significant reduction in the presence of tufa and travertine in the coarse fraction of soil thin sections representing phase two reflects this shift in transport and deposition processes due to the restructuring of the rock shelter and a likely increase in the sedimentation rates. Soil samples collected for pollen analysis from S.U. V (lower) were found to be sterile, however, despite this, $\delta^{13}C_{wax}$ values at this part of the sequence confirm the presence of a C3 vegetation signal. VPD values fluctuate through S.U. V (lower) and are generally higher in S.U. V (upper), indicating a high evaporative demand of ambient air and a trend toward more arid regional environmental conditions, consistent with the presence of the *Glomus* sp palynomorph, which is common in dry or desiccated areas soils and reached the highest values in S.U. V. Our finding also supports the results presented in Fagoaga et al. (2019), which point to arid conditions during the deposition of S.U. V (upper) based on analysis of the micro-vertebrate assemblage. Regional aridification and climatic deterioration in the area around Alcoy would undoubtedly have affected the availability of critical resources that Neanderthal groups depended on for their survival. The results of our study add new detail and help frame the abrupt decrease in evidence for Neanderthal occupation during phase two at El Salt, adding weight to the argument that the breakdown of regional Neanderthal populations in Eastern Iberia occurred around the time of HE 5 and before the onset HE 4 (Galván et al., 2014). A similar scenario is described by Wolf et al. (2018) who observe that loess deposition and regional aridification in the Upper Tagus Basin occurred between HE 5 and HE 4, coinciding with the disappearance of Neanderthal populations in Central Iberia.

In the fifth chapter of this thesis, our experimental study addresses a significant research gap by exploring potential biases which could arise when using δ^2H_{wax} as a climatic proxy in archaeological contexts affected by anthropogenic combustion activities. Although much has been published on the range of environmental and physiological factors affecting ^2H fractionation in plants (Kahmen et al., 2011; Liu and An, 2018; Sachse et al., 2009, 2006; Schwab et al., 2015), the potential impact of human activities on δ^2H_{wax} has largely been overlooked in previous studies since the development and application of this proxy have mostly focused on sediments which are presumed to be unaffected by human activities. It is critically important that this gap in our knowledge is addressed, particularly as δ^2H_{wax} increasingly comes to be applied in archaeological contexts where combustion activities are ubiquitous and the mixing of fine charred particles in sediments is commonplace. This study revealed that variation in δ^2H_{wax} with increasing temperature differs between plant organs and tissue types, with a high variation corresponding to low alkane concentrations in bark and xylem samples. Significantly, changes in δ^2H_{wax} of leaf, which is the predominant source of *n*-alkanes in sediments, showed a high degree of variation at temperatures ≥ 450 °C. This result highlights the importance of first characterising the depositional environment before sampling sediments for δ^2H_{wax}. It is proposed here that soil micromorphology represents the most robust and comprehensive technique for identifying fine charred particles in archaeological deposits and could be used to help eliminate potential sources of bias in δ^2H_{wax} and lead to more secure palaeoenvironmental interpretations.

Another significant observation from the fifth chapter results was that variation in δ^2H_{wax} from leaf samples at temperatures ≤ 350 °C was generally small. Although further analyses are required to investigate whether this result is repeated across different plant species, it suggests that δ^2H_{wax} could theoretically be utilised to target thermally altered archaeological combustion substrates, providing a new source temporally and spatially resolved onsite climate data that can be directly linked to archaeological datasets. Considering recent advances in high-precision radiocarbon dating, including ongoing developments and improvements in the application of Bayesian statistical analyses (Bayliss, 2015; Carleton, 2021; Pettitt and Zilhão, 2015), the potential to yield molecular climate data directly from anthropogenic combustion features is significant. This approach could offer a powerful means to construct new well-dated onsite paleoclimate records against which longstanding deterministic models of human responses to climatic change can be tested. These methods would also be well complemented by the analysis of δ^2H values of lipid biomarkers preserved on other archaeological materials, which has recently been investigated by Roffet-Salque et al. (2018). These advances are especially pertinent for understanding significant biogeographic, cultural, and evolutionary changes of the Pleistocene, such as the demise of Neanderthal populations at the MUPT, where long-term continuous palaeoenvironmental sequences are mostly absent or far removed from the relevant archaeological assemblages.

6.2. Hypotheses

The hypotheses defined in Section 1.7 are tested against the evidence presented from the studies outlined in this thesis. The null hypothesis (H_0) is proposed and either retained or rejected in favour of an alternative hypothesis (H_1).

6.2.1. Hypothesis I

H_0 - Archaeosediments from Middle Palaeolithic sites in Eastern Iberia *do not* preserve a microscopic and molecular record of Pleistocene climate conditions.

Several studies have highlighted the potential to trace climatic and environmental signals in soil micromorphological thin sections (Macphail et al., 2010; Macphail and Goldberg, 2018; Nicosia and Stoops, 2017; Nieuwendam et al., 2020; Vliet-Lanoë et al., 2004) and through compound-specific isotope analysis of sedimentary fossil leaf waxes (Diefendorf and Freimuth, 2017; Eley et al., 2016; Garcin et al., 2014; Ramos-Román et al., 2018; Yamamoto et al., 2010). However, most of these studies have focused on Holocene sediments or sites where organic preservation is generally good, limiting our understanding of how these signals might present in archaeosediments of Pleistocene age. The study sites investigated in this thesis, Abric del Pastor (MIS 5/4) and El Salt (MIS 3), are ideal for addressing these issues given their respective chronologies, the generally inorganic nature of their sediments, and their geographic setting in Eastern Iberia which experiences both Mediterranean and Atlantic climate influences. Data presented in chapter 3 and chapter 4 of this thesis demonstrate that sedimentary microstructures and fossil leaf waxes are preserved at Abric del Pastor and El Salt and responsive to dynamic external environmental and climatic processes.

The null hypothesis (H_0) is therefore rejected. The following alternative hypothesis (H_1) is proposed: **Archaeosediments from Middle Palaeolithic sites in Eastern Iberia *do* preserve a microscopic and molecular record of Pleistocene climate conditions.**

6.2.2. Hypothesis II

H_0 – **Combined microscopic and molecular analyses of sediments at the study sites *do not* allow accurate and precise reconstruction of past climatic and environmental conditions.**

Chapter 3 and chapter 4 combined archaeological soil micromorphology, lipid biomarker analyses of sedimentary fossil leaf waxes, and compound-specific isotope analyses to investigate past environmental and climatic conditions from Abric del Pastor and El Salt. In both cases, these techniques have been applied alongside other palaeoenvironmental proxies more traditionally employed in archaeology. Similar to other studies which used molecular and isotopic analyses of sedimentary lipid biomarkers in the Iberian Peninsula, we conclude changes in precipitation amount, temperature, local vegetation structure, water stress, and moisture source are the predominant drivers of molecular and isotopic changes (Schäfer et al., 2018; Schirrmacher et al., 2020; Toney et al., 2020). It is widely recognised that there are significant challenges disentangling these variables (Liu and An, 2018; Sachse et al., 2012), which is greatly exacerbated in older archaeological contexts where comparative climate records are typically more fragmentary. We have demonstrated in chapters 3 and 4 that soil micromorphology *can*, if somewhat tentatively, contribute supplementary information about the environmental and depositional context that can help to resolve this. At Abric del Pastor, cold climate conditions throughout the sequence are evidenced at the microstratigraphic level, and these conditions are corroborated in S.U. IVc and IVd through comparison with data from the other palaeoenvironmental proxies. Given the site's chronology, this is also congruent with palaeoenvironmental data for the Iberian Peninsula based on marine sediment core datasets (Sánchez Goñi et al., 1999).

Soil micromorphology also highlighted likely changes in sedimentary rates at both Abric del Pastor and El Salt, which has significant implications for interpreting sedimentary lipid biomarker and compound-specific isotope results. Understanding changes in the mode or rate of sedimentation provide clues not only for understanding the duration of exposure of human occupation surfaces and activities which occurred thereon but critically, this technique helps reduce time-averaging or palimpsest effects and to characterise the sensitivity of the sedimentary environment to a range of relevant climatic and post-depositional variables (Bailey, 2007; Courty and Vallverdu, 2001). Furthermore, the experimental study we present in chapter 5 highlights the importance of identifying whether fine charred particles are present in sediments before sampling for lipid biomarkers. With this in mind, we propose that the combine application of soil micromorphology can contribute to more robust palaeoclimate reconstructions. The results presented in chapters 3 and 4 support the notion that sedimentary microscopic and molecular evidence from Abric del Pastor and El Salt reflect genuine Pleistocene climatic and environmental conditions, though these lines of evidence are no doubt enhanced by cross-validation with other palaeoenvironmental proxies.

The null hypothesis (H_0) is therefore rejected. The following alternative hypothesis (H_1) is proposed: **Combined microscopic and molecular analyses of sediments at the study sites *do* allow accurate and precise reconstruction of past climatic and environmental conditions.**

6.2.3. Hypothesis III

***H_0* – Sedimentary microscopic and molecular climate proxies *cannot* be usefully compared with traditional palaeoenvironmental proxies used in archaeological research.**

Chapters 3 and 4 provide useful case studies for exploring the ways that microscopic and molecular climate proxies can be compared with palaeoenvironmental data gleaned from the study of archaeological materials from the same sites, such as charcoal and faunal assemblages, as well as other sedimentary proxies such as microvertebrate remains and pollen/non-pollen palynomorphs. It is clear from the evidence presented in chapter 3 that practical and theoretical challenges exist linking palaeoenvironmental proxies which are responsive to climatic and environmental variables across different spatial and temporal scales. In practical terms, though our microscopic and molecular proxies cover the full sedimentary sequence at the site, the other proxy datasets are incomplete and could only be compared for S.U. IVd and, in the case of charcoal, also IVc. Also, we must consider that soil microstructures may reflect seasonal freeze-thaw processes, molecular and isotopic changes in fossil leaf waxes may be controlled by centennial to millennial-scale shifts in precipitation amount or North Atlantic Oscillation (NAO), the charcoal assemblage at the site is mostly if not totally the result of intermittent Neanderthal occupation activity and no doubt biased toward more favourable and available fuel sources. In contrast, the microvertebrate assemblage is linked to the Eurasian eagle-owl activities (*Bubo bubo*) whose range may extend beyond the limits of the ravine where the site is located. Emphasis on differences of scale, particularly concerning time, has been the focus of much discussion and debate in archaeology (Bailey, 2007, 1983; Holdaway and Wandsnider, 2008; Lucas, 2004). By combining climatic and environmental proxies which respond to different phenomena and vary in terms of their respective spatial and temporal resolution, archaeologists will have the opportunity to address questions about relationships between different kinds of processes. The results presented in chapter 3 demonstrate that while inherent uncertainties may prevent direct correlations between individual datapoints from different proxies, broad relationships and inferences about regional environmental conditions can be discerned. Chapter 4 also reveals how our microscopic and molecular approach can complement other palaeoenvironmental proxies by overcoming issues surrounding preservation—for instance, sediment samples collected for pollen analysis from S.U. V (lower) at El Salt were found to be sterile, however, our lipid biomarker and compound-specific isotope results confirmed the regional presence of C3 vegetation during the deposition of this unit, while the presence of local vegetation cover in the immediate area around the site was evidenced by the occurrence of *Celtis sp.* seed coatings in our soil micromorphological samples.

The null hypothesis (H_0) is therefore rejected. The following alternative hypothesis (H_1) is proposed: **Sedimentary microscopic and molecular climate proxies *can* be usefully compared with traditional palaeoenvironmental proxies used in archaeological research.**

6.2.4. Hypothesis IV

H_0 – Sedimentary microscopic and molecular climate proxies *do not* indicate unstable environmental conditions during MIS 3 in Eastern Iberia.

It has been argued that MIS 3 was characterised by abrupt and unstable climatic changes marked by significant drops in temperatures and episodes of widespread aridification, producing environmental conditions and resource distributions not typically found in modern environments (Stewart, 2005). At a global and continental scale, this climatic instability has been recorded by several different proxies, including $\delta^{18}O$ of Greenland ice-cores (NGRIP), evidence of ice-rafted debris (IRD) from North Atlantic marine sediment cores, and isotope records of planktonic and benthic foraminifera, among other sources (Adams et al., 1999; Birner et al., 2016; Blockley et al., 2014; Maslin et al., 2013; North Greenland Ice Core Project members, 2004; Rasmussen et al., 2014; Sánchez Goñi et al., 2008). This has led many researchers to implicate climatic crises during MIS 3 in Neanderthal demise in the Iberian Peninsula (Finlayson, 2004; Finlayson and Carrión, 2007; Jiménez–Espejo et al., 2007; Müller et al., 2011; Wolf et al., 2018). As set out in chapter 1, however, it is unclear the extent to which reconstructions based on coarse proxies such as these reflect conditions at a regional scale. Given the large error range in the available MIS 3 chronometric dates from the study sites investigated in this thesis, attempts to link our microscopic and lipid molecular records with larger climate datasets remain speculative. Nevertheless, the results from both sites demonstrate millennial scale climatic variability throughout MIS 3. This variability is particularly prounounced at El Salt in the observed fluctuations in *n*-alkane molecular ratios such as CPI, ACL, and VPD, as well as in compound-specific carbon and hydrogen isotope values. The formation of phosphatic crusts, observed in our micromorphological samples, are also interpreted as evidence of intermittent surface stabilisation linked to broad changes in regional environmental conditions and vegetation structure.

The null hypothesis (H_0) is therefore rejected. The following alternative hypothesis (H_1) is proposed: **Sedimentary microscopic and molecular climate proxies *do* indicate unstable environmental conditions during MIS 3 in Eastern Iberia.**

6.2.5. Hypothesis V

***H_0* – There is *no* consistent relationship between climate change or abrupt climate events and Neanderthal activity at the selected study sites.**

Global cooling during MIS 4, climatic instability and rapid ecological turnover during MIS 3, and abrupt climate events such as HE 5 (*c.* 50 - 47 kya) and HE 4 (*c.* 39 kya) have long been implicated in the demise of Neanderthal populations in the Iberian Peninsula (Finlayson, 2004; Finlayson and Carrión, 2007; Mallol et al., 2019; Mellars, 2006; Müller et al., 2011; Sepulchre et al., 2007). In chapter 3 and chapter 4 of this thesis, we have provided new lines of evidence for investigating the relationship between Neanderthal occupations in the Alcoy region of Eastern Iberia and fluctuations in environmental conditions through the course of MIS 4 and MIS 3. The results of our multiproxy study presented in chapter 3 indicate regional climatic and environmental fluctuations through the sedimentary sequence at Abric del Pastor, despite which there is abundant evidence for repeated short-term Neanderthal occupation events dated between 48 kya ± 5 (MIS 3) and 62 kya ± 12 (MIS 4). Recent technical and spatial studies of lithic refits from S.U. IV (IVb, IVc, IVd) at the site indicate a minimum of 9 distinct Neanderthal occupation episodes, represented by broadly similar hearth-related assemblages (Machado et al., 2019, 2013). Although the overall number of occupation events is too low to meaningfully discern causal or correlative relationships between the palaeoenvironmental and archaeological records, it is notable that the most intense occupation activity is recorded in S.U. IVd, which is dated by OSL to 63 kya ± 5. This may be pronounced by palimpsest effects due to a slowing down in the rates of sedimentation at this part of the sequence, as indicated by our soil micromorphology samples. Alternatively, this may reflect a real, if somewhat modest, increase in human occupation of the rock shelter linked to a downturn in wider regional environmental conditions.

It is also noteworthy that the last chronometric dates for Neanderthal activity at Abric del Pastor, 48 kya ± 5 (S.U. IVb), overlap with the dates from the nearby site of El Salt where the final Neanderthal occupations are recorded *c.* 45 kya (Galván et al., 2014). There, our palaeoenvironmental results point to unstable environmental conditions in S.U. VIII - VI, with turnover in local vegetation structure linked to episodic fluctuations in humidity and intermittent periods of soil surface stabilisation. During this time, evidence for Neanderthal occupation activities is abundant both at the microscopic scale through soil micromorphology and at the macroscopic scale of excavation. However, our results reveal that the final Neanderthal occupations at El Salt are coincident with an abrupt change in sedimentary dynamics recorded in S.U. V and the onset of regional aridification following HE 5 but prior to the commencement of HE 4, in line with previous studies from this site and elsewhere (Fagoaga et al., 2019; Galván et al., 2014; Kehl et al., 2013; Wood et al., 2013).

The palaeoclimate and palaeoenvironmental records for both Abric del Pastor and El Salt exhibit high variability. Despite evidence for aridification at El Salt around the time of the final Neanderthal occupations, and the disappearance of Neanderthals from Abric del Pastor around the same time, the evidence presented in this thesis does not provide sufficient grounds in and of itself to support arguments in favour of a consistent relationship between climate change or abrupt climate events and Neanderthal activity at the selected study sites. The evidence presented here certainly does not preclude such relationships, or otherwise suggest that Neanderthal activity at the sites is unconnected to climatic processes. However, there are confounding differences in resolution and completeness between archaeological and palaeoclimatic datasets that demand further evidence to meaningfully link local environmental conditions and Neanderthal social and cultural processes through time.

The null hypothesis (H_0) is therefore retained.

6.3. Conclusion

The work presented in this thesis has highlighted the applicability and potential value of systematically combining archaeological soil micromorphology and compound-specific isotope analysis of sedimentary lipid biomarkers for reconstructing palaeoenvironmental conditions from well-described archaeological contexts and providing new lines of evidence for investigating the relationship between past peoples and their environments. The results presented here have also added new levels of detail to our understanding of the regional palaeoclimatic and environmental variability of MIS 4 through MIS 3, which framed the disappearance of Neanderthals in the Alcoy region of Eastern Iberia. Combined microscopic and molecular approaches such as this present an opportunity to not only enhance existing onsite palaeoenvironmental records but crucially, to reconstruct conditions even in archaeological contexts where post-depositional disturbance or poor preservation renders other proxies such as charcoal or pollen obsolete. Chapter 1 argued reconstructions based on ice-core and deep-sea sediments, or discontinuous terrestrial palynological sequences, lack the spatio-temporal resolution to meaningfully investigate the role of climate in Neanderthal social and cultural evolution at a regional scale. As demonstrated in chapter 3 and chapter 4, regional and local variability is an important feature of Abric del Pastor and El Salt's palaeoenvironmental records. Despite our microscopic and molecular approach, there are still significant challenges linking palaeoenvironmental and archaeological records due to spatial or temporal resolution differences and inherent chronological uncertainties.

It is anticipated that archaeological soil micromorphology and compound-specific isotope analysis of lipid biomarkers will increasingly be utilised to investigate archaeosediments to elucidate links between past climate changes and trends in human cultural evolution. Based on this thesis's results, the combined future application of these techniques should focus on integrating methods or approaches for establishing improved chronologies and spatial resolution. To this end, researchers will no doubt benefit from recent advances in Bayesian statistical analysis of high-precision radiocarbon dates, as well as recent breakthroughs in compound-specific radiocarbon analysis (CSRA) of individual lipid compounds (Casanova et al., 2020; Deviese et al., 2018; Smyth et al., 2019). Recent research has also revealed exciting possibilities for targeted molecular and isotopic analysis of lipid biomarkers from polyester resin-impregnated soil micromorphology sediment slabs (Rodríguez de Vera et al., 2020). Future work that combines these advances with the approach set out in this thesis has the potential to provide unprecedentedly detailed reconstructions of regional and local climatic variability from onsite records and facilitate robust explorations of links between palaeoenvironmental and archaeological records. Developments in this direction will offer exciting new avenues for investigating the complex mechanisms that underpin how past societies responded to environmental or climatic changes, helping researchers gain a more nuanced understanding of the role of climate in Neanderthal social and cultural evolution.

Chapter 7: Bibliography

Adams, J., Maslin, M., Thomas, E., 1999. Sudden climate transitions during the Quaternary. *Progress in Physical Geography: Earth and Environment* 23, 1–36.

Agafonoff, V., 1929. Sur quelques sols rouges et Bienhoa de l'Indochine (Suite et fin). *Journal d'agriculture traditionnelle et de botanique appliquée* 9, 120–126.

AHE. 2016. SIARE (Servidor de Información de Anfibios y Reptiles de España). Asociación Herpetológica Española. [accessed November 2018 at http://siare.herpetologica.es/bdh].

Albert, R.M., Cabanes, D., 2007. Fire in prehistory: An experimental approach to combustion processes and phytolith remains. *Israel Journal of Earth Sciences* 56 (2–4), 175–189.

Alcaraz–Castaño, M., Alcolea–González, J., Kehl, M., Albert, R.–M., Baena–Preysler, J., de Balbín–Behrmann, R., Cuartero, F., Cuenca–Bescós, G., Jiménez–Barredo, F., López–Sáez, J.–A., Piqué, R., Rodríguez–Antón, D., Yravedra, J., Weniger, G.–C., 2017. A context for the last Neandertals of interior Iberia: Los Casares cave revisited. *PLoS One* 12, e0180823.

Aldeias, V., 2017. Experimental Approaches to Archaeological Fire Features and Their Behavioral Relevance. *Current Anthropology* 58, 191 – 205.

Aldeias, V., Bicho, N., 2016. Embedded Behavior: Human Activities and the Construction of the Mesolithic Shellmound of Cabeco da Amoreira, Muge, Portugal. Geoarchaeology 31, 530–549.

Aldeias, V., Gur–Arieh, S., Maria, R., Monteiro, P., Cura, P., 2016. Shell we cook it? An experimental approach to the microarchaeological record of shellfish roasting. *Archaeological and Anthropological Sciences* 11, 389–407.

Allen, V.T., 1930. *Petrographic studies bearing on the genesis and morphology of Illinois soils*. Proceedings of Second International Congress on Soil Science, 113–117.

Allué, E., Cabanes, D., Solé, A., Sala, R., 2012. Hearth Functioning and Forest Resource Exploitation Based on the Archeobotanical Assemblage from Level J. In: Roura, E.C. (Ed.) *High Resolution Archaeology and Neanderthal Behavior, Vertebrate Paleobiology and Paleoanthropology*. Springer Netherlands, 373–385.

Anderson, R.S., Homola, R.L., Davis, R.B., Jacobson, G.L., Jr., 1984. Fossil remains of the mycorrhizal fungal Glomus fasciculatum complex in postglacial lake sediments from Maine. *Canadian Journal of Botany* 62, 2325–2328.

Andrews, P., 1990. *Owls, Caves and Fossils*. Natural History Museum Publications, London.

Andrews, P., Evans, E.M.N., 1983. Small mammal bone accumulations produced by mammalian carnivores. *Paleobiology* 9, 289–307.

Angelucci, D.E., 2010. The recognition and description of knapped lithic artifacts in thin section. *Geoarchaeology* 25(2), 220–232.

Angelucci, D.E., Zambaldi, M., Tessari, U., Vaccaro, C., Arnaud, J., Berruti, G.L.F., Daffara, S., Arzarello, M., 2019. New insights on the Monte Fenera Palaeolithic, Italy: Geoarchaeology of the Ciota Ciara cave. *Geoarchaeology* 34, 413–429.

Arponen, V.P.J., Dörfler, W., Feeser, I., Grimm, S., Groß, D., Hinz, M., Knitter, D., Müller–Scheeßel, N., Ott, K., Ribeiro, A., 2019. Environmental determinism and archaeology. Understanding and evaluating determinism in research design. *Archaeological Dialogues* 26, 1–9.

Badal, E. 1992. L'anthracologie préhistorique: à propos de certains problèmes méthodologiques, in J.–L. Vernet (dir.), *Les charbons de bois, les anciens écosystèmes et le rôle de l'homme, Montpellier*. Société botanique de France (Bulletin de la Société botanique de France 139), 167–190.

Badal, E., Heinz, C., 1991. Méthodes utilisées en Anthracologie pour l'étude de sites préhistoriques. *BAR International Series* 573, 17–47.

Bailey, G., 2007. Time perspectives, palimpsests and the archaeology of time. *Journal of Anthropological Archaeology* 26, 198–223.

Bailey, G.N., 1983. Concepts of Time in Quaternary Prehistory. *Annual Review of Anthropology* 12, 165–192.

Bailon, S., 1991. *Amphibiens et reptiles du Pliocene et du Quaternaire de France et d´Espagne: mise en place et evolution des faunes*. Ph.D. Thesis, Universite de Paris VII (Unpublished).

Bailon, S., 1999 *Différenciation ostéologique des anoures (Amphibia, Anura) de France*. In: Desse, J., DesseBerset, N. (Eds.) Fiches d'Ostéologie Animale pour l'Archéologie, Antibes, Centre de Recherches Archéologiques du CNRS, APDCA, série C, 1–42.

Banks, W.E., d'Errico, F., Peterson, A.T., Kageyama, M., Sima, A., Sánchez–Goñi, M.–F., 2008. Neanderthal extinction by competitive exclusion. *PLoS One* 3, e3972.

Barahona, F., 1996. *Osteología craneal de lacértidos de la Península Ibérica e Islas Canarias: análisis sistemático filogenético*. Ph.D. Thesis, Universidad Autónoma de Madrid (Unpublished).

Barahona, F., Barbadillo, L.J., 1997. Identification of some Iberian lacertids using skull characters. *Revista Española de Herpetología* 11, 47–62.

Barnes, J., Dove, M.R., 2015. *Climate Cultures: Anthropological Perspectives on Climate Change*. Yale University Press.

Barnes, J., Paul, N., Percy, K., Broadbent, P., McLaughlin, C., Mullineaux, P., Creissen, G., Wellburn, A., 1994. *Effects of UV–B Radiation on Wax Biosynthesis. Air Pollutants and the Leaf Cuticle.* In: Percy K.E., Cape J.N., Jagels R., Simpson C.J. (Eds.) Air pollutants and the leaf cuticle, NATO ASI Series 36. Berlin, Springer–Verlag, 195–205.

Bayliss, A., 2015. Quality in Bayesian chronological models in archaeology. *World Archaeology* 47, 677–700.

Bencatel, J., Álvares, F., Moura, A.E., Barbosa, A.M., 2017. *Atlas de Mamíferos de Portugal*. Universidade de Évora, Portugal.

Benetti, M., Steen–Larsen, H.C., Reverdin, G., Sveinbjörnsdóttir, Á.E., Aloisi, G., Berkelhammer, M.B., Bourlès, B., Bourras, D., de Coetlogon, G., Cosgrove, A., Faber, A.–K., Grelet, J., Hansen, S.B., Johnson, R., Legoff, H., Martin, N., Peters, A.J., Popp, T.J., Reynaud, T., Winther, M., 2017. Stable isotopes in the atmospheric marine boundary layer water vapour over the Atlantic Ocean, 2012–2015. *Scientific Data* 4, 160128.

Beresford–Jones, D.G., Johnson, K., Pullen, A.G., Pryor, A.J.E., Svoboda, J., Jones, M.K., 2010. Burning wood or burning bone? A reconsideration of flotation evidence from Upper Palaeolithic (Gravettian) sites in the Moravian Corridor. *Journal of Archaeological Science* 37, 2799–2811.

Berna, F., Goldberg, P., Horwitz, L.K., Brink, J., Holt, S., Bamford, M., Chazan, M., 2012. Microstratigraphic evidence of in situ fire in the Acheulean strata of Wonderwerk Cave, Northern Cape province, South Africa. *Proceedings of the National Academy of Sciences of the United States of America* 109, E1215–20.

Bi, X., Sheng, G., Liu, X., Li, C., Fu, J., 2005. Molecular and carbon and hydrogen isotopic composition of n–alkanes in plant leaf waxes. *Organic Geochemistry* 36, 1405–1417.

Biltekin, D., Burjachs, F., Vallverdú, J., Sharp, W.D., Mertz–Kraus, R., Gema Chacón, M., Saladié, P., Bischoff, J.L., Carbonell, E., 2019. Vegetation and climate record from Abric Romaní (Capellades, northeast Iberia) during the Upper Pleistocene (MIS 5d−3). *Quaternary Science Reviews* 220, 154–164.

Binford, L.R., 1964. A Consideration of Archaeological Research Design. *American Antiquity* 29, 425–441.

Binford, L.R., 1981. *Bones: Ancient Men and Modern Myths, Studies in Archaeology*. Academic Press, New York.

Binford, L.R., 1983. *In Pursuit of the Past: Decoding the Archaeological Record*. Thames and Hudson, London and New York.

Binford, L.R., 1996. *Hearth and home: the spatial analysis of ethnographically documented rock shelter occupations as a template for distinguishing between human and hominid use of sheltered space*. In: XIII UISPP Congress Proceedings– Forli, 8–14 September 1996, 229–239.

Birner, B., Hodell, D.A., Tzedakis, P.C., Skinner, L.C., 2016. Similar millennial climate variability on the Iberian margin during two early Pleistocene glacials and MIS 3: Early Pleistocene millennial variability. *Paleoceanography* 31, 203–217.

Bischoff, J.L., Rosenbauer, R.J., Tavoso, A., de Lumley, H., 1988. A test of uranium–series dating of fossil tooth enamel: results from Tournal Cave, France. *Applied Geochemistry* 3, 145–151.

Blain, H.A., 2009. Contribution de la paléoherpétofaune (Amphibia and Squamata) à la connaissance de l´évolution du climat et du paysage du Pliocène supérieur au Pléistocène moyen d´Espagne. *Treballs del Museu de Geologia de Barcelona* 16, 39–170.

Blain, H.A., Bailon, S., Cuenca–Bescós, G., Arsuaga, J.L., Bermúdez de Castro, J.M., Carbonell, E., 2009. Long–term climate record inferred from Early–Middle Pleistocene amphibian and squamate reptile assemblages at the Gran Dolina cave, Atapuerca, Spain. *Journal of Human Evolution* 56, 55–65.

Blain, H.–A., Gleed–Owen, C.P., López–García, J.M., Carrión, J.S., Jennings, R., Finlayson, G., Finlayson, C., Giles–Pacheco, F., 2013. Climatic conditions for the last Neanderthals: Herpetofaunal record of Gorham's Cave, Gibraltar. *Journal of Human Evolution* 64, 289–299.

Blain, H.A., Laplana, C., Sevilla, P., Arsuaga, J.L., Baquedano, E., Pérez–González, A., 2014. MIS 5/4 transition in a mountain environment: herpetofaunal assemblages from Cueva del Camino, central Spain. *Boreas* 43, 107–120.

Blain, H.–A., Lozano–Fernández, I., Agustí, J., Bailon, S., Menéndez, L.G., Espígares, P.O.M., Ros–Montoya, S., Jiménez, J.M.A., Toro–Moyano, I., Martínez–Navarro, B., Sala, R., 2016. Redefining upon the climatic background of the early Pleistocene hominid settlement in western Europe: Barranco Leon and Fuente Nueva–3 (Guadix–Baza basin, SE Spain). *Quaternary Science Reviews* 144, 132–144.

Blockley, S.P.E., Ramsey, C.B., Higham, T.F.G., 2008. The Middle to Upper Paleolithic transition: dating, stratigraphy, and isochronous markers. *Journal of Human Evolution* 55, 764–771.

Blockley, S.P.E., Bourne, A.J., Brauer, A., Davies, S.M., Hardiman, M., Harding, P.R., Lane, C.S., MacLeod, A., Matthews, I.P., Pyne-O'Donnell, S.D.F., Rasmussen, S.O., Wulf, S., Zanchetta, G., 2014. Tephrochronology and the extended intimate (integration of ice-core, marine and terrestrial records) event stratigraphy 8–128 ka b2k. *Quaternary Science Reviews* 106, 88–100.

Blomquist, G.J., Tillman, J.A., Mpuru, S., Seybold, S.J., 2019. *The Cuticle and Cuticular Hydrocarbons of Insects: Structure, Function, and Biochemistry*. In: Vander Meer, R.K., Breed, M.D., Winston, M., Espelie, K.E. (Eds.) Pheromone Communication in Social Insects. CRC Press.

Bocquet–Appel, J.P., Demars, P.Y., 2000. Neanderthal contraction and modern human colonization of Europe. *Antiquity* 74, 544–552.

Bottema, S., 1975. The interpretation of pollen spectra from prehistoric settlements (with special attention of Liguliflorae). *Palaeohistoria* 17–35.

Braadbaart, F., Poole, I., 2008. Morphological, chemical and physical changes during charcoalification of wood and its relevance to archaeological contexts. *Journal of Archaeological Science* 35, 2434–2445.

Bradtmöller, M., Pastoors, A., Weninger, B., Weniger, G.C., 2012. The repeated replacement model – Rapid climate change and population dynamics in Late Pleistocene Europe. *Quaternary International* 247, 38–49.

Bray, E.E., Evans, E.D., 1961. Distribution of n –paraffins as a clue to recognition of source beds. *Geochimica et Cosmochimica Acta* 22, 2–15.

Brennan, B.J., Rink, W.J., McGuirl, E.L., Schwarcz, H.P., Prestwich, W.V., 1997. Beta doses in tooth enamel by "one–group" theory and the ROSY ESR dating software. *Radiation Measurements* 27, 307–314.

Brittingham, A., Hren, M.T., Hartman, G., 2017. Microbial alteration of the hydrogen and carbon isotopic composition of n–alkanes in sediments. *Organic Geochemistry* 107, 1–8.

Brittingham, A., Petrosyan, Z., Hepburn, J.C., Richards, M.P., Hren, M.T., Hartman, G., 2019. Influence of the North Atlantic Oscillation on δD and δ18O in meteoric water in the Armenian Highland. *Journal of Hydrology* 575, 513–522.

Brose, D.S., 1970. *The Summer Island site: A study of prehistoric cultural ecology and social organization in the Northern Lake Michigan area*. Case Western Reserve University.

Bullock, P., Fedoroff, N., Jongerius, A., Stoops, G., Tursina, T., 1985. *Handbook for soil thin section description*. Waine Research.

Bunn, H.T., 1986. Patterns of skeletal representation and hominid subsistence activities at Olduvai Gorge, Tanzania, and Koobi Fora, Kenya. *Journal of Human Evolution* 15, 673–690.

Buonasera, T., Herrera–Herrera, A.V., Mallol, C., 2019. Experimentally Derived Sedimentary, Molecular, and Isotopic Characteristics of Bone–Fueled Hearths. *Journal of Archaeological Method and Theory* 26, 1327–1375.

Buonasera, T.Y., Tremayne, A.H., Darwent, C.M., Eerkens, J.W., Mason, O.K., 2015. Lipid biomarkers and compound specific δ13C analysis indicate early development of a dual–economic system for the Arctic Small Tool tradition in northern Alaska. *Journal of Archaeological Science* 61, 129–138.

Burgoyne, T.W., Hayes, J.M., 1998. Quantitative Production of H2 by Pyrolysis of Gas Chromatographic Effluents. *Analytical Chemistry* 70, 5136–5141.

Burjachs, F., 1990. *Palinologia dels dolmenes de l'Alt Empordà i dels diposits quaternaris de la cova de l'Arbreda (Serinyà, Pla de l'Estany) i del Pla de l'Estany (Olot, Garrotxa).Evolució del paisatge vegetal i del clima des de fa més de 140.000 anys al NE de la Península Ibèrica, Bellaterra, Barcelona*, Ph.D. Thesis. Universitat Autònoma de Barcelona, Barcelona.

Burjachs, F., Julià, R., 1994. Abrupt Climatic Changes during the Last Glaciation Based on Pollen Analysis of the Abric Romani, Catalonia, Spain. *Quaternary Research* 42, 308–315.

Burjachs, F., López–García, J.M., Allué, E., Blain, H.–A., Rivals, F., Bennàsar, M., Expósito, I., 2012. Palaeoecology of Neanderthals during Dansgaard–Oeschger cycles in northeastern Iberia (Abric Romaní): From regional to global scale. *Quaternary International* 247, 26–37.

Burjachs, F., López–Sáez, J.A., Iriarte, M.J., 2003. *Metodología arqueopalinológica.* In: Buxó, R., Piqué, R. (Eds.), La recogida de muestras en arqueobotànica: objetivos y propuestas metodológicas. Museu d'Arqueologia de Catalunya, Barcelona, 11–18.

Burke, A., Levavasseur, G., James, P.M.A., Guiducci, D., Izquierdo, M.A., Bourgeon, L., Kageyama, M., Ramstein, G., Vrac, M., 2014. Exploring the impact of climate variability during the Last Glacial Maximum on the pattern of human occupation of Iberia. *Journal of Human Evolution* 73, 35–46.

Bush, R.T., McInerney, F.A., 2013. Leaf wax n–alkane distributions in and across modern plants: Implications for paleoecology and chemotaxonomy. *Geochimica et Cosmochimica Acta* 117, 161–179.

Butler, D.H., Koivisto, S., Brumfeld, V., Shahack–Gross, R., 2019. Early Evidence for Northern Salmonid Fisheries Discovered using Novel Mineral Proxies. *Scientific Reports* 9, 147.

Butzer, K.W., 1982. *Archaeology as Human Ecology: Method and Theory for a Contextual Approach*. Cambridge University Press.

Cacho, I., Grimalt, J.O., Pelejero, C., Canals, M., Sierro, F.J., Flores, J.A., Shackleton, N., 1999. Dansgaard–Oeschger and Heinrich event imprints in Alboran Sea paleotemperatures. *Paleoceanography* 14, 698–705.

Carleton, W.C., 2021. Evaluating Bayesian Radiocarbon-dated Event Count (REC) models for the study of long-term human and environmental processes. *Journal of Quaternary Science* 36, 110–123.

Carr, A.S., Boom, A., Grimes, H.L., Chase, B.M., Meadows, M.E., Harris, A., 2014. Leaf wax n–alkane distributions in arid zone South African flora: Environmental controls, chemotaxonomy and palaeoecological implications. *Organic Geochemistry* 67, 72–84.

Carrión, J.S., 1992. Late Quaternary pollen sequence from Carihuela Cave, southeastern Spain. *Review of Palaeobotany and Palynology* 71, 37–77.

Carrión, J.S., Munuera, M., 1997. Upper Pleistocene palaeoenvironmental change in Eastern Spain: new pollen–analytical data from Cova Beneito (Alicante). *Palaeogeography, Palaeoclimatology, Palaeoecology* 128, 287–299.

Casanova, E., Knowles, T.D.J., Bayliss, A., Dunne, J., Barański, M.Z., Denaire, A., Lefranc, P., di Lernia, S., Roffet–Salque, M., Smyth, J., Barclay, A., Gillard, T., Claßen, E., Coles, B., Ilett, M., Jeunesse, C., Krueger, M., Marciniak, A., Minnitt, S., Rotunno, R., van de Velde, P., van Wijk, I., Cotton, J., Daykin, A., Evershed, R.P., 2020. Accurate compound–specific 14 C dating of archaeological pottery vessels. *Nature* 1–5.

Chabal, L., 1997. *Forêts et sociétés en Languedoc (Néolithique final, Antiquité tardive) : l'anthracologie, méthode et paléoécologie*. Éditions de la Maison des sciences de l'homme. Paris.

Chazan, M., 2017. Toward a Long Prehistory of Fire. *Current Anthropology* 58, 351–359.

Cheng, G., Huang, H., Zhou, L., He, S., Zhang, Y., Cheng, X. 'an, 2019. Chemical composition and water permeability of the cuticular wax barrier in rose leaf and petal: A comparative investigation. *Plant Physiology and Biochemistry* 135, 404–410.

Choy, K., Potter, B.A., McKinney, H.J., Reuther, J.D., Wang, S.W., Wooller, M.J., 2016. Chemical profiling of ancient hearths reveals recurrent salmon use in Ice Age Beringia. *Proceedings of the National Academy of Sciences of the United States of America* 113, 9757–9762.

Clark, J.S., 1988. Particle motion and the theory of charcoal analysis: Source area, transport, deposition, and sampling. *Quaternary Research* 30, 67–80.

Cliquet, D., Dumont, J.L., Dupont, J.P., Fosse, G., Jouis, M., Lanoe, B., Mante, C., Morel, J., Quillard, J., Thiébault, S., Others, 1989. *Approche d'une étude comparative des matières organiques de foyers préhistoriques et de foyers expérimentaux: l'exemple du gisement moustérien de Saint–Germain–des–Vaux (Manche)*. Association pour la promotion de la recherche archéologique en Ile de France.

Collins, J.A., Carr, A.S., Schefuß, E., Boom, A., Sealy, J., 2017. Investigation of organic matter and biomarkers from Diepkloof Rock Shelter, South Africa: Insights into Middle Stone Age site usage and palaeoclimate. *Journal of Archaeological Science* 85, 51–65.

Collins, J.A., Schefuß, E., Mulitza, S., Prange, M., Werner, M., Tharammal, T., Paul, A., Wefer, G., 2013. Estimating the hydrogen isotopic composition of past precipitation using leaf–waxes from western Africa. *Quaternary Science Reviews* 65, 88–101.

Conard, N.J., 2011. *The Demise of the Neanderthal Cultural Niche and the Beginning of the Upper Paleolithic in Southwestern Germany*. In: Conard, N.J., Richter, J. (Eds.) Neanderthal Lifeways, Subsistence and Technology: One Hundred Fifty Years of Neanderthal Study. Springer Netherlands, Dordrecht, 223–240.

Connolly, R., Jambrina–Enríquez, M., Herrera–Herrera, A.V., Vidal-Matutano, P., Fagoaga, A., Marquina–Blasco, R., Marin–Monfort, M.D., Ruiz–Sánchez, F.J., Laplana, C., Bailon, S., Pérez, L., Leierer, L., Hernández, C.M., Galván, B., Mallol, C., 2019. A multiproxy record of palaeoenvironmental conditions at the Middle Palaeolithic site of Abric del Pastor (Eastern Iberia). *Quaternary Science Reviews* 225, 106023.

Contreras, D.A., 2016. *Correlation is not enough: building better arguments in the archaeology of human–environment interactions*. In: Contreras, D. (Ed.) The Archaeology of Human–Environment Interactions. Routledge, 17–36.

Coombes, P., Barber, K., 2005. Environmental determinism in Holocene research: causality or coincidence? *Area* 37 (3), 303–311.

Cornwall, I.W., 1958. *Soils for the Archaeologist*. Phoenix, London.

Costa, M., Morla, C., Sainz, H., 2005. *Los bosques ibéricos: una interpretación geobotánica*. Editorial Planeta, Barcelona.

Costamagno, S., Théry–Parisot, I., Brugal, J.–P., Guibert, R., 2005. *Taphonomic consequences of the use of bones as fuel. Experimental data and archaeological applications*. In: O'Connor, T. (Ed.) Biosphere to Lithosphere: New Studies in Vertebrate Taphonomy. Oxbow Books Oxford, 51–62.

Courty, M.A., 2001. Microfacies Analysis Assisting Archaeological Stratigraphy. In: Goldberg, P., Holliday, V.T., Reid Ferring, C. (Eds.) *Earth Sciences and Archaeology*, 205–239.

Courty, M.A., Fedoroff, N., 1985. Micromorphlogy of recent and buried soils in a semi–arid region of northwestern India. *Geoderma* 35, 287–332.

Courty, M.A., Goldberg, P., Macphail, R.I., 1989. *Soils and Micromorphology in Archaeology, Cambridge Manuals in Archaeology*. Cambridge University Press, Cambridge.

Courty, M.A., Vallverdu, J., 2001. The microstratigraphic record of abrupt climate changes in cave sediments of the Western Mediterranean. *Geoarchaeology* 16, 467–499.

Courty, M.A., Vallverdu, J., 2001. The microstratigraphic record of abrupt climate changes in cave sediments of the Western Mediterranean. *Geoarchaeology* 16, 467–499.

Cranwell, P.A., 1981. Diagenesis of free and bound lipids in terrestrial detritus deposited in a lacustrine sediment. *Organic Geochemistry* 3, 79–89.

Cranwell, P.A., Eglinton, G., Robinson, N., 1987. Lipids of aquatic organisms as potential contributors to lacustrine sediments—II. *Organic Geochemistry* 11, 513–527.

Crass, BA, Kedrowski, BL, Baus, J, Behn JA. 2011. *Residue analysis of bone–fueled Pleistocene hearths.* In: Goebelt, T., Buvit, I. (Eds.) From the Yenisei to the Yukun. Interpreting lithic assemblage variability in Late Pleistocene/Early Holocene Beringia. Texas A and M University Press.

Cuenca–Bescós, G., Rofes, J., García–Pimienta, J.C., 2005. *Early Europeans and environmental change across the Early–Middle Pleistocene transition: small mammalian evidence from Trinchera Dolina cave, Atapuerca, Spain.* In: Head, M.J., Gibbard, P.L. (Eds.) Early–middle Pleistocene Transitions: the Landocean Evidence 247, 277–286. Geological Society of London, Special Publications, London.

d'Errico, F., Sánchez Goñi, M.F., 2003. Neandertal extinction and the millennial scale climatic variability of OIS 3. *Quaternary Science Reviews* 22, 769–788.

d'Errico, F., Zilhão, J., Julien, M., Baffier, D., Pelegrin, J., 1998. Neanderthal Acculturation in Western Europe? A Critical Review of the Evidence and Its Interpretation. *Current Anthropology* 39, S1–S44.

Daams, R., 1981. *The dental pattern of the dormice Dryomys, Myomimus, Microdyromys and Peridyromys, vol. 3*. Utrecht Micropaleontological Bulletins. Special Publications, 1–115.

Dalrymple, J.B., 1958. The application of soil micromorphology to fossil soils and other deposits from archaeological sites. *Journal of Soil Science* 9, 199–209.

Dansgaard W., 1964. Stable isotopes in precipitation. *Tellus* 16, 436–68.

Daura, J., Sanz, M., Allué, E., Vaquero, M., López–García, J.M., Sánchez–Marco, A., Domènech, R., Martinell, J., Carrión, J.S., Ortiz, J.E., Torres, T., Arnold, L.J., Benson, A., Hoffmann, D.L., Skinner, A.R., Julià, R., 2017. Palaeoenvironments of the last Neanderthals in SW Europe (MIS 3): Cova del Coll Verdaguer (Barcelona, NE of Iberian Peninsula). *Quaternary Science Reviews* 177, 34–56.

Daura, J., Sanz, M., Julià, R., García–Fernández, D., Fornós, J.J., Vaquero, M., Allué, E., López–García, J.M., Blain, H.A., Ortiz, J.E., Torres, T., Albert, R.M., Rodríguez–Cintas, À., Sánchez–Marco, A., Cerdeño, E., Skinner, A.R., Asmeron, Y., Polyak, V.J., Garcés, M., Arnold, L.J., Demuro, M., Pike, A.W.G., Euba, I., Rodríguez, R.F., Yagüe, A.S., Villaescusa, L., Gómez, S., Rubio, A., Pedro, M., Fullola, J.M., Zilhão, J., 2015. Cova del Rinoceront (Castelldefels, Barcelona): a terrestrial record for the Last Interglacial period (MIS 5) in the Mediterranean coast of the Iberian Peninsula. *Quaternary Science Reviews* 114, 203–227.

Davis OK, Buchmann SL., 1994. *Insect sources of pollen clumps in archaeological sites in southestern USA: ground–nesting bees and mites*. In: Davis O.K. (Ed.). Aspects of Archaeological Palynology: Methodology and Applications. American Association of Stratigraphic Palynologists Contributions Series 29, 63–73.

Defleur, A.R., Desclaux, E., 2019. Impact of the last interglacial climate change on ecosystems and Neanderthals behavior at Baume Moula–Guercy, Ardèche, France. *Journal of Archaeological Science* 104, 114–124.

Delage, A., Lagatu, H., 1904. *Sur la constitution de la terre arable*. Compte–rendu Académie des Sciences, Paris 109, 1043–1044.

Denys, C., Patou–Mathis, M., 2014. *Manuel de taphonomie*. Editions Errance.

Deviese, T., Comeskey, D., McCullagh, J., Bronk Ramsey, C., Higham, T., 2018. New protocol for compound–specific radiocarbon analysis of archaeological bones. *Rapid Communications in Mass Spectrometry* 32, 373–379.

Dibble, H.L., Abodolahzadeh, A., Aldeias, V., Goldberg, P., McPherron, S.P., Sandgathe, D.M., 2017. How Did Hominins Adapt to Ice Age Europe without Fire? *Current Anthropology* 58, 278–287.

Dibble, H.L., Sandgathe, D., Goldberg, P., McPherron, S., Aldeias, V., 2018. Were Western European Neandertals Able to Make Fire? *Journal of Paleolithic Archaeology* 1–26.

Diefendorf, A.F., Freeman, K.H., Wing, S.L., 2014. A comparison of terpenoid and leaf fossil vegetation proxies in Palaeocene and Eocene Bighorn Basin sediments. *Organic Geochemistry* 71, 30–42.

Diefendorf, A.F., Freeman, K.H., Wing, S.L., Graham, H.V., 2011. Production of n–alkyl lipids in living plants and implications for the geologic past. *Geochimica et Cosmochimica Acta* 75, 7472–7485.

Diefendorf, A.F., Freimuth, E.J., 2017. Extracting the most from terrestrial plant–derived n–alkyl lipids and their carbon isotopes from the sedimentary record: A review. *Organic Geochemistry* 103, 1–21.

Diefendorf, A.F., Leslie, A.B., Wing, S.L., 2015a. Leaf wax composition and carbon isotopes vary among major conifer groups. *Geochimica et Cosmochimica Acta* 170, 145–156.

Diefendorf, A.F., Sberna, D.T., Taylor, D.W., 2015b. Effect of thermal maturation on plant–derived terpenoids and leaf wax n–alkyl components. *Organic Geochemistry* 89–90, 61–70.

Diefendorf, A.F., Mueller, K.E., Wing, S.L., Koch, P.L., Freeman, K.H., 2010. Global patterns in leaf 13C discrimination and implications for studies of past and future climate. *Proceedings of the National Academy of Sciences of the United States of America* 107, 5738–5743.

Diefendorf, A.F., Patterson, W.P., Holmden, C., Mullins, H.T., 2008. Carbon isotopes of marl and lake sediment organic matter reflect terrestrial landscape change during the late Glacial and early Holocene (16,800 to 5,540 cal yr BP): a multiproxy study of lacustrine sediments at Lough Inchiquin, western Ireland. *Journal of Paleolimnology* 39, 101–115.

Dodson, P., Wexlar, D., 1979. Taphonomic investigations of owl pellets. *Paleobiology* 5, 275–284.

Domínguez–Rodrigo, M., Yravedra, J., 2009. Why are cut mark frequencies in archaeofaunal assemblages so variable? A multivariate analysis. *Journal of Archaeological Science* 36, 884–894.

Dupin, A., Sordoillet, D., Fréville, K., Girardclos, O., Gauthier, E., 2019. The taphonomic characterization of a charcoal production platform. Contribution of an innovative pair of methods: Raman analysis and micromorphology. *Journal of Archaeological Science* 107, 87–99.

Eckmeier, E., Wiesenberg, G.L.B., 2009. Short–chain n–alkanes (C16–20) in ancient soil are useful molecular markers for prehistoric biomass burning. *Journal of Archaeological Science* 36, 1590–1596.

Eglinton, G., Hamilton, R.J., 1967. Leaf epicuticular waxes. *Science* 156, 1322–1335.

Eglinton, G., Hamilton, R.J., Raphael, R.A., Gonzalez, A.G., 1962. Hydrocarbon constituents of the wax coatings of plant leaves: a taxonomic survey. *Nature* 193, 739–742.

Eglinton, G., Scott, P.M., Belsky, T., Burlingame, A.L., Calvin, M., 1964. Hydrocarbons of Biological Origin from a One–Billion–Year–Old Sediment. *Science* 145, 263–264.

Eley, Y., Dawson, L., Pedentchouk, N., 2016. Investigating the carbon isotope composition and leaf wax n–alkane concentration of C3 and C4 plants in Stiffkey saltmarsh, Norfolk, UK. *Organic Geochemistry* 96, 28–42.

Eley, Y.L., Hren, M.T., 2018. Reconstructing vapor pressure deficit from leaf wax lipid molecular distributions. *Scientific Reports* 8, 3967.

Esteban, I., Albert, R.M., Eixea, A., Zilhão, J., Villaverde, V., 2017. Neanderthal use of plants and past vegetation reconstruction at the Middle Paleolithic site of Abrigo de la Quebrada (Chelva, Valencia, Spain). *Archaeological and Anthropological Sciences* 9, 265–278.

Evershed, R.P., 1993. Biomolecular archaeology and lipids. *World Archaeology* 25, 74–93.

Evershed, R.P., Dudd, S.N., Charters, S., Mottram, H., Stott, A.W., Raven, A., van Bergen, P.F., Bland, H.A., 1999. Lipids as carriers of anthropogenic signals from prehistory. *Philosophical Transactions of the Royal Society B: Biological Sciences* 354, 19–31.

Fagoaga, A., Laplana, C., Marquina–Blasco, R., Machado, J., Marin–Monfort, M.D., Crespo, V.D., Hernández, C.M., Mallol, C., Galván, B., Ruiz–Sánchez, F.J., 2019. Palaeoecological context for the extinction of the Neanderthals: A small mammal study of Stratigraphic Unit V of the El Salt site, Alcoi, eastern Spain. *Palaeogeography, Palaeoclimatology, Palaeoecology* 530, 163–175.

Fagoaga, A., Ruiz–Sánchez, F.J., Laplana, C., Blain, H.–A., Marquina, R., Marin–Monfort, M.D., Galván, B., 2018. Palaeoecological implications of Neanderthal occupation at Unit Xb of El Salt (Alcoi, eastern Spain) during MIS 3 using small mammals proxy. *Quaternary International* 481, 101–112.

Farquhar, G.D., Ehleringer, J.R., Hubick, K.T., 1989. Carbon Isotope Discrimination and Photosynthesis. *Annual Review of Plant Physiology and Plant Molecular Biology* 40, 503–537.

Fedele, F.G., Giaccio, B., Isaia, R., Orsi, G., Carroll, M., Scaillet, B., 2016. *The Campanian Ignimbrite factor: towards a reappraisal of the Middle to Upper Palaeolithic "transition."* In: Grattan, J., Torrence, R. (Eds.) Living Under the Shadow, 29–51. Routledge.

Fedoroff, N., Courty, M.A., 1987. *Morphology and distribution of textural features in arid and semi–arid regions*. VII Micromorphologie des sols. Plaisir-Grignon, AFES, 213–220.

Fedoroff, N., Goldberg, P., 1982. Comparative micromorphology of two late Pleistocene paleosols (in the Paris Basin). *Catena* 9, 227–251.

Fernandes, R., Eley, Y., Brabec, M., Lucquin, A., Millard, A., Craig, O.E., 2018. Reconstruction of prehistoric pottery use from fatty acid carbon isotope signatures using Bayesian inference. *Organic Geochemistry* 117, 31–42.

Fernández Peris, J., González, V.B., Blasco, R., Cuartero, F., Fluck, H., Sañudo, P., Verdasco, C., 2012. The earliest evidence of hearths in Southern Europe: The case of Bolomor Cave (Valencia, Spain). *Quaternary International* 247, 267–277.

Fernández–García, M., López–García, J.M., Royer, A., Lécuyer, C., Allué, E., Burjachs, F., Chacón, M.G., Saladié, P., Vallverdú, J., Carbonell, E., 2020. Combined palaeoecological methods using small–mammal assemblages to decipher environmental context of a long–term Neanderthal settlement in northeastern Iberia. *Quaternary Science Reviews* 228, 106072.

Fernández–Jalvo, Y., Andrews, P., 1992. Small mammal taphonomy of gran dolina, Atapuerca (Burgos), Spain. *Journal of Archaeological Science* 19 (4), 407–428.

Fernández–Jalvo, Y., Andrews, P., 2016. *Atlas of Taphonomic Identifications. 1001+ Images of Fossil and Recent Mammal Bone Modification*. Springer.

Fernández–Jalvo, Y., Andrews, P., Denys, C., Sesé, C., Stoetzel, E., Marin–Monfort, D., Pesquero, D., 2016. Taphonomy for taxonomists: implications of predation in small mammal studies. *Quaternary Science Reviews* 139, 138–157.

Ferrio, J.P., Alonso, N., Lopez, J.B., Araus, J.L., Voltas, J., 2006. Carbon isotope composition of fossil charcoal reveals aridity changes in the NW Mediterranean Basin. *Global Change Biology* 12, 1253–1266.

Ficken, K.J., Barber, K.E., Eglinton, G., 1998. Lipid biomarker, δ13C and plant macrofossil stratigraphy of a Scottish montane peat bog over the last two millennia. *Organic Geochemistry* 28, 217–237.

Ficken, K.J., Li, B., Swain, D.L., Eglinton, G., 2000. An n–alkane proxy for the sedimentary input of submerged/ Øoating freshwater aquatic macrophytes. *Organic Geochemistry* 31, 745–749.

Finlayson, C., 2004. *Neanderthals and Modern Humans: An Ecological and Evolutionary Perspective*. Cambridge University Press.

Finlayson, C., Carrión, J.S., 2007. Rapid ecological turnover and its impact on Neanderthal and other human populations. *Trends in Ecology and Evolution* 22, 213–222.

Finlayson, C., Vidal, J.–N.R.–G., Pacheco, F.G., 2007. *Where the Last Neanderthals Lived: A Study of Neanderthal and Modern Human Behavioural Ecology in a Glacial Refugium*. Oxbow Books, Limited.

Fletcher, W.J., Sánchez Goñi, M.F., Allen, J.R.M., Cheddadi, R., Combourieu–Nebout, N., Huntley, B., Lawson, I., Londeix, L., Magri, D., Margari, V., Müller, U.C., Naughton, F., Novenko, E., Roucoux, K., Tzedakis, P.C., 2010. Millennial–scale variability during the last glacial in vegetation records from Europe. *Quaternary Science Reviews* 29, 2839–2864.

Freeman, K.H., Pancost, R.D., 2013. *Biomarkers for terrestrial plants and climate, in: Treatise on Geochemistry: Second Edition*. Elsevier, 395–416.

Friesem, D.E., Zaidner, Y., Shahack–Gross, R., 2014. Formation processes and combustion features at the lower layers of the Middle Palaeolithic open–air site of Nesher Ramla, Israel. *Quaternary International* 331, 128–138.

Frost, D.R., 2015. Amphibian Species of the World: an Online Reference. Version 6.0. http://research.amnh.org/herpetology/amphibia/index.html. [accessed November 2018]

Fumanal, P., 1994. El yacimiento musteriense de El Salt (Alcoi, País Valenciano): rasgos geomorfológicos y climatoestratigrafía de sus registros. *Saguntum PLAV* 27 39–55.

Galbraith, R.F., Roberts, R.G., Laslett, G.M., Yoshida, H., Olley, J.M., 1999. Optical dating of single and multiple grains of quartz from Jinmium Rock Shelter, Northern Australia: Part I, Experimental design and statistical models. *Archaeometry* 41, 339–364.

Galván Santos, B., Hernández Gómez, C.M, Francisco Ortega, M.I., 2007. Elementos líticos apuntados en el Musteriense alcoyano. El Abric del Pastor (Alicante). *Veleia* 24–25, 367–383.

Galván, B., Hernández Gómez, C.M., Alberto Barroso, V., Barro Rois, A., Francisco Ortega, M., Rodríguez Rodríguez, A., 2001. Las sociedades cazadoras–recolectoras neandertalianas en los Valles de Alcoi (Alicante, España). El Salt como un centro de intervención referencial. *Tabona Revista de Prehistoria y Arqueología* 10, 7–33.

Galván, B., Hernández, C.M., Mallol, C., Mercier, N., Sistiaga, A., Soler, V., 2014. New evidence of early Neanderthal disappearance in the Iberian Peninsula. *Journal of Human Evolution* 75, 16–27.

Galván, B., Hernández, C.M., Mallol, C., Mercier, N., Sistiaga, A., Soler, V., 2014. New evidence of early Neanderthal disappearance in the Iberian Peninsula. *Journal of Human Evolution* 75, 16–27.

Gamarra, B., Sachse, D., Kahmen, A., 2016. Effects of leaf water evaporative 2 H–enrichment and biosynthetic fractionation on leaf wax n–alkane δ2 H values in C3 and C4 grasses. *Plant Cell and Environment* 39, 2390–2403.

Gamble, C., 1999. *The Palaeolithic Societies of Europe*. Cambridge University Press.

Gao, X., Zhang, S., Zhang, Y., Chen, F., 2017. Evidence of Hominin Use and Maintenance of Fire at Zhoukoudian. *Current Anthropology* 58, 267–277.

Garcin, Y., Schefuß, E., Schwab, V.F., Garreta, V., Gleixner, G., Vincens, A., Todou, G., Séné, O., Onana, J.–M., Achoundong, G., Sachse, D., 2014. Reconstructing C3 and C4 vegetation cover using n–alkane carbon isotope ratios in recent lake sediments from Cameroon, Western Central Africa. *Geochimica et Cosmochimica Acta* 142, 482–500.

Garcin, Y., Schwab, V.F., Gleixner, G., Kahmen, A., Todou, G., Séné, O., Onana, J.–M., Achoundong, G., Sachse, D., 2012. Hydrogen isotope ratios of lacustrine sedimentary n–alkanes as proxies of tropical African hydrology: Insights from a calibration transect across Cameroon. *Geochimica et Cosmochimica Acta* 79, 106–126.

Garralda, M.D., Galván, B., Hernández, C.M., Mallol, C., Gómez, J.A., Maureille, B., 2014. Neanderthals from El Salt (Alcoy, Spain) in the context of the latest Middle Palaeolithic populations from the southeast of the Iberian Peninsula. *Journal of Human Evolution* 75, 1–15.

Gauch, H.G., 1989. *Multivariate Analysis in Community Ecology*. Cambridge University Press, Cambridge.

Gibbs, A., Pomonis, J.G., 1995. Physical properties of insect cuticular hydrocarbons: The effects of chain length, methyl–branching and unsaturation. *Comparative Biochemistry and Physiology - Part B: Biochemistry & Molecular Biology* 112, 243–249.

Gilpin, W., Feldman, M.W., Aoki, K., 2016. An ecocultural model predicts Neanderthal extinction through competition with modern humans. *Proceedings of the National Academy of Sciences of the United States of America* 113, 2134–2139.

Glauberman, P., Gasparyan, B., Sherriff, J., Wilkinson, K., Li, B., Knul, M., Brittingham, A., Hren, M.T., Arakelyan, D., Nahapetyan, S., Raczynski–Henk, Y., Haydosyan, H., Adler, D.S., 2020. Barozh 12: Formation processes of a late Middle Paleolithic open–air site in western Armenia. *Quaternary Science Reviews* 236, 106276.

Goeury, C., de Beaulieu, J.L., 1979. À propos de la concentration du pollen à l'aide de la liqueur de Thoulet dans les sédiments minéraux. *Pollen et Spores XXI* (1–2), 239–251.

Goldberg, P., 1979. Micromorphology of sediments from Hayonim cave, Israel. *Catena* 6 (2), 167–181.

Goldberg, P., 1980. Micromorphology in Archaeology and Prehistory. *Paléorient* 6, 159–164.

Goldberg, P., Berna, F., 2010. Micromorphology and context. *Quaternary International* 214, 56–62.

Goldberg, P., Dibble, H., Berna, F., Sandgathe, D., McPherron, S.J.P., Turq, A., 2012. New evidence on Neandertal use of fire: Examples from Roc de Marsal and Pech de l’Azé IV. *Quaternary International* 247, 325–340.

Goldberg, P., Macphail, R.I., 2008. *Practical and theoretical geoarchaeology*. Blackwell, Oxford.

Goldberg, P., Miller, C.E., Mentzer, S.M., 2017. Recognizing Fire in the Paleolithic Archaeological Record. *Current Anthropology* 58, 175–190.

Goldberg, P., Miller, C.E., Schiegl, S., Ligouis, B., Berna, F., Conard, N.J., Wadley, L., 2009. Bedding, hearths, and site maintenance in the Middle Stone Age of Sibudu Cave, KwaZulu–Natal, South Africa. *Archaeological and Anthropological Sciences* 1, 95–122.

Goldfield, A.E., Booton, R., Marston, J.M., 2018. Modeling the role of fire and cooking in the competitive exclusion of Neanderthals. *Journal of Human Evolution* 124, 91-104.

Golovanova, L.V., Doronichev, V.B., 2010. Significance of ecological factors in the Middle to Upper Paleolithic transition. *Current Anthropology* 51 (5), 655-691.

Gómez de la Rua, D., Mallol, C., Galván, B., Hernández Gómez, C.M., 2010. Una visión geoarqueológica general del yacimiento musteriense de El Salt (Alcoy, Alicante) a partir de la micromorfología de suelos. Recerques del Museu d'Alcoi 19, 19–32.

Gómez–Orellana, L., Ramil–Rego, P., Sobrino, C.M., 2007. The Würm in NW Iberia, a pollen record from area Longa (Galicia). *Quaternary Research* 67, 438–452.

González–Sampériz, P., 1998. Estudio palinológico de la cueva de En Pardo (planes, Alicante) Primeros resultados. *Cuaternario y Geomorfología* 12, 45–61.

Gowlett, J.A.J., Wrangham, R.W., 2013. Earliest fire in Africa: towards the convergence of archaeological evidence and the cooking hypothesis. *Azania: Archaeological Research in Africa* 48, 5–30.

Gravina, B., Mellars, P., Ramsey, C.B., 2005. Radiocarbon dating of interstratified Neanderthal and early modern human occupations at the Chatelperronian type–site. *Nature* 438, 51–56.

Greenbaum, G., Friesem, D.E., Hovers, E., Feldman, M.W., Kolodny, O., 2018. Was inter–population connectivity of Neanderthals and modern humans the driver of the Upper Paleolithic transition rather than its product? *Quaternary Science Reviews* 217, 316-329.

Grimm, E.C., 1987. CONISS: a FORTRAN 77 program for stratigraphically constrained cluster analysis by the method of incremental sum of squares. *Computers and Geosciences* 13, 13–35.

Grimm, E.C., 1991–2015. TiliaIT. [accessed at: https://www.tiliait.com/]

Grün, R., 2009. The DATA program for the calculation of ESR age estimates on tooth enamel. *Quaternary Geochronology* 4, 231–232.

Grün, R., Katzenberger–Apel, O., 1994. An alpha irradiator for ESR dating. *Ancient TL* 12, 35–38.

Gunderson, L.H., 2000. Ecological Resilience—In Theory and Application. *Annual Review of Ecology, Evolution, and Systematics* 31, 425–439.

Haaland, M.M., Friesem, D.E., Miller, C.E., Henshilwood, C.S., 2017. Heat–induced alteration of glauconitic minerals in the Middle Stone Age levels of Blombos Cave, South Africa: Implications for evaluating site structure and burning events. *Journal of Archaeological Science* 86, 81–100.

Haaland, M.M., Miller, C.E., Unhammer, O.F., Reynard, J.P., van Niekerk, K.L., Ligouis, B., Mentzer, S.M., Henshilwood, C.S., 2020. Geoarchaeological investigation of occupation deposits in Blombos Cave in South Africa indicate changes in site use and settlement dynamics in the southern Cape during MIS 5b–4. *Quaternary Research*, 1-54.

Hayes, J.M., Freeman, K.H., Popp, B.N., Hoham, C.H., 1990. Compound–specific isotopic analyses: a novel tool for reconstruction of ancient biogeochemical processes. *Organic Geochemistry* 16, 1115–1128.

Henry, A., Théry–Parisot, I., 2014. From Evenk campfires to prehistoric hearths: charcoal analysis as a tool for identifying the use of rotten wood as fuel. *Journal of Archaeological Science* 52, 321-336.

Henry, D., 2012. The palimpsest problem, hearth pattern analysis, and Middle Paleolithic site structure. *Quaternary International* 247, 246–266.

Hernández, F.J.M., Vinagre, A.T., Galván Santos, B., Hernández Gómez, C.M., 2010. Áreas de aprovisionamiento de sílex en el Paleolítico Medio en torno al Abric del Pastor (Alcoi, Alicante). Estudio macroscópico de la producción lítica de la colección Brotons. *Recerques del Museu d'Alcoi* 19, 65–80.

Hernández–Fernández M, Peláez–Campomanes P., 2003. The bioclimatic model: a method of palaeoclimatic. *Global Ecology and Biogeography* 12: 507–517.

Hernández–Fernández M., 2001. Bioclimatic discriminant capacity of terrestrial mammal faunas. *Global Ecology and Biogeography* 10, 189–204.

Hernández Fernández, M., 2006. Rodent paleofaunas as indicators of climatic change in Europe during the last 125,000 years. *Quaternary Research* 65, 308–323.

Herrera–Herrera, A.V., Mallol, C., 2018. Quantification of lipid biomarkers in sedimentary contexts: Comparing different calibration methods. *Organic Geochemistry* 125, 152–160.

Higham, T., Douka, K., Wood, R., Ramsey, C.B., Brock, F., Basell, L., Camps, M., Arrizabalaga, A., Baena, J., Barroso–Ruíz, C., Bergman, C., Boitard, C., Boscato, P., Caparrós, M., Conard, N.J., Draily, C., Froment, A., Galván, B., Gambassini, P., Garcia–Moreno, A., Grimaldi, S., Haesaerts, P., Holt, B., Iriarte–Chiapusso, M.–J., Jelinek, A., Jordá Pardo, J.F., Maíllo–Fernández, J.–M., Marom, A., Maroto, J., Menéndez, M., Metz, L., Morin, E., Moroni, A., Negrino, F., Panagopoulou, E., Peresani, M., Pirson, S., de la Rasilla, M., Riel–Salvatore, J., Ronchitelli, A., Santamaria, D., Semal, P., Slimak, L., Soler, J., Soler, N., Villaluenga, A., Pinhasi, R., Jacobi, R., 2014. The timing and spatiotemporal patterning of Neanderthal disappearance. *Nature* 512, 306–309.

Hijmans, R.J., Cameron, S.E., Parra, J.L., Jones, P.G., Jarvis, A., 2005. Very high–resolution interpolated climate surfaces for global land areas. *International Journal of Climatology* 25, 1965–1978.

Hilkert, A.W., Douthitt, C.B., Schlüter, H.J., Brand, W.A., 1999. Isotope ratio monitoring gas chromatography/Mass spectrometry of D/H by high temperature conversion isotope ratio mass spectrometry. *Rapid Communications in Mass Spectrometry* 13, 1226–1230.

Hockett, B., Haws, J.A., 2005. Nutritional ecology and the human demography of Neandertal extinction. *Quaternary International* 137, 21–34.

Holdaway, S., Wandsnider, L., 2008. *Time in Archaeology: Time Perspectivism Revisited*. University of Utah Press.

Holling, C.S., 1973. Resilience and stability of ecological systems. *Annual Review of Ecology, Evolution, and Systematics* 4, 1–23.

Hublin, J.–J., 2015. The modern human colonization of western Eurasia: when and where? *Quaternary Science Reviews* 118, 194–210.

IAEA/WMO, 2006. Global Network of Isotopes in Precipitation. The GNIP Database. [Accessed at: http://www.iaea.org/water]

Jacquiot, C., Trenard, Y., Dirol, D., 1973. *Atlas d'anatomie des bois des angiosperms (Essences feuillues)*. Centre Technique du Bois, Paris.

Jambrina-Enríquez, M., Herrera-Herrera, A.V., Rodríguez de Vera, C., Leierer, L., Connolly, R., Mallol, C., 2019. n-Alkyl nitriles and compound-specific carbon isotope analysis of lipid combustion residues from Neanderthal and experimental hearths: Identifying sources of organic compounds and combustion temperatures. *Quaternary Science Reviews* 222, 105899.

Jambrina–Enríquez, M., Herrera–Herrera, A.V., Mallol, C., 2018. Wax lipids in fresh and charred anatomical parts of the Celtis australis tree: Insights on paleofire interpretation. *Organic Geochemistry* 122, 147–160.

Jambrina–Enríquez, M., Recio, C., Vega, J.C., Valero–Garcés, B., 2017. Tracking climate change in oligotrophic mountain lakes: Recent hydrology and productivity synergies in Lago de Sanabria (NW Iberian Peninsula). *Science of the Total Environment*, 579–591.

Jambrina–Enríquez, M., Sachse, D., Valero–Garcés, B.L., 2016. A deglaciation and Holocene biomarker–based reconstruction of climate and environmental variability in NW Iberian Peninsula: the Sanabria Lake sequence. *Journal of Paleolimnology* 56, 49–66.

Jansen, B., Wiesenberg, G.L.B., 2017. Opportunities and limitations related to the application of plant–derived lipid molecular proxies in soil science. *SOIL Discussions*, 1–53.

Jaworski, J.G., Tai, H., Ohlrogge, J.B., Post–Beittenmiller, D., 1994. The initial reactions of fatty acid biosynthesis in plants. *Progress in Lipid Research* 33, 47–54.

Jeannet, M., 2000. *Gruta da Figueira Brava: les rongeurs*. Memórias da Academia das Ciências de Lisboa. Classe de Ciências 38, 179 –243.

Jenks, M.A., Joly, R.J., Peters, P.J., Rich, P.J., Axtell, J.D., Ashworth, E.N., 1994. Chemically Induced Cuticle Mutation Affecting Epidermal Conductance to Water Vapor and Disease Susceptibility in Sorghum bicolor (L.) Moench. *Plant Physiology* 105, 1239–1245.

Jennings, R., Finlayson, C., Fa, D., Finlayson, G., 2011. Southern Iberia as a refuge for the last Neanderthal populations: Southern Iberia as a Neanderthal refugium. *Journal of Biogeography* 38, 1873–1885.

Jiménez–Espejo, F.J., Martínez–Ruiz, F., Finlayson, C., Paytan, A., Sakamoto, T., Ortega–Huertas, M., Finlayson, G., Iijima, K., Gallego–Torres, D., Fa, D., 2007. Climate forcing and Neanderthal extinction in Southern Iberia: insights from a multiproxy marine record. *Quaternary Science Reviews* 26, 836–852.

Jones, J.R., Richards, M.P., Straus, L.G., Reade, H., Altuna, J., Mariezkurrena, K., Marín-Arroyo, A.B., 2018. Changing environments during the Middle-Upper Palaeolithic transition in the eastern Cantabrian Region (Spain): direct evidence from stable isotope studies on ungulate bones. *Scientific Reports* 8, 14842.

Jordan, S.F., Murphy, B.T., O'Reilly, S.S., Doyle, K.P., Williams, Grey, A., Lee, S., McCaul, M.V., Kelleher, B.P., 2017. Mid–Holocene climate change and landscape formation in Ireland: Evidence from a geochemical investigation of a coastal peat bog. *Organic Geochemistry* 109, 67–76.

Jordan, S.F., Murphy, B.T., O'Reilly, S.S., Doyle, K.P., Williams, Grey, A., Lee, S., McCaul, M.V., Kelleher, B.P., 2017. Mid–Holocene climate change and landscape formation in Ireland: Evidence from a geochemical investigation of a coastal peat bog. *Organic Geochemistry* 109, 67–76.

Kaal, J., Lantes–Suárez, O., Martínez Cortizas, A., Prieto, B., Prieto Martínez, M.P., 2014. How Useful is Pyrolysis–GC/MS for the Assessment of Molecular Properties of Organic Matter in Archaeological Pottery matrix? An Exploratory Case Study from North–West Spain. *Archaeometry* 56, 187–207.

Kahmen, A., Dawson, T.E., Vieth, A., Sachse, D., 2011. Leaf wax n–alkane δD values are determined early in the ontogeny of Populus trichocarpa leaves when grown under controlled environmental conditions. *Plant, Cell and Environment* 34, 1639–1651.

Kahmen, A., Schefuß, E., Sachse, D., 2013. Leaf water deuterium enrichment shapes leaf wax n–alkane δD values of angiosperm plants I: Experimental evidence and mechanistic insights. *Geochimica et Cosmochimica Acta* 111, 39–49.

Kaplan, J.O., Colin Prentice, I., Buchmann, N., 2002. The stable carbon isotope composition of the terrestrial biosphere: Modeling at scales from the leaf to the globe. Global Biogeochemical Cycles 16 (4), 8-1-8-11.

Karkanas, P., 2017. *Guano*. In: Nicosia, C., Stoops, G. (Eds.) Archaeological Soil and Sediment Micromorphology. John Wiley and Sons Ltd., UK, 83–89.

Karkanas, P., Bar–Yosef, O., Goldberg, P., Weiner, S., 2000. Diagenesis in prehistoric caves: the use of minerals that form in situ to assess the completeness of the archaeological record. *Journal of Archaeological Science* 27 (10), 915-929.

Karkanas, P., Goldberg, P., 2018. *Phosphatic Features.* In: Stoops, G., Marcelino, V., Mees, F. (Eds.) Interpretation of Micromorphological Features of Soils and Regoliths (Second Edition). Amsterdam, Elsevier, 323–346.

Karkanas, P., Koumouzelis, M., Kozlowski, J.K., Sitlivy, V., Sobczyk, K., Berna, F., Weiner, S., 2004. The earliest evidence for clay hearths: Aurignacian features in Klisoura Cave 1, southern Greece. *Antiquity* 78 (301), 513-525.

Kedrowski, B.L., Crass, B.A., Behm, J.A., Luetke, J.C., 2009. GC/MS analysis of fatty acids from ancient hearth residues at the Swan Point archaeological site. *Archaeometry* 51 (1), 110-122.

Kehl, M., Burow, C., Hilgers, A., Navazo, M., Pastoors, A., Weniger, G.–C., Wood, R., Jordá Pardo, J.F., 2013. Late Neanderthals at Jarama VI (central Iberia)? *Quaternary Research* 80, 218–234.

Klavina, L., Kviesis, J., 2015. Solid Phase Extraction of Bryophyte Lipids. *Materials Science and Applied Chemistry* 32, 58–67.

Klein, R.G., 2003. Whither the Neanderthals? *Science* 299, 1525–1527.

Klein, R.G., 2009. *The Human Career: Human Biological and Cultural Origins, Third Edition*. University of Chicago Press.

Kohn, M.J., 2010. Carbon isotope compositions of terrestrial C3 plants as indicators of (paleo) ecology and (paleo) climate. *Proceedings of the National Academy of Sciences of the United States of America* 107, 19691–19695.

Kolattukudy, P.E., 1968. Further Evidence for an Elongation–Decarboxylation Mechanism in the Biosynthesis of Paraffins in Leaves. *Plant Physiology* 43, 375-383.

Kolodny, O., Feldman, M.W., 2017. A parsimonious neutral model suggests Neanderthal replacement was determined by migration and random species drift. *Nature Communications* 8, 1040.

Korth, W.W., 1979. Taphonomy of microvertebrate fossil assemblages. *Annals of the Carnegie Museum* 48, 235–285.

Krajcarz, M., Krajcarz, M.T., 2019. Post–depositional bone destruction in cave sediments: a micromorphological study of the MIS 5a–d cave bear strata of Biśnik Cave, Poland. *Journal of Quaternary Science* 34, 138–152.

Kreutzer, S., Martin, L., Guérin, G., Tribolo, C., Selva, P., Mercier, N., 2018. Environmental dose rate determination using a passive dosimeter: Techniques and workflow for α–Al2O3: C chips. *Geochronometria* 45, 56–67.

Kubiëna, W.L., 1938. *Micropedology*. Collegiate Press, Ames, Iowa.

Kubiëna, W.L., 1958. The Classification of Soils. *European Journal of Soil Science* 9, 9–19.

Kubiëna, W.L., Ruhe, R.V., 1970. Micromorphological Features of Soil Geography. Rutgers University Press

Kuder, T., Kruge, M.A., 1998. Preservation of biomolecules in sub–fossil plants from raised peat bogs – a potential paleoenvironmental proxy. *Organic Geochemistry* 29, 1355–1368.

Kuhlwilm, M., Gronau, I., Hubisz, M.J., de Filippo, C., Prado–Martinez, J., Kircher, M., Fu, Q., Burbano, H.A., Lalueza–Fox, C., de la Rasilla, M., Rosas, A., Rudan, P., Brajkovic, D., Kucan, Ž., Gušic, I., Marques–Bonet, T., Andrés, A.M., Viola, B., Pääbo, S., Meyer, M., Siepel, A., Castellano, S., 2016. Ancient gene flow from early modern humans into Eastern Neanderthals. *Nature* 530, 429–433.

Kunst, L., Samuels, A.L., 2003. Biosynthesis and secretion of plant cuticular wax. *Progress in Lipid Research* 42, 51–80.

Kusmer, K.D., 1990. Taphonomy of Owl Pellet Deposition. *Journal of Paleontology* 64, 629–637.

Ladd, S.N., Sachs, J.P., 2013. Positive correlation between salinity and n–alkane δ13C values in the mangrove Avicennia marina. *Organic Geochemistry* 64, 1–8.

Laplana, C., Sevilla, P., 2013. Documenting the biogeographic history of Microtus cabrerae through its fossil record. *Mammal Review* 43, 309–332.

Laville, H., 1976. Deposits in calcareous rock shelters: analytical methods and climatic interpretation. *Geoarchaeology* 137–155.

Lebedeva–Verba, M.P., Gerasimova, M.I., 2009. Micromorphology of diagnostic horizons in aridic soils (complementary to the new classification system of soils of Russia). *Eurasian Soil Science* 42, 1427–1434.

Leierer, L., Alonso, Á.C., Pérez, L., Lagunilla, Á.H., Herrera–Herrera, A.V., Connolly, R., Jambrina–Enríquez, M., Hernández Gómez, C.M., Galván, B., Mallol, C., 2020. It's getting hot in here – Microcontextual study of a potential pit hearth at the Middle Paleolithic site of El Salt, Spain. *Journal of Archaeological Science* 123, 105237.

Leierer, L., Jambrina–Enríquez, M., Herrera–Herrera, A.V., Connolly, R., Hernández, C.M., Galván, B., Mallol, C., 2019. Insights into the timing, intensity and natural setting of Neanderthal occupation from the geoarchaeological study of combustion structures: A micromorphological and biomarker investigation of El Salt, unit Xb, Alcoy, Spain. *PLoS One* 14, e0214955.

Lejay, M., Alexis, M., Quénéa, K., Sellami, F., Bon, F., 2016. Organic signatures of fireplaces: Experimental references for archaeological interpretations. *Organic Geochemistry* 99, 67–77.

Leroyer, C., 1988. *Des occupations castelperroniennes et aurignaciennes dans leur cadre chrono–climatique*. In: Otte, M. (Ed.) L'Homme de Neanderthal. La mutation 8. Études et Recherches Archéologiques de l'Université de Liège, 103–108.

Leroyer, C., Leroi–Gourhan, A., 1983. Problèmes de chronologie: le castelperronien et l'aurignacien. *Bulletin de la Société Préhistorique Française* 80, 41–44.

Liu, J., An, Z., 2018. A hierarchical framework for disentangling different controls on leaf wax δD n–alkane values in terrestrial higher plants. *Quaternary Science Reviews* 201, 409–417.

Liu, W., Yang, H., 2008. Multiple controls for the variability of hydrogen isotopic compositions in higher plant n–alkanes from modern ecosystems. *Global Change Biology* 14, 2166–2177.

Liu, Z., Henderson, A.C.G., Huang, Y., 2008. Regional moisture source changes inferred from late holocene stable isotope records. *Advances in Atmospheric Sciences* 25, 1021–1028.

Lloveras, L., Moreno–García, M., Nadal, J., Thomas, R., 2014. Blind test evaluation of accuracy in the identification and quantification of digestion corrosion damage on leporid bones. *Quaternary International* 330, 150–155.

López, P., Martín, J., 2018. Enciclopedia Virtual de los Vertebrados Espanoles. Museo Nacional de Ciencias Naturales (CSIC). [accessed at: http://www.vertebradosibericos.org].

López–García, J.M., Blain, H.A., Bennàsar, M., Fernández–García, M., 2014. Environmental and climatic context of Neanderthal occupation in southwestern Europe during MIS3 inferred from the small–vertebrate assemblages. *Quaternary International* 326–327, 319–328.

López–García, J.M., Blain, H.–A., Bennàsar, M., Sanz, M., Daura, J., 2013. Heinrich event 4 characterized by terrestrial proxies in southwestern Europe. *Climate of the Past* 9, 1053–1064.

López–García, J.M., Blain, H.–A., Sanz, M., Daura, J., 2012. A coastal reservoir of terrestrial resources for neanderthal populations in north–eastern Iberia: palaeoenvironmental data inferred from the small–vertebrate assemblage of Cova del Gegant, Sitges, Barcelona. *Journal of Quaternary Science* 27 (1), 105-113.

López–Sáez, J.A., Van Geel, B., Sánchez, M.M., 2000. *Aplicación de los microfósiles no polínicos en Palinología Arqueológica*. In: Vitor Oliveira, J. (Ed.) Actas Do 3° Congresso de Arqueologia Peninsular. Faculty of Science (FNWI). Institute for Biodiversity and Ecosystem Dynamics (IBED), 11–20.

Loublier, I., 1978. *Application de l'analyse pollinique à l'étude du paleoenvironnement du remplissage Würmien de la grotte de L'Arbreda (Espagne)*. PhD Thesis. U.S.T. Ls, Montpellier.

Lucas, G., 2004. *The Archaeology of Time*. Routledge.

Lucquin, A., Colonese, A.C., Farrell, T.F.G., Craig, O.E., 2016. Utilising phytanic acid diastereomers for the characterisation of archaeological lipid residues in pottery samples. *Tetrahedron Letters* 57, 703–707.

Lyman, R.L., 1984. Bone density and differential survivorship of fossil classes. *Journal of Anthropological Archaeology* 3, 259–299.

Lyman, R.L., 1985. Bone frequencies: differential transport, in situ destruction, and the MGUI. *Journal of Archaeological Science* 12, 221–236.

Lyman, R.L., 1994. *Vertebrate taphonomy, Cambridge Manuals in Archaeology*. Cambridge Unviersity Press, Camdridge.

Lynch, T.F., 1986. Climate change and human settlement around the late–glacial laguna De Punta Negra, northern Chile: The preliminary results. *Geoarchaeology* 1, 145–161.

Machado, J., Hernández, C.M., Mallol, C., Galván, B., 2013. Lithic production, site formation and Middle Palaeolithic palimpsest analysis: in search of human occupation episodes at Abric del Pastor Stratigraphic Unit IV (Alicante, Spain). *Journal of Archaeological Science* 40, 2254–2273.

Machado, J., Mallol, C., Hernández, C.M., 2015. *Insights into Eurasian Middle Palaeolithic settlement dynamics: the palimpsest problem*. In: Conard N.J., Delagnes, A. (Ed.) Settlement dynamics of the Middle Paleolithic and Middle Stone Age. Tübingen, Kerns.

Machado, J., Mayor, A., Hernández, C.M., Galván, B., 2019. Lithic refitting and the analysis of Middle Palaeolithic settlement dynamics: a high–temporal resolution example from El Pastor rock shelter (Eastern Iberia). *Archaeological and Anthropological Sciences* 11, 4539–4554.

Machado, J., Molina, F.J., Hernández, C.M., Tarriño, A., Galván, B., 2017. Using lithic assemblage formation to approach Middle Palaeolithic settlement dynamics: El Salt Stratigraphic Unit X (Alicante, Spain). *Archaeological and Anthropological Sciences* 9, 1715–1743.

Machado, J., Pérez, L., 2015. Temporal frameworks to approach human behavior concealed in Middle Palaeolithic palimpsests: A high–resolution example from El Salt Stratigraphic Unit X (Alicante, Spain). *Quaternary International* 417, 66-81.

Macphail, R.I., 1987. *A review of soil science in archaeology in England*. In: Keeley, H. C. M. (Ed.) Environmental archaeology: a regional review 2. London, English Heritage Occasional Paper 1, 332–379.

Macphail, R.I., Allen, M.J., Crowther, J., Cruise, G.M., Whittaker, J.E., 2010. Marine inundation: Effects on archaeological features, materials, sediments and soils. *Quaternary International* 214, 44–55.

Macphail, R.I., Courty, M.A., Goldberg, P., 1990. Soil and Micromorphology in Archaeology. *Endeavour* 14, 163–171.

Macphail, R.I., Goldberg, P., 2018. *Applied Soils and Micromorphology in Archaeology*. Cambridge University Press.

Magill, C.R., Ashley, G.M., Domínguez–Rodrigo, M., Freeman, K.H., 2016. Dietary options and behavior suggested by plant biomarker evidence in an early human habitat. *Proceedings of the National Academy of Sciences of the United States of America* 113, 2874–2879.

Magill, C.R., Ashley, G.M., Freeman, K.H., 2013. Ecosystem variability and early human habitats in eastern Africa. *Proceedings of the National Academy of Sciences of the United States of America* 110, 1167–1174.

Magill, C.R., Eglinton, G., Eglinton, T.I., 2019. Isotopic variance among plant lipid homologues correlates with biodiversity patterns of their source communities. *PLoS One* 14, e0212211.

Mallol, C., 2006. What's in a beach? Soil micromorphology of sediments from the Lower Paleolithic site of 'Ubeidiya, Israel. *Journal of Human Evolution* 51, 185–206.

Mallol, C., Cabanes, D., Baena, J., 2010. Microstratigraphy and diagenesis at the upper Pleistocene site of Esquilleu Cave (Cantabria, Spain). *Quaternary International* 214, 70–81.

Mallol, C., Henry, A., 2017. Ethnoarchaeology of Paleolithic Fire: Methodological Considerations. *Current Anthropology* 58 (16), 217-229.

Mallol, C., Hernández, C., Mercier, N., Falguères, C., Carrancho, Á., Cabanes, D., Vidal-Matutano, P., Connolly, R., Pérez, L., Mayor, A., Ben Arous, E., Galván, B., 2019. Fire and brief human occupations in Iberia during MIS 4: Evidence from Abric del Pastor (Alcoy, Spain). *Scientific Reports* 9, 18281.

Mallol, C., Hernández, C.M., Cabanes, D., Machado, J., Sistiaga, A., Pérez, L., Galván, B., 2013. Human actions performed on simple combustion structures: An experimental approach to the study of Middle Palaeolithic fire. *Quaternary International* 315, 3–15.

Mallol, C., Hernández, C.M., Cabanes, D., Sistiaga, A., Machado, J., Rodríguez, Á., Pérez, L., Galván, B., 2013. The black layer of Middle Palaeolithic combustion structures. Interpretation and archaeostratigraphic implications. *Journal of Archaeological Science* 40, 2515–2537.

Mallol, C., Mentzer, S.M., Wrinn, P.J., 2009. A micromorphological and mineralogical study of site formation processes at the late Pleistocene site of Obi–Rakhmat, Uzbekistan. *Geoarchaeology* 24, 548–575.

March, R.J., 1999. Chimie organique appliquée à l'étude des structures de combustion du site de Tunel I (Terre de Feu, Argentine). *ArchéoSciences, revue d'Archéométrie* 23, 127–156.

March, R.J., 2013. *Searching for the functions of fire structures in Eynan (Mallaha) and their formation processes: a geochemical approach*. In: Bar-Yosef, O., Valla, F. R. (Eds.) Natufian Foragers in the Levant. Ann Arbor, International Monographs in Prehistory, 227–283.

March, R.J., Baldessari, A., Gross, E.G., 1989. *Determinación de compuestos orgánicos en estructuras de combustión arqueológicas*. In: Olive, M., Taborin, Y. (Eds.) Nature et Funtion Des Foyes Préhistoriques. Actes Du Colloque International de Nemours. Mémoires Du Musée Du Préhistoire D'Ile de France. 47–58.

March, R.J., Lucquin, A., Joly, D., Ferreri, J.C., Muhieddine, M., 2014. Processes of Formation and Alteration of Archaeological Fire Structures: Complexity Viewed in the Light of Experimental Approaches. *Journal of Archaeological Method and Theory* 21, 1–45.

Marín–Arroyo, A.B., Rios–Garaizar, J., Straus, L.G., Jones, J.R., de la Rasilla, M., González Morales, M.R., Richards, M., Altuna, J., Mariezkurrena, K., Ocio, D., 2018. Chronological reassessment of the Middle to Upper Paleolithic transition and Early Upper Paleolithic cultures in Cantabrian Spain. *PLoS One* 13, e0194708.

Maslin, M., Seidov, D., Lowe, J., 2013. *Synthesis of the Nature and Causes of Rapid Climate Transitions During the Quaternary*. Geophysical Monograph Series 126, 9–52.

Mayhew, D.F., 1977. Avian predators as accumulators of fossil mammal material. *Boreas* 6, 25–31.

McAdams, C., Morley, M.W., Fu, X., Kandyba, A.V., Derevianko, A.P., Nguyen, D.T., Doi, N.G., Roberts, R.G., 2019. The Pleistocene geoarchaeology and geochronology of Con Moong Cave, North Vietnam: Site formation processes and hominin activity in the humid tropics. *Geoarchaeology* 4, 14.

McCoy, R.C., Wakefield, J., Akey, J.M., 2017. Impacts of Neanderthal–Introgressed Sequences on the Landscape of Human Gene Expression. *Cell* 168, 916–927.e12.

McInerney, F.A., Helliker, B.R., Freeman, K.H., 2011. Hydrogen isotope ratios of leaf wax n–alkanes in grasses are insensitive to transpiration. *Geochimica et Cosmochimica Acta* 75, 541–554.

McPherron, A., 1967. *The Juntunen site and the late woodland prehistory of the Upper Great Lakes Area*. Ann Arbor, Museum of Anthropology, University of Michigan.

Mellars, P., 2004. Neanderthals and the modern human colonization of Europe. *Nature* 432, 461–465.

Mellars, P., 2006. A new radiocarbon revolution and the dispersal of modern humans in Eurasia. *Nature* 439, 931–935.

Mellars, P., Stringer, C., 1989. *The Human Revolution: Behavioural and Biological Perspectives on the Origins of Modern Humans*. Edinburgh University Press.

Mellett, J.S., 1974. Scatological origin of microvertebrate fossil accumulations. *Science* 185 (4148), 349–350.

Mentzer, S.M., 2014. Microarchaeological approaches to the identification and interpretation of combustion features in prehistoric archaeological sites. *Journal of Archaeological Method and Theory* 21, 616–668.

Mihailović, D., 2019. Push–and–pull factors of the Middle to Upper Paleolithic transition in the Balkans. *Quaternary International* 551, 47-62.

Miller, C.E., Sievers, C., 2012. An experimental micromorphological investigation of bedding construction in the Middle Stone Age of Sibudu, South Africa. *Journal of Archaeological Science* 39, 3039–3051.

Miller, C.E., Conard, N.J., Goldberg, P., Berna, F., 2010. Dumping, sweeping and trampling: experimental micromorphological analysis of anthropogenically modified combustion features. *Palethnologie* 2, 25-37.

Miller, C.E., Goldberg, P., Berna, F., 2013. Geoarchaeological investigations at Diepkloof Rock Shelter, Western Cape, South Africa. *Journal of Archaeological Science* 40, 3432–3452.

Miola, A., 2012. Tools for Non–Pollen Palynomorphs (NPPs) analysis: A list of Quaternary NPP types and reference literature in English language (1972–2011). *Review of Palaeobotany and Palynology* 186, 142–161.

Molina, F.J., Tarriño, A., Galván Santos, B., Hernández, C.M, 2010. Áreas de aprovisionamiento de sílex en el Paleolítico medio en torno al Abric del Pastor (Alcoi, Alicante). *Recerques del Museu d'Alcoi* 19.

Moore, P.D., Webb, J.A., Collinson, M.E., 1991. *Pollen Analysis*. Blackwell Scientific Publications, Oxford.

Morales JV, Sanchis A., 2009. The Quaternary fossil record of the genus Testudo in the Iberian Peninsula. Archaeological implications and diachronic distribution in the western Mediterranean. *Journal of Archaeological Science* 36, 1152–1162.

Morin, E., 2010. Taphonomic implications of the use of bone as fuel. *Palethnologie* 2, 209–217.

Morley, M., 2012. The Campanian–Ignimbrite (CI) tephra at Crvena Stijena Rockshelter, Montenegro: A Key Marker Horizon for the Middle to Upper Palaeolithic Transition in Southern Europe. *Quaternary International* 279–280, 337–338.

Morley, M.W., Goldberg, P., Sutikna, T., Tocheri, M.W., Prinsloo, L.C., Jatmiko, Saptomo, E.W., Wasisto, S., Roberts, R.G., 2017. Initial micromorphological results from Liang Bua, Flores (Indonesia): Site formation processes and hominin activities at the type locality of Homo floresiensis. *Journal of Archaeological Science* 77, 125–142.

Müller, U.C., Pross, J., Tzedakis, P.C., Gamble, C., Kotthoff, U., Schmiedl, G., Wulf, S., Christanis, K., 2011. The role of climate in the spread of modern humans into Europe. *Quaternary Science Reviews* 30, 273–279.

Muñoz–Díaz, D., Rodrigo, F.S., 2004. Impacts of the North Atlantic Oscillation on the probability of dry and wet winters in Spain. *Climate Research* 27, 33–43.

Nabais, M., Zilhão, J., 2019. The consumption of tortoise among Last Interglacial Iberian Neanderthals. *Quaternary Science Reviews* 217, 225-246.

Naughton, F., Sánchez Goñi, M.F., Kageyama, M., Bard, E., Duprat, J., Cortijo, E., Desprat, S., Malaizé, B., Joly, C., Rostek, F., Turon, J.–L., 2009. Wet to dry climatic trend in north–western Iberia within Heinrich events. *Earth and Planetary Science Letters* 284, 329–342.

Nicosia, C., Stoops, G., 2017. *Archaeological Soil and Sediment Micromorphology*. John Wiley and Sons.

Niedermeyer, E.M., Forrest, M., Beckmann, B., Sessions, A.L., Mulch, A., Schefuß, E., 2016. The stable hydrogen isotopic composition of sedimentary plant waxes as quantitative proxy for rainfall in the West African Sahel. *Geochimica et Cosmochimica Acta* 184, 55–70.

Nieuwendam, A., Vieira, G., Schaefer, C., Woronko, B., Johansson, M., 2020. Reconstructing cold climate paleoenvironments from micromorphological analysis of relict slope deposits (Serra da Estrela, Central Portugal). *Permafrost Periglacial Processes* 31 (4), 567-586.

Nigst, P.R., 2019. Approaching the Neanderthal–modern human replacement with population contact scenarios. In: Ramsl, P.C., Rebay–Salisbury, K., Trebsche , P. (Ed.) *Schichtengeschichten. Festschrift Für Otto H. Urban*. Bonn, Universitätsforschungen Zur Prähistorischen Archäologie 328, 261–279.

Nigst, P.R., Haesaerts, P., Damblon, F., Frank–Fellner, C., Mallol, C., Viola, B., Götzinger, M., Niven, L., Trnka, G., Hublin, J.–J., 2014. Early modern human settlement of Europe north of the Alps occurred 43,500 years ago in a cold steppe–type environment. *Proceedings of the National Academy of Sciences of the United States of America* 111, 14394–14399.

Norström, E., Katrantsiotis, C., Smittenberg, R.H., Kouli, K., 2017. Chemotaxonomy in some Mediterranean plants and implications for fossil biomarker records. *Geochimica et Cosmochimica Acta* 219, 96–110.

Norström, E., Norén, G., Smittenberg, R.H., Massuanganhe, E.A., Ekblom, A., 2018. Leaf wax δD inferring variable medieval hydroclimate and early initiation of Little Ice Age (LIA) dryness in southern Mozambique. *Global and Planetary Change* 170, 221–233.

North Greenland Ice Core Project members, 2004. High–resolution record of Northern Hemisphere climate extending into the last interglacial period. *Nature* 431 (7005), 147–151.

Ochando, J., Carrión, J.S., Blasco, R., Fernández, S., Amorós, G., Munuera, M., Sañudo, P., Fernández Peris, J., 2019. Silvicolous Neanderthals in the far west: the mid–Pleistocene palaeoecological sequence of Bolomor Cave (Valencia, Spain). *Quaternary Science Reviews* 217, 247-267.

Ohlrogge, J.B., Jaworski, J.G., Post–Beittenmiller, D., 1993. *De Novo Fatty Acid Biosynthesis*. In: Moore Jr., T.S. (Ed.) Lipid Metabolism in Plants. Boca Raton, FL, CRC Press, 3–32.

Ordóñez, S., Cuevas, J., Benavente, D., García del Cura, M.A., 2016. Architecture of Pleistocene fluvial tufa systems associated with waterfalls: El Salt (Alcoy, Spain). *Geogaceta* 59, 7–10.

Ortiz, J.E., Gallego, J.L.R., Torres, T., Díaz–Bautista, A., Sierra, C., 2010. Palaeoenvironmental reconstruction of Northern Spain during the last 8000 cal yr BP based on the biomarker content of the Roñanzas peat bog (Asturias). *Organic Geochemistry* 41, 454–466.

Palomo, L.J., Gisbert, J., Blanco, J.C., 2007. *Atlas y Libro Rojo de los Mamíferos Terrestres de Espana*. Dirección General de Conservación de la Naturaleza, SECEM, SECEMU, Madrid.

Patania, I., Goldberg, P., Cohen, D.J., Wu, X., Zhang, C., Bar–Yosef, O., 2019. Micromorphological analysis of the deposits at the early pottery Xianrendong cave site, China: formation processes and site use in the Late Pleistocene. *Archaeological and Anthropological Sciences* 11, 4229–4249.

Pérez, L., Sanchis, A., Hernández, C.M., Galván Santos, B., 2017. *Paleoecología de macromamíferos aplicada a los conjuntos zooarqueológicos de El Salt y el Abric del Pastor (Alcoy, Alicante)*. In: Sanchis, A., Pascual, J.L. (Eds.) Interaccions entre felins i humans. III Jornades d'arqueozoologia, Museu Prehistòria de València, Valencia, 327–353.

Peters, K.E., Walters, C.C., Moldowan, J.M., 2005. *The Biomarker Guide. Biomarkers and isotopes in the environment and human history, vol. 1*. Cambridge University Press.

Pettitt, P., Zilhão, J., 2015. Problematizing Bayesian approaches to prehistoric chronologies. *World Archaeology* 47 (4), 525-542.

Pires, L.F., Cooper, M., Cássaro, F.A.M., Reichardt, K., Bacchi, O.O.S., Dias, N.M.P., 2008. Micromorphological analysis to characterize structure modifications of soil samples submitted to wetting and drying cycles. *Catena* 72, 297–304.

Pita, R., Mira, A., Beja, P., 2014. Microtus cabrerae (rodentia: cricetidae). *Mammalian Species* 46 (912), 48–70.

Pleguezuelos, J. M., Márquez, M., and Lizana, M. 2002. *Atlas y Libro Rojo de los anfibios y reptiles de España*. Dirección General de Conservación de la Naturaleza. Asociación Herpetológica Española, Madrid.

Poch, R.M., Artieda, O., Lebedeva, M., 2018. Chapter 10 – Gypsic Features. In: Stoops, G., Marcelino, V., Mees, F. (Eds.), Interpretation of Micromorphological Features of Soils and Regoliths (Second Edition). Elsevier, 259–287.

Pokines, J.T. 2000. Microfaunal research design in the Cantabrian Spanish Paleolithic. *Journal of Anthropological Research* 56 (1), 95–112.

Post–Beittenmiller, D., 1996. Biochemistry and Molecular Biology of Wax Production in Plants. *Annual Review of Plant Physiology and Plant Molecular Biology* 47, 405–430.

Poynter, J.G., Farrimond, P., Brassell, S.C., Eglington, G., 1989. *Molecular Stratigraphic Study of Sediments from Holes 658A and 660A, Leg 108*. In: Barbu, E.M. (Ed.) Proceedings of the Ocean Drilling Program 108 Scientific Results. Texas A&M University, 387–396.

Price, M., 2020. Africans, too, carry Neanderthal genetic legacy. *Science* 367, 497.

Prüfer, K., Racimo, F., Patterson, N., Jay, F., Sankararaman, S., Sawyer, S., Heinze, A., Renaud, G., Sudmant, P.H., de Filippo, C., Li, H., Mallick, S., Dannemann, M., Fu, Q., Kircher, M., Kuhlwilm, M., Lachmann, M., Meyer, M., Ongyerth, M., Siebauer, M., Theunert, C., Tandon, A., Moorjani, P., Pickrell, J., Mullikin, J.C., Vohr, S.H., Green, R.E., Hellmann, I., Johnson, P.L.F., Blanche, H., Cann, H., Kitzman, J.O., Shendure, J., Eichler, E.E., Lein, E.S., Bakken, T.E., Golovanova, L.V., Doronichev, V.B., Shunkov, M.V., Derevianko, A.P., Viola, B., Slatkin, M., Reich, D., Kelso, J., Pääbo, S., 2014. The complete genome sequence of a Neanderthal from the Altai Mountains. *Nature* 505, 43–49.

Rabeder, G., 1981. Die Arvicoliden (Rodentia, Mammalia) aus dem Pliozan und dem älteren Pleistozän von Niederösterreich. *Beiträge zur Paläontologie Österreich* 8, 1–373.

Raczyński, J., Ruprecht, A.L., 1974. The effect of digestion on the osteological composition of owl pellets. *Acta Ornithologica* 14, 25–38.

Rajčević, N., Janaćković, P., Dodoš, T., Tešević, V., Marin, P.D., 2014. Biogeographic variation of foliar n–alkanes of Juniperus communis var. saxatilis Pallas from the Balkans. *Chemistry and Biodiversity* 11, 1923–1938.

Ramos–Román, M.J., Jiménez–Moreno, G., Camuera, J., García–Alix, A., Anderson, R.S., Jiménez–Espejo, F.J., Sachse, D., Toney, J.L., Carrión, J.S., Webster, C., Others, 2018. Millennial–scale cyclical environment and climate variability during the Holocene in the western Mediterranean region deduced from a new multi–proxy analysis from the Padul record (Sierra Nevada, Spain). *Global and Planetary Change* 168, 35-53.

Rasmussen, S.O., Bigler, M., Blockley, S.P., Blunier, T., Buchardt, S.L., Clausen, H.B., Cvijanovic, I., Dahl–Jensen, D., Johnsen, S.J., Fischer, H., Others, 2014. A stratigraphic framework for abrupt climatic changes during the Last Glacial period based on three synchronized Greenland ice–core records: refining and extending the INTIMATE event stratigraphy. *Quaternary Science Reviews* 106, 14–28.

Real, C., 2012. Aproximación metodológica y nuevos datos sobre los conjuntos arqueozoológicos del Magdaleniense superior de la Cova de les Cendres. *Archivo de prehistoria levantina* 29, 99–120.

Real, C., 2016. *Estudio arqueozoológico y tafonómico del Magdaleniense de la Cova de les Cendres (Teulada–Moraira, Alicante).* PhD Thesis. Universitat de València.

Reicosky, D.A., Hanover, J.W., 1978. Physiological Effects of Surface Waxes: I. Light Reflectance for Glaucous and Nonglaucous Picea pungens. *Plant Physiology* 62, 101–104.

Reidsma, F.H., van Hoesel, A., van Os, B.J.H., Megens, L., Braadbaart, F., 2016. Charred bone: Physical and chemical changes during laboratory simulated heating under reducing conditions and its relevance for the study of fire use in archaeology. *Journal of Archaeological Science*: *Reports* 10, 282–292.

Reille, M., 1992. *Pollen et Spores d'Europe et d'Afrique du nord*. Laboratoire de Botanique Historique et Palynologie, Marseille.

Reille, M., 1995. *Pollen et Spores d'Europe et d'Afrique du Nord (Supplément 1)*. Laboratoire de Botanique Historique et Palynologie, Marseille.

Reitz, E.J., Wing, E.S., 2008. *Zooarchaeology 2nd edition. Archaeological theory and methods*. Cambridge University Press.

Reumer, J. W. F., 1984. Rusician and early Pleistocene Soricidae (Insectívora, mammalia) from tegelen (The Netherlands) and Hungary. *Scripta Geologica* 73, 1–173.

Richards, M.P., Trinkaus, E., 2009. Isotopic evidence for the diets of European Neanderthals and early modern humans. *Proceedings of the National Academy of Sciences* 106, 16034–16039.

Riederer, M., Schreiber, L., 2001. Protecting against water loss: analysis of the barrier properties of plant cuticles. *Journal of Experimental Botany* 52 (363), 2023–2032.

Rivas–Martınez, S., 1987. M*apas y memoria de las series de vegetación de Espana (1: 400000)*. Icona, Madrid.

Roberts, M.F., Bricher, S.E., 2018. Modeling the disappearance of the Neanderthals using principles of population dynamics and ecology. *Journal of Archaeological Science* 100, 16–31.

Roček, Z., 1984. *Lizards (Reptilia: Sauria) form the Lower Miocene locality Dolnice (Bohemia, Czechoslovakia).* Rozpravy Československé akademie věd, ř. mat. Přir. 94, 1–69.

Rodríguez de Vera, C., Herrera–Herrera, A.V., Jambrina–Enríquez, M., Sossa–Ríos, S., González–Urquijo, J., Lazuen, T., Vanlandeghem, M., Alix, C., Monnier, G., Pajović, G., Tostevin, G., Mallol, C., 2020. Micro–contextual identification of archaeological lipid biomarkers using resin–impregnated sediment slabs. *Scientific Reports* 10, 20574.

Rodríguez J., 2013. *Paleoecología*. In: García–Díez, M., Zapata, L. (Eds.) Métodos y Técnicas de Análisis y Estudio en Arqueología Prehistórica: de lo técnico a la reconstrucción de los grupos humanos. Servicio Editorial Argitalpen–Zerbitzua, 315–340.

Rodríguez–Cintas, Á., Cabanes, D., 2017. Phytolith and FTIR studies applied to combustion structures: The case of the Middle Paleolithic site of El Salt (Alcoy, Alicante). *Quaternary International* 431, 16–26.

Roebroeks, W., 2008. Time for the Middle to Upper Paleolithic transition in Europe. *Journal of Human Evolution* 55, 918–926.

Roebroeks, W., Villa, P., 2011. On the earliest evidence for habitual use of fire in Europe. *Proceedings of the National Academy of Sciences of the United States of America* 108 (13) 5209-5214.

Roffet–Salque, M., Marciniak, A., Valdes, P.J., Pawłowska, K., Pyzel, J., Czerniak, L., Krüger, M., Roberts, C.N., Pitter, S., Evershed, R.P., 2018. Evidence for the impact of the 8.2–kyBP climate event on Near Eastern early farmers. *Proceedings of the National Academy of Sciences of the United States of America* 115 (35), 8705–8709.

Romans, J.C.C., Robertson, L., 1983. *The general effects of early agriculture on the soil*. In: Maxwell, G.S. (Ed.) The impact of aerial reconnaissance on archaeology. Council for British Archaeology Research Report 49, 136–141.

Rosell, J., Blasco, R., 2019. The early use of fire among Neanderthals from a zooarchaeological perspective. *Quaternary Science Reviews* 217, 268-283.

Rottlander, R.C.A., 1989. Chemische untersuchungen an sedimenten der Höhle Geissenklösterle bei Blaubeuren. *Fundberichte Aus Baden–Württemberg* 14, 23–32.

Rottlander, R.C.A., 1990. Die Resultate der modernen Fettanalytik und irhe Anwendung auf die prähistorische Forschung. *Archaeo-Physik* 12, 1–354.

Roucoux, K.H., de Abreu, L., Shackleton, N.J., Tzedakis, P.C., 2005. The response of NW Iberian vegetation to North Atlantic climate oscillations during the last 65 kyr. *Quaternary Science Reviews* 24, 1637–1653.

Roucoux, K.H., Shackleton, N.J., de Abreu, L., Schönfeld, J., Tzedakis, P.C., 2001. Combined Marine Proxy and Pollen Analyses Reveal Rapid Iberian Vegetation Response to North Atlantic Millennial–Scale Climate Oscillations. *Quaternary Research* 56, 128–132.

Rowe, J.S., 1956. Uses of underground plant species in forestry. *Ecology* 37, 461–473.

Sachse, D., Billault, I., Bowen, G.J., Chikaraishi, Y., Dawson, T.E., Feakins, S.J., Freeman, K.H., Magill, C.R., McInerney, F.A., van der Meer, M.T.J., Polissar, P., Robins, R.J., Sachs, J.P., Schmidt, H.–L., Sessions, A.L., White, J.W.C., West, J.B., Kahmen, A., 2012. Molecular Paleohydrology: Interpreting the Hydrogen–Isotopic Composition of Lipid Biomarkers from Photosynthesizing Organisms. *Annual Review of Earth and Planetary Sciences* 40, 221–249.

Sachse, D., Kahmen, A., Gleixner, G., 2009. Significant seasonal variation in the hydrogen isotopic composition of leaf–wax lipids for two deciduous tree ecosystems (Fagus sylvativa and Acerpseudoplatanus). *Organic Geochemistry* 40, 732–742.

Sachse, D., Radke, J., Gleixner, G., 2006. δD values of individual n–alkanes from terrestrial plants along a climatic gradient—Implications for the sedimentary biomarker record. *Organic Geochemistry* 37, 469–483.

Sánchez Goñi, M.F., d'Errico, F., 2005. *La historia de la vegetación y el clima del último ciclo climático (OIS5–OIS1, 140.000–10.000 años BP) en la Península Ibérica y su posible impacto sobre los grupos paleolíticos*. Museo de Altamira. MONOGRAFÍAS 20, 115–129.

Sánchez Goñi, M.F., Eynaud, F., Turon, J.L., Shackleton, N.J., 1999. High resolution palynological record off the Iberian margin: direct land–sea correlation for the Last Interglacial complex. *Earth and Planetary Science Letters* 171, 123–137.

Sánchez Goñi, M.F., Harrison, S.P., 2010. Millennial–scale climate variability and vegetation changes during the Last Glacial: Concepts and terminology. *Quaternary Science Reviews* 29, 2823–2827.

Sánchez Goñi, M.F., Landais, A., Fletcher, W.J., Naughton, F., Desprat, S., Duprat, J., 2008. Contrasting impacts of Dansgaard–Oeschger events over a western European latitudinal transect modulated by orbital parameters. *Quaternary Science Reviews* 27, 1136–1151.

Sánchez–Bragado, R., Serret, M.D., Marimon, R.M., Bort, J., Araus, J.L., 2019. The Hydrogen Isotope Composition δ2H Reflects Plant Performance. *Plant Physiology* 180, 793–812.

Sánchez–Hernández, C., Rivals, F., Blasco, R., Rosell, J., 2014. Short, but repeated Neanderthal visits to Teixoneres Cave (MIS 3, Barcelona, Spain): a combined analysis of tooth microwear patterns and seasonality. *Journal of Archaeological Science* 49, 317–325.

Sanchis, A., Morales, J.V., Pérez, L.J., Hernández, C.M., Galván Santos, B., 2015. *La tortuga mediterránea en yacimientos valencianos del Paleolítico medio: distribución, origen de las acumulaciones y nuevos datos procedentes del Abric del Pastor (Alcoi, Alacant)*. In: Sanchis, A., Pasual, J.L. (Eds.) Preses petites i grups humans en el passat. II Jornades d’arqueozologia, Valencia, Museu Prehistòria de València, 97–120.

Sankararaman, S., Mallick, S., Dannemann, M., Prüfer, K., Kelso, J., Pääbo, S., Patterson, N., Reich, D., 2014. The genomic landscape of Neanderthal ancestry in present–day humans. *Nature* 507, 354–357.

Schaefer, C.E.G.R., Lima, H.N., Gilkes, R.J., Mello, J.W.V., 2004. Micromorphology and electron microprobe analysis of phosphorus and potassium forms of an Indian Black Earth (IBE) Anthrosol from Western Amazonia. *Australian Journal of Soil Research* 42, 401–409.

Schäfer, I.K., Bliedtner, M., Wolf, D., Kolb, T., Zech, J., Faust, D., Zech, R., 2018. A δ13C and δ2H leaf wax record from the Late Quaternary loess–paleosoil sequence El Paraíso, Central Spain. *Palaeogeography, Palaeoclimatology, Palaeoecology* 507, 52–59.

Schiffer, M.B., 1972. Archaeological Context and Systemic Context. *American Antiquity* 37, 156–165.

Schiffer, M.B., 1987. *Formation Processes of the Archaeological Record*. University of New Mexico Press.

Schirrmacher, J., Andersen, N., Schneider, R.R., Weinelt, M., 2020. Fossil leaf wax hydrogen isotopes reveal variability of Atlantic and Mediterranean climate forcing on the southeast Iberian Peninsula between 6000 to 3000 cal. BP. *PLoS One* 15, e0243662.

Schuldenrein, J., 1986. Paleoenvironment, prehistory, and accelerated slope erosion along the central Israeli coastal plain (Palmahim): A geoarchaeological case study. *Geoarchaeology* 1 (1), 61–81.

Schwab, V.F., Garcin, Y., Sachse, D., Todou, G., Séné, O., Onana, J.–M., Achoundong, G., Gleixner, G., 2015. Effect of aridity on δ 13 C and δD values of C 3 plant–and C 4 graminoid–derived leaf wax lipids from soils along an environmental gradient in Cameroon (Western Central Africa). *Organic Geochemistry* 78, 99–109.

Schweingruber, F.H., 1976. *Mikroskopische holzanatomic, Anatomie microscopique de bois*. Birmensdorf, Institut féderal de recherches forestières, Zurcher AG.

Schweingruber, F.H., 1990. *Anatomie europäischer Hölzer*. Bern, Haupt.

Sedov, S., Solleiro–Rebolledo, E., Fedick, S.L., Pi–Puig, T., Vallejo–Gómez, E., de Lourdes Flores–Delgadillo, M., 2008. *Micromorphology of a Soil Catena in Yucatán: Pedogenesis and Geomorphological Processes in a Tropical Karst Landscape.* In: Kapur S., Mermut A., Stoops G. (Eds.) New Trends in Soil Micromorphology. Berlin, Heidelberg, Springer, 19–37.

Sepulchre, P., Ramstein, G., Kageyama, M., Vanhaeren, M., Krinner, G., Sánchez–Goñi, M.–F., d'Errico, F., 2007. H4 abrupt event and late Neanderthal presence in Iberia. *Earth and Planetary Science Letters* 258, 283–292.

Shahack-Gross, R., Berna, F., Karkanas, P., Weiner, S., 2004. Bat guano and preservation of archaeological remains in cave sites. *Journal of Archaeological Science* 31 (9), 1259–1272.

Shea, J.J., 2003. Neandertals, competition, and the origin of modern human behavior in the Levant. *Evolutionary Anthropology* 12, 173–87.

Shillito, L.M., Almond, M.J., Nicholson, J., Pantos, M., Matthews, W., 2009. Rapid characterisation of archaeological midden components using FT–IR spectroscopy, SEM–EDX and micro–XRD. *Spectrochimica Acta Part A: Molecular and Biomolecular Spectroscopy* 73, 133–139.

Shipman, P., 1981. *Life History of a Fossil. An introduction to taphonomy and paleoecology*. Harvard University Press, Boston.

Shipman, P., Rose, J., 1983. Early hominid hunting, butchering, and carcass–processing behaviors: Approaches to the fossil record. *Journal of Anthropological Archaeology* 2 (1), 57–98.

Simpson, I.A., Barrett, J.H., 1996. Interpretation of Midden Formation Processes at Robert's Haven, Caithness, Scotland using Thin Section Micromorphology. *Journal of Archaeological Science* 23, 543–556.

Sistiaga, A., Mallol, C., Galván, B., Summons, R.E., 2014. The Neanderthal meal: a new perspective using faecal biomarkers. *PLoS One* 9, e101045.

Smyth, J., Berstan, R., Casanova, E., McCormick, F., Mulhall, I., Sikora, M., Synnott, C., Evershed, R.P., 2019. Four millennia of dairy surplus and deposition revealed through compound–specific stable isotope analysis and radiocarbon dating of Irish bog butters. *Scientific Reports* 9, 4559.

Sorensen, A.C., 2017. On the relationship between climate and Neandertal fire use during the Last Glacial in south–west France. *Quaternary International* 436, A, 114–128.

Stahl, P.W., 1996. The recovery and interpretation of microvertebrate bone assemblages from archeological contexts. *Journal of Archaeological Method and Theory* 3 (1), 31–75.

Stahlschmidt, M.C., Miller, C.E., Ligouis, B., Hambach, U., Goldberg, P., Berna, F., Richter, D., Urban, B., Serangeli, J., Conard, N.J., 2015. On the evidence for human use and control of fire at Schöningen. *Journal of Human Evolution* 89, 181–201.

Stahlschmidt, M.C., Nir, N., Greenbaum, N., Zilberman, T., Barzilai, O., Ekshtain, R., Malinsky–Buller, A., Hovers, E., Shahack–Gross, R., 2018. Geoarchaeological Investigation of Site Formation and Depositional Environments at the Middle Palaeolithic Open–Air Site of 'Ein Qashish, Israel. *Journal of Paleolithic Archaeology* 1, 32–53.

Staubwasser, M., Drăgușin, V., Onac, B.P., Assonov, S., Ersek, V., Hoffmann, D.L., Veres, D., 2018. Impact of climate change on the transition of Neanderthals to modern humans in Europe. *Proceedings of the National Academy of Sciences of the United States of America* 115, 9116–9121.

Stephens, M., Rose, J., Gilbertson, D.D., Canti, M.G., 2005. Micromorphology of Cave Sediments in the Humid Tropics: Niah Cave, Sarawak. *Asian Perspectives* 44, 42–55.

Stewart, J.R., 2005. The ecology and adaptation of Neanderthals during the non-analogue environment of Oxygen Isotope Stage 3: armageddon or entente? The demise of the European Neanderthals in Isotope Stage 3. *Quaternary International* 137, 35–46.

Stiner, M.C., Kuhn, S.L., Weiner, S., Bar–Yosef, O., 1995. Differential Burning, Recrystallization, and Fragmentation of Archaeological Bone. *Journal of Archaeological Science* 22, 223–237.

Stoops, G., 2003. *Guidelines for analysis and description of soil and regolith thin sections*. Soil Science Society of America, Madison, WI.

Stoops, G., Marcelino, V., Mees, F., 2010. *Interpretation of Micromorphological Features of Soils and Regoliths*. Elsevier.

Struck, J., Bliedtner, M., Strobel, P., Schumacher, J., Bazarradnaa, E., Zech, R., 2020. Leaf wax n–alkane patterns and compound–specific δ13C of plants and topsoils from semi–arid and arid Mongolia. *Biogeosciences* 17, 567–580.

Swain, A.M., 1973. A history of fire and vegetation in northeastern Minnesota as recorded in lake sediments. *Quaternary Research* 3, 383–396.

Szyndlar, Z., 1984. Fossil snakes from Poland. *Acta Zoologica Cracoviensia* 28, 1–156.

Tinto, W.F., Elufioye, T.O., Roach, J., 2017. *Waxes*. In: Badal, S., Delgoda, R. (Eds.) Pharmacognosy. Boston, Academic Press, 443–455.

Tipple, B.J., Berke, M.A., Hambach, B., Roden, J.S., Ehleringer, J.R., 2015. Predicting leaf wax n–alkane 2H/1H ratios: controlled water source and humidity experiments with hydroponically grown trees confirm predictions of Craig–Gordon model. *Plant, Cell and Environment* 38. 6, 1035–1047.

Toffolo, M.B., Ritchie, M., Sellers, I., Morin, J., Lyons, N., Caldwell, M., Albert, R.M., Letham, B., Berna, F., 2019. Combustion features from short–lived intermittent occupation at a 1300–year–old Coast Salish rock shelter, British Columbia: The microstratigraphic data. *Journal of Archaeological* Science: *Reports* 23, 646–661.

Toney, J.L., García–Alix, A., Jiménez–Moreno, G., Anderson, R.S., Moossen, H., Seki, O., 2020. New insights into Holocene hydrology and temperature from lipid biomarkers in western Mediterranean alpine wetlands. *Quaternary Science Reviews* 240, 106395.

Torres, T., Ortiz, J.E., Blázquez, A.M., Ruiz Zapata, B., Gil, M.J., Martín, T., Sánchez–Palencia, Y., 2015. The MIS 5 palaeoenvironmental record in the SE Mediterranean coast of the Iberian Peninsula (Río Antas, Almería, Spain). *Climate of the Past* 11, 3897–3936.

Trinkaus, E., 1995. Neanderthal mortality patterns. *Journal of Archaeological Science* 22, 121–142.

Trinkaus, E., 2011. Late Pleistocene adult mortality patterns and modern human establishment. *Proceedings of the National Academy of Sciences of the United States of America* 108 (4) 1267-1271.

Uerpmann, H.P., 1973. Animal bone finds and economic archaeology: a critical study of Osteoarchaeological method. *World Archaeology* 4, 307–322.

Uetz, P. and Hošek, J., 2015. The Reptile Database. [accessed at http://www.reptile–database.org].

Underdown, S., 2008. A potential role for transmissible spongiform encephalopathies in Neanderthal extinction. *Medical Hypotheses* 71, 4–7.

Uno, K.T., Polissar, P.J., Kahle, E., Feibel, C., Harmand, S., Roche, H., deMenocal, P.B., 2016. A Pleistocene palaeovegetation record from plant wax biomarkers from the Nachukui Formation, West Turkana, Kenya. *Philosophical Transactions of the Royal Society B: Biological Sciences* 371 (1698), 20150235.

Urban, T.M., Rasic, J.T., Alix, C., Anderson, D.D., Chisholm, L., Jacob, R.W., Manning, S.W., Mason, O.K., Tremayne, A.H., Vinson, D., 2019. Magnetic detection of archaeological hearths in Alaska: A tool for investigating the full span of human presence at the gateway to North America. *Quaternary Science Reviews* 211, 73–92.

Vallverdú–Poch, J., Courty, M.A., 2012. *Microstratigraphic Analysis of Level J Deposits: A Dual Paleoenvironmental–Paleoethnographic Contribution to Paleolithic Archeology at the Abric Romaní.* In: Roura, E.C. (Ed.) High Resolution Archaeology and Neanderthal Behavior, Vertebrate Paleobiology and Paleoanthropology. Netherlands, Springer, 77–133.

Val–Peón, C., Expósito, I., Soto, M., Burjachs, F., 2019. A taphonomic approach to the pollen assemblage from layer M of the Abric Romaní archaeological site (NE Iberian Peninsula). *Review of Palaeobotany and Palynology* 270, 19–39.

van Andel, T.H., Davies, W., 2003. *Neanderthals and modern humans in the European landscape during the last glaciation: archaeological results of the Stage 3 Project*. Cambridge, McDonald Institute for Archaeological Research monographs.

van der Meulen, A., 1973. Middle Pleistocene smaller mammals from the montepeglia (orvieto, Italy), with special reference to the phylogeny of Microtus (arvicolidae, rodentia). *Quaternaria* 17, 1–144.

van der Weerd, A., 1976. *Rodents Faunas of the Mio–Pliocene Sediments of the Teruel–alfambra Region, Spain, vol. 2*. Utrecht Micropaleontological Bulletins Special Publication, 1–217.

Van Geel, B., Coope, G.R., Van Der Hammen, T., 1989. Palaeoecology and stratigraphy of the lateglacial type section at Usselo (the Netherlands). *Review of Palaeobotany and Palynology* 60, 25–129.

van Hoeve, M.L., Hendrikse, M., 1998. *A study of non–pollen objects in pollen slides*. Unpublished Report, University of Amsterdam.

Vidal-Matutano, P., 2018. Anthracological data from Middle Palaeolithic contexts in Iberia: What do we know? *Munibe Antropologia-Arkeologia* 69

Vidal-Matutano, P., Pérez–Jordà, G., Hernández, C.M., Galván, B., 2018. Macrobotanical evidence (wood charcoal and seeds) from the Middle Palaeolithic site of El Salt, Eastern Iberia: Palaeoenvironmental data and plant resources catchment areas. *Journal of Archaeological Scienc*e: *Reports* 19, 454–464.

Vidal-Matutano, P., Henry, A., Théry–Parisot, I., 2017. Dead wood gathering among Neanderthal groups: Charcoal evidence from Abric del Pastor and El Salt (Eastern Iberia). *Journal of Archaeological Science* 80, 109–121.

Vidal-Matutano, P., Hernández, C.M., Galván, B., Mallol, C., 2015. Neanderthal firewood management: evidence from Stratigraphic Unit IV of Abric del Pastor (Eastern Iberia). *Quaternary Science Reviews* 111, 81–93.

Vigne, J.D., Valladas, H., 1996. Small mammal fossil assemblages as indicators of environmental change in northern Corsica during the last 2500 years. Journal of Archaeological Science 23 (2), 199–215.

Villa, P., Mahieu, E., 1991. Breakage patterns of human long bones. *Journal of Human Evolution* 21, 27–48.

Villa, P., Pollarolo, L., Conforti, J., Marra, F., Biagioni, C., Degano, I., Lucejko, J.J., Tozzi, C., Pennacchioni, M., Zanchetta, G., Nicosia, C., Martini, M., Sibilia, E., Panzeri, L., 2018. From Neandertals to modern humans: New data on the Uluzzian. *PLoS One* 13, e0196786.

Villa, P., Roebroeks, W., 2014. Neandertal demise: an archaeological analysis of the modern human superiority complex. *PLoS One* 9, e96424.

Villanea, F.A., Schraiber, J.G., 2019. Multiple episodes of interbreeding between Neanderthal and modern humans. *Nature Ecology and Evolution* 3, 39–44.

Vliet–Lanoë, B., Fox, C.A., Gubin, S.V., 2004. *Micromorphology of Cryosols*. In: Kimble, J.M. (Ed.) Cryosols. Berlin, Heidelberg. Springer, 365-390.

Vliet–Lanoë, B.V., 2010. *Frost Action*. In: Stoops, G., Marcelino, V., Mees, F. (Eds.) Interpretation of Micromorphological Features of Soils and Regoliths (Second Edition). Amsterdam, Elsevier, 81–108.

von Wettstein–Knowles, P., 1982. Elongase and epicuticular wax biosynthesis. Physiologie Végétale 20, 797–809.

Wakano, J.Y., Gilpin, W., Kadowaki, S., Feldman, M.W., Aoki, K., 2018. Ecocultural range–expansion scenarios for the replacement or assimilation of Neanderthals by modern humans. Theoretical Population Biology.

Walter H. 1973. *Vegetation of the Earth*. The English University Press, London.

Wang, C., Eley, Y., Oakes, A., Hren, M., 2017. Hydrogen isotope and molecular alteration of n–alkanes during heating in open and closed systems. *Organic Geochemistry* 112, 47–58.

Wang, C., Eley, Y., Oakes, A., Hren, M., 2017. Hydrogen isotope and molecular alteration of n–alkanes during heating in open and closed systems. *Organic Geochemistry* 112, 47–58.

Wang, J., Xu, Y., Zhou, L., Shi, M., Axia, E., Jia, Y., Chen, Z., Li, J., Wang, G., 2018. Disentangling temperature effects on leaf wax n–alkane traits and carbon isotopic composition from phylogeny and precipitation. *Organic Geochemistry* 126, 13–22.

Wang, X., Huang, X., Sachse, D., Ding, W., Xue, J., 2016. Molecular Paleoclimate Reconstructions over the Last 9 ka from a Peat Sequence in South China. *PLoS One* 11, e0160934.

Ward, I., Moe–Astrup, P., Merigot, K., 2019. At the water's edge: Micromorphological and quantitative mineral analysis of a submerged Mesolithic shell midden at Hjarnø Sund, Denmark. *Journal of Archaeological Science* 102, 11–25.

Wattez, J., Courty, M.A., Macphail, R.I., 1990. *Burnt Organo–Mineral Deposits Related to Animal and Human Activities in Prehistoric Caves*. In: Douglas, L.A. (Ed.), Soil Micromorphology: a Basic and Applied Science, Developments in Soil Science. Amsterdam, Elsevier, 431–439.

Weiner, S., 2010. *Microarchaeology: Beyond the Visible Archaeological Record*. Cambridge University Press.

Weiner, S., Schiegl, S., Goldberg, P., Bar–Yosef, O., 1995. Mineral Assemblages in Kebara and Hayonim Caves, Israel: Excavation Strategies, Bone Preservation, and Wood Ash Remnants. *Israel Journal of Chemistry* 35 (2), 143–154.

Welker, F., Hajdinjak, M., Talamo, S., Jaouen, K., Dannemann, M., David, F., Julien, M., Meyer, M., Kelso, J., Barnes, I., Brace, S., Kamminga, P., Fischer, R., Kessler, B.M., Stewart, J.R., Pääbo, S., Collins, M.J., Hublin, J.J., 2016. Palaeoproteomic evidence identifies archaic hominins associated with the Châtelperronian at the Grotte du Renne. *Proceedings of the National Academy of Sciences of the United States of America* 113 (40), 11162–11167.

Whitau, R., Vannieuwenhuyse, D., Dotte–Sarout, E., Balme, J., O'Connor, S., 2018. Home Is Where the Hearth Is: Anthracological and Microstratigraphic Analyses of Pleistocene and Holocene Combustion Features, Riwi Cave (Kimberley, Western Australia). *Journal of Archaeological Method and Theory* 25, 739–776.

Whitlock, C., Larsen, C., 2001. *Charcoal as a Fire Proxy*. In: Smol, J.P., Birks, H.J.B., Last, W.M., Bradley, R.S., Alverson, K. (Eds.) Tracking Environmental Change Using Lake Sediments: Terrestrial, Algal, and Siliceous Indicators. Netherlands, Dordrecht, Springer, 75–97.

Whittaker, R.H., 1948. *A Vegetation Analysis of the Great Smoky Mountains*. PhD Thesis. University of Illinois.

Wiesenberg, G.L.B., Lehndorff, E., Schwark, L., 2009. Thermal degradation of rye and maize straw: Lipid pattern changes as a function of temperature. *Organic Geochemistry* 40, 167–174.

Wilson, D.E., Reeder, D.M., 2005. *Mammal Species of the World: a Taxonomic and Geographic Reference*. Baltimore, Johns Hopkins University Press.

Wintle, A.G., Murray, A.S., 2000. Quartz OSL: Effects of thermal treatment and their relevance to laboratory dating procedures. *Radiation Measurements* 32, 387–400.

Wirth, S.B., Sessions, A.L., 2016. Plant–wax D/H ratios in the southern European Alps record multiple aspects of climate variability. *Quaternary Science Reviews* 148, 176–191.

Wolf, D., Kolb, T., Alcaraz–Castaño, M., Heinrich, S., Baumgart, P., Calvo, R., Sánchez, J., Ryborz, K., Schäfer, I., Bliedtner, M., Zech, R., Zöller, L., Faust, D., 2018. Climate deteriorations and Neanderthal demise in interior Iberia. *Scientific Reports* 8, 7048.

Wolff, H., Greenwood, A.D., 2010. Did viral disease of humans wipe out the Neandertals? *Medical Hypotheses* 75, 99–105.

Wood, R.E., Barroso–Ruíz, C., Caparrós, M., Jordá Pardo, J.F., Galván Santos, B., Higham, T.F.G., 2013. Radiocarbon dating casts doubt on the late chronology of the Middle to Upper Palaeolithic transition in southern Iberia. *Proceedings of the National Academy of Sciences of the United States of America* 110, 2781–2786.

Wrangham, R., Carmody, R., 2010. Human adaptation to the control of fire. *Evolutionary Anthropology* 19, 187–199.

Wroth, K., Cabanes, D., Marston, J.M., Aldeias, V., Sandgathe, D., Turq, A., Goldberg, P., Dibble, H.L., 2019. Neanderthal plant use and pyrotechnology: phytolith analysis from Roc de Marsal, France. *Archaeological and Anthropological Sciences* 11, 4325–4346.

Wu, M., Zhuang, G., Hou, M., Miao, Y., 2018. Ecologic shift and aridification in the northern Tibetan Plateau revealed by leaf wax n–alkane δ2H and δ13C records. *Palaeogeography, Palaeoclimatology, Palaeoecology* 514, 464–473.

Xie, S., Nott, C.J., Avsejs, L.A., Maddy, D., chambers, F.M., Evershed, R.P., 2004. Molecular and isotopic stratigraphy in an ombrotrophic mire for paleoclimate reconstruction. *Geochimica et Cosmochimica Acta* 68, 2849–2862.

Yamamoto, S., Kawamura, K., Seki, O., Meyers, P.A., Zheng, Y., Zhou, W., 2010. Environmental influences over the last 16ka on compound–specific δ13C variations of leaf wax n–alkanes in the Hani peat deposit from northeast China. *Chemical Geology* 277, 261–268.

Yang, H., Huang, Y., 2003. Preservation of lipid hydrogen isotope ratios in Miocene lacustrine sediments and plant fossils at Clarkia, northern Idaho, USA. *Organic Geochemistry* 34, 413–423.

Yokoyama, Y., Nguyen, H.V., 1980. *Direct and non–destructive dating of marine sediments, manganese nodules and corals by high resolution gamma–ray spectrometry*. In: Goldberg, E.D., Horibe, Y., Saruhashi, K. (Eds.) Isotope Marine Chemistry. Tokyo, Uchida Rokakuho, 259–2890.

Zhang, Y., Liu, X., Lin, Q., Gao, C., Wang, J., Wang, G., 2014. Vegetation and climate change over the past 800 years in the monsoon margin of north eastern China reconstructed from n–alkanes from the Great Hinggan Mountain ombrotrophic peat bog. *Organic Geochemistry* 76, 128–135.

Zhao, L., Wang, L., Cernusak, L.A., Liu, X., Xiao, H., Zhou, M., Zhang, S., 2016. Significant Difference in Hydrogen Isotope Composition Between Xylem and Tissue Water in Populus Euphratica. *Plant, Cell and Environment* 39, 1848–1857.

Zilhão, J., 2006. Chronostratigraphy of the Middle–to–Upper Paleolithic Transition in the Iberian Peninsula. *Pyrenae* 7–84.

Zilhão, J., Pettitt, P., 2006. On the new dates for Gorham's Cave and the late survival of Iberian Neanderthals. *Before Farming* 2006 (3), 95–122.

APPENDIX 1

Supplementary Material

for

Chapter 3: A multiproxy record of palaeoenvironmental conditions at the Middle Palaeolithic site of Abric del Pastor (Eastern Iberia)

Contents:

Chapter 3: Material and methods (extended)

Dosimetry on site

10 Al2O3:C dosimeters were inserted (S.U. I to VI) and remained in place for a duration of five months. Doses were measured following Kreutzer et al. (2018). Obtained dose rates (gamma + cosmic) are low and do not show significant variation through the stratigraphic sequence (from 317 to 388 µGy/a). This likely corresponds with the calcareous nature of the sediments. These external dose rates were used for calculating the ages of both the tooth and sediment samples.

Dated sediment samples

Sediment was collected from S.U. IVd in absolute darkness and dated using Optically Stimulated Luminescence (OSL). Quartz grains (60-80µm) were extracted by sieving and subsequently purified using acids (HCl and H2SiF6). The Single Aliquot Regenerative (SAR) dose protocol (Wintle and Murray, 2000) was applied to large aliquots (6mm in diameter) for measuring the fast component of the OSL signal. A preheating plateau test was carried out, which indicated no dependence of the equivalent doses (De) on temperature (200 - 260°C). Following this, a dose recovery test was conducted and yielded a value close to one (1.02 ± 0.02). A series of 20 aliquots were then analysed and the representative De was calculated using the Central Age Model (Galbraith et al., 1999). Determination of U, Th, K contents in the sediment was carried out by gamma spectrometric analysis, allowing for the alpha and beta external dose rates received by the 60-80µm grains to be calculated.

Dated Teeth

Two herbivore teeth were selected for combined ESR / U-series dating. An Equidae premolar recovered from S.U. IVb (sample AP1601) and a Bovinae tooth recovered from S.U. VI (sample AP1602). Enamel, dentin and cement in AP1601 were separated mechanically. Alpha-ray spectrometry was used to measure the radio-isotope content in the dentin and cement following standard methods (Bischoff et al., 1988), and by gamma-ray spectrometry (Yokoyama, and Nguyen, 1980). Analysis was carried out at the Institut de Paléontologie Humaine (IPH), Paris.

ESR measurements were carried out using an EMX Bruker ESR spectrometer applying the following parameters: 1mW microwave power, 0.1mT modulation amplitude, room temperature (19°C), 10mT scan range, 4min scan time and 100kHz frequency modulation. A minimum of three measurements was recorded for each dose on different days. The equivalent doses (DE) were determined from the asymmetric enamel T1-B2 signal at $g = 2.001853$ and fitted from the experimental data using an exponential function (SSE) with Microcal Origin Pro 8 software with $1/I^2$ weighting. The DE were calculated from mean values obtained from three repeated measurements for each aliquot. ESR age calculations were achieved using the ESR-DATA program (Grün, 2009), which utilises an alpha efficiency of 0.13 ± 0.02 (Grün and Katzenberger-Apel, 1994) and Monte-Carlo beta attenuation factors (Brennan et al., 1997) determined by the thickness of the tooth enamel and outer layers removed. The analysis was carried out at the Institut de Paléontologie Humaine (IPH), Paris.

Microvertebrate study (IVd)

The minimum number of individuals (MNI) was calculated to establish the abundance of each species in the fossil assemblage. In order to reconstruct the palaeoenvironmental context of S.U. IVd from Abric del Pastor, the Habitat Weighting method developed by Whittaker (1948), Rowe (1956) and Gauch (1989) was employed. This procedure consists of defining a value, in a range between 0 and 1, for each species in each habitat where it is found. Following Cuenca-Bescós et al. (2005), the habitats considered in this work are: Open dry (OD), meadows under seasonal climate change; Open humid (OH), evergreen meadows with dense pastures and suitable topsoil; Woodland (W), mature forest; Open Woodlands (OWo), woodland margins and forest patches, with moderate ground cover; Rocky (R), areas with a suitable rocky or stone substratum and Water (Wa), areas along streams, lakes and ponds. The ecological preferences of the different taxa described in the present work have been taken from Pleguezuelos et al. (2002), Palomo et al. (2007), Bencatel et al. (2017) and López and Martín (2018).

Prior to palaeoclimatic and palaeoenvironmental interpretation it is necessary to conduct a taphonomic study to identify predator(s) species responsible for the small mammal assemblage (e.g. Andrews, 1990; Vigne and Valladas, 1996; Pokines, 2000). Predation is the main factor involved in the accumulation of small mammal assemblages (Dodson and Wexlar, 1979; Korth, 1979; Andrews and Evans, 1983; Andrews, 1990; Kusmer, 1990; Stahl, 1996 amongst others) and it can be recognised by the presence of fossil digested remains (Raczyński and Ruprecht, 1974; Mellet, 1974; Mayhew, 1977; Andrews, 1990; Fernández-Jalvo and Andrews, 1992; Lloveras et al., 2014; Fernández-Jalvo et al., 2016). In this preliminary taphonomic study, the degree and frequency of digestive corrosion on both bones and dental elements have been examined. For the identification of the source of taphonomic information we used the criteria provided by Andrews (1990), Fernández-Jalvo and Andrews (1992) and Fernández-Jalvo et al. (2016).

Macrofaunal study (IVd) - Material and methods (extended)

All remains were analysed taphonomically using macroscopic and microscopic techniques (Leuchtturm hand lens up to 20x and Leica M165C stereo light, magnification ranging from 10x to 120x) to identify biostratinomic and diagenetic modifications. In the fracture analysis, we classified all of the fragments by fracture type following the criteria established by Villa and Mahieu (1991) and the morphotypes created by Real (2012; 2016). All dimensions were measured for each bone fragment. Bone surface modifications were observed and quantified to identify damage caused by anthropogenic activity (thermal alteration, percussion and butchering marks) or predator damage (tooth marks, digestion), as well as the diverse diagenetic processes that produce alterations on bone surfaces (erosion, sediment concreteness, roots marks, weathering, pigmentation, trampling) (Binford, 1981; Shipman, 1981; Shipman and Rose, 1983; Lyman, 1994; Reitz and Wing, 2008; Domínguez Rodrigo and Yravedra, 2009; Denys and Patou-Mathis, 2014; Fernandez-Jalvo and Andrews, 2016).

Chapter 3: Results (extended)

	Type	Layer	U	Th	K	α-efficiency	Internal	+-	external	+-	annual	+-	De	+-	Age	+-
			(ppm)	(ppm)	(%)				dose rate (μGy/a)				(Gy)		(ka)	
OSL1	Sediment	IVd	1.31	0.70	0.13	5	0	0	681	21	681	21	43	1	63	5
AP1601	Tooth	IVb	1.31	0.70	0.13		326	36	356	23	682	51	33	1	48	5
AP1602	Tooth	VI	1.31	0.70	0.13		749	155	378	23	1127	164	70	4.1	62	12/-9

Table 1 OSL and ESR dates from Abric del Pastor. Errors at the 1-sigma (1σ) confidence level (Mallol et al., 2019)

.

Sample	Type	Layer	p-value					
			enamel	±	dentine	±	cement	±
AP1601	Tooth	IVb	-0.69	0.12	-0.76	0.12	-49	0.14
AP1602	Tooth	VI	-0.7	0.19	-89	0.15	--	--

Table 2 Reported p-values for ESR dates from Abric del Pastor (Mallol et al., 2019).

	I	I	III	IVA	IVB	IVB	IVC	IVD	IVD	V	VI
C_{18}	-	-	-	0.0247 ± 0.0021	-	-	0.0019 ± 0.0007	-	-	-	-
C_{19}	-	-	-	0.0054 ± 0.0064	-	-	-	0.0035 ± 0.0028	-	-	-
C_{20}	-	0.0026 ± 0.0004	-	0.0073 ± 0.0003	-	-	-	0.0078 ± 0.0036	-	-	-
C_{21}	0.0008 ± 0.0002	0.0059 ± 0.0021	-	0.0125 ± 0.0012	-	-	0.0037 ± 0.001	0.0102 ± 0.0024	-	-	-
C_{22}	0.0006 ± 0.0004	0.005 ± 0.0004	-	0.0142 ± 0.0006	-	-	0.0068 ± 0.0012	0.0147 ± 0.0016	-	-	-
C_{23}	0.0115 ± 0.0001	0.0097 ± 0.0006	-	0.0221 ± 0.0057	0.0018 ± 0.0011	-	0.0163 ± 0.0037	0.0234 ± 0.0009	-	-	-
C_{24}	0.0008 ± 0.0116	0.006 ± 0.0002	-	0.028 ± 0.0013	-	-	0.0185 ± 0.0021	0.0335 ± 0.0031	-	-	-
C_{25}	0.024 ± 0.0011	0.0203 ± 0.0001	0.0034	0.0317 ± 0.0006	-	-	0.0258 ± 0.0052	0.045 ± 0.0031	-	-	0.0006 ± 0.0025
C_{26}	0.0151 ± 0.0046	0.0101 ± 0.0002	-	0.0246 ± 0.0262	-	-	0.0292 ± 0.0035	0.0501 ± 0.0029	0.0007 ± 0.0004	-	-
C_{27}	0.0657 ± 0.0015	0.0442 ± 0.0002	0.0088 ± 0.0001	0.0687 ± 0.0027	0.0083 ± 0.0012	0.0053 ± 0.0007	0.0336 ± 0.0039	0.0546 ± 0.0032	0.0057 ± 0.0016	-	0.0112 ± 0.0012
C_{28}	0.0459 ± 0.0007	0.0263 ± 0.0008	-	0.0391 ± 0.0007	-	-	0.0303 ± 0.0028	0.0514 ± 0.0045	-	-	-
C_{29}	0.1232 ± 0.002	0.0866 ± 0.0017	0.0261 ± 0.0003	0.1477 ± 0.0168	0.02 ± 0.0001	0.017 ± 0.0014	0.0384 ± 0.0038	0.0499 ± 0.0041	0.0145 ± 0.0021	0.0049 ± 0.0027	0.0248 ± 0.0018
C_{30}	0.0625 ± 0.0051	0.0346 ± 0.0035	-	0.0442 ± 0.0019	-	-	0.0271 ± 0.0046	0.0382 ± 0.0023	-	-	-
C_{31}	0.18 ± 0.0025	0.1199 ± 0.0056	0.0387 ± 0.0002	0.1878 ± 0.0052	0.0257 ± 0.0021	0.022 ± 0.0016	0.0401 ± 0.0028	0.0379 ± 0.0027	0.0182 ± 0.0011	0.0096	0.0291 ± 0.0017
C_{32}	0.1005 ± 0.0014	0.0488 ± 0.0002	-	0.0638 ± 0.018	-	-	0.0168 ± 0.0068	0.0232 ± 0.0019	-	-	-
C_{33}	0.2758 ± 0.011	0.1724 ± 0.0014	0.0444 ± 0.0055	0.2174 ± 0.0038	0.016 ± 0.001	0.0138 ± 0.0022	0.0257 ± 0.0045	0.0187 ± 0.0026	0.0097	-	0.0092
C_{34}	0.1479 ± 0.0182	0.042 ± 0.0087	0.0215 ± 0.0031	0.2472 ± 0.0232	0.0289 ± 0.0021	-	0.0323 ± 0.0164	-	0.0181 ± 0.0073	0.0227 ± 0.0071	-
C_{35}	0.3307 ± 0.0086	0.1113 ± 0.0238	0.0473 ± 0.0064	0.4029 ± 0.1461	0.0397	-	-	-	-	-	-

Table 3 Concentration of individual *n*-alkanes, errors reported as standard deviation.

Taphonomic remarks on the microfaunal assemblage

Evidence of digestion damage is detected in cranial and postcranial elements indicating that the fossil assemblage is produced by predation. The total percentage of digested incisors is close to 31% while in molars it is around 19%. The most frequent degree of digestion observed is light followed by moderate. Samples with a heavy degree of digestion were scarce and only detected in molars. No evidence of extreme degree was observed either on molars or on incisors. Digestion of long bones on proximal ends of femurs and distal ends of humeri affects 38% and 36% of the assemblage, respectively. Based on the overall results, the evidence from S.U. IVd at Abric del Pastor points to category 3 digestion (Andrews, 1990; Fernández-Jalvo and Andrews, 1992; Fernández-Jalvo et al., 2016) in which the Eurasian eagle-owl (*Bubo bubo*) and the tawny owl (*Strix aluco*) are the most probable predators. Both predators fall under “intermediate modification” according to Andrews (1990), although *Bubo bubo* may fit better with data obtained from Abric del Pastor for the present study.

Taphonomic data and anthropogenic alterations - macrofaunal assemblage

Regarding surface features informative of anthropogenic activities, anthropogenic marks are sparse. They were identified on 26 bones or fragments (5.4% NR). Slicing marks and notches prevail, followed by scraping marks and a few cases of crenulated edges and peeling (Table 4). These features are concentrated on bones of *Capra pyrenaica*, *Cervus elaphus*, *Testudo hermanni* and medium-weight animals. Nevertheless, the distribution and nature of the marks suggest on-site butchering activity, including disarticulation, evisceration, defleshing, periosteum removal, percussion, and flexion. Thermally altered bone remains are common (14.7% NISP), particularly Mediterranean tortoises and undetermined bone fragments. These mainly exhibit incipient alteration and carbonisation

(200-400ºC), although some are strongly burned and calcined (600-700ºC). None of the remains shows burning over the entire surface. In the tortoise, thermal alteration is present mainly on the exterior face of plates. This relates to cooking practices and has been demonstrated in others works from Abric del Pastor (Sanchis et al., 2015), Gruta da Figueira Brava and Gruta da Oliveira (Nabais and Zilhão, 2019). Finally, lagomorphs, carnivores and birds within the assemblage do not appear to be associated with human activity, based on the absence of anthropogenic features.

Taxa	**Slicing marks**	**Scraping marks**	**Notches**	**Crenulated edge**	**Peeling**	**Thermal Alteration**
Capra pyrenaica	2		1			1
Cervidae			**1**			
Cervus elaphus	1	1	1			
Testudo hermanni	5	2	1	1	1	33
Testudo sp.						1
Birds						1
Total NISP	**8**	**3**	**4**	**1**	**1**	**36**
Medium size	5		1			6
Small size	1				1	2
Undetermined	1					26
Total NR	**7**	**0**	**1**	**0**	**1**	**34**

Table 4 Quantity and taxa distribution of the determined biostratinomic alteration.

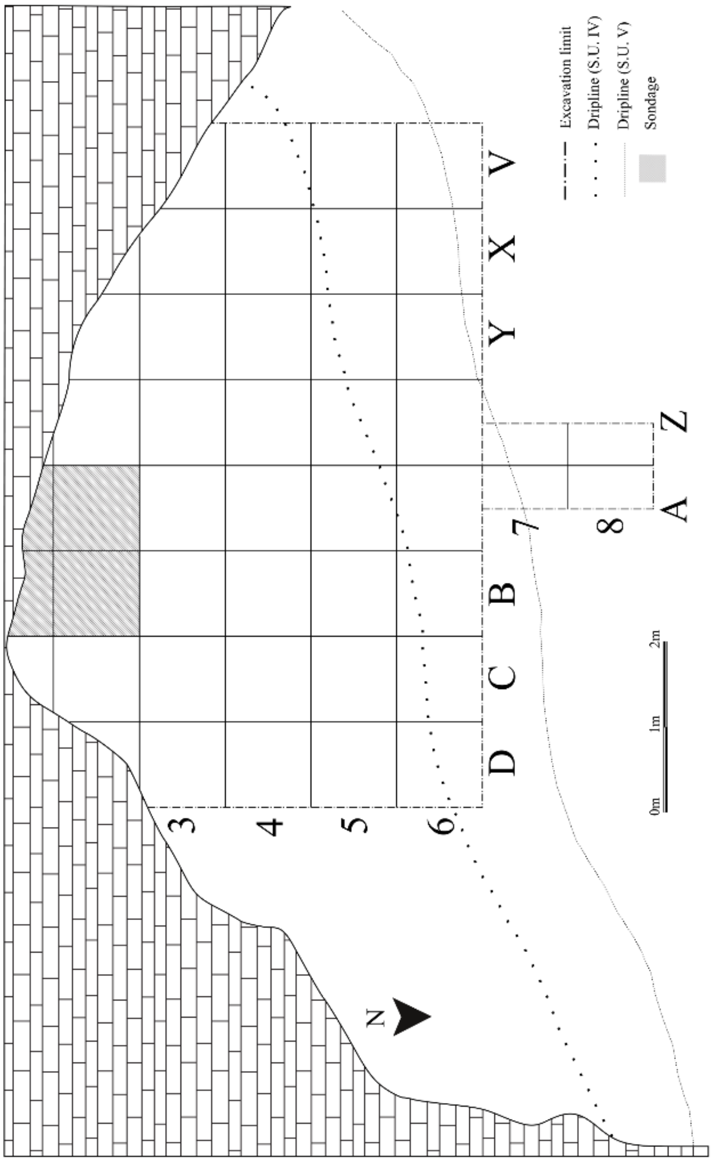

Figure 1 Plan of excavation area at Abric del Pastor (after Machado et al., 2013).

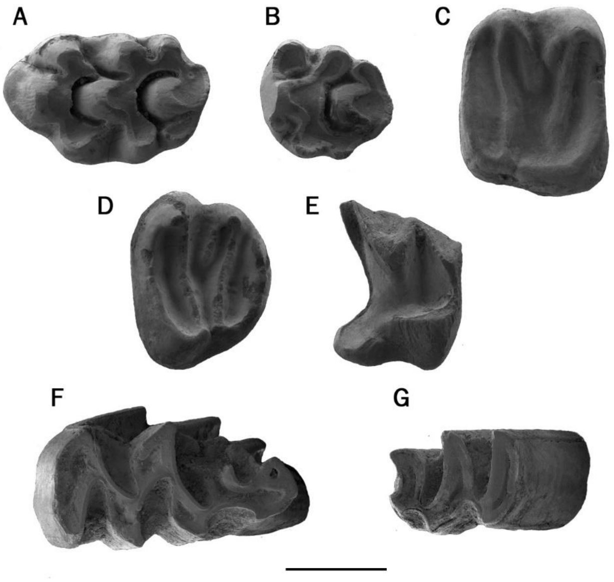

Figure 2 Small mammal remains from S.U. IVd of Abric del Pastor. A) *Apodemus sylvaticus*, AP-IVd-x-35, M1 left; B) *Apodemus sylvaticus*, AP-IVd-x-47, M2 right; C) *Eliomys quercinus*, AP-IVd-x-126, M1-2 right; D) *Eliomys quercinus*, AP-IVd-x-122, M3 left; E) *Crocidura* gr. *russula-gueldenstaedtii* AP-IVd-x-143, M1 right; F) *Microtus cabrerae*. AP-IVd-x-130, M3 right; G) *Microtus cabrerae*, AP-IVd-x-134, m3 left.

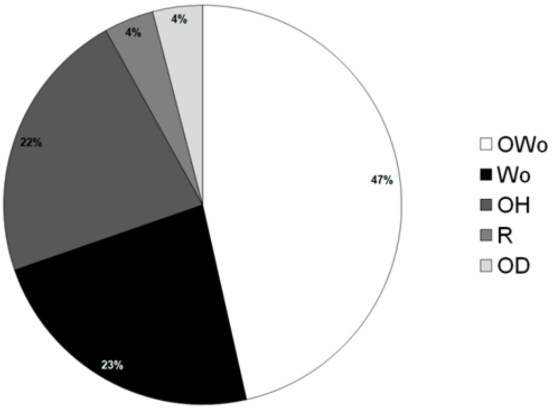

Figure 3 Percentage of the different habitats with a representation in the surroundings of the site at the time of the formation of Abric del Pastor S.U. IVd, based on analysis of the microvertebrate assemblage. OH: Open Humid; OD: Open Dry; R: Rocky; Wo: Woodland; OWo: Open Woodland.

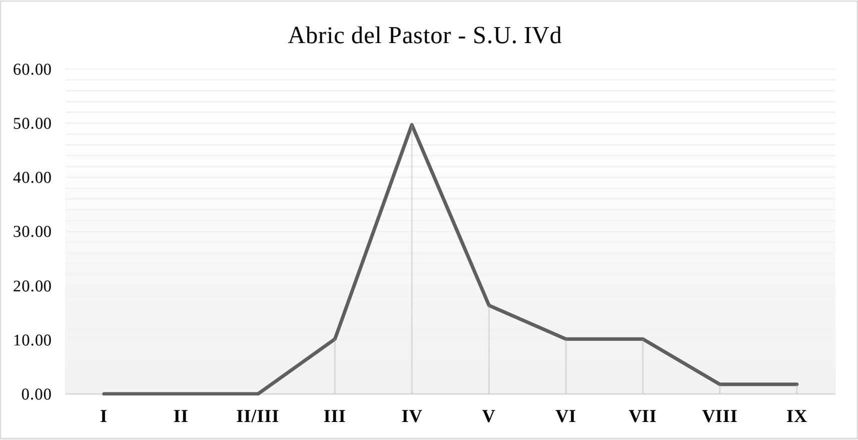

Figure 4 Chart displaying bioclimatic component (BC) values from Abric del Pastor S.U. IVd.

Sample	MFU	MF Type	S.U	Voids	Frequency	Pedality and microstructure	Components	*b*-fabric	Sedimentary features	Postdepositional features
AP-10-1a	1	1	IVe/f	compound packing voids	30-50%	unaccomodated crumb double spaced fine enaulic (c/f $_{30\mu m}$ 1:2)	fissured clasts bone fragments ash charcoal	calcitic crystallitic	fine clay cappings dusty clay coatings	-
	2	1		planes vesicles chambers	30-50% 15-30% 5-15%	unaccomodated crumb single spaced fine enaulic single spaced porphyric (c/f $_{30\mu m}$ 1:4)				
AP-10-1b	1	1a	IVd	compound packing voids planes	30-50% 5-15%	unaccomodated crumb/granular single spaced fine enaulic (c/f $_{30\mu m}$ 2:1)	fissured clasts well-rounded clasts ash bone fragments	calcitic crystallitic	dusty clay infillings dusty clay coatings platy gravels clay cappings	-
	2	2		planes	30-50%	partially accomodated weakly lenticular double spaced fine enaulic (c/f $_{30\mu m}$ 1:4)	fissured clasts well-rounded clasts bone fragments			
AP-10-1c	1	1a	IVf/g	compound packing voids planes	30-50% 5-15%	unaccomodated crumb/granular single spaced fine enaulic (c/f $_{30\mu m}$ 1:4)	well-rounded clasts ash charcoal	calcitic crystallitic	dusty clay coatings	Fe segregation
AP-10-2a	1	4a	IVa	vesicles vughs	5-15% 5-15%	massive double spaced porphyric (c/f $_{30\mu m}$ 1:6)	fissured clasts bone fragments	calcitic crystallitic	dusty clay coatings	root bioturbation
AP-10-2b	1	2	IVa	planes	30-50%	partially accomodated weakly lenticular double spaced fine enaulic (c/f $_{30\mu m}$ 1:3)	ash bone fragments fissured clasts	calcitic crystallitic	limpid clay infillings dusty clay coatings	-

	2	1a		vesicles chambers	15-30% 5-15%	unaccomodated crumb/granular single spaced fine enaulic (c/f 30µm 1:4)	bone fragments tortoise bone fragment ash fissured clasts			
	3	4a		vesicles	5-15%	massive double spaced porphyric (c/f 30µm 1:9)	ash bone fragments fissured clasts			
AP-10-2c	1	1b	IVb	compound packing voids	30-50%	unaccomodated crumb/granular single spaced fine enaulic (c/f 30µm 1:4)	ash charcoal bone fragments fissured clasts well rounded clasts	calcitic crystallitic	dusty clay coatings platy gravels clay cappings	Fe segregation calcite dissolution
	2	3		vughs vesicles compound packing voids	30-50% 5-15% 5-15%	unaccomodated vughy single spaced fine enaulic (c/f 30µm 1:4)				
AP-10-3a	1	1a	IVg	compound packing voids	30-50%	unaccomodated crumb/granular single spaced fine enaulic (c/f 30µm 1:4)	well-rounded clasts bone fragments	calcitic crystallitic	dusty clay coatings	Mn and Fe nodules
AP-10-3b	1	1a	IVg	compound packing voids planes	30-50% 5-15%	unaccomodated crumb/granular weakly lenticular single spaced fine enaulic (c/f 30µm 2:1)	fissured clasts well-rounded clasts bone fragments	calcitic crystallitic	dusty clay coatings	Mn and Fe nodules
AP-10-3c	1	1	V	compound packing voids vesicles	30-50% 5-15%	unaccomodated crumb/granular single spaced fine enaulic (c/f 30µm 1:4)	bone fragments charcoal	calcitic crystallitic	dusty clay coatings dusty clay infillings	Fe segregation neomorphic calcite
AP-10-4b	1	1	Id	compound packing voids channels	30-50% 15-30%	unaccomodated crumb/granular single spaced fine enaulic (c/f 30µm 1:4)	well-rounded clasts coprolites (massive) snail shell bone fragments	calcitic crystallitic	dusty clay coatings	root bioturbation

AP-10-4c	1	1	Id - III	compound packing voids channels	30-50% 15-30%	unaccomodated crumb/granular single spaced fine enaulic (c/f 30µm 1:4)	well-rounded clasts faecal spherulites bone fragments	calcitic crystallitic	dusty clay coatings	root bioturbation
AP-10-5a	1	4	II	vughs vesicles chambers	5-15% 5-15% 5-15%	massive double spaced porphyric (c/f 30µm 1:9)	corroded clasts ash bone fragments	calcitic crystallitic	dusty clay coatings	-
AP-10-5b	1	4	II	vughs vesicles chambers	5-15% 5-15% 5-15%	massive double spaced porphyric (c/f 30µm 1:9)	corroded clasts tooth fragment bone fragments	calcitic crystallitic	dusty clay coatings/hypocoatings	root bioturbation
AP-10-6	1	3	IVb	vughs compound packing voids	30-50% 5-15%	unaccomodated vughy single spaced fine enaulic (c/f 30µm 1:4)	ash exogenous flint bone fragments	calcitic crystallitic	dusty clay coatings dusty clay infillings	root biotrurbation Fe segregation
AP-13-1a	1	1	VI 1-2	compound packing voids	30-50%	unaccomodated crumb/granular single spaced fine enaulic (c/f 30µm 1:4)	platy clasts fissured clasts bone fragments	calcitic crystallitic	clay cappings dusty clay infillings	-
AP-13-1b	1	1	VI 2-3	compound packing voids	30-50%	unaccomodated crumb single spaced fine enaulic (c/f 30µm 1:3)	platy clasts corroded clasts ash	calcitic crystallitic	dusty clay coatings	-
	2			compound packing voids	30-50%	unaccomodated crumb/granular single spaced fine enaulic (c/f 30µm 1:6)	fissured clasts corroded clasts char burned bone bone fragments charcoal ash		anorthic nodule limpid clay infillings dusty clay coating guano	

AP-13-2	1	1	VI 1-2	compound packing voids vesicles	30-50% 5-15%	unaccomodated crumb single spaced fine enaulic (c/f $_{30\mu m}$ 1:3)	faecal spherulites charred plant tissue ash ash nodule burned bone bone fragments char charcoal	calcitic crystallitic	dusty clay coatings	root bioturbation
AP-13-3	1	1	VI 3	compound packing voids vesicles vughs	30-50% 30-50% 5-15%	unaccomodated crumb/granular, locally compacted single spaced fine enaulic (c/f $_{30\mu m}$ 1:5)	-	calcitic crystallitic	dusty clay infillings dusty clay nodules needle fibre calcite	-
AP-13-4-1	1	1a	IVd 1-2	compound packing voids	30-50%	unaccomodated crumb single spaced fine enaulic (c/f $_{30\mu m}$ 1:3)	-	calcitic crystallitic	dusty clay coatings	-
Ap-13-4-2	1	1a	IVd 1-2	compound packing voids	30-50%	unaccomodated crumb single spaced fine enaulic (c/f $_{30\mu m}$ 1:4)	fissured clasts well-rounded clasts	calcitic crystallitic	dusty clay coatings dsuty clay nodules dusty clay infillings anorthic nodule	Mn segregation
AP-13-5-1	1	1a	IVd 2	compound packing voids	30-50%	unaccomodated crumb single spaced fine enaulic (c/f $_{30\mu m}$ 1:4)	well-rounded clasts bone charcoal	calcitic crystallitic	dusty clay coatings organic rich anorthic nodule	-
AP-13-5-2	1	1a	IVd 2	compound packing voids	30-50%	unaccomodated crumb single spaced fine enaulic (c/f $_{30\mu m}$ 1:4)	-	calcitic crystallitic	dusty clay coatings	-

AP-13-7	1	1	IIa (H7)	compound packing voids vesicles vughs	30-50% 15-30% 5-15%	unaccomodated crumb/granular single spaced fine enaulic (c/f 30µm 1:5)	bone fragments carnivore coprolite ash burned bone	calcitic crystallitic	dusty clay coatings orthic nodules	-
AP-13-8	1	1	IVd 3-4 (H9)	compound packing voids vesicles	30-50% 5-15%	unaccomodated crumb/granular, locally compacted single spaced fine enaulic (c/f 30µm 1:4)	charcoal bone fragments	calcitic crystallitic	crusts anorthic nodule dusty clay coating	root bioturbation
AP-13-9	1	1	IVd 3-4 (H8)	compound packing voids vesicles	30-50% 5-15%	unaccomodated crumb/granular single spaced fine enaulic (c/f 30µm 1:4)	charcoal	calcitic crystallitic	dusty clay coatings organic rich anorthic nodule	root bioturbation
AP-13-10	1	1a	IVd 3-4 (H10)	compound packing voids	30-50%	unaccomodated granular single spaced fine enaulic (c/f 30µm 1:4)	fissured clasts well-rounded clasts shell fragments charcoal burned bone bone fragments ash	calcitic crystallitic	dusty clay coatings faecal pellets	biotubation
	2			vughs planes	5-15% 5-15%	weakly accomodated subangular blocky single spaced fine enaulic (c/f 30µm 1:5)	fissured clasts well-rounded clasts charcoal burned bone bone fragments ash massive coprolite		dusty clay coatings faecal pellets needle fibre calcite	bioturbation

	3			vesicles planes	5-15% 5-15%	massive single spaced porphyric (c/f 30µm 1:5)	fissured clasts well-rounded clasts shell fragments charcoal burned bone bone fragments		dusty clay coatings	-
AP-13-11	1	1a	IVd 4	compound packing voids	30-50%	unaccomodated granular single spaced fine enaulic (c/f 30µm 1:4)	well-rounded clasts bone fragments	calcitic crystallitic	dusty clay coatings	Mn segregation root bioturbation
	2	3		vesicles vughs	30-50% 5-15%	spongy single spaced fine enaulic (c/f 30µm 1:4)	well-rounded clasts bone fragments charcoal		dusty clay coatings faecal pellets	bioturbation
AP-15-1	1	1a	IVd/e	compound packing voids	30-50%	unaccomodated crumb single spaced fine enaulic (c/f 30µm 1:3)	well-rounded clasts	calcitic crystallitic	dusty clay coatings limpid clay infillings	root bioturbation
AP-15-2	1	1a	IVd	compound packing voids	30-50%	unaccomodated crumb/granular single spaced fine enaulic (c/f 30µm 1:3)	well-rounded clasts	calcitic crystallitic	dusty clay coatings	-
AP-15-3	1	3	IVd (H14)	vesicles	30-50%	spongy single spaced fine enaulic (c/f 30µm 1:4)	well-rounded clasts	calcitic crystallitic	dusty clay coatings	-
	2	1a		compound packing voids	30-50%	unaccomodated crumb/granular single spaced fine enaulic (c/f 30µm 1:4)	well-rounded clasts			

AP-15-4	1	1a	IVd (H13)	compound packing voids	30-50%	unaccomodated crumb/granular single spaced fine enaulic (c/f $_{30\mu m}$ 1:4)	vertically oriented clasts platy clasts well-rounded clasts bone fragments	calcitic crystallitic	dusty clay coatings organic rich anorthic nodule clay cappings	-
	2	3		vesicles vughs	30-50% 15-30%	spongy single spaced fine enaulic (c/f $_{30\mu m}$ 1:4)	platy clasts well-rounded clasts		dusty clay coatings limpid clay infillings	
AP-15-5	1	1a	IVd 5	compound packing voids vesicles	30-50% 5-15%	unaccomodated crumb/granular, locally spongy single spaced fine enaulic (c/f $_{30\mu m}$ 1:4)	well-rounded clasts fissured clasts platy clasts burned bone char charcoal	calcitic crystallitic	dusty clay coatings clay cappings	root bioturbation
AP-15-6	1	3	IVd (H16)	vesicles vughs	30-50% 30-50%	spongy single spaced fine enaulic (c/f $_{30\mu m}$ 1:4)	well-rounded clasts char bone fragments	calcitic crystallitic	dusty clay coatings	-

Table 5 Descriptions of micromorphological thin sections from Abric del Pastor discussed in chapter 3.

APPENDIX 2

Supplementary Material

for

Chapter 4: Investigating the palaeoenvironmental context for the disappearance of Neanderthals in Eastern Iberia: a multiproxy study of Stratigraphic Units VIII – V (upper) at El Salt (Alcoy)

Contents:

Chapter 4: Soil micromorphology results (extended)

Sample	Profile	MFU	S.U	LT	Microstructure	c/f rd	Porosity	*b*-fabric	Sedimentary features	Components
SALT-08-3	1	3	VII	A	no pedality; intergrain microaggregate; locally compacted	single spaced porphyric $c/f_{20\mu m}$	complex packing voids; channels; vesicles	undifferentiated to calcitic crystallitic	matrix locally decalcified; Fe and Mn nodules; faecal pellets	*Celtis sp.* seed coatings; guano; charcoal fragments; bone fragments; microfauna; fine black OM particles; massive and fibrous coprolites
		2		C			complex packing voids; channels; locally vughy	calcitic crystallitic	dusty clay infillings; gypsum infillings; gypsum coating bone fragment; Fe and Mn nodules	*Celtis sp.* seed coatings; charcoal fragments; bone fragments; microfauna; fine black OM; massive coprolites
		1	VIII	A			complex packing voids; planes; locally compact;	undifferentiated	matrix decalcified; gypsum infillings; Fe and Mn nodules	*Celtis sp.* seed coatings; charcoal; bone fragments; microfauna; fine black OM
SALT-08-04	1	2	V	B	no pedality; intergrain microaggregate	single spaced porphyric $c/f_{20\mu m}$	complex packing voids; channels	calcitic crystallitic	matrix rich in micritic calcite; Fe and Mn nodules; Fe mottling; gypsum infillings	*Celtis sp.* seed coatings; massive and fibrous coprolites; bone fragments; guano; charcoal fragments; microfauna
		1	VI	A			complex packing voids; channels; locally vughy	undifferentiated to calcitic crystallitic	matrix locally decalcified; gypsum infillings; Fe and Mn nodules	*Celtis sp.* seed coatings; guano; charcoal fragments
SALT-08-05	1	3	VI	A	no pedality; intergrain microaggregate	single spaced porphyric $c/f_{20\mu m}$	complex packing voids; vesicles	calcitic crystallitic	anorthic clay nodules; faecal pellets;	*Celtis sp.* seed coatings; bone fragments; microfauna; guano

		2		C	no pedality; intergrain microaggregate; locally massive		complex packing voids; locally vughy;			*Celtis sp.* seed coatings; charcoal fragments; bone fragments; massive coprolites;
		1	VII	A	no pedality; intergrain microaggregate; channel microstructure		complex packing voids; vesicles; channels		locally bioturbated; faecal pellets	*Celtis sp.* seed coatings; guano; bone fragments; microfauna; massive coprolites; flint microflakes; fine black OM
SALT-08-06	1	2	IV	B	no pedality; intergrain microaggregate (open)	double spaced porphyric c/f $_{20\mu m}$	open	calcitic crystallitic		
		1	V		no pedality; intergrain microaggregate; locally massive	single spaced porphyric c/f $_{20\mu m}$	complex packing voids; vughs; channels		matrix rich in micritic calcite; Fe and Mn nodules; faecal pellets; gypsum infillings	*Celtis sp.* seed coatings; bone fragments; guano; massive coprolites
SALT-08-26	3	2	VII	C	no pedality; intergrain microaggregate	single spaced porphyric c/f $_{20\mu m}$	complex packing voids; channels; chambers	calcitic crystallitic; locally undifferentiated	dusty clay infillings;	*Celtis sp.* seed coatings; bone fragments; microfauna; fine black OM
		1	VIII		no pedality; intergrain microaggregate; locally massive				matrix decalcified	*Celtis sp.* seed coatings; large flint microflake; charcoal fragments; bone fragments; microfauna; fine black OM
SALT-08-32	3	3	V	B	no pedality; intergrain microaggregate;	single spaced porphyric c/f $_{20\mu m}$	complex packing voids; channels	undifferentiated to calcitic crystallitic	wasp nests; locally bioturbated; faecal pellets; gypsum infillings	*Celtis sp.* seed coatings; guano; bone fragments; charcoal fragments
		2	V - VI	A	no pedality; intergrain microaggregate; locally granular				dusty clay coatings (thin); wasp nests; faecal pellets; anorthic nodules	*Celtis sp.* seed coatings; bone fragments; fine black OM; guano

		1	VI		no pedality; intergrain microaggregate				matrix decalcified; gypsum infillings; locally bioturbated	*Celtis sp.* seed coatings; bone fragments; fine black OM; massive coprolites; guano; microfauna
SALT-08-37	3	4	VI	A	no pedality; intergrain microaggregate	single spaced porphyric c/f $_{20\mu m}$	complex packing voids;	calcitic crystallitic	anorthic clay nodules; faecal pellets; gypsum infillings; recrystalised calcite coatings	*Celtis sp.* seed coatings; charcoal fragments; bone fragments; calcitic wood ash; flint microflakes; fibrous coprolites; fine black OM
		3	VII			single spaced porphyric c/f $_{20\mu m}$	complex packing voids; channels; chambers;	undifferentiated to calcitic crystallitic	locally bioturbated; faecal pellets; Fe and Mn nodules	*Celtis sp.* seed coatings; bone fragments; charcoal fragments; fine black OM; guano; massive and fibrous coprolites; flint microflakes; calcitic wood ash
		2					complex packing voids; planes	undifferentiated	gypsum infillings; faecal pellets; anorthic clay nodules	*Celtis sp.* seed coatings; fine black OM; burned bone; charcoal fragments
		1			no pedality; intergrain microaggregate; locally fissured (thin section artefact)			calcitic crystallitic		*Celtis sp.* seed coatings; bone fragments; charcoal fragments; fine black OM; guano; massive and fibrous coprolites; microfauna; calcitic wood ash; tooth fragment; fat-derived char
SALT-10-13	13	1	VIII	C	no pedality; intergrain microaggregate; locally compacted	single to double spaced porphyric c/f $_{20\mu m}$	complex packing voids; channels	calcitic crystallitic	matrix decalcified; gypsum infillings; reaction rims; faecal pellets; phosphatic crust	*Celtis sp.*seed coatings; bone fragments; guano; fine black OM; phytoliths; charcoal fragments; microfauna; shell fragments; massive coprolites; flint microflakes; tooth fragment

SALT-10-16			VI	A	no pedality; massive; locally intergrain microaggregate/crumb	single spaced porphyric c/f 20µm	complex packing voids; channels	calcitic crystallitic	matrix locally decalcified; faecal pellets; wasp nests	*Celtis sp.*seed coatings; bone fragments; fine black OM; massive coprolites; guano; microfauna
SALT-10-17	20	1	V	B	no pedality; intergrain microaggregate	single spaced porphyric c/f 20µm	complex packing voids; channels	calcitic crystallitic	Fe and Mn nodules; gypsum infillings	*Celtis sp.* seed coatings; bone fragments; guano; phytoliths; massive and fibrous coprolites; charcoal fragments;
SALT-10-18	20	2	V	B*	no pedality; intergrain microaggregate; locally compacted	single spaced porphyric c/f 20µm	complex packing voids; channels	undifferentiated to calcitic crystallitic	dusty clay coatings; faecal pellets; gypsum infillings	*Celtis sp.* seed coatings; bone fragments; guano; massive and fibrous coprolites; charcoal fragments
		1		B				calcitic crystallitic	Fe and Mn nodules; gypsum infillings	*Celtis sp.* seed coatings; bone fragments; phytoliths; guano; massive and fibrous coprolites; charcoal fragments
SALT-10-19	21	4	V	B*	no pedality; intergrain microaggregate	single spaced porphyric c/f 20µm	complex packing voids; channels	calcitic crystallitic	matrix rich in micritic calcite; limpid clay infillings; orthic nodules; faecal pellets; gypsum infillings	*Celtis sp.* seed coatings; charcoal fragments; bone fragments; fibrous coprolites; guano
		3	VI	A					matrix locally decalcified; Fe and Mn nodules; faecal pellets	*Celtis sp.* seed coatings; bone fragments; charcoal fragments; fine black OM; guano; fibrous coprolites; microfauna; shell fragments; phytoliths
		2		D	no pedality; intergrain microaggregate			undifferentiated	matrix decalcified;	*Celtis sp.* seed coatings; fine black OM; burned bone; charcoal fragments; guano

		1						undifferentiated to calcitic crystallitic	matrix locally decalcified; Fe and Mn nodules; faecal pellets	*Celtis sp.* seed coatings; guano; fine black OM; fibrous coprolites
SALT-10-20	24	6	V	B	no pedality; intergrain microaggregate; locally crumb	single spaced porphyric c/f $_{20\mu m}$	complex packing voids; channels; vughs; planes	undifferentiated to calcitic crystallitic	faecal pellets; Fe and Mn nodules; organic rich anorthic nodules; gypsum infillings	*Celtis sp.* seed coatings; guano; charcoal fragments; bone fragments; phytoliths
		5	VI	E	sub-angular blocky peds (partially accommodated); internally massive		vughs; planes		anorthic organic rich nodules	bone fragments (very degraded); fine black OM; phytoliths
		4			no pedality; vughy		vughs; channels;	undifferentiated	phosphatic crust; anorthic clay nodules; Fe and Mn nodules	
		3		A	no pedality; intergrain microaggregate; locally crumb		complex packing voids; channels; chambers	undifferentiated to calcitic crystallitic	matrix locally decalcified; faecal pellets; calcite coatings; anorthic clay rich nodules	*Celtis sp.* seed coatings; guano; fine black OM; bone fragments; microfauna; charcoal fragments; fibrous coprolites
		2							matrix mildly decalcified; faecal pellets; anorthic clay rich nodules	
		1							matrix mildly decalcified; faecal pellets; calcite coatings around voids; anorthic clay rich nodules	

Table 5 Descriptions of micromorphological thin sections from El Salt discussed in chapter 4.